Molecular and Cellular Aspects of

DNA-end Resection by Human CtIP

DISSERTATION

ZUR

ERLANGUNG DER NATURWISSENSCHAFTLICHEN DOKTORWÜRDE

(Dr. sc. nat.)

VORGELEGT DER

MATHEMATISCH-NATURWISSENSCHAFTLICHEN FAKULTÄT

DER

UNIVERSITÄT ZÜRICH

VON

OLGA MURINA

AUS

RUSSLAND

PROMOTIONSKOMITEE:

PROF. DR. ALESSANDRO A. SARTORI (VORSITZ UND LEITUNG DER DISSERTATION)

PROF. DR. PRIMO LEO SCHÄR

PROF. DR. MASSIMO LOPES

PD DR. MANUEL STUCKI

ZÜRICH, 2014

TABLE OF CONTENTS

ZUSAMMENFASSUNG

Die Erbinformation (DNA) in unseren Zellen wird durch eine Vielzahl von Umwelteinflüssen konstant beschädigt. DNA Doppelstrangbrüche (DSB) gehören zu den gefährlichsten aller DNA Schäden, weil sie ohne Reparatur zum Tod einer Zelle führen können. Zudem besteht eine direkte Verbindung zwischen falscher DSB Reparatur und Krebs. Zellen besitzen zwei verschiedene Systeme für die DSB Reparatur: Nicht-homologe Enden-Verknüpfung (NHEJ) und Homologe Rekombination (HR). Im Unterschied zu NHEJ, müssen für HR die Enden der Brüche zuerst prozessiert werden, sodass einzelsträngige DNA Überhänge entstehen. An diesem Schritt, der als 'DNA-Endresektion' bezeichnet wird, ist das CtIP Protein massgeblich beteiligt.

Der erste Teil meiner Doktorarbeit beschäftigt sich mit der Frage ob CtIP auch in der Reparatur von kovalent-quervernetzten DNA Strängen, sogenannten 'interstrand crosslinks' (ICL), eine Rolle spielt und ob ein Zusammenspiel zwischen DNA-Endresektion und dem *Fanconi anemia* (FA) Signalweg existiert. Die FA-Proteine steuern die komplexe Reparatur von ICLs, indem sie diese im Chromatin erkennen, prozessieren und, in Zusammenarbeit mit anderen Reparatursystemen inklusive der HR, korrigieren. Wir zeigen, dass die Bindung von CtIP an ICL-geschädigtes Chromatin von der Funktion des FA-Kernkomplexes und der Mono-Ubiquitinierung des FANCD2 Proteins abhängig ist. Wir legen außerdem dar, dass die Lokalisierung von CtIP an ICLs durch die direkte Interaktion von CtIP mit FANCD2 vermittelt und möglicherweise durch die Fähigkeit von CtIP ubiquitinierte Substrate zu binden verstärkt wird. Bemerkenswerterweise haben Zellen in denen FANCD2 inaktiviert ist, einen ähnlichen Defekt in der DNA-Endresektion wie CtIP-defiziente Zellen. Zudem haben wir eine FANCD2-Bindestelle innerhalb des CtIP Proteins identifizieren können, welche für eine fehlerfreie Reparatur von ICLs erforderlich ist und somit potentielle, durch NHEJ-verursachte, chromosomale Aberrationen verhindert. Interessant ist auch, dass charakteristische Phänotypen von FANCD2-defizienten Zellen, wie genomische Instabilität und Hypersensitivität gegenüber ICL-induzierenden Stoffen, durch eine zusätzlichen Verlust von CtIP verschlimmert werden. Daraus schließen wir, dass CtIP auch in Abwesenheit von FANCD2 eine bedeutende Funktion für die ICL Reparatur hat. Insgesamt zeigen unsere Ergebnisse, dass FANCD2 ein wichtiger Regulator der CtIP-

vermittelten DNA-Endresektion darstellt und dass CtIP eine essenzielle Rolle in der Aufrechterhaltung der Stabilität unseres Genoms spielt.

Im zweiten Teil meiner Doktorarbeit untersuchen wir eine spezielle Klasse von Mutationen des menschlichen RAD50 Proteins, genannt RAD50S, die in Hefe zu einer Trennung verschiedener Funktionalitäten des Proteins führt. Bei RAD50 handelt es sich um eine Untereinheit des MRE11-RAD50-NBS1 (MRN) Komplexes, der mit CtIP interagiert und mehrere Aufgaben in der DSB Reparatur spielt. Wir zeigen, dass RAD50S Mutationen die DNA-Endresektion und DSB Reparatur beeinträchtigt, vor allem wenn Zellen mit DNA Topoisomerase-hemmenden Substanzen behandelt werden. RAD50S Mutationen führten jedoch weder zu einer veränderten Struktur des MRN Komplexes, noch zu einer Beeinträchtigung MRN-abhängiger Signalwege nach Behandlung von Zellen mit anderen DNA-schädigenden Substanzen. Basierend auf unseren biochemischen Daten kommen wir zum Schluss, dass die von uns beobachteten zellulären Phänotypen höchstwahrscheinlich durch eine Störung der Interaktion zwischen RAD50S und CtIP hervorgerufen werden, welche besonders für die Reparatur blockierter Topoisomerase Moleküle an DSB Enden von Bedeutung ist.

Beide Studien eingeschlossen, belegen unsere Ergebnisse dass CtIP durch Interaktionen mit FANCD2 und RAD50 eine Schlüsselrolle bei der Reparatur von DNA Schäden spielt und somit womöglich ein wichtiger Faktor zur Verhinderung von Krebs ist.

SUMMARY

Our genome is under constant threat from DNA damage that inflicts different kinds of lesions including DNA double-strand breaks (DSBs). Failure to correctly repair DSBs can cause gross chromosomal aberrations, which are a hallmark of cancer. Cells have evolved two major pathways to repair DSBs: non-homologous end-joining (NHEJ) and homologous recombination (HR). Human CtIP promotes DNA-end resection, which commits cells to error-free HR and prevents aberrant repair by NHEJ, hence it is a critical determinant of DSB repair pathway choice. However, the cellular response to DNA damage involves a complex interplay between different genome maintenance pathways and the role of CtIP in this multifaceted network is still poorly understood.

In the first part of my PhD study, we addressed the functional interplay between CtIP-dependent resection and the *Fanconi anemia* (FA) pathway during the repair of DNA interstrand crosslinks (ICLs). *Fanconi anemia* is an inherited disorder associated with a high risk to develop cancer and is caused by mutations in sixteen *FA* genes. Together, the FA proteins orchestrate ICL incision, translesion synthesis and HR. We demonstrate that chromatin association of CtIP in response to ICL-induced damage is strictly dependent on a functional FA core complex and FANCD2 monoubiquitination. Furthermore, we show that CtIP recruitment to ICL lesions is mediated by its direct interaction with FANCD2 and might be further reinforced by the discovered ability of CtIP to recognize ubiquitinated substrates. Remarkably, cells lacking FANCD2 akin to CtIP-depleted cells are impaired in DNA-end resection. We have identified FANCD2-binding sites on CtIP and provide evidence that CtIP-FANCD2 complex is required for the faithful repair of ICLs, meanwhile counteracting mutagenic NHEJ pathway. Interestingly, the phenotypes of *FA* cells such as genome instability and ICL hypersensitivity are further aggravated by CtIP depletion, indicating the significance of CtIP even in the absence of proficient FA pathway. Taken together, our data establish FANCD2 as a critical regulator of CtIP-mediated DNA-end resection and emphasize the essential role of CtIP in maintaining genome stability in response to ICL damage.

In the second part, we examined the phenotypes of the separation-of-function (S) mutations in human RAD50, a subunit of the MRE11-RAD50-NBS1 (MRN) complex that interacts with CtIP and plays crucial roles in DSB signaling and processing. We demonstrate that RAD50S mutants compromise resection and repair of DSBs induced specifically by DNA topoisomerase poisons, but do neither alter MRN complex integrity

nor significantly affect MRN-dependent signaling in response to other types of DNA damaging agents. Based on our biochemical data we suggest that these phenotypes are caused by the impaired interaction between RAD50S mutants and CtIP, which is particularly important for the processing of topoisomerases trapped to DNA ends.

Collectively, our results establish a key role for CtIP in the repair of ICLs and also highlight the significance of CtIP-MRN association for the processing of toxic protein-DNA adducts. Work presented in my thesis thus advances the understanding of how the DNA-end resection activity of CtIP is regulated to preserve genome stability.

ABBREVIATIONS

53BP1	p53-binding protein 1
aa	amino acid
APLF	apraxin and polynucleotide kinase-like factor
AT	ataxia telangiectasia
ATM	ataxia telangiectasia mutated
ATR	ataxia telangiectasia mutated and Rad3 related
bp	base pair
BRCA1/2	breast cancer susceptibility gene 1/2
BRCT	BRCA1 C-terminus domain
CHK1/2	checkpoint kinase 1/2
CDKs	cyclin-dependent kinases
CDC	cell division cycle
CIN	chromosomal instability
CPT	camptothecin
CSR	class switch recombination
CtBP	carboxy-terminal binding protein
CtIP	CtBP interacting protein
CO	crossover
DDR	DNA damage response
DNA-PK	DNA-dependent protein kinase
DNA-PKcs	DNA-PK catalytic subunit
ssDNA	single stranded DNA
dsDNA	double stranded DNA
dHJ	double Holliday junction
DSB	double strand break
EXO1	exonuclease 1
ETOP	etoposide
FA	Fanconi anaemia
FANCD2	Fanconi anemia complementation group D type 2
FAN1	FANCD2-associated nuclease 1
FHA	forkhead-associated domain
GFP	green fluorescent protein
HR	homologous recombinaton
ICL	interstrand crosslink
IR	ionizing radiation
LigIV	DNA ligase IV
MDC1	mediator of DNA damage checkpoint 1
MEFs	mouse embryonic fibroblasts
MMC	mitomycin C
MMS	methyl methanesulfonate
MRE11	meiotic recombination 11 homolog 1
MRN	MRE11-RAD50-NBS1
MSI	microsatellite instability
NBS1	Nijmegen breakage syndrome 1
NCO	non-crossover
NER	nucleotide excision repair
NHEJ	non-homologous end-joining

alt-NHEJ	alternative NHEJ
c-NHEJ	classical NHEJ
PCNA	proliferating cell nuclear antigen
PIKK	phosphatidylinositol 3-kinase-like protein kinase
PLA	proximity ligation assay
PNKP	polynucleotide kinase/phosphatase
PTMs	post-translational modifications
pRb	retinoblastoma protein
RAD50	radiation sensitive 50
RAD50S	RAD50 separation-of-function mutation
RIF1	Rap-interacting factor 1
RPA	replication protein A
RNF8	ring finger protein 8
ROS	reactive oxygen species
Sae2	sporulation in absence of spo11
SDSA	synthesis dependent strand annealing
SD	standard deviation
SEM	standard error of the mean
SMC	structural maintenance of chromosomes
Spo11	sporulation-specific protein 11
SSA	single-strand annealing
TLS	translesion DNA synthesis
Top I/II	topoisomerase I/II
UBD	ubiquitin-binding domain
UBZ	ubiquitin-binding zinc finger
UV	ultraviolet light
XLF	XRCC4-like factor
XRCC4	X-ray repair cross-complementing protein 4
Xrs2	X-ray sensitive protein 2

1. INTRODUCTION

1.1. DNA damage response, genome stability and cancer

Genetic information in all known organisms is encoded in DNA that has to be faithfully propagated to subsequent generations. However, the integrity of DNA is under constant threat of DNA damage from both internal and external sources [1]. Spontaneous DNA alterations can be caused by inaccurate DNA replication or reactive-oxygen species (ROS) that arise during normal cellular metabolism [2,3]. Furthermore, DNA lesions can be induced by exposure to ionizing irradiation (IR), UV light or chemical compounds used in chemotherapy, hence representing major triggers of exogenous DNA damage [4]. Each cell in the human body experience about 10^4-10^6 DNA lesions per day [5]. Failure to correctly repair DNA lesions gives rise to mutations and genomic alterations that eventually can threaten cell viability [1]. Uncontrolled cell proliferation and oncogenic transformation are the other dangerous consequences of mutations inactivating tumor suppressor genes or triggering activation of oncogenes [6]. Consequently, eukaryotic cells have evolved different repair strategies to maintain genomic integrity. Depending on the type of lesion, specialized repair pathways are activated to remove the damage (Figure 1) [1]. Subtle modifications of DNA, including small alkylation products and oxidative lesions are repaired by base excision repair (BER) via incision of the damaged base [7]. Deletions, insertions and mismatched base pairs incorporated during DNA replication are corrected by the mismatch repair (MMR) pathway [8]. Nucleotide excision repair (NER) eliminates more complex helix-distorting DNA damage such as pyrimidine dimers and intrastrand crosslinks by removal of a short oligonucleotide containing the damaged base [9]. DNA double-strand breaks (DSBs) are the substrates of either homologous recombination (HR) repair or non-homologous end-joining (NHEJ) [10]. Notably, some DNA lesions that block replication fork progression are not repaired but instead are bypassed by translesion synthesis (TLS) polymerases with less stringent base-pairing requirements than replicative polymerases [11]. Interstrand crosslinks (ICLs) covalently blocking two opposite DNA strands are removed by a complex interplay between the Fanconi anemia (FA) repair pathway and proteins of NER, TLS and HR pathways [12]. The DSB and ICL repair pathways are described in detail in the following sections.

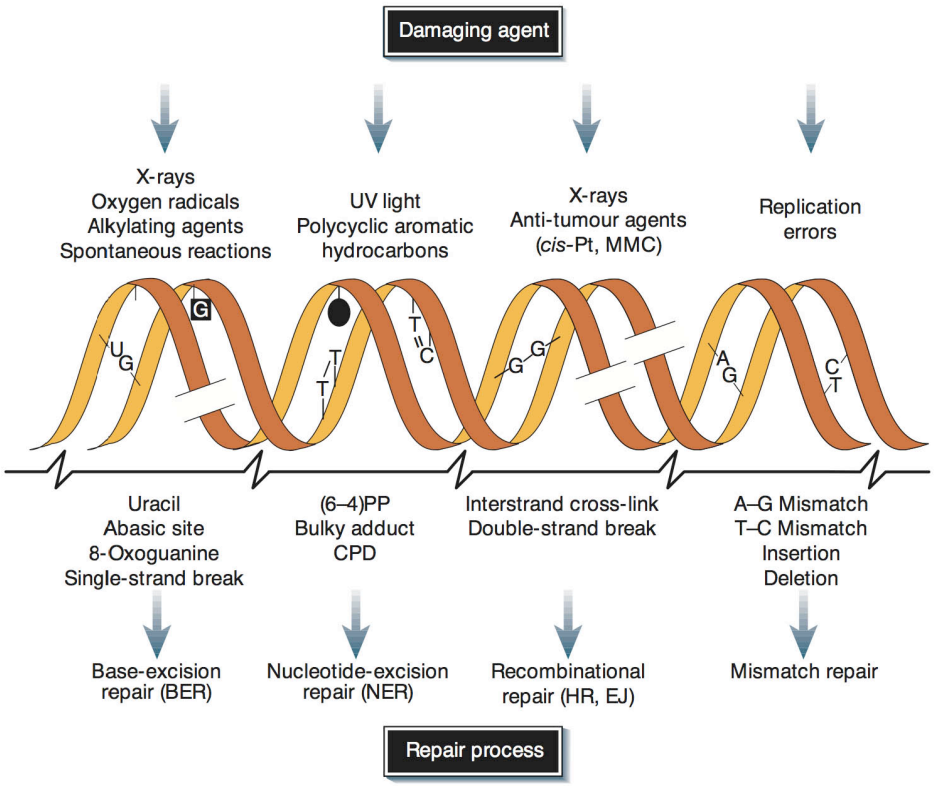

Figure 1. DNA damage and DNA repair mechanisms. Different DNA damaging agents generate various types of DNA lesions that are removed by specialized DNA repair mechanisms. Abbreviations: *cis*-Pt, cisplatin; MMC, mitomycin C; (6-4)PP, 6-4 photoproduct; CPD, cyclobutane pyrimidine dimer; BER, base excision repair; NER, nucleotide excision repair; HR, homologous recombination; EJ, end joining. Adapted from [1].

The repair of DNA lesions requires activation of the DNA damage response (DDR), a sophisticated cellular network that senses and signals the presence of DNA damage to effector proteins to regulate numerous biological responses, including DNA repair, transient cell cycle arrest, transcription and apoptosis (Figure 2) [13]. The DDR signaling cascade is mainly controlled by three phosphatidylinositol 3-kinase-like protein kinases (PIKKs): ataxia telangiectasia-mutated (ATM), ATM and Rad3-related kinase (ATR) and DNA-dependent protein kinase (DNA-PK) [14]. Activation of ATM and DNA-PK is primarily triggered by DSB formation, whereas ATR is activated by single-stranded DNA (ssDNA) generated during replicative stress or DNA-end resection of DSBs [15,16]. PIKKs are recruited to sites of DNA lesions via conserved interactions with DNA damage sensor proteins [14]. ATM activation is triggered by the recruitment of the MRE11-RAD50-NBS1 (MRN) complex to DSBs [17]. ATM exists as an inactive dimer, but in response to DSB-inducing agents it undergoes MRN-mediated activation, dimer

dissociation and autophosphorylation [18]. Once activated, it phosphorylates various downstream targets including the MRN complex itself, histone variant H2AX at serine 139 (S139) producing γH2AX, and checkpoint kinase 2 (CHK2) [19,20]. CHK2 kinase activated via phosphorylation at a specific threonine 68 (T68) acts on multiple substrates such as p53 and cell division cycle 25 (CDC25) phosphatases [21,22]. CDC25 phosphatases control cell cycle transition by removing inhibitory phosphorylation from cyclin-dependent kinases (CDKs) [23]. Phosphorylation of CDC25 phosphatases leads to their inactivation and inhibition of CDKs that delays the progression of the cell cycle at the G1-S, intra-S and G2-M cell cycle checkpoints, thereby giving sufficient time for DNA repair before replication or entering mitosis [24]. The major sensor of DNA damage promoting activation of ATR kinase is a replication protein A (RPA) complex [15]. It consists of three subunits RPA1, RPA2 and RPA3 and binds to ssDNA regions protecting them from the nuclease degradation and preventing formation of secondary structures that may interfere with subsequent recombination events [25]. Moreover, RPA-ssDNA complex plays a crucial role in activation and maintenance of ATR-mediated checkpoint by recruiting ATR kinase via its functional partner, ATR-interacting protein (ATRIP), to the sites of DNA damage and to the stalled replication forks [26,27]. Following activation, ATR kinase acts on various substrates including checkpoint kinase 1 (CHK1) that gets phosphorylated on serine 317 and serine 345 [28,29]. Similar to CHK2, CHK1 also limits the activity of CDKs, thereby triggering activation of cell cycle checkpoint [30]. In parallel, the DDR coordinates the action of DNA repair pathways by other post-translational modifications (PTMs) such as acetylation, sumoylation and ubiquitylation [31]. Once DNA repair is completed, the DDR gets inactivated, allowing resumption of the cell cycle. However, if the damage cannot be removed, constitutive DDR signaling triggers cell death by apoptosis or cellular senescence, both of which prevent propagation of mutations and hence have critical antitumor function [14]. Consequently, DDR plays an essential role in maintaining genome integrity.

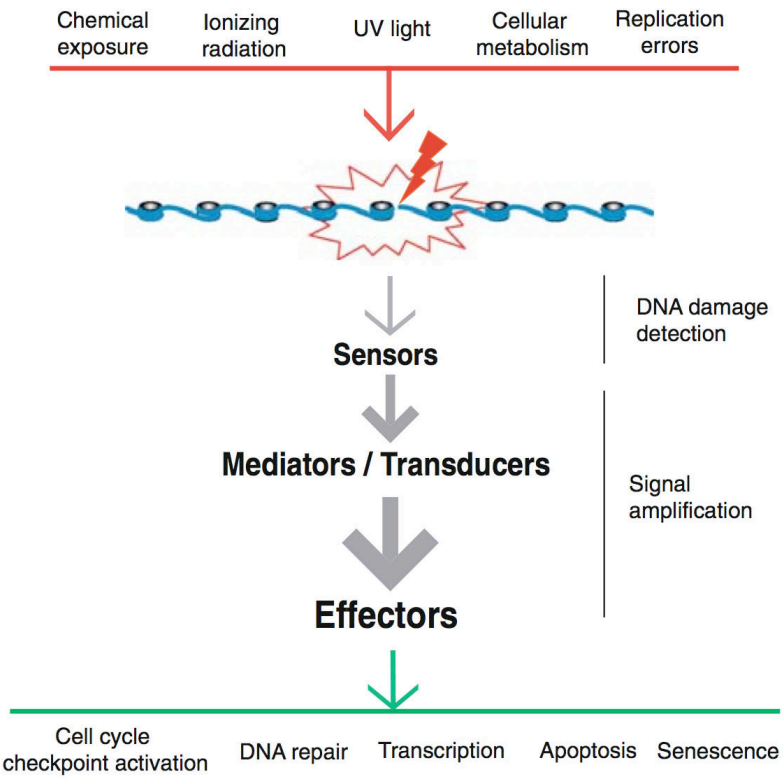

Figure 2. The DNA damage response cascade. DNA damage induced by endogenous or exogenous sources is recognized by sensor proteins (e.g. MRN, RPA). Through the recruitment of mediator proteins the presence of the lesion is signaled and the signal is amplified by transducers (e.g. ATM, ATR). The signal reaches the effector proteins (e.g. CHK1, CHK2) to initiate a cellular response, including cell cycle arrest, activation of DNA repair and transcriptional program, and, in case the damage is too severe, apoptosis or senescence. Adapted from [17].

Genomic instability is a hallmark of cancer [5]. Cancer cells have also other characteristics such as self-sufficiency in growth signals, insensitivity to anti-growth signals, evasion of apoptosis, sustained angiogenesis, tissue invasion and metastasis, unlimited replication potential [32]. Remarkably, genomic instability is present in all stages of cancer, from precancerous lesions to advanced malignancies [33]. There are various forms of genomic instability with chromosomal instability (CIN) being the major one. CIN is referred to different types of chromosomal aberrations such as changes in chromosome structure (e.g. translocations, deletions) and in chromosome number [34]. Another form of genomic instability is microsatellite instability (MSI) characterized by the expansion or reduction of the number of oligonucleotide repeats present in microsatellite sequences [35]. Hereditary cancers such as non-polyposis colon cancer, breast and ovarian cancer, and leukemias are driven by mutations in DNA repair genes

and demonstrate genomic instability [5]. Importantly, inherited defects in DDR genes can cause tumorigenesis in precancerous lesions by enhancing the accumulation of spontaneous mutations [36]. Although sporadic (non-hereditary) cancers also show genomic instability, they rarely contain mutations in DNA repair genes [14]. Instead, they are often triggered by constitutive activation of proto-oncogenes and inactivation of tumor suppressors that elicit a growth- and, associated with it, a replication-rate increase, which eventually leads to the activation of the DDR [37]. Indeed, the DDR is commonly activated in early neoplastic lesions and presumably protects against malignancy [38]. However, constitutive activation of DDR also leads to elevated levels of errors during DNA replication and repair, favoring the transition of a precancerous lesion into cancer [30]. Therefore, coordination and tight regulation of DNA repair processes and DDR play critical role in preventing tumorigenesis.

1.2. MRE11-RAD50-NBS1 (MRN) complex

1.2.1. Structure and functions of the MRN complex

DSBs are one of the most deleterious DNA lesions that can lead to genome rearrangements and carcinogenesis if they are misrepaired. The MRE11-RAD50-NBS1 (MRN) complex plays a crucial role in DSB repair due to its ability to recognize and to maintain the broken ends in close proximity, thereby facilitating repair [39]. It also promotes DNA-end resection of the breaks and activation of DSB response. In addition, to its function in DSB repair, the MRN complex is associated with the replication forks and telomeres promoting their maintenance [40]. This complex is highly conserved and orthologues of MRE11 and RAD50 are found in all taxonomic kingdoms [41]. Yeast strains bearing null mutations of *Rad50*, *Mre11* or *Xrs2*, which is an orthologue of human NBS1 in budding yeast, are viable, but show similar phenotypes such as poor vegetative growth, hypersensitivity to DSB-inducing agents and defects in meiosis [39]. However, all three components of the mammalian MRN complex are essential for survival as knockout mice display early embryonic lethality [42-44]. Hypomorphic mutations in *NBS1* in humans cause Nijmegen breakage syndrome (NBS), a rare autosomal recessive disorder characterized by microcephaly, immunodeficiency and cancer predisposition [45,46]. Hypomorphic mutations in *RAD50* lead to phenotypes similar to NBS that are

classified as an NBS-like disorder (NBSLD), but only one patient has been reported so far [47]. Mutations in *MRE11* gene trigger ataxia-telangiectasia-like disorder (ATLD) [48]. ATLD patients display ataxia and neurodegeneration and resemble the phenotypes of ATM deficiency [49]. Given the importance of the MRN complex in the activation of ATM kinase, cells from patients with hypomorphic mutations in *MRE11*, *RAD50* or *NBS1* genes exhibit defective ATM-mediated signaling, radiosensitivity and chromosomal instability [50].

RAD50 is the largest component of the MRN complex. It has both sequence and structure homology to SMC family members, involved in sister-chromatid cohesion and chromosome condensation, and plays essential role in tethering broken DNA ends [17]. The N- and C-termini contain Walker A and Walker B motifs, respectively, that can associate forming a bipartite ATP-binding cassette (ABC)-type ATPase domain that possesses both ATPase and DNA-binding activity (Figure 3) [51-53]. The central part of RAD50 consists of two large coiled-coil structures with a zinc-hook motif (CXXC) in the middle that can coordinate a zinc ion to form an interaction interface between two RAD50 molecules [54]. Mutations targeting the invariant cysteines of the RAD50 hook domain globally disrupt functions of the MRN complex and phenocopy the null *Rad50* mutation in yeast, fail to support viability in mice and lead to severe defects in ATM activation and repair in human cells [54-57]. RAD50 also contains MRE11-binding sites located at the intersection of coiled-coil and ATPase domains [52,53].

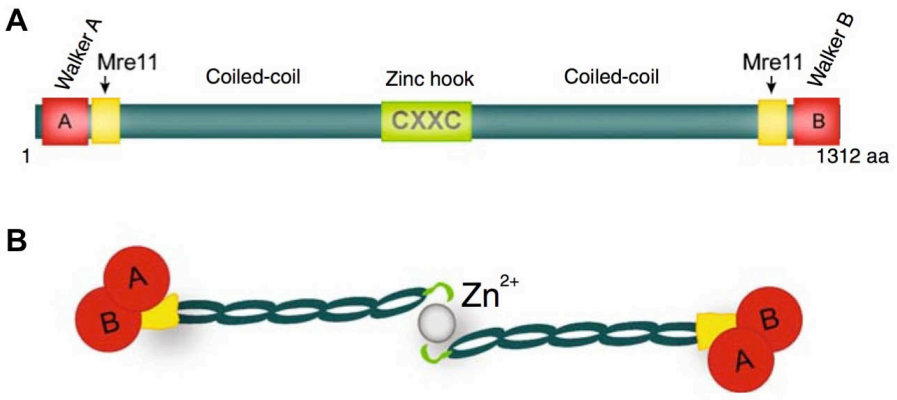

Figure 3. Structure of RAD50. (A) The domain structure of RAD50. RAD50 contains Walker A and B motifs in N- and C-terminus, respectively, that are responsible for ATPase activity of RAD50. The central part of RAD50 consists of two coiled-coil regions that are linked by zinc-hook motif in the middle. MRE11 interacts with RAD50 via two regions localized at the intersection of coiled-coil and ATPase domains. **(B)** Schematic representation of RAD50 dimerization. RAD50 molecule can fold back on itself and form a dimer with another RAD50 molecule via zinc-hook domain in presence of a Zn^{2+} ion. A globular head formed by the Walker motifs and MRE11-interacting regions binds DNA. Adapted from [17].

MRE11 is composed of an N-terminal phosphoesterase domain that harbors the nuclease active site, dimerization motifs and an interaction region with NBS1 [52,58]. The central and C-terminal parts contain DNA-binding sites and RAD50 interaction domain. MRE11 possesses intrinsic DNA-binding activity, endo- and 3'-5' exonuclease activities *in vitro* that are required for the function of the MRN complex in DNA-end resection [59-63]. Atomic force and electron microscopic imaging indicate that each MRE11 molecule binds to a single RAD50 and they form a heterotetrameric core complex consisting of $MRE11_2RAD50_2$ (M2R2) *in vivo* [52-54,64]. The third subunit, NBS1/Xrs2 interacts with the core complex through binding to MRE11 forming a functional MRN dimer [40,65]. Given the importance of these interactions for the MRN complex stability, depletion of individual subunits leads to the destabilization of the whole complex [45,47,48].

NBS1 contains N-terminal forkhead-associated domain (FHA) domain followed by two adjacent breast cancer susceptibility protein 1 C-terminus domain (BRCT) motifs [66,67]. Both of them can recognize and bind to phosphoproteins, therefore NBS1 acts as an adapter linking the MRN complex to proteins phosphorylated in response to DNA damage [41]. Notably, such phospho-specific interaction of NBS1 with MDC1 mediates stable association of the MRN complex with damaged chromatin [66,68,69]. In fission yeast, Nbs1 recognizes phosphorylated Ctp1 and recruits Ctp1 to DSB ends to promote resection [66,70-72]. Similar mechanism to regulate DNA-end resection has been

proposed for NBS1 and human CtIP, an orthologue of Ctp1, however the MRN complex is not required for CtIP recruitment to DSBs in human cells [73-75]. The C-terminus of NBS1 harbors MRE11 and ATM-binding sites. Interaction of NBS1 with MRE11 is critical for the nuclear localization of the MRN complex and may also stimulate its DNA-binding and endonuclease activities [45,76]. NBS1 directly binds to ATM kinase that triggers its full activation and autophosphorylation at serine 1981 (S1981) and several other sites [18,77,78]. Noteworthy, the MRN complex is not absolutely required for it as ATM can still be activated in ATLD and NBS patient cells upon DNA damage, though at a much reduced efficiency [79].

The relationships between the MRN complex conformations and their biological functions for a long time remained enigmatic. Recent structural analysis of the bacterial and archaeal Rad50 and Mre11 proteins revealed that in the absence of ATP Walker A and B domains of Rad50 bound to Mre11 persist in open configuration [80,81]. ATP-binding by Rad50 dramatically alters the conformation of the complex leading to the closed configuration [82,83]. ATP-bound state is associated with a higher affinity of the MRN complex for DNA ends and with DNA tethering as well as with stimulation of Mre11 endonuclease activity to initiate DNA-end resection [81,84]. Following ATP hydrolysis, complex configuration changes back from closed to the open state that facilitates Mre11 exonuclease activity to continue DSB resection [84]. Therefore, Rad50-mediated ATP hydrolysis acts as a molecular switch that regulates Mre11 nuclease activity and DNA-end resection. Moreover, there is a temporal sequence of DNA-end tethering followed by DNA-end resection that is orchestrated by the MRN complex.

1.2.2. Separation-of-function RAD50 (RAD50S) mutations

Given the critical role of the MRN complex in DSB repair, it is also required for the processing of DSBs formed during meiosis [85]. Meiotic DSBs are induced by topoisomerase-like transferase Spo11 that cuts both strands of a DNA molecule and remains covalently attached to 5'-ends [86]. To allow DNA-end processing and subsequent homologous recombination repair, Spo11 needs to be released from DNA ends. The MRN complex is required for the removal of Spo11 [85]. In budding yeast *Saccharomyces cerevisiae* (*S. cerevisiae*) it is also essential for the formation of meiotic DSBs together with Spo11 [87,88]. Thus, mutants lacking any subunit of the MRX

complex fail to generate meiotic DSBs [89]. A specific class of separation-of-function mutations located in the N-terminus of *Rad50*, named *rad50S*, allows Spo11-induced formation of the break, but is totally defective in processing of meiotic DSBs in *S. cerevisiae* [90]. Hence, rad50S mutants accumulate unprocessed DSBs with covalently attached Spo11 in meiosis [86]. Despite a strong defect in meiotic recombination, these mutations show no overt mitotic phenotype and nearly wild-type resistance to DNA-damaging agent methyl methanesulfonate (MMS) [90]. Notably, seven out of nine *Rad50S* mutations are clustered at a surface patch forming a putative protein interaction site, suggesting that the cause of the *rad50S* phenotype can be due to an interaction defect with a meiosis-specific protein rather than impaired ATP-binding or hydrolysis [51].

Removal of Spo11 from DSBs requires both the nuclease activity of the MRX complex and Sae2 [61,91-93]. Akin to rad50S mutations, deletion of *Sae2* also leads to the accumulation of unprocessed DSBs during meiosis [85,94]. Remarkably, *Sae2* overexpression could partially rescue the DNA processing defects of *rad50S,* implying that *rad50S* mutations may impair the interaction between Rad50 and Sae2 [91]. The activity affected in *rad50S* and *sae2*Δ strains seems to be required for the processing of DNA ends blocked by covalently bound protein, such as Spo11 described above or DNA topoisomerase cleavage complexes [95]. DNA topoisomerases are enzymes that release torsional stress in the DNA or resolve DNA catenanes through a DNA breakage and rejoining mechanism during DNA replication and transcription [96]. In order to form a break, the topoisomerases get first covalently bound to the DNA and then reversibly released. DNA topoisomerase poisons such as camptothecin (CPT) or etoposide (ETOP) increase the half-life of the Top I-DNA and Top II-DNA cleavage complexes, respectively [97]. Due to prolonged presence of these complexes ssDNA breaks induced by Top I get converted into toxic DSBs in replicating cells, whereas Top II initially generates DSBs. To support cell viability, these toxic topoisomerase-DNA adducts have to be removed and the remaining DNA breaks need to be repaired. The MRN/X-mediated processing of blocked DNA ends seems to be one of major pathways promoting cellular resistance to CPT and ETOP, but the detailed molecular mechanism is still unclear [41]. Remarkably, reminiscent of the phenotypes observed in budding yeast, *rad50S (K81I)* mutation in fission yeast *Schizosaccharomyces pombe* (*S. pombe*) as well as deletion of *Ctp1*, an orthologue of *Sae2* in fission yeast, result in hypersensitivity to DNA topoisomerase poisons [71,98,99].

Yeast *rad50S* mutations were also modeled in mouse [100]. However, two out of three tested *RAD50S* alleles were embryonic lethal and thus only *Rad50-K22M* allele, corresponding to yeast *rad50-R20M*, was analyzed [101]. Though Rad50S mice were fertile, they had strong spermatogenic and hematopoietic attrition resulted in severe anemia and shortened lifespan [101]. Apoptosis in the hematopoietic and spermatogenic lineages of Rad50S mice was triggered by chronic ATM activation [101-103]. A similar constitutive activation of Tel1, an orthologue of ATM kinase in budding yeast, was also observed in rad50S mutants [104]. Though the mechanisms underlying these phenotypes remain elusive, the increased spontaneous chromosomal instability observed in mutant cell indicates unprocessed DNA damage accumulating in *Rad50S* background [101]. Furthermore, mouse cells expressing a *RAD50S* allele conferred hypersensitivity to both Top I and Top II poisons, but not to other DSB-inducing agents such as ionizing radiation, suggesting that Rad50S mutations specifically affect the processing of DSB ends blocked by topoisomerase cleavage complexes by a yet unknown mechanism [100-103].

1.3. CtIP

1.3.1. Role in DNA repair and tumorigenesis

Human CtIP, the CtBP (carboxi-terminal binding protein) interacting protein, was first described as a binding partner of the transcriptional corepressor CtBP [105]. CtIP contains PLDLS sequence representing a PXDLS motif for CtBP binding that is highly conserved among other CtBP interaction partners (Figure 4) [106,107]. Subsequently, CtIP was shown to associate with two *bona fide* tumor suppressor proteins, BRCA1 and retinoblastoma (pRb), thereby it also acquired another name, retinoblastoma-binding protein 8 or RBBP8 [108-110]. CtIP is essential for embryonic development as $Ctip^{-/-}$ mouse embryos were reported to die at a very early stage during embryogenesis [111]. Remarkably, the heterozygous $Ctip^{+/-}$ mice were viable, but their life span, compare to $Ctip^{+/+}$, was shortened by the development of multiple types of tumors, predominantly, large lymphomas, indicating that CtIP haploinsufficiency promotes tumorigenesis. CtIP frameshift mutations caused by microsatellite instability were found in colorectal and endometrial cancers [112,113]. Moreover, low expression of CtIP correlates with high-

grade breast cancer and is associated with resistance to tamoxifen treatment, further supporting the idea that CtIP might be a tumor suppressor gene itself [114,115].

The CtIP in complex with pRb functions in the regulation of G1/S cell cycle progression [116]. The interaction between CtIP and pRb is mediated by a pRb-binding motif LECEE in the N-terminus of CtIP [110]. CtIP binds pRb releasing it from the E2F-responsive promoters in G1 phase of the cell cycle. The inactivation of pRb-mediated transcriptional repression leads to the expression of E2F-responsive genes such as CtIP itself and cyclin D1 and promotes G1/S transition [116]. Accordingly, G1 arrest observed in mouse embryonic fibroblasts (MEFs) lacking CtIP was circumvented by absence of pRb, indicating the role for CtIP in counteracting pRb-mediated G1 restraint and facilitating G1/S progression [111].

At the molecular level human CtIP is a nuclear protein of 897 amino acids (aa) [105]. The amino acid sequence of CtIP is relatively well conserved among mammals. There are also conserved limited regions in human CtIP and its functional orthologues in budding and fission yeast, Sae2 and Ctp1, respectively, as well as in other species [117]. The C-terminal domain (CTD) of CtIP is the most evolutionary conserved region and is required for its function in DNA-end resection [118-120]. The RPA-bound ssDNA generated during resection serves as the signal for sustained ATR-CHK1 checkpoint signaling [27]. Due to its crucial function in DNA-end resection, CtIP is essential for maintaining both the intra-S- and G2-phase checkpoints in response to DNA damage [121]. Noteworthy, mutations in CtIP leading to a truncated protein that lacks the whole C-terminus cause related disorders, Seckel and Jawad syndromes, characterized by congenital microcephaly, impaired DNA-end resection and ATR-mediated signaling [122].

Little is known about the structure of CtIP. It contains two putative coiled-coil domains located near the N- and C-termini [110]. The N-terminus of CtIP, particularly the residues 20-45, are required for CtIP dimer formation [123,124]. Dimerization of CtIP is essential for proper localization to the DSBs and its function in DNA-end resection [124]. The central region of CtIP contains replication foci targeting sequence (RFTS, 515-537 aa) that includes consensus PCNA-interacting protein (PIP) box mediating both the CtIP-PCNA interaction and the assembly of CtIP into replication foci during S-phase [125]. Though the exact function of the PIP-box remains elusive, it was suggested that PCNA might facilitate CtIP localization to replication foci. Accumulation of CtIP at laser-induced DNA damage sites requires a "damage recruitment (DR) motif" (509-557 aa) [74]. The N-terminus of DR motif contains two critical lysines K513 and K515, which

are conserved from chicken to humans. These residues are essential for direct DNA-binding of CtIP, but do not overlap with the PIP-box, suggesting distinct modes of CtIP recruitment to the DNA lesions.

To promote DNA-end resection CtIP directly interacts with the MRN complex [118,126,127]. Multiple regions of CtIP seem to be involved in binding to the MRN complex: both N-terminus, especially residues 22-45, and conserved C-terminus (790-897 aa) mediate CtIP-MRN complex formation [118,126,127]. In addition, it was recently reported that several CDK-dependent phosphorylation sites in the central region of human CtIP contributes to its binding to NBS1 in response to DNA damage [73].

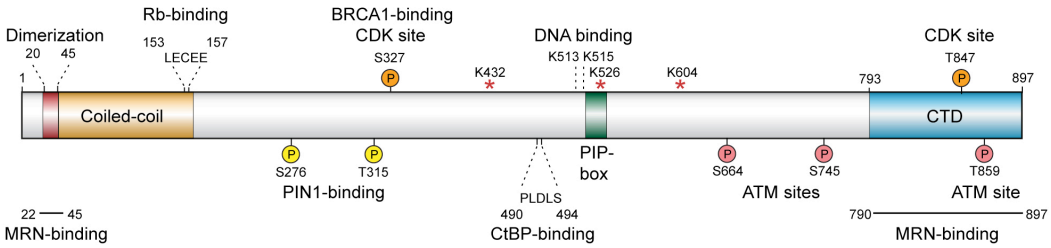

Figure 4. Protein domains of human CtIP. The N-terminus of CtIP contains a dimerization region (20-45 aa), a coiled-coil domain (45-160 aa) and a consensus motif for Rb-binding (LECEE). The middle region consists of a CtBP interaction sequence (PLDLS), two conserved lysines (K513 and K515) important for DNA-binding and a PIP-box (515-537 aa) mediating interaction with PCNA. Two sites (S276 and T315) phosphorylated by proline-directed kinases are required for PIN1-binding and CtIP isomerization. CDK phosphorylation at S327 mediates interaction with BRCA1. Three lysine residues (K432, K526 and K604) are constitutively acetylated and undergo SIRT6-mediated deacetylation in response to DNA damage. The C-terminal domain (CTD, 793-897 aa) is conserved from yeast to humans and contains CDK phosphorylation sites T847 essential for CtIP function in DNA-end resection. Three ATM phosphorylation sites (S664, S745 and T859) are conserved in vertebrates. MRN-binding regions are located in both N- (22-45 aa) and C-terminus (790-897 aa) of CtIP. Adapted from [117].

1.3.2. Regulation of CtIP

To ensure that DNA-end resection takes place only in appropriate stages of the cell cycle the function of CtIP is tightly regulated both at the level of protein expression and posttranslational modifications (PTMs) (Figure 4). Transcript levels of CtIP are relatively constant throughout the cell cycle, however protein levels of CtIP are remarkably lower in G1 compared to other cell cycle phases [128,129]. A possible E3 ubiquitin ligase

promoting polyubiquitination and subsequent proteasomal degradation of CtIP in G1 is SIAH-1 [130].

During S and G2 phases, CtIP is phosphorylated in a CDK-dependent manner on several sites including serine 327 (S327) and threonine 847 (T847) [120,131]. Phosphorylation on S327 mediates CtIP interaction with BRCA1, whereas phosphorylation on T847 is required for DNA-end resection [120,131]. Although the function of BRCA1-CtIP complex in resection remains controversial, it plays an important role in G2/M checkpoint control and in suppression of NHEJ [132,133]. Mutation of T847 causes cellular hypersensitivity to DSB-inducing agents and chromosomal rearrangements, indicating the importance of CDK-dependent phosphorylation for CtIP function in repair and maintaining genome stability [120].

The cellular response to genotoxic stress is mediated via a protein phosphorylation cascade propagated by DNA damage-activated protein kinases such as ATM and ATR kinases [4]. CtIP recruitment to DSBs was shown to be dependent on ATM and partially on ATR kinase activities [74,134]. CtIP is phosphorylated by ATM on at least three residues, serine 664 (S664), serine 745 (S745) and threonine (T859) [73,74]. However, recruitment of CtIP mutant lacking all three phosphorylation sites (CtIP-3A) to DSBs is not affected [74]. Remarkably, CtIP-3A mutant cells are impaired in DNA-end resection, suggesting the role for ATM-mediated phosphorylation of CtIP in promoting repair [73].

An important regulatory mechanism of CtIP stability by a phosphorylation-specific prolyl isomerase PIN1 was recently discovered in our lab [135]. PIN1 binds to CtIP phosphorylated on serine 276 (S276) and threonine 315 (T315) by a proline-directed kinase and CDK2, respectively, and triggers its conformational change that results in ubiquitination and subsequent proteasomal degradation of CtIP. Therefore, PIN1-mediated isomerization of CtIP plays an important role in counteracting DNA-end resection and in the regulation of DSB repair.

Deacetylation of CtIP represents another layer of its regulation. Human CtIP is constitutively acetylated at lysine 432 (K432), lysine 526 (K526) and lysine 604 (K604) that maintains the protein in the inactive state [136]. In response to DNA damage CtIP undergoes deacetylation mediated by SIRT6, a member of the sirtuin family of protein lysine deacetylases. Deacetylation of CtIP facilitates its ability to promote DNA-end resection, thus contributing to DSB processing and genome stability.

In summary, CtIP is a multifunctional protein involved in cell cycle control, checkpoint signaling, transcription and DNA repair. Due to the crucial role of CtIP-dependent DNA-

end resection in homologous recombination, CtIP appears to be one of the major determinants influencing DSB repair pathway choice. Therefore, proper regulation of CtIP is of particular importance for maintaining genome stability.

1.4. DNA-end resection

DNA-end resection is the first step of homologous recombination (HR) and plays crucial role in the DSB repair pathway choice [10]. Once the DSB is formed, both the MRN complex and Ku heterodimer can bind the DNA ends to initiate distinct modes of DSB repair [137]. Remarkably, cells lacking non-homologous end-joining (NHEJ) factors demonstrate enhanced HR frequency, suggesting that there is a competition between Ku-mediated DNA-end protection resulting in NHEJ and DNA-end resection triggering HR [138,139]. The MRX complex can remove Ku from DNA ends to facilitate HR in budding yeast [140]. Furthermore, once the DSB ends are processed, they are no longer suitable substrates for Ku binding and, thus, for the repair by NHEJ [141]. However, the MRN/X complex alone is not sufficient to promote DNA-end resection and requires additional factors. The process of 5'-3' DNA-end resection is conserved in different organisms [141]. In budding yeast MRX complex cooperates with Sae2 endonuclease during DNA-end resection (Figure 5) [142]. Human CtIP and its counterpart Ctp1 in fission yeast physically interact with the MRN complex and promote DNA-end resection, though it is still unknown whether they possess endonuclease activity similar to Sae2 [71,118]. Importantly, human CtIP can stimulate MRE11-RAD50-dependent endonuclease activity *in vitro* [118]. Whereas the MRN complex in conjunction with CtIP initiates and promotes short-range resection, other nucleases, such as EXO1 or DNA2 in complex with BLM helicase, or its orthologue in budding yeast Sgs1, are involved in the extensive, long-range 5'-3' resection [141]. The MRN/X complex and CtIP/Sae2 are required for both EXO1-dependent resection and its recruitment to DSBs [75,143,144]. Furthermore, they also stimulate resection mediated by DNA2-BLM/Sgs1 complex [144,145]. Since only simultaneous depletion of EXO1 and DNA2-BLM/Sgs1 severely impairs ssDNA formation, EXO1 and DNA2-BLM/Sgs1 seem to play redundant roles during DNA-end resection [145-147]. Though many aspects of how DNA-end resection is executed remain enigmatic, recent study on processing of DNA ends which are blocked by a protein complex such as Spo11, suggest that it can be a bidirectional process [62].

As mentioned previously, upon generation of DSB in meiosis, Spo11 stays covalently attached to the 5'-end of DNA [86]. To remove Spo11, Mre11 endonuclease in conjunction with Sae2 creates a nick in DNA strand up to 300 nucleotides from the 5'-terminus of the DSB. The subsequent repair requires Mre11 exonuclease activity in the 3'-5' direction towards the end, meanwhile Exo1 and Dna2-Sgs1 promote DNA resection in the opposing 5'-3' direction that result in formation of long ssDNA regions. Similar mechanism is proposed for DNA-end resection of all DSB ends that are blocked by a protein complex that prevents direct exonuclease-mediated processing of the DSBs [62]. Given the conservation of the DNA-end resection mechanisms, human MRN complex and CtIP also play a critical role in the processing of DNA ends containing protein adducts [41,118]. Accordingly, depletion of CtIP confers cellular hypersensitivity to a wide range of DSB-inducing agents, and particularly to the inhibitors of DNA topoisomerases I and II, such as camptothecin (CPT) and etoposide (ETOP), respectively [118,120].

To ensure that HR takes place in S/G2 when a template for recombination is available, DNA-end resection is tightly regulated during cell cycle [141]. As we briefly discussed above, cyclin-dependent kinases (CDKs) are the master regulators of cell cycle progression [24]. Remarkably, CDK activity that increases in S/G2 is required for DNA-end resection and HR [148,149]. Human CtIP, as well as its yeast counterpart Sae2, are the CDK substrates [117]. Similar to T847 in CtIP, phosphorylation on serine 267 (S267) in Sae2 by CDK is essential for its function in resection and HR, however molecular mechanism of CtIP/Sae2 activation by CDK phosphorylation still remains to be elucidated [119,120]. CtIP phosphorylation on S327 mediates its interaction with E3 ubiquitin ligase BRCA1 as well as the assembly of MRN-CtIP-BRCA1 complex [126,150]. BRCA1-mediated ubiquitination of CtIP does not target it for degradation, but, instead, was reported to be important for CtIP association with chromatin following DNA damage [150]. Furthermore, MRE11 by direct interaction with CDK2 facilitates phosphorylation of CtIP at S327 and CtIP-BRCA1 complex formation [151]. CtIP-BRCA1 complex is required for the activation of the DNA damage-induced G2/M checkpoint, but the role of this complex in DNA-end resection is disputable [131]. CtIP-BRCA1 association was proposed to promote resection and efficient processing of DNA ends that are covalently trapped by DNA topoisomerases in chicken DT40 cells [129,152]. However, mouse cells, in which the formation of CtIP-BRCA1 complex is abrogated, did not display severe defects in HR, implicating that this interaction may not

be required for DNA-end resection in mammalian cells [132]. Instead, CtIP-BRCA1 association may facilitate the suppression of aberrant NHEJ in S/G2 [133]. Other factors involved in DNA-end resection also undergo CDK-mediated phosphorylation, further supporting the significance of this regulation in DSB repair [153].

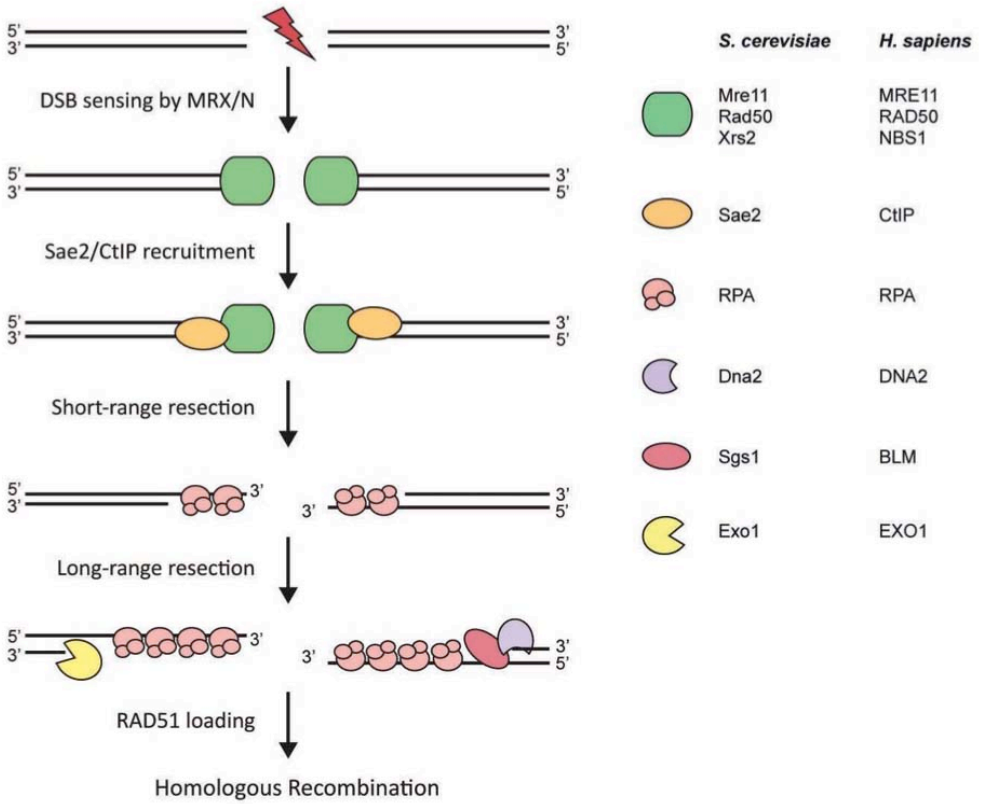

Figure 5. Mechanism of DNA-end resection. Following formation of a DSB, the MRX/N complex rapidly binds to the damaged DNA. In S/G2 phases of the cell cycle, DSB repair via HR is initiated by DNA-end resection. The MRX/N complex in conjunction with Sae2/CtIP promotes short-range resection by trimming DNA ends and generating short 3′-ssDNA overhangs, which are immediately coated by replication protein A (RPA). Subsequent long-range resection is carried out either by the 5′-3′ exonuclease Exo1 or the helicase Sgs1/BLM in complex with the endonuclease Dna2. RPA is then replaced by RAD51 recombinase performing strand invasion of the sister chromatid that is required for downstream steps of HR. Adapted and modified from [153].

1.5. DNA double-strand break (DSB) repair

DSBs are one of the most toxic lesions with respect to survival and maintenance of genomic integrity. Ionizing radiation (IR), radiomimetic drugs (e.g. bleomycin and neocarzinostatin) and chemical agents such as poisons of DNA topoisomerases (e.g. camptothecin, etoposide and their derivatives) are the major exogenous sources of DSBs

[97,154]. Endogenously generated reactive oxygen species, conversion of stalled replication forks or single-strand DNA nicks encountered by replication fork also result in DSB formation [155,156]. In certain contexts, DSBs are generated in a controlled manner. Programmed DSBs occur during meiosis to trigger strand exchange between homologous chromosomes or during class-switch recombination (CSR) and V(D)J recombination in B- and T-lymphocytes to provide antibody diversity [87,157]. Failure to repair DSBs leads to genetic alterations including deletions, translocations, chromosome loss or fusion, which enhance genome instability and may trigger either apoptosis or carcinogenesis [14]. Therefore, the recognition and repair of DSBs is a multifaceted and tightly regulated process involving a multitude of proteins. Two major pathways promote DSB repair: non-homologous end-joining (NHEJ) and homologous recombination (HR) [4]. Whereas NHEJ does not require extensive resection of the break, HR depends on the generation of ssDNA tracts as repair intermediate [158,159]. In addition, DSBs containing complementary sequences flanking broken DNA ends can be repaired via alternative NHEJ (alt-NHEJ), in case of microhomology (5-25 bp), or via single-strand annealing (SSA), in case of longer repeats [158]. Similar to HR, both of the mechanisms require DNA-end resection promoted by the MRN complex and CtIP that gives rise to DNA strands, which subsequently are annealed [129,160,161]. However, given that alt-NHEJ and SSA are intramolecular mechanisms leading to the loss of the intervening sequence, in contrast to HR, they are highly mutagenic [158].

1.5.1. Non-homologous end-joining

Non-homologous end-joining (NHEJ), also called as classical NHEJ (c-NHEJ), is a prominent DSB repair pathway in mammalian cells that is active throughout the cell cycle [162]. NHEJ does not require extensive DNA-end processing and can perform direct ligation of broken DNA ends [163]. However, radiation-induced DSBs often contain chemically modified ends such as 5'-hydroxyl and 3'-phosphate groups that cannot be joined without some limited processing. Since removal of these altered nucleotides or joining of DSBs present in different genomic locations results in mutations or chromosomal aberrations, NHEJ is considered to be error-prone [159].

Ku70 and Ku80 form the Ku heterodimer, which has high affinity for DNA ends [164]. Ku rapidly binds to DSBs, thus allowing NHEJ to make the first attempt in rejoining DSBs [63,165]. Once bound to DNA, Ku recruits the catalytic subunit of the DNA-

dependent protein kinase (DNA-PKcs) to form the active DNA-PK holoenzyme (Figure 6) [166]. The key role of DNA-PK is to stabilize DSB ends in close proximity and to promote DNA-end processing through phosphorylation and recruitment of downstream NHEJ factors [163]. Subsequently, DNA-PKcs autophosphorylation at six SQ/TQ sites within the ABCDE cluster domain destabilizes its interaction with DNA and, therefore, facilitates the access of DNA-end processing factors and subsequent religation steps [167]. In contrast, DNA-PKcs autophosphorylation at five SQ/TQ sites within the PQR cluster domain was reported to inhibit extensive end processing, thus protecting DNA ends from repair via HR. Remarkably, SQ/TQ sites within the ABCDE cluster can be also phosphorylated by ATM to stimulate HR in case of NHEJ failure [168]. Mutations in these clusters as well as chemical inhibition of DNA-PKcs increase cellular sensitivity to DSB-inducing agents, indicating that phosphorylation-induced alterations in DNA-PKcs are critical for DSB repair [169-171]. As mentioned above, DNA termini containing incompatible end groups require additional processing before ligation can take place. One of the main factors involved in DNA-end processing during NHEJ is Artemis, a member of the vertebrate SNM1 endonuclease family [172]. Artemis was first characterized as an enzyme possessing DNA hairpin-opening activity during V(D)J recombination [172,173]. Artemis interacts with and is phosphorylated by DNA-PKcs at its C-terminus that is required for its endonuclease activity [173,174]. Artemis also possesses 5'-3' exonuclease activity and can endonucleolytically process 3'- and 5'-overhangs during NHEJ [173]. Another group of proteins promoting end processing includes aprataxin, aprataxin-PNKP-like factor (APLF) and polynucleotide kinase/phosphatase (PNKP) [159]. The latter exhibits both 5'-kinase and 3'-phosphatase activity and therefore generates ligatable 5'-phosphate and 3'-hydroxyl termini [175]. Short gaps on DNA strands that can arise during the DSB processing steps are filled-in by X family DNA polymerases such as polμ and polλ, though these polymerase are only required for a subset of NHEJ-mediated repair events [176,177].

After DNA-end processing, two juxtaposed ends are joined together by the coordinated action of DNA ligase IV (Lig IV) in complex with XRCC4 and XLF (XRCC4-like factor) [163]. Hypomorphic mutations in genes encoding for NHEJ factors such as Lig IV or Artemis lead to immunodeficiency and radiosensitivity, indicating that despite being potentially error-prone, NHEJ activity in higher eukaryotes is critically important for V(D)J recombination and cell survival [178].

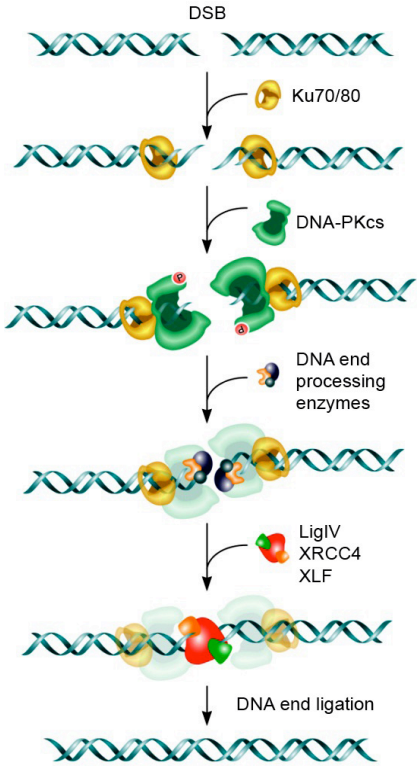

Figure 6. Mechanism of c-NHEJ. Rapid binding of the Ku70/80 heterodimer to both ends of the DSB promotes recruitment of DNA-PKcs. The DNA-PK holoenzyme tethers the DNA ends together and stimulates the subsequent association of DNA-end processing factors such as Artemis and PNKP. Finally, LigIV/XRCC4/XLF complex repairs the break by ligating the DNA ends. Adapted from [178].

1.5.2. Homologous recombination (HR)

HR employs the undamaged sister chromatid as a template for error-free repair and is therefore restricted to S and G2 phases of the cell cycle, being most pronounced in mid-S phase [154,179]. HR is initiated via recognition of the DSBs by the MRN complex that tethers broken DNA ends together and promotes repair by performing short-range DNA-end resection in complex with CtIP (Figure 7) [118,126]. Subsequent extensive DNA-end resection is mediated by BLM together with DNA2 nuclease and EXO1 exonuclease, resulting in formation of ssDNA up to several kilobases in length [75,145,146]. To promote the recombination steps, RPA is displaced from ssDNA by RAD51 recombinase resulting in formation of presynaptic filament. The loading of RAD51 onto ssDNA and stabilization of presynaptic filament requires additional factors called recombination mediators [180]. The key complex promoting RAD51 assembly in mammalian cells consists of a breast cancer 1 (BRCA1) and its partner BRCA1-associated RING domain

protein 1 (BARD1), BRCA2 (also known as FANCD1), and PALB2, a partner and localizer of BRCA2 (also known as FANCN) [181,182]. BRCA2 can directly bind to RAD51 and promote RAD51 loading onto ssDNA meanwhile suppressing RAD51 assembly on dsDNA [183,184]. In absence of functional BRCA1, BRCA2 or PALB2 alternative HR factor RAD52 was shown to support RAD51-dependent recombination in human cells [185]. Another group of recombination mediators includes five RAD51 paralogues that form two distinct complexes: RAD51B-RAD51C-RAD51D-XRCC2 (BCDX2) and RAD51C-XRCC3 (CX3) [186]. Whereas BCDX2 complex facilitates RAD51 assembly and stability of presynaptic filament, CX3 is implicated in HR downstream of RAD51 recruitment, but its exact function is unknown [187]. At this step, HR can still be reversed by antirecombinases such as RECQ5 helicase that dismantle RAD51-ssDNA filaments to prevent illegitimate recombination events [10].

The formed RAD51-ssDNA nucleoprotein filament invades the duplex DNA and searches for homology to produce a displacement loop (D-loop) intermediate. Once the D-loop is formed, the 3'-end of the filament primes DNA synthesis using the homologous partner as a template resulting in the D-loop extension. The D-loop can be dissociated by the antirecombinases like RTEL1 helicase and the extended 3'-invading strand anneals to the processed second end of the break [188]. This pathway is called SDSA and it gives rise to non-crossover (NCO) products with short gene conversion tracts [189]. The D-loop can also capture the second DNA end generating a double Holliday junction (dHJ) that is further processed and leads to the formation of either crossover (CO) or NCO products. dHJs are also able to undergo branch migration along DNA that is promoted by RAD54 and result in increasing or decreasing lengths of heteroduplex DNA [190]. Most dHJs are processed as NCOs by the BLM-TOPIII-RMI1-RMI2 (BTR) complex, the mechanism that is termed as dHJ dissolution [191,192]. BLM helicase promotes convergent branch migration of the dHJ, while TOPIII decatenates the intervening strands. Alternatively, dHJs can be resolved by nucleases. The majority of mitotic COs in mammalian cells is produced by the cooperation of SLX1-SLX4 and MUS81-EME1 endonucleases [193-195]. Structure-specific endonuclease SLX4 (also known as BTBD12 or FANCP) functions as a scaffold protein for SLX1 and MUS81-EME1 and coordinates their activities during dHJ resolution [196-199]. Another pathway to resolve dHJ is mediated by endonuclease GEN1, though it was shown to play a minor role in dHJ processing [193,195,200]. Given that HR is the only pathway generating crossovers

(COs) as repair products and leading to genetic diversity by creating new allele combinations, it is particularly important for the repair of meiotic DSBs [201].

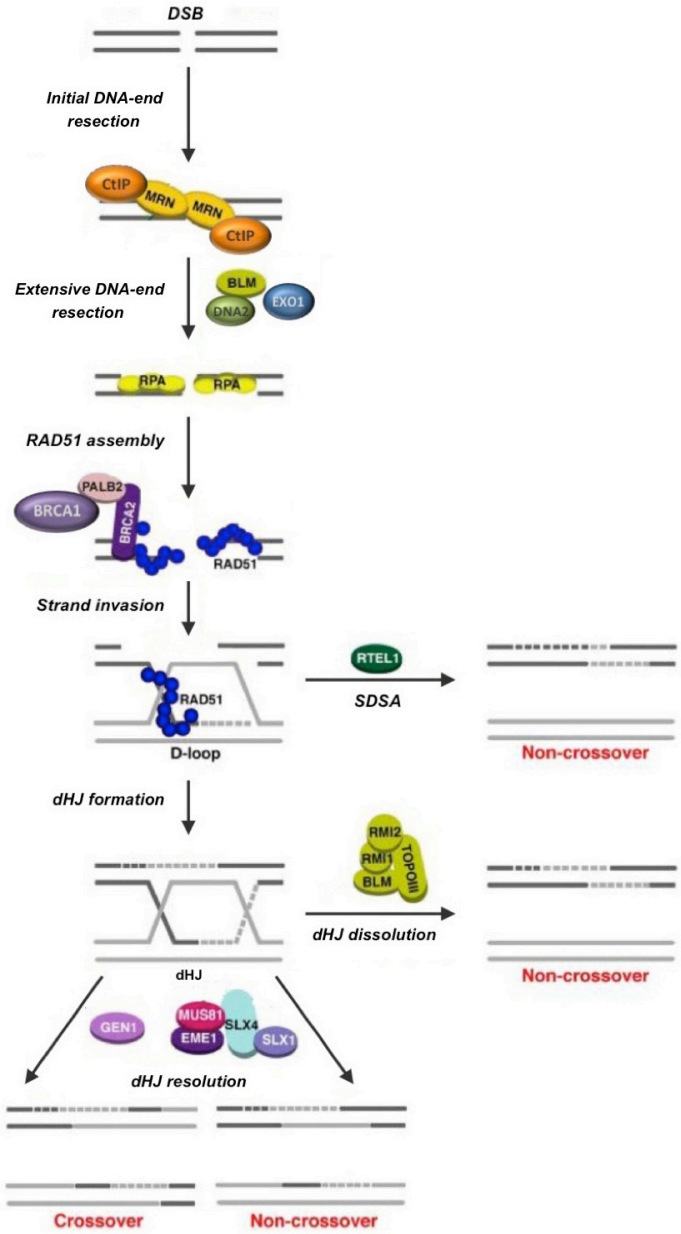

Figure 7. Mechanism of homologous recombination. Following DSB formation, the MRN complex binds to DNA ends and initiates DNA-end in conjunction with CtIP. BLM in complex with DNA2 and EXO1 promote extensive DNA-end processing generating long stretches of ssDNA. RPA protects ssDNA from degradation and is then exchanged by RAD51 with the help of BRCA1-BRCA2-PALB2 proteins. RAD51 nucleoprotein filament promotes search for homology sequence and strand invasion, forming D-loop. D-loop structure formed after strand invasion can be displaced by RTEL1 during SDSA generating non-crossover products. If the second DNA end is captured by the D-loop, it results in the dHJ formation. This intermediate can be processed either by dissolution involving BLM-TopIII complex or by resolution promoted by GEN1 or by SLX4-SLX1 and MUS81-EME1 complex to form non-crossover and crossover products. Adapted and modified from [4].

1.5.3. DSB repair pathway choice

The choice of an appropriate repair pathway is required for maintaining genomic integrity [10]. Although the detailed molecular mechanism of DSB repair pathway choice remains unclear, given that DNA-end resection irreversibly commits cells to HR, the competition between DNA-end protection and resection seems to determine it [137]. The two tumor suppressors 53BP1 and BRCA1 are the critical regulators of DSB repair pathway choice [10]. Recruitment of both proteins to chromatin is mediated by the ubiquitin-dependent signaling activated in response to DNA damage [202]. Though both 53BP1 and BRCA1 are effectors of the RNF8 E3-ligase-dependent ubiquitination pathway, they play antagonistic roles in DSB repair: 53BP1 promotes NHEJ, while BRCA1 channels DSB repair into HR (Figure 8) [10]. BRCA1 deficiency is associated with genome instability and predisposes carriers to breast and ovarian cancer [203-205]. Mice expressing mutant *Brca1*$^{\Delta 11/\Delta 11}$ allele show increased tumorigenesis and chromosomal abnormalities due to impaired HR [206]. Remarkably, these phenotypes can be alleviated by 53BP1 deletion indicating that BRCA1 acts as a suppressor of aberrant 53BP1-mediated NHEJ [206,207]. However, deletion of classical NHEJ factors, for instance DNA Ligase IV, could not rescue HR defect of BRCA1-deficient cells, indicating that the lack of NHEJ *per se* is not responsible for the restoration of DNA-end resection in absence of 53BP1 [206]. In wild-type cells, 53BP1 promotes NHEJ in G1, but is inhibited in S/G2, and this regulation seems to be altered in BRCA1-deficient cells [208]. Insights into how 53BP1 acts to promote NHEJ came from several recent studies characterizing RIF1, a downstream effector of 53BP1 [133,209-212]. RIF1, the mammalian orthologue of the yeast Rap1-interacting factor 1, binds to 53BP1 in ATM-dependent manner inhibiting DNA-end resection and damage-induced BRCA1 foci formation in G1 [133,209,211,212]. On the other hand, BRCA1 strongly diminishes RIF1 localization at DSBs in S/G2 in a CtIP-dependent manner [133]. Accordingly, both depletion of CtIP and abrogation of CDK-mediated phosphorylation of CtIP on S327 or T847 lead to the increased RIF1 foci formation in S/G2 [133]. Given the significance of CDK-dependent phosphorylation in suppressing RIF1 and facilitating resection, CDK-mediated regulation is one the important mechanisms to insure the switch of DSB repair from NHEJ in G1 to HR in S/G2 phases [153,208]. In addition, CtIP protein levels are low in G1, but high during S/G2 phases, therefore triggering HR when sister chromatid is available [128]. Due to the crucial role of CtIP in conjunction with the MRN complex in promoting DNA-end

resection and suppression of RIF1, it is likely that DSB resection does not only produce a substrate for HR, but also inhibits the accumulation of pro-NHEJ factors such as RIF1 at the sites of damage [213]. Therefore, the formation of ssDNA regions as a result of DNA-end resection regulates the DSB repair pathway choice: it prevents NHEJ and represents the commitment step for HR.

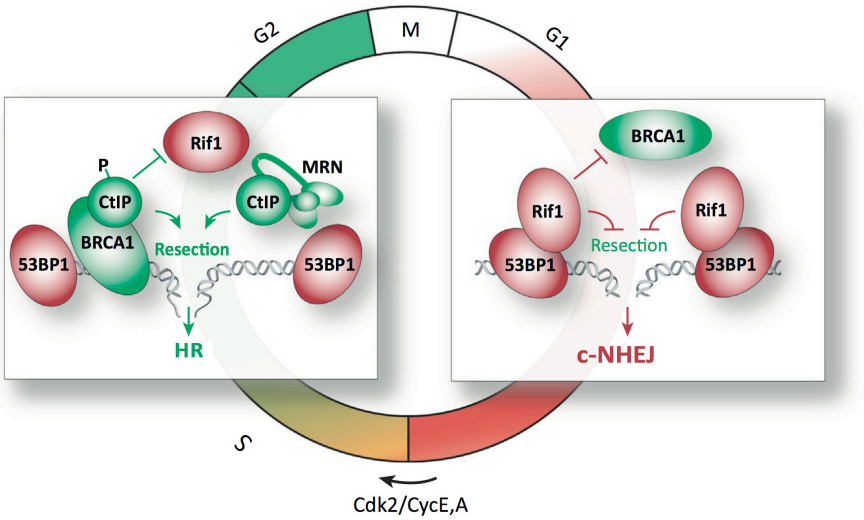

Figure 8. Cell cycle dependent, antagonistic relationships of 53BP1-RIF1 and BRCA1-CtIP in DSB repair. During G1 phase of cell cycle RIF1, a downstream effector of 53BP1, prevents the accumulation of BRCA1 at DSBs, thus promoting c-NHEJ and inhibiting DNA-end resection and HR. As cells enter S-phase, CtIP is phosphorylated in a CDK-dependent manner. Phosphorylated CtIP together with BRCA1 antagonizes the accumulation of RIF1 at sites of DNA damage and in conjunction with the MRN complex initiates DNA-end resection, which commits cells to HR. Adapted from [208].

In contrast to 53BP1, RIF1 deficiency does not fully restore HR in BRCA1-deficient cells, implying the existence of additional 53BP1 effector proteins inhibiting HR [212]. Such 53BP1 effector, a PAX transactivation domain-interacting protein or PTIP, has been recently identified [214]. It interacts with phosphorylated 53BP1 via its BRCT domain and, similar to RIF1, is recruited to DSBs in a 53BP1- and ATM-dependent manner [214,215]. Both PTIP and RIF1 block DNA-end resection and promote NHEJ repair, however, unlike RIF1, ablation of PTIP efficiently rescues the HR defect in BRCA1-deficient cells, indicating a more prominent role for PTIP in NHEJ [214]. On the other hand, whereas RIF1 is essential for 53BP1-initiated NHEJ during class switch recombination (CSR) in B cells, PTIP is dispensable for CSR, demonstrating two distinct functions of PTIP and RIF1 [216]. However, the mechanism of DNA-end resection inhibition by 53BP1 and its effectors still remains elusive. It is known that 53BP1 binds

methylated and ubiquitinated nucleosomes minimally as a dimer and thus may act in a wheel clamp-like manner or as a factor bridging adjacent nucleosomes, making chromatin refractory to the resection machinery in G1 [217]. Furthermore, PTIP and RIF may block the chromatin accessibility for BRCA1 or nucleases that mediate resection [213]. Alternatively, 53BP1 is evicted from the core of IR-induced foci in S phase in a BRCA1-dependent manner [218]. Though the mechanism of 53BP1 inhibition by BRCA1 is not clear, it is plausible that BRCA1 modulates ubiquitination events at chromatin flanking DSBs, thereby protecting DNA ends from NHEJ factors and granting access for the end resection machinery [10]. While E3-ubiquitin ligase activity of BRCA1 seems to be dispensable for promoting HR and NHEJ suppression, BRCA1 may antagonize the ubiquitin-dependent recruitment of 53BP1 and its effectors to damaged chromatin via the interaction with deubiquitinating enzymes such as BRCC36 [133,219,220]. Multiple other factors including ubiquitin and SUMO E3 ligases are involved in the regulation of repair [202].

DSB repair occurs in the context of chromatin, therefore the complexity of chromatin structure influence pathway choice. DSBs in the heterochromatin regions that represent tightly packed DNA require remodeling prior to repair and mainly undergo slow repair by HR, whereas DSBs in more open euchromatic regions are repaired by NHEJ [221]. Repair of breaks in heterochromatin requires ATM-mediated phosphorylation of transcriptional corepressor Krüppel-associated box (KRAB)-associated protein KAP1 [222,223]. KAP-1 forms densely packed chromatin by recruiting CHD3, HP1 and other remodeling factors [224,225]. Phosphorylation of KAP1 on serine 824 (S824) leads to the dissociation of KAP1 and CHD3, resulting in chromatin relaxation that facilitates repair [222,225,226]. Recruitment of another ATP-dependent chromatin remodeler SMARCAD1 to DSBs weakens histone-DNA interactions in nucleosomes flanking breaks and stimulates end resection and HR [227,228]. In summary, the balance between HDR and NHEJ is tightly controlled at different levels to ensure maintenance of genome stability since deregulation of DSB repair mechanisms may lead to apoptosis or tumorigenesis.

1.6. DNA interstrand crosslink (ICL) repair

1.6.1. DNA interstrand crosslinks

DNA interstrand crosslinks (ICLs) are highly toxic DNA lesions generated by chemical compounds that covalently link two bases on the complementary DNA strands [229]. The mechanism of action of ICL-inducing drugs is broadly similar. The formation of a DNA interstrand crosslink requires an initial reaction to produce a monoadduct and subsequent slow conversion of monoadduct into crosslink [230]. Furthermore, ICL-inducing agents cause a wide variety of DNA lesions in addition to ICLs, such as monoadducts, DNA-protein crosslinks and intrastrand crosslinks when adjacent DNA bases on the same DNA strand are covalently linked. However, ICLs are the most toxic lesions because they prevent DNA strand separation and thus block essential cellular processes such as DNA replication and transcription [231]. Given the detrimental effect of ICLs on rapidly dividing cells, ICL-inducing agents are widely used in chemotherapy. Mitomycin C (MMC) and psoralen combined with ultraviolet-A irradiation (PUVA) as well as nitrogen mustards and platinum compounds, such as cisplatin, are applied for treatment of different types of cancer including lymphomas, ovarian, breast and colorectal cancer [229,231]. Endogenous compounds arising from normal cellular metabolism such as malondialdehydes or acetaldehydes produced during lipid peroxidation and ethanol oxidation, respectively, can also induce ICLs [232,233]. A well-orchestrated multicomponent machinery, consisting of Fanconi Anemia (FA) proteins, aided by factors of nucleotide excision repair (NER), translesion DNA synthesis (TLS) and HR removes ICLs during DNA replication (Figure 9) [234]. ICLs in actively transcribed genes can be encountered by the transcription machinery and repaired via transcription-coupled ICL repair involving NER proteins and TLS polymerases independently of FA pathway [231]. However, ICL repair is mainly active during S-phase, implying that ICLs predominantly affect DNA replication [235,236].

1.6.2. *Fanconi anemia* pathway

Fanconi anemia (FA) is a rare hereditary disorder characterized by progressive bone marrow failure, congenital abnormalities and susceptibility to both solid tumors and acute myeloid leukemia (AML) [237]. FA is genetically heterogeneous disorder. So far, sixteen

FA genes that constitute the FA repair pathway have been identified as mutated in patients (Table 1) [231]. The predisposition of FA patients to cancer is attributed to the essential role of FA pathway in DNA repair, particularly in the repair of ICLs. Cells isolated from FA patients display chromosomal instability and hypersensitivity to ICL-inducing agents such as MMC and cisplatin that is used as a diagnostic test for FA [238]. The FA pathway orchestrates replication-coupled ICL repair involving nucleolytic incision of the crosslink, TLS and HR and therefore maintains genomic stability [12]. The replication fork stalling at ICLs serve as a signal to initiate the repair and currently different models with one or two replication forks converging on ICL are discussed [239]. Complex consisting of FANCM DNA translocase in conjunction with FA-associated protein 24 kDa (FAAP24) and two histone-fold-containing FANCM-associated proteins, MHF1 and MHF2, recognizes the stalled replication fork structure, initiates ATR-mediated checkpoint signaling and promotes recruitment of the FA core complex to chromatin (Figure 9) [240-243]. Upon ATR activation multiple FA proteins undergo phosphorylation representing a close connection of the FA pathway with DDR signaling [244]. FA core complex consists of FANCA, FANCB, FANCC, FANCE, FANCF, FANCG, FANCL, FAAP20 and FANCM in subcomplex with FAAP24 and MHF1-2 [231]. Members of the core complex stabilize the complex via protein-protein interactions and are essential for proper downstream signaling, particularly for monoubiquitination of FANCD2 and FANCI (FANCD2-I) heterodimer [245]. A FANCL subunit is an E3 ubiquitin ligase that in concert with the UBE2T E2 enzyme conjugates a single ubiquitin to lysine 561 (K561) and lysine 523 (K523) of human FANCD2 and FANCI, respectively [246-248]. Monoubiquitination of FANCD2-I by the FA core complex is a critical regulatory step in ICL repair required for both stable association of FANCD2-I complex on damaged chromatin and coordination of crosslink repair activities together with downstream FA proteins (FANCD1, J, N, O, P, Q) [12]. Efficient monoubiquitination of FANCD2-I is independent of subsequent events such as nucleolytic processing of ICLs, but requires phosphorylation of FA core complex and FANCD2-I (ID) by ATR kinase [247,249,250]. FANCD2 is also monoubiquitinated during S-phase progression that might be important for the its function in protecting stalled replication forks from degradation [251,252].

Remarkably, monoubiquitinated FANCD2 is considered to be a platform for recruiting proteins that contain ubiquitin-binding domain (UBD). One of such proteins is FA-

associated nuclease 1 (FAN1) harboring an ubiquitin-binding zinc finger 4 (UBZ4) motif in the N-terminus required for specific recognition of ubiquitin moiety of FANCD2 [253-256]. FA complementation group P (FANCP or SLX4) protein also contains a UBZ motif that is implicated in the binding to monoubiquitinated FANCD2 and is essential for its localization at sites of ICL-induced damage at least in chicken DT40 cells [257]. Therefore modified FANCD2 can specifically recruit UBD-containing proteins to damaged chromatin. Deubiquitination of FANCD2 is mediated by deubiquitinating (DUB) enzyme USP1 (ubiquitin-specific peptidase 1) in complex with its activating partner UAF1 (USP1-associated factor 1) [258,259]. Given the importance of FANCD2 deubiquitination for the completion of repair, genetic disruption of murine *Usp1* gene results in a phenotype similar to FA and *Usp1*$^{-/-}$ cells are hypersensitivity to ICL-inducing agents [260].

Intriguingly, recent study using single-molecule technique for visualizing encounters of replication forks with ICLs in living cells revealed a frequent pattern consistent with replication traverse of the ICL without repair of the lesion [261]. It implies that DNA synthesis can resume past an ICL leaving behind still crosslinked parental strands. Replication traverse is promoted by the translocase and DNA-binding activities of FANCM-MHF1-2 independently of FA core complex, whereas FA proteins could participate in postreplication repair of the lesion. Though details of the regulation of this mechanism remain to be elucidated, it is a first indication that ICLs are not always absolute blocks to DNA replication.

Table 1. *Fanconi anemia* genes and their role in ICL repair. Adapted and modified from [231].

Gene name	Function in ICL repair
FANCA	Core complex member
FANCB	Core complex member
FANCC	Core complex member
FANCD1/BRCA2	Loading of RAD51 onto ssDNA
FANCD2	DNA binding, promotes DNA damage signaling and recruitment of other repair proteins
FANCE	Core complex member
FANCF	Core complex member
FANCG	Core complex member
FANCI	DNA binding, promotes DNA damage signaling and recruitment of other repair proteins
FANCJ/BRIP1/BACH1	3'-5' DNA helicase, preferred substrate is branched DNA
FANCL	Core complex member, E3 ubiquitin ligase responsible for FANCD2 and FANCI monoubiquitination
FANCM	DNA translocase, binds branched DNA structures and recruits the core complex to the ICLs, involved in activation of checkpoint
FANCN/PALB2	Assists in BRCA2 localization to DNA and RAD51 loading
FANCO/RAD51C	Involved in HR during ICL repair
FANCP/SLX4/BTBD12	Scaffold protein for endonucleases
FANCQ/XPF/ERCC4	Structure-specific endonuclease with a preference for 3'-flaps

1.6.3. Structure-specific nucleases

Following activation of the FA pathway, the crosslink has to be unhooked to allow subsequent repair to proceed. Excision of ICL requires two endonucleolytic incisions in one strand of the duplex on both 5'- and 3'-side of the lesion [12]. Though unhooking of a

crosslink is not sufficient for it complete removal, it permits DNA synthesis past the lesion. The FA pathway has been implicated in the recruitment and regulation of several nucleases such as MUS81-EME1, XPF-ERCC1, SLX4-SLX1, FAN1 and SNM1A [231]. However, given the variety of nucleases involved in ICL repair, the extent of the redundancy and their precise role in processing of the lesion still remain to be elucidated.

MUS81-EME1 is DNA structure-specific endonuclease preferentially cleaving 3′-flap structures, aberrant replication fork structures and nicked HJ [262-264]. The formation of DSBs in response to ICL-inducing agents was shown to be dependent on MUS81-EME1, suggesting a critical role for this complex in promoting incision of crosslink on one side of the lesion [265,266]. To complete the unhooking of ICL, a second incision on the other side of the lesion is required. It is not clear, which endonuclease promotes this step. One of the candidates is XPF-ERCC1 endonuclease that functions both in NER and ICL repair [267]. In contrast to other factor involved in NER of bulky DNA adducts, only depletion of XPF-ERCC1 confers cellular hypersensitivity to ICL-inducing agents [249]. Moreover, mutations in XPF-ERCC1 impairing its interaction with NER proteins do not affect ICL repair, suggesting that specific protein-protein interactions regulate distinct roles of this complex in NER and ICL repair [268]. Remarkably, mutations in XPF that caused abnormal nuclease activity of the protein strongly disrupted the function of XPF in ICL, but not in NER repair, and resulted in FA phenotype, defining XPF as a novel FA complementation group, FANCQ [269].

Another recently identified FA protein is SLX4 or FANCP that plays role of a scaffold and regulator of the three structure-specific nucleases XPF-ERCC1, MUS81-EME1 and SLX1 that is considered to be a key function of SLX4 in ICL repair [197-199,270]. Disruption of *Slx4* in mice recapitulates many key features of FA [271]. SLX4 contains a UBZ domain that is required for its recruitment to ICLs via recognition of monoubiquitinated FANCD2 or other ubiquitinated substrates and ICL resistance [257]. Mutation analysis of SLX4 revealed that its interaction with XPF-ERCC1 is absolutely essential for resistance to ICL-inducing agents, whereas complex formation with MUS81-EME1 or SLX1 is less important [194,249,272].

Though XPF-ERCC1 has an ability to perform both 5' and 3' incisions at the site of ICL, it was reported to preferentially cleave 3′-flap structures, implying additional nucleases to be involved in ICL incision [262,273,274]. FAN1 is a 5'-3' exonuclease and endonuclease with a preference for 5'-flaps [253-256]. It is recruited to ICLs through direct binding to monoubiquitinated FANCD2 via its UBZ4 domain and might play a role in the initial

incision of ICL, though it is currently unknown at which stage FAN1 acts. Furthermore, cells depleted of FAN1 show hypersensitivity to ICL-inducing agents and increased chromosomal instability, strongly suggesting a role in ICL repair [253,255]. However, patients with FAN1 deficiency do not display any characteristic symptoms of FA [275]. The 5'-3' exonuclease SNM1A is also required for ICL resistance and is implicated in the processing of the crosslink after the initial incision [276]. *In vitro*, it can digest a DNA substrate containing a crosslink starting from a single nick, and therefore generating a favorable intermediate for TLS [276].

1.6.4. Translesion DNA synthesis

After ICL unhooking, the lesion has to be bypassed by a TLS polymerase in order to extend the leading strand that serves as a template for HR, whereas the unhooked ICL is eventually removed by nucleotide excision repair [12]. TLS is a mechanism for DNA damage tolerance or post-replication repair [277]. It allows replication over DNA lesion without initiating the repair of the lesion though predominantly in an error-prone manner. TLS requires replacement of the replicative polymerases by specialized translesion polymerases that have usually low fidelity and processivity and are characterized by a larger active site, which allows them to insert a base opposite the lesion [11]. The switch from replicative to translesion polymerases is mediated by the ubiquitination of proliferating cell nuclear antigen, PCNA [278]. PCNA is a polymerase processivity factor that functions as a moving platform along the strand to ensure DNA synthesis. Upon stalling of replication fork, PCNA gets monoubiquitinated on lysine 164 (K164) by the E2-E3 ubiquitin ligase complex RAD6-RAD18 [279,280]. Many TLS polymerases in addition to PIP-box also contain a UBD, such as the ubiquitin-binding motif (UBM) of REV1 or the UBZ3 motif of Pol η to specifically recognize monoubiquitinated form of PCNA [281,282].

REV1 and Pol ζ, a heterodimer of REV3 and REV7, play critical role in TLS synthesis during ICL repair as cells lacking either one of these genes are hypersensitive to ICL-inducing agents [283,284]. REV1 functions as a scaffold for recruiting and coordinating other TLS polymerases such as Pol ζ [285]. REV1 binds to REV7 via its C-terminus and mediates loading of Pol ζ to the lesion [286]. Given the critical role of this interaction, its disruption renders cells hypersensitive to cisplatin [287]. Furthermore, REV1 was

reported to stimulate Pol ζ extension *in vitro*, implicating a role for REV1 in regulating enzymatic activity of the recruited TLS polymerases [288].

FA core complex coordinates REV1-dependent TLS pathway both by promoting FANCD2 monoubiquitination and ICL incision and directly by interacting with REV1 via FAAP20 [12]. FAAP20 is an integral subunit of FA core complex that binds to FANCA and also interacts with REV1 stabilizing its nuclear foci [289,290]. Remarkably, FAAP20-REV1 complex formation is enhanced in response to ICL damage through the interaction of FAAP20 UBZ4 domain with monoubiquitinated form of REV1 [290]. Therefore, FA core complex promotes stable association of the REV1 in conjunction with PCNA to replicate over a DNA lesion. Other TLS polymerases such as Pol η and Pol κ are also likely to play role in the repair of a subset of ICL lesions, but their significance for ICL repair still remains to be determined [231].

1.6.5. Role of HR factors in ICL repair

The incision of the crosslink converts the stalled replication fork into a DSB intermediate that is primarily resolved by HR using the homologous strand restored by TLS as a template for repair [12]. The key steps of HR involve loading of RAD51 onto newly resected DNA and subsequent RAD51-mediated strand invasion of the restored sister chromatid. Downstream FA proteins such as FANCD1/BRCA2 and FANCN/PALB2 in complex with BRCA1 promote loading of RAD51 on RPA-coated single-stranded DNA [181,291,292]. FANCO/RAD51C and additional RAD51 paralogues also facilitate the RAD51 loading [293,294]. 5'-3' helicase FANCJ/BRIP1 (BRCA1-interacting protein C-terminal helicase 1) acts downstream from RAD51 to complete HR by preventing promiscuous recombination [295,296]. Inhibition of RAD51 in *Xenopus* egg extracts blocks replication-coupled ICL repair, indicating a functional link between the FA and HR pathways [297]. Though recombination takes place after nucleolytic incision of ICL, RAD51 was shown to bind ICL-stalled replication forks even before FANCD2-I monoubiquitination [297]. The loading of RAD51 on ssDNA at stalled forks may function to prevent fork breakage or degradation in favor of proper incisions regulated by the FA pathway [298,299].

Mutations in downstream FA genes frequently cause breast and ovarian cancer, underlining the connection between FA and breast cancer, so called FA-BRCA pathway associated with impaired HR [12]. Whereas FA pathway-deficient cells are compromised

in HR, the level of HR impairment detected by classical GFP reporter assays is relatively mild when compared with the severe defects observed in BRCA1- or BRCA2-mutant cells [247,300]. However, ICL-induced HR, measured using a modified GFP reporter that is able to replicate, was substantially compromised in FANCA-deficient cells, indicating that the FA pathway is specifically involved in replication-coupled HR repair, though its direct contribution to HR still remains to be elucidated [299]. Remarkably, inactivation of NHEJ pathway by depleting NHEJ factors such as Ku70, DNA-PKcs and Lig IV or by applying specific DNA-PKcs inhibitor in FA-deficient background partially rescues the hypersensitivity of FA cells to ICL-inducing agents [301,302]. Therefore, FA pathway not only promotes error-free HR, but also seems to play a critical role in inhibiting aberrant repair of DSB intermediates by NHEJ, thereby suppressing chromosomal rearrangements during ICL repair [237]. However, recent mouse knockout studies demonstrated that deletion of either Ku or 53BP1 aggravates genomic instability in cells lacking FANCD2, suggesting that FANCD2 provides a key activity in ICL repair that cannot be bypassed only by ablation of NHEJ [303]. One of the critical determinants of the DSB repair pathway choice is DNA-end resection that channels repair into HR and inhibits NHEJ [10]. Cells lacking DNA-end resection factors such as the MRN complex, CtIP, BLM or DNA2 and EXO1 are hypersensitive to ICL-inducing agents, implicating their role in ICL repair, however the connection between the FA pathway and resection machinery is poorly investigated [304-308]. Furthermore, FANCD2 was shown to interact with NBS1, DNA2 and BLM, indicating a putative regulation of DNA-end resection by FANCD2 [304-307].

Collectively, extensive studies of the replication-coupled ICL repair have revealed a complex interplay of nucleolytic incision, TLS and HR repair mechanisms regulated by the FA pathway. FANCD2 monoubiquitination is a prerequisite for ICL repair, connecting signaling with enzymatic repair steps. Deciphering further details about the molecular mechanism of ICL repair will provide better understanding of FA as a disease and a rationale for ICL-based chemotherapy in cancer treatment.

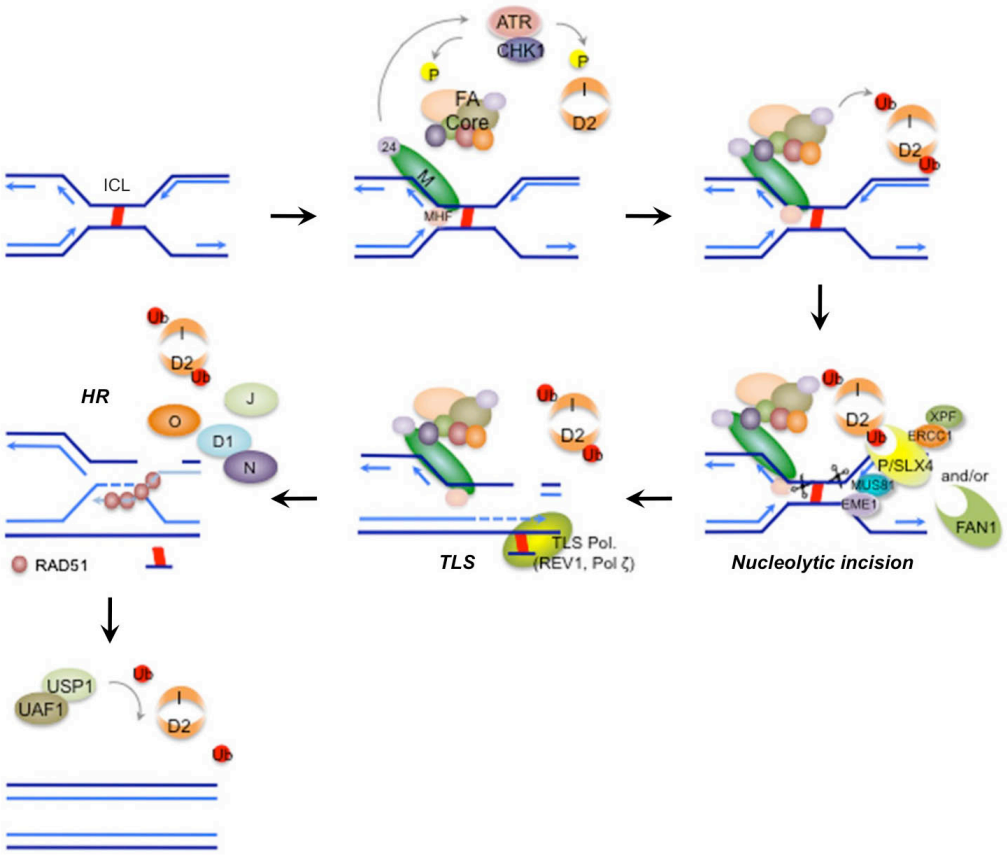

Figure 9. Model of replication-coupled ICL repair. Upon stalling of the replication fork, the FA core complex is phosphorylated by ATR kinase and is recruited to the lesion by FANCM, FAAP24 and MHF1-2. This complex possesses ubiquitin E3 ligase activity and monoubiquitinates FANCD2-FANCI heterodimer to promote its stable association with damaged chromatin. Monoubiquitinated FANCD2 serves as a scaffold to recruit multiple nucleases such as SLX4/FANCP in complex with MUS81-EME1 and XPF-ERCC1, and FAN1 that perform the incision of the crosslink. Translesion polymerases REV1 and Pol ζ fill in the gap opposite the unhooked oligonucleotide, which is then released by nucleotide excision repair. Incision creates DSB intermediates that are repaired via HR machinery, including FANCD1/BRCA2, FANCN/PALB2, FANCJ/BRIP1 and FANCO/RAD51C factors. To complete the repair, the USP1-UAF1 DUB complex deubiquitinates FANCD2-I heterodimer. Adapted and modified from [12].

2. AIMS

DSBs are the most deleterious lesions with respect to survival and preservation of genomic integrity. If left unrepaired, they lead to cell death and, if misrepaired, they trigger genomic instability, a hallmark of almost all human cancers. On the other hand, DSBs are induced by chemo- or radiotherapy as a means to treat cancer. Therefore, a detailed understanding of the molecular mechanisms promoting DSB repair is of particular importance. The major goal of my thesis is to further expand our knowledge on the role of CtIP in DNA-end resection, which initiates error-free repair of DSBs by homologous recombination (HR).

2.1. Addressing the interplay between CtIP-dependent DNA-end resection and the *Fanconi anemia* pathway during DNA interstrand crosslink repair

Distinct DNA repair activities are required for the resolution of DNA interstrand crosslinks (ICLs), including the recognition of the lesion by proteins of the *Fanconi anemia* (FA) pathway, nucleolytic incision of the crosslink, and HR. Remarkably, DSBs formed as intermediates during ICL processing are preferentially repaired via HR, whereas DSB repair by the more mutagenic non-homologous end-joining (NHEJ) pathway is suppressed. FANCD2 monoubiquitination and CtIP-mediated DNA-end resection represent key events in FA and HR pathway activation, respectively, but very little is known about their functional relationship. Therefore, the first aim of my thesis was to investigate the physical and functional interplay between CtIP and the FA pathway during ICL repair. We first analyzed the phenotypes of cells lacking CtIP and FANCD2 in response to ICL damage and revealed that both factors are required for DNA-end resection and faithful ICL repair. Furthermore, we examined the interdependence of CtIP and FANCD2 regarding their localization to damaged chromatin and discovered that CtIP is recruited to ICLs in a FANCD2-dependent manner. We also addressed the physical interaction between CtIP and FANCD2 and identified a minimal FANCD2-binding region on CtIP, highlighting the functional significance of CtIP-FANCD2 interaction for ICL repair. Moreover, we elucidated the contribution of CtIP-mediated DNA-end resection to the maintenance of genome stability in FANCD2-deficient cells. The obtained data were compiled into manuscript that has recently been accepted for

publication in the peer-reviewed Cell Reports journal. The scientific manuscript is included in section 3.1.

2.2. Functional characterization of human RAD50S mutants in the DNA damage response

The MRE11-RAD50-NBS1 (MRN) complex plays an essential role in the sensing and signaling of DSBs, as well as in HR, by promoting the resection of DSBs in collaboration with CtIP. However, the molecular mechanism by which MRN and CtIP cooperate in DNA-end resection still remains largely elusive. Thus, the second part of my thesis focused on the analysis of human RAD50 separation-of-function mutants (RAD50S), which were originally described in budding yeast to impair meiosis but to have no overt mitotic phenotype. Subsequently, RAD50S mutants were characterized in fission yeast and mice. To study the function of RAD50S mutants in human cells, we complemented a patient-derived RAD50 hypomorphic cell line, F239, with wild-type *RAD50 o*r different *RAD50S* alleles and analyzed their phenotypes both in absence and presence of genotoxic stress. Hypothesizing that some of the RAD50S phenotypes might be attributed to alterations in MRN-CtIP complex formation, we also examined the impact of human RAD50S mutations on the interaction between MRN and CtIP. Results from these studies are presented in section 3.2.

3. RESULTS

3.1. FANCD2 and CtIP cooperate to repair DNA interstrand crosslinks

Olga Murina, Christine von Aesch, Ufuk Karakus, Lorenza P. Ferretti, Hella A. Bolck, Kay Hänggi and Alessandro A. Sartori

article published in Cell Reports, 2014

I designed the research together with A.A.S. and performed most of the experiments with the help of C.A. and U.K. The laser microirradiation experiments were performed by L.P.F. H.A.B. helped with the ubiquitin-binding assay. K.H. generated the inducible $MRC5^{shCtIP}$ cell line. I also analyzed the data and wrote the manuscript together with A.A.S.

Please cite this article in press as: Murina et al., FANCD2 and CtIP Cooperate to Repair DNA Interstrand Crosslinks, Cell Reports (2014), http://dx.doi.org/10.1016/j.celrep.2014.03.069

Cell Reports
Report

OPEN ACCESS
CellPress

FANCD2 and CtIP Cooperate to Repair DNA Interstrand Crosslinks

Olga Murina,[1] Christine von Aesch,[1] Ufuk Karakus,[1] Lorenza P. Ferretti,[1] Hella A. Bolck,[1] Kay Hänggi,[1,2] and Alessandro A. Sartori[1,*]
[1]Institute of Molecular Cancer Research, University of Zurich, Winterthurerstrasse 190, 8057 Zürich, Switzerland
[2]Institute of Experimental Immunology, University of Zurich, Winterthurerstrasse 190, 8057 Zürich, Switzerland
*Correspondence: sartori@imcr.uzh.ch
http://dx.doi.org/10.1016/j.celrep.2014.03.069

SUMMARY

The resolution of DNA interstrand crosslinks (ICLs) requires a complex interplay between several processes of DNA metabolism, including the Fanconi anemia (FA) pathway and homologous recombination (HR). FANCD2 monoubiquitination and CtIP-dependent DNA-end resection represent key events in FA and HR activation, respectively, but very little is known about their functional relationship. Here, we show that CtIP physically interacts with both FANCD2 and ubiquitin and that monoubiquitinated FANCD2 tethers CtIP to damaged chromatin, which helps channel DNA double-strand breaks generated during ICL processing into the HR pathway. Consequently, CtIP mutants defective in FANCD2 binding fail to associate with damaged chromatin, which leads to increased levels of nonhomologous end-joining activity and ICL hypersensitivity. Interestingly, we also observe that CtIP depletion aggravates the genomic instability in FANCD2-deficient cells. Thus, our data indicate that FANCD2 primes CtIP-dependent resection during HR after ICL induction but that CtIP helps prevent illegitimate recombination in FA cells.

INTRODUCTION

Fanconi anemia (FA) is a rare hereditary disorder characterized by bone marrow failure, developmental abnormalities, and cancer predisposition (Moldovan and D'Andrea, 2009). Cells isolated from FA patients display chromosomal instability and hypersensitivity to DNA interstrand crosslink (ICL)-inducing agents such as mitomycin C (MMC) and cisplatin. The high cytotoxicity of MMC, a property exploited in cancer therapy, is primarily based on the strong inhibitory effect of unrepaired ICLs on DNA replication (Deans and West, 2011). Recent studies indicate that the FA pathway orchestrates replication-coupled ICL repair—involving nucleolytic incision, translesion DNA synthesis (TLS), and homologous recombination (HR)—to maintain genomic stability (Knipscheer et al., 2009). In response to ICL damage, the FA core complex, consisting of eight proteins (FANCA, B, C, E, F, G, L, and M), promotes monoubiquitination of FANCD2 and FANCI (Garcia-Higuera et al., 2001; Smogorzewska et al., 2007). The ubiquitinated FANCD2/I complex relocalizes to damaged chromatin, where it coordinates downstream repair events (Kim and D'Andrea, 2012). ICL repair is initiated by nucleolytic incisions on either side of the crosslink and carried out by SLX4-associated XPF-ERCC1 and MUS81-EME1 nucleases and FAN1 (Kottemann and Smogorzewska, 2013). ICL incision converts the stalled replication fork into a one-ended DNA double-strand break (DSB), which is repaired by HR. Interestingly, FA phenotypes can be partially rescued by inhibition of nonhomologous end-joining (NHEJ), suggesting that the FA pathway not only promotes error-free HR but also actively suppresses inappropriate repair of DSB intermediates by NHEJ in order to prevent chromosomal instability (Adamo et al., 2010; Pace et al., 2010).

Although FANCD2 is critically important for ICL repair, its contribution to HR remains largely elusive (Nakanishi et al., 2011; Smogorzewska et al., 2007). HR is initiated by DNA-end resection, which occurs in human cells through the combined action of CtIP and the MRE11-RAD50-NBS1 (MRN) complex, together with DNA2 or EXO1 nucleases (Nimonkar et al., 2011; Sartori et al., 2007). Importantly, DNA-end resection is a key determinant of DSB repair pathway choice, as it commits cells to HR, while, at the same time, suppresses NHEJ (Chapman et al., 2012). A putative connection between the resection machinery and the FA pathway was recently proposed, based on data showing that DNA2 and EXO1 depletion leads to cisplatin hypersensitivity (Karanja et al., 2012). Additionally, CtIP was shown to accumulate at sites of locally induced ICLs (Duquette et al., 2012). However, the contribution of DNA-end resection to ICL repair and the regulation of CtIP by the FA pathway have not yet been thoroughly investigated.

RESULTS

FANCD2 Is Required for CtIP Localization to ICL Damage

Similar to FA cells, we observed that CtIP depletion results in hypersensitivity and increased chromosomal aberrations following MMC treatment, implicating a key role for CtIP in ICL repair (Figures 1A, S1A, and S1B). Because FANCD2 monoubiquitination constitutes a key step of the FA pathway, we investigated

OPEN ACCESS
CellPress

Please cite this article in press as: Murina et al., FANCD2 and CtIP Cooperate to Repair DNA Interstrand Crosslinks, Cell Reports (2014), http://dx.doi.org/10.1016/j.celrep.2014.03.069

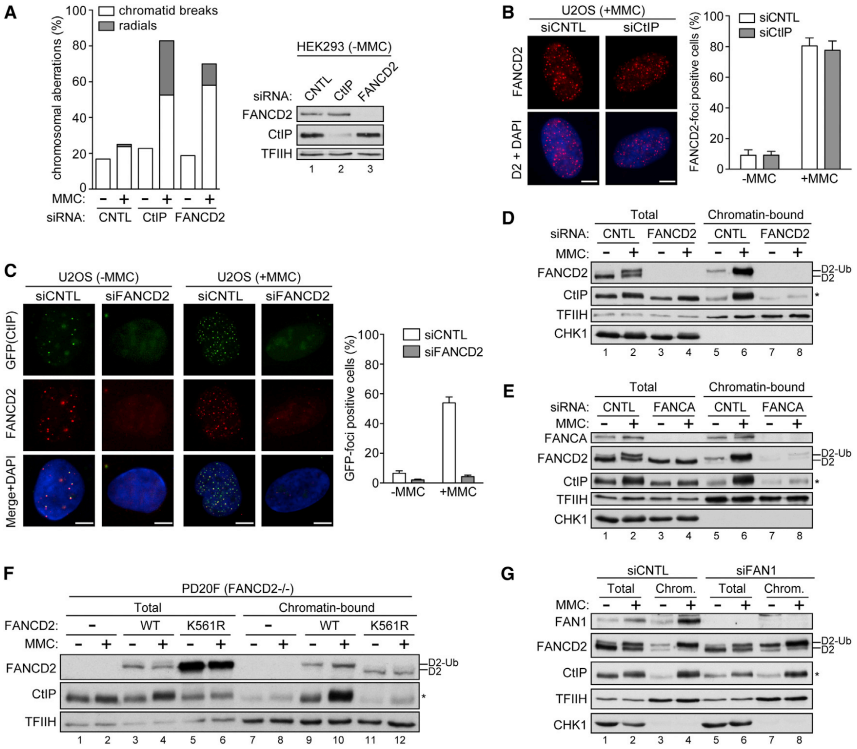

Figure 1. FANCD2 Is Required for the Accumulation of CtIP at Sites of ICL Damage

(A) Metaphase spreads from HEK293 cells transfected with the indicated small interfering RNAs (siRNAs) and treated for 20 hr with MMC (25 ng/ml) were analyzed for chromosomal aberrations. A total of 100 metaphase spreads from three independent experiments were analyzed for each condition. The percentages of cells displaying chromatid breaks or radial chromosomes are shown (see also Figure S1B).

(B) After 48 hr of transfection with indicated siRNAs, U2OS cells grown on coverslips were treated for 24 hr with MMC (120 ng/ml), pre-extracted, fixed, and immunostained for FANCD2. Nuclei were visualized by DAPI-staining. Graph shows the percentage of cells displaying more than ten FANCD2 foci/nuclei.

(C) U2OS cells stably expressing GFP-tagged CtIP were transfected with indicated siRNAs, and 48 hr later, cells grown on coverslips were treated as in (B) and immunostained for FANCD2. Graph shows the percentage of cells displaying more than ten GFP-CtIP foci/nuclei.

(D and E) U2OS cells were transfected with indicated siRNAs, and 48 hr later, cells were treated as in (B) and extracts were analyzed by immunoblotting.

(F) FANCD2 mutant human fibroblasts (PD20F) and PD20F stably expressing wild-type FANCD2 (WT) or K561R mutant FANCD2 were treated as in (B) and harvested for immunoblot analysis (see also Figure S1H).

(G) U2OS cells were transfected with FAN1 siRNA and processed as in (D).

In (B) and (C), for each condition, at least 100 cells were scored and the data are presented as the mean ± SD (n = 3). The scale bar represents 5 μm.

whether CtIP affects FANCD2 foci formation. However, silencing of CtIP did not significantly change the assembly of FANCD2 foci after MMC treatment (Figure 1B). Moreover, FANCD2 monoubiquitination and chromatin assembly still efficiently occurred in CtIP-depleted cells (Figures S1C and S1D). Recently, it was shown that the knockdown of CtIP leads to a 2-fold reduction in FANCD2 accumulation at ICLs induced by 8-methoxypsoralen plus UVA laser microirradiation (PUVA) (Duquette et al., 2012). Therefore, we subjected CtIP-depleted cells to PUVA treatment and noticed partially reduced levels of monoubiquitinated FANCD2 on chromatin (Figures S1E and S1F). Taken together, our data indicate that CtIP is not strictly required for FANCD2 monoubiquitination in response to ICL-inducing agents but that its loss may lead to a negative feedback loop limiting FA pathway activation during ICL repair.

We also noticed that CtIP was highly enriched on chromatin upon MMC or PUVA treatment (Figures S1C and S1F). Consistent with this, ICL damage caused a strong increase in CtIP foci that colocalized with FANCD2 (Figure 1C). Remarkably, both spontaneous and damage-induced CtIP foci were abrogated in FANCD2-depleted cells (Figure 1C). Accordingly, FANCD2 depletion impaired CtIP chromatin association in

Please cite this article in press as: Murina et al., FANCD2 and CtIP Cooperate to Repair DNA Interstrand Crosslinks, Cell Reports (2014), http://dx.doi.org/10.1016/j.celrep.2014.03.069

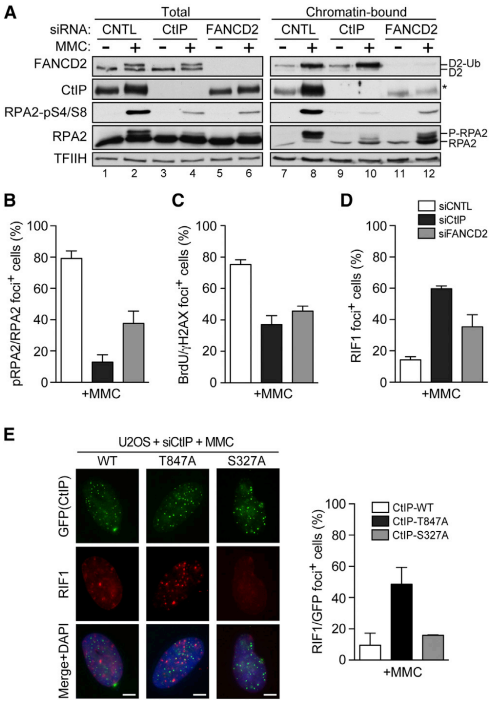

Figure 2. FANCD2 and CtIP Promote DNA-End Resection during ICL Repair

(A) U2OS cells were transfected with indicated small interfering RNAs (siRNAs), and 48 hr after siRNA transfection, cells were either mock-treated or treated for 24 hr with MMC (120 ng/ml) and extracts were analyzed by immunoblotting. RPA2 and P-RPA2 represent nonmodified and hyperphosphorylated forms of RPA2, respectively.

(B) Same cells as in (A) were grown on coverslips, pre-extracted, fixed, and coimmunostained for RPA2-pS4/S8 (pRPA2) and RPA2 (see also Figure S2C). Graph shows the percentage of RPA2-foci-positive cells displaying more than ten pRPA2 foci.

(C) Same cells as in (A) were coimmunostained for γH2AX and BrdU to visualize single-stranded DNA under nondenaturing conditions (see also Figure S2D). Graph shows the percentage of γH2AX-foci-positive cells displaying more than ten BrdU foci.

(D) Same cells as in (A) were immunostained for RIF1 (see also Figure S2E). Graph shows the percentage of nuclei displaying more than ten RIF1 foci.

(E) U2OS cells were transfected with CtIP siRNA, and 24 hr post-siRNA transfection, cells were transfected with siRNA-resistant GFP-tagged CtIP wild-type (WT), T847A, or S327A mutant CtIP (see also Figure S2F). After 48 hr of siRNA transfection, cells were treated as in (A) and immunostained for RIF1. Graph shows the percentage of GFP-foci positive cells displaying more than 10 RIF1 foci. The scale bar represents 5 μm.

In (B)–(E), for each condition, at least 100 cells were scored and data are presented as the mean ± SEM (n = 3).

MMC- and PUVA-treated cells (Figures 1D and S1G). In response to ICL damage, FANCD2 becomes monoubiquitinated at K561 by the FA core complex (Garcia-Higuera et al., 2001; Meetei et al., 2003). Depletion of FANCA, a subunit of the FA core complex, abolished both FANCD2 and CtIP association with damaged chromatin (Figure 1E). Importantly, impaired CtIP accumulation at ICLs in FANCD2-deficient fibroblasts (PD20F) was restored by complementation with wild-type (WT) FANCD2, but not with the K561R mutant (Figures 1F and S1H). In addition, CtIP failed to form MMC-induced foci in cells pretreated with the proteasome inhibitor MG-132, which leads to the sequestration of ubiquitin in the cytoplasm, further indicating that FANCD2 monoubiquitination is a prerequisite for CtIP localization to ICLs (Figure S1I).

During the initial processing of DSBs, CtIP acts together with the MRE11-RAD50-NBS1 (MRN) complex. We therefore explored whether efficient localization of CtIP to ICLs may require the MRN complex. However, while NBS1 downregulation resulted in defective chromatin association of MRE11, the levels of chromatin-bound FANCD2 and CtIP remained unaltered (Figure S1J). On the other hand, monoubiquitinated FANCD2 was reported to directly interact with and recruit FAN1 and SLX4 to coordinate ICL incision (Kottemann and Smogorzewska, 2013; Yamamoto et al., 2011). However, depletion of FAN1 or SLX4 did not significantly affect the binding of CtIP to damaged chromatin (Figures 1G and S1K). Collectively, our results suggest that proper localization of CtIP to ICLs is controlled by FANCD2 but occurs independently of both MRN and structure-specific nucleases involved in ICL incision.

FANCD2 Facilitates CtIP-Mediated DNA-End Resection during ICL Repair

We observed that both MMC and PUVA treatment resulted in robust RPA2-S4/S8 phosphorylation (Figures S2A and S1E). RPA2 phosphorylation, particularly at S4 and S8, has been widely used as a surrogate marker for single-stranded DNA (ssDNA) that is generated by DNA-end resection (Kousholt et al., 2012). Remarkably, knockdown of CtIP or FANCD2 strongly impaired RPA2 hyperphosphorylation in response to ICL-inducing agents, which was particularly evident in the chromatin-bound fractions (Figures 2A and S2B). Likewise, the percentage of cells with RPA2-pS4/S8 foci was significantly reduced in CtIP- or FANCD2-depleted cells (Figures 2B and S2C). Moreover, by immunostaining of cells with anti-bromodeoxyuridine (anti-BrdU), we found that MMC triggered substantial ssDNA formation, which was reduced upon depletion of CtIP or FANCD2 (Figures 2C and S2D). Impaired DNA-end resection commits cells to error-prone repair of DSBs by NHEJ. Recently, RIF1 was characterized as a key NHEJ-promoting factor by virtue of its role in counteracting resection (Chapman et al., 2013; Di Virgilio et al., 2013; Escribano-Díaz et al., 2013; Zimmermann et al., 2013). Indeed, MMC-induced RIF1 foci were elevated in CtIP- or FANCD2-depleted cells, further supporting the idea that both factors promote DNA-end resection and, thus, suppress NHEJ during ICL repair (Figures 2D and S2E).

To further substantiate the role of CtIP-dependent resection in ICL repair, we monitored RIF1 foci in cells expressing GFP-tagged CtIP-WT, CtIP-T847A, or CtIP-S327A (Figure S2F). The mutated residues in CtIP represent CDK phosphorylation sites required for resection (T847A) or for interaction with BRCA1 (S327A) (Figure S2G) (Huertas and Jackson, 2009; Yu and

OPEN ACCESS CellPress

Please cite this article in press as: Murina et al., FANCD2 and CtIP Cooperate to Repair DNA Interstrand Crosslinks, Cell Reports (2014), http://dx.doi.org/10.1016/j.celrep.2014.03.069

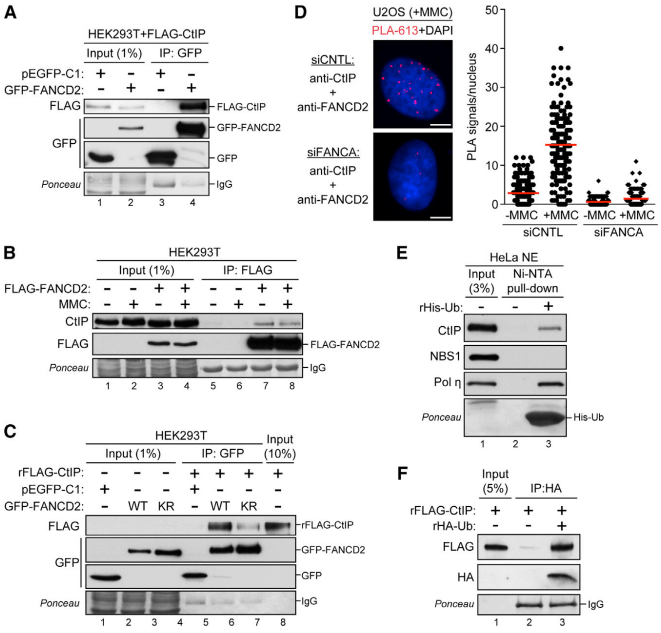

Figure 3. CtIP Physically Interacts with FANCD2 and Ubiquitin

(A) HEK293T cells were cotransfected with FLAG-CtIP along with either empty vector or GFP-FANCD2, and 48 hr after transfection, cells were lysed in NP-40 buffer and whole cell extracts were analyzed before (input) or after immunoprecipitation (IP) with anti-GFP (see also Figure S3A).

(B) HEK293T cells were transfected with either empty vector or FLAG-FANCD2, and 48 hr post-transfection, cells were either mock-treated or treated for 24 hr with MMC (120 ng/ml). Cells were lysed in Triton-X buffer, and whole-cell extracts were analyzed before (input) or after IP using anti-FLAG M2 affinity resin.

(C) HEK293T cells were transfected with empty vector, GFP-FANCD2 (WT), or GFP-FANCD2 K561R (KR). Then 48 hr after transfection, cells were lysed in NP-40 buffer and whole-cell extracts were subjected to IP with anti-GFP. After stringent washings, immunoprecipitated GFP-tagged proteins were incubated with 0.5 μg of recombinant FLAG-tagged CtIP (rFLAG-CtIP; see also Figure S3B). Inputs and recovered protein complexes were analyzed by immunoblotting.

(D) U2OS cells transfected with the indicated siRNAs were left untreated or treated as in (B). After pre-extraction, cells were fixed on coverslips and incubated with antibodies against CtIP and FANCD2 before the detection of protein-protein interactions using a fluorescently labeled probe (PLA-613). Nuclei were visualized by DAPI staining. Graph shows the quantification of the PLA signals/nucleus. PLA signals from at least 100 cells were analyzed (n = 3) (see also Figures S3C and S3D). The scale bar represents 5 μm.

(E) His alone (–) or recombinant His-tagged ubiquitin (rHis-Ub) coupled to nickel nitrilotriacetic acid (Ni-NTA) agarose beads were incubated with HeLa nuclear extracts (NE). Input and precipitated bead fractions from the pull-downs were subjected to immunoblotting. Ponceau staining is shown to indicate the amounts of rHis-Ub used in the pull-down assay.

(F) Recombinant FLAG-tagged CtIP was incubated either alone or together with recombinant hemagglutinin (HA)-tagged ubiquitin and the samples were subjected to IP with anti-HA. Inputs and recovered protein complexes were analyzed by immunoblotting.

Chen, 2004). Our analysis revealed a strong increase in RIF1 foci in MMC-treated T847A mutant cells, whereas the S327A mutation had no significant impact on RIF1 foci formation (Figure 2E). In agreement with this result, T847A mutant cells were hypersensitive to MMC, whereas the viability of cells expressing CtIP-S327A was similar to CtIP-WT cells, further supporting the idea that BRCA1-CtIP interaction is not required for resection during ICL repair (Figures S2H and S2I) (Reczek et al., 2013). Thus far, our findings suggest a pivotal regulatory role for FANCD2 in priming CtIP-mediated DNA-end resection to prevent aberrant NHEJ activity following ICL damage.

CtIP Physically Interacts with FANCD2 and Ubiquitin

Given that CtIP localization to sites of ICL damage is facilitated by FANCD2, we next addressed whether they exist in a complex and found that FLAG-CtIP efficiently coimmunoprecipitated with GFP-FANCD2, and vice versa (Figures 3A and S3A). Moreover, we were able to specifically detect endogenous CtIP coimmunoprecipitating with FLAG-FANCD2 but did not observe significant changes in complex formation upon MMC treatment, suggesting that monoubiquitination of FANCD2 may not be essential for CtIP binding (Figure 3B). In order to further address this issue, we mixed recombinant CtIP purified from insect cells with GFP-FANCD2 immunoprecipitated from human embryonic kidney 293T (HEK293T) cells. While CtIP efficiently bound to FANCD2-WT, it only weakly interacted with the FANCD2-K561R mutant, indicating that FANCD2 and CtIP physically interact and that complex formation might be reinforced by FANCD2 monoubiquitination (Figures 3C and S3B).

To verify the existence of endogenous CtIP-FANCD2 complexes, we performed proximity ligation assays (in situ PLA). As shown in Figure 3D, we could readily detect nuclear PLA signals in undamaged cells, which significantly increased in numbers upon MMC treatment, indicating that the FANCD2-CtIP interaction is enhanced following ICL damage. Moreover, we observed a strong reduction in CtIP-FANCD2 complex formation in FANCA-depleted, but not SLX4- or FAN1-depleted, cells (Figures 3D, S3C, and S3D). These findings further support the importance of FANCD2 monoubiquitination for the accumulation of CtIP at damaged chromatin, presumably by facilitating FANCD2-CtIP interaction. Although sequence analysis revealed that CtIP does not contain any known ubiquitin-binding motifs (Hofmann,

Please cite this article in press as: Murina et al., FANCD2 and CtIP Cooperate to Repair DNA Interstrand Crosslinks, Cell Reports (2014), http://dx.doi.org/10.1016/j.celrep.2014.03.069

2009), our results prompted us to examine whether CtIP can bind to ubiquitin. As shown in Figure 3E, we discovered that CtIP is able to interact with ubiquitin, although less efficiently compared to Polη that contains a ubiquitin-binding domain (UBD) (Bienko et al., 2005; Plosky et al., 2006). Furthermore, we observed comparable ubiquitin binding abilities of GFP-CtIP and UBZ-domain containing GFP-SLX4 (Figure S3E) (Yamamoto et al., 2011). However, while the ubiquitin I44A mutant completely abolished UBZ-mediated interactions of SLX4 and Polη with ubiquitin, it did not affect the binding of CtIP, implicating a distinct type of ubiquitin recognition (Figure S3F). We were also able to detect an interaction between purified, recombinant proteins, implying that CtIP can directly recognize ubiquitin (Figure 3F). Collectively, these data demonstrate that CtIP interacts with FANCD2 and that FANCD2 monoubiquitination enhances FANCD2-CtIP complex formation, perhaps owing to the ability of CtIP to bind ubiquitin.

FANCD2-CtIP Interaction Promotes Crosslink Resistance

To establish the functional significance of the FANCD2-CtIP interaction for ICL repair, we sought to identify the FANCD2-binding motif in CtIP. Whereas FANCD2 did not bind to a region of CtIP containing putative coiled-coil motifs (45–160), it bound efficiently to fragments of CtIP comprising amino acid (aa) residues 45–298 or 45–371 (Figure 4A), highlighting the region between aa residues 160–298 of CtIP to be important for FANCD2 binding. Detailed protein sequence analysis of this region revealed four motifs with high sequence conservation between vertebrates (Figure S4A). Remarkably, cells expressing RRK/AAA or RYIE/AAIA mutant variants of CtIP were impaired in MMC-induced GFP-CtIP foci formation and showed increased RIF1 foci (Figures S4B and S4C). Consistent with a defect in CtIP foci formation, RRK/AAA and RYIE/AAIA mutants exhibited reduced FANCD2 binding in glutathione S-transferase (GST) pull-down experiments (Figures 4B and 4C). Moreover, PLA signals were reduced in both CtIP mutants after MMC treatment, further supporting the role of RRK and RYIE motifs in CtIP-FANCD2 interaction (Figures 4D and 4E). MMC-induced CtIP foci were also abrogated in U2OS cells stably expressing GFP-tagged CtIP-RRK/AAA and -RYIE/AAIA mutants, whereas RIF1 foci were significantly increased in those cells (Figure 4F). However, both CtIP mutants were efficiently recruited to DSB-containing tracks generated by laser microirradiation (Figure S4D). Underscoring a differential regulation of CtIP in response to ICL damage, CtIP recruitment to laser-induced DNA lesions was FANCD2-independent (Figure S4E). Of note, a truncated CtIP mutant lacking residues 153–322 was still proficient in ubiquitin binding, indicating that neither RRK (aa 177–179) nor RYIE (aa 185-188) sequence motifs are required for the interaction between CtIP and ubiquitin (Figures S4F and S4G). Finally, both RRK/AAA and RYIE/AAIA mutant cells were hypersensitive to MMC, further supporting the idea that FANCD2 regulates CtIP functionality during ICL repair (Figure 4G).

CtIP Counteracts ICL-Induced DNA Damage in the Absence of FANCD2 Activation

To genetically determine the epistatic relationship between CtIP and FANCD2 in ICL repair, we generated an MRC5 cell line stably expressing doxycycline (DOX)-inducible small hairpin RNA (shRNA) against CtIP (Figure 5A). Interestingly, depletion of FANCD2 in DOX-treated MRC5 cells led to a further increase in MMC hypersensitivity (Figures 5A and 5B). In agreement with this, survival of PD20 cells upon MMC treatment was further reduced after silencing of CtIP (Figure S5A). CtIP/FANCD2-deficient MRC5 cells also showed elevated levels of MMC-induced RIF1 foci and radial chromosomes compared to cells depleted for either factor alone, indicative of potent, illegitimate repair of DSBs by NHEJ (Figures 5C, 5D, S5B, and S5C). Previously, BRCA1 has been reported to regulate the accumulation of FANCD2 into repair foci and CtIP recruitment to PUVA-induced ICLs (Garcia-Higuera et al., 2001; Duquette et al., 2012). Further supporting a dual, nonredundant role for CtIP in ICL repair, knockdown of BRCA1 in DOX-treated MRC5^{shCtIP} cells resulted in increased MMC sensitivity (Figure S5D). Thus, our data suggest that CtIP-dependent DNA-end resection is essential to counteract the toxic effects of ICL damage when the FA/BRCA signaling pathway is compromised.

ATR kinase is a major regulator of the FA pathway and promotes FANCD2/I monoubiquitination (Andreassen et al., 2004; Smogorzewska et al., 2007). Recently, both ATM and ATR kinases have been implicated in DNA-damage-induced CtIP phosphorylation (Peterson et al., 2013; Wang et al., 2013). In order to gain further mechanistic insight into the regulation of CtIP during ICL repair, we applied selective ATR and/or ATM inhibitors prior to MMC treatment (Reaper et al., 2011). CtIP and RPA2 phosphorylation was strongly elevated after ATR inhibition; meanwhile, FANCD2 monoubiquitination and CHK1 phosphorylation were reduced as expected (Figure 5E, lane 2). Interestingly, MMC-induced hyperphosphorylation of CtIP and, to a lesser extent, of RPA2 was reversed when both inhibitors were combined (Figure 5E, lane 4). These data suggest that ATM gets hyperactivated when ATR kinase is blocked, probably as a result of prevalent cleavage of collapsed replication forks into DSBs. The structure-specific endonuclease MUS81-EME1 has been implicated in the conversion of stalled replication forks into DSBs, particularly in checkpoint-deficient cells (Hanada et al., 2006; Murfuni et al., 2013). Indeed, inhibition of ATR combined with MUS81 depletion significantly reduced the phosphorylation of H2AX and KAP1, both established ATM targets, indicating that MUS81 is at least partially required for the processing of ICL-stalled forks into DSBs (Figure 5F). Remarkably, phosphorylation levels of CtIP were also decreased, further implying CtIP in promoting DNA-end resection and HR of replication-associated DSBs in the absence of a fully functional FA pathway. Taken together, our results demonstrate that during conventional ICL repair, CtIP-mediated DNA-end resection is regulated by FANCD2 but that CtIP also helps prevent illegitimate repair of stalled forks in FA-pathway-defective cells.

DISCUSSION

CtIP is an essential factor required for the initiation of DNA-end resection during HR and, thus, for the suppression of DSB repair by NHEJ. Given that FA-pathway-deficient cells exhibit increased chromosomal instability in response to ICL damage, FA proteins have also been implicated in NHEJ inhibition. Indeed, we

OPEN ACCESS CellPress

Please cite this article in press as: Murina et al., FANCD2 and CtIP Cooperate to Repair DNA Interstrand Crosslinks, Cell Reports (2014), http://dx.doi.org/10.1016/j.celrep.2014.03.069

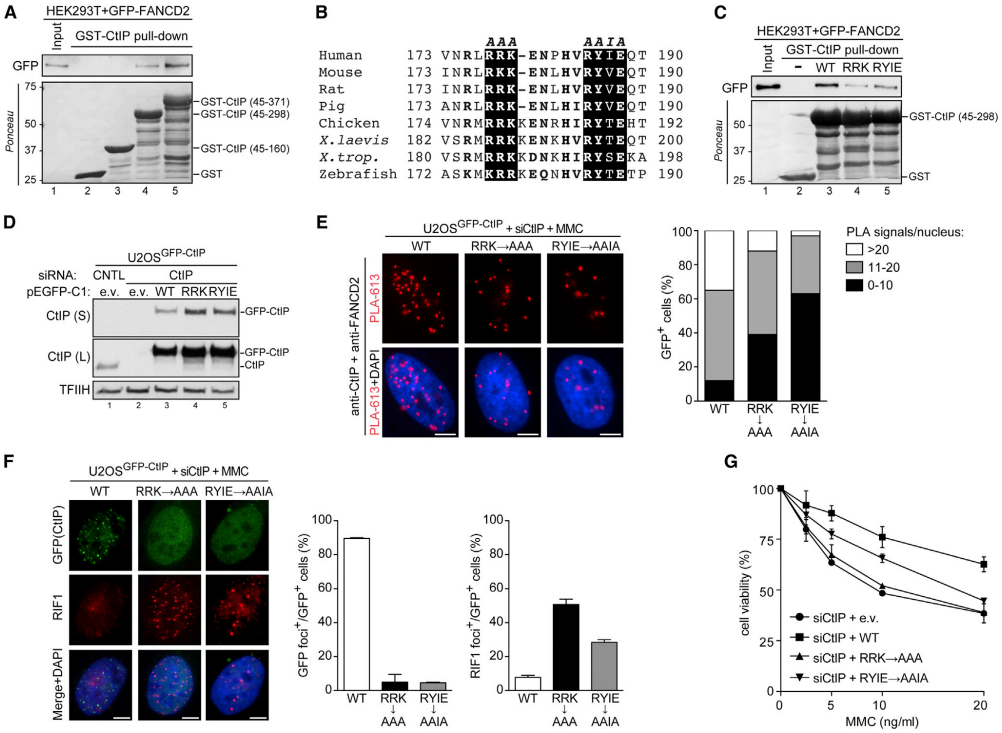

Figure 4. Functional Characterization of CtIP Mutants Impaired in FANCD2 Binding

(A) GST or GST-CtIP proteins were coupled to glutathione Sepharose beads and incubated with HEK293T cell lysates transiently overexpressing GFP-FANCD2. The recovered materials were analyzed by immunoblotting.

(B) Alignment of the putative FANCD2-interacting region in CtIP orthologs. RRK and RYxE motifs are highlighted in black boxes. Other, highly conserved amino acid residues are marked in bold typeface (see also Figure S4A).

(C) GST or indicated GST-CtIP (45–298) proteins were coupled to glutathione Sepharose beads and incubated with HEK293T cell lysates transiently overexpressing GFP-FANCD2. The recovered materials were analyzed by immunoblotting.

(D) U2OS cells stably expressing siRNA-resistant GFP-tagged wild-type (WT) and mutant (RRK/AAA and RYIE/AAIA) CtIP were transfected with CtIP siRNA for 72 hr, and whole-cell extracts were analyzed by immunoblotting. (S) and (L) indicate short and long exposures of the same immunoblot, respectively.

(E) Same cells as in (D) were transfected with CtIP siRNA. After 48 hr of siRNA transfection, cells grown on coverslips were treated for 24 hr with MMC (120 ng/ml), fixed, and incubated with antibodies against CtIP and FANCD2 before the detection of protein-protein interactions using a fluorescently labeled probe (PLA-613). Graph shows the quantification of the PLA signals/nucleus in GFP-positive cells. PLA signals from at least 100 cells were analyzed (n = 2).

(F) Same cells as in (E) were fixed and immunostained for RIF1. Graphs show the percentage of GFP-positive cells displaying more than ten GFP-CtIP foci or more than ten RIF1 foci, respectively. For each condition, at least 100 cells were scored. Data are presented as the mean ± SEM (n = 2).

(G) Same cells as in (D) were either mock-treated or continuously treated with the indicated doses of MMC, and the survival was determined after 5 days using the CellTiter-Blue cell viability assay. Data are presented as the mean ± SD (n = 3).

In (E) and (F), the scale bar represents 5 μm.

observed that depletion of CtIP or FANCD2 leads to an increase in radial chromosome formation and RIF1 foci after MMC treatment, indicative of enhanced NHEJ activity. Accordingly, DNA-end resection, as measured by phosphorylated RPA2 and BrdU focus formation, was reduced in CtIP- or FANCD2-depleted cells. Several mechanisms have been proposed how FA proteins prevent NHEJ, including the restriction of NHEJ factors to access DNA termini, cryptic exonuclease, or nucleosome-assembly activity of FANCD2 (Adamo et al., 2010; Pace et al., 2010; Sato et al., 2012). Based on our data, we propose that FANCD2 suppresses error-prone NHEJ through promoting CtIP-dependent resection (Figure S6).

We observed that monoubiquitinated FANCD2 tethers CtIP to damaged chromatin and identified two short, highly conserved motifs within CtIP responsible for CtIP-FANCD2 interaction. Consequently, CtIP mutants defective in FANCD2 binding are

Please cite this article in press as: Murina et al., FANCD2 and CtIP Cooperate to Repair DNA Interstrand Crosslinks, Cell Reports (2014), http://dx.doi.org/10.1016/j.celrep.2014.03.069

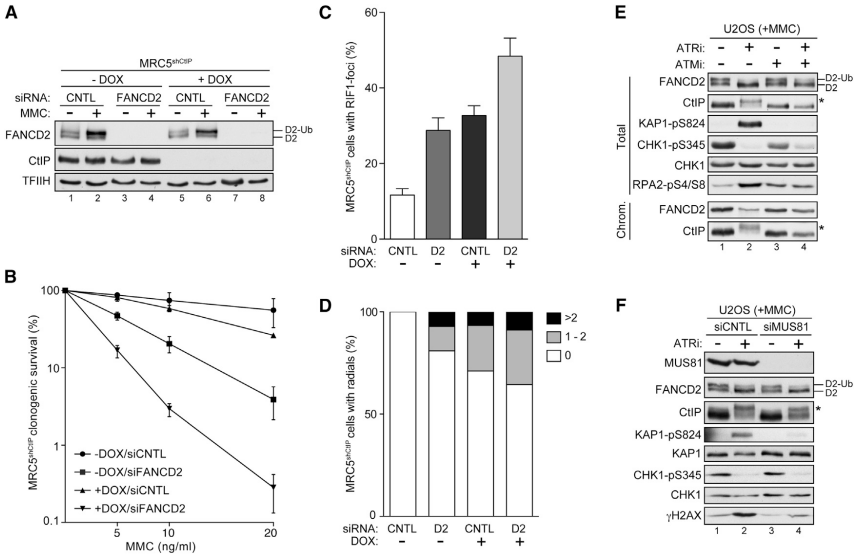

Figure 5. CtIP Contributes to Genome Stability in FA-Pathway-Deficient Cells

(A) MRC5 cells stably expressing doxycycline (DOX)-inducible shRNA against CtIP (MRC5^{shCtIP}) were transfected with indicated siRNAs. Then 24 hr after siRNA transfection, cells were cultivated in the absence or presence of DOX (1 μg/ml) for 48 hr. Cells were treated with MMC (120 ng/ml) for 24 hr and subjected to immunoblotting.

(B) Same cells as in (A) were treated for 24 hr with indicated doses of MMC, and survival was determined after 10 days by colony-formation assay. Data are presented as the mean ± SD (n = 3).

(C) Same cells as in (A) were immunostained for RIF1. Graph shows the percentage of RIF1-foci-positive cells displaying more than ten RIF1 foci. For each condition, at least 100 cells were scored. Data are presented as the mean ± SD (n = 3) (see also Figure S5B).

(D) Metaphase spreads from the same cells as in (A) treated for 20 hr with MMC (20 ng/ml) were analyzed for chromosomal aberrations. A total of 45 metaphase spreads from three independent experiments were analyzed for each condition. The percentages of cells displaying radial chromosomes are shown (see also Figure S5C).

(E) U2OS cells were pretreated for 15 min with DMSO, ATR inhibitor (VE-821, 1 μM), ATM inhibitor (KU-55933, 10 μM), or both inhibitors together. Cells were then treated for 20 hr with MMC (120 ng/ml), and extracts were analyzed by immunoblotting.

(F) U2OS cells were transfected with MUS81 siRNA, and 48 hr after siRNA transfection, cells were pretreated for 15 min with DMSO or ATR inhibitor (VE-821, 1 μM). Cells were then treated as in (E) and harvested for immunoblot analysis.

impaired in the formation of MMC-induced foci. Whereas FANCD2 monoubiquitination may not be essential for the physical interaction with CtIP, it is required to retain CtIP on damaged chromatin. Remarkably, we show that CtIP directly interacts with ubiquitin in vitro. Although bioinformatic analysis failed to predict any motifs resembling known UBDs in CtIP, it is plausible that the FANCD2-CtIP interaction is reinforced by the ability of CtIP to recognize ubiquitin. However, a CtIP mutant lacking both FANCD2-interacting motifs was proficient in ubiquitin binding. Furthermore, a mutant form of ubiquitin (I44A) defective in most UBD-mediated interactions was still able to interact with CtIP. Therefore, one could hypothesize that CtIP may employ a dual mode of recognizing monoubiquitinated FANCD2, but, if so, binds ubiquitin by a unique mechanism that involves a new type of UBD (Bomar et al., 2007). Clearly, further investigations are needed to establish the role of CtIP-ubiquitin interaction in the DNA damage response. On the other hand, it was proposed that monoubiquitination of FANCD2 could alter FANCD2 conformation (Joo et al., 2011). Thus, it is tempting to speculate that such structural changes in FANCD2 stimulate CtIP-FANCD2 interaction. Finally, the FANCD2/I complex may also facilitate CtIP recruitment to damaged chromatin via its histone chaperone activity (Sato et al., 2012). Increased MMC-induced sensitivity and RIF1 foci formation in cells expressing CtIP mutants (RRK/AAA and RYIE/AAIA) further strengthen the significance of CtIP-FANCD2 interaction in ICL repair. Notably, R177Q and Y186C, two cancer-associated missense mutations in human CtIP, map exactly to the region implicated in FANCD2 interaction (Figure S4A). Given that RRK and RYIE motifs reside in a highly conserved stretch of 12 amino acids, it is also reasonable to think that they constitute a single FANCD2 interaction "domain." These data are similar to those described in the accompanying paper by Unno et al. (2014) published in this issue of *Cell Reports*.

Depletion of CtIP in FANCD2-deficient cells aggravates the phenotypes of cells lacking either factor alone, indicating that CtIP contributes to genome stability in FA-pathway-defective

OPEN ACCESS CellPress

Please cite this article in press as: Murina et al., FANCD2 and CtIP Cooperate to Repair DNA Interstrand Crosslinks, Cell Reports (2014), http://dx.doi.org/10.1016/j.celrep.2014.03.069

cells. Likewise, inactivation of FAN1 or SLX4 enhanced crosslink sensitivity of cells compromised in FANCD2 activation, suggesting that these proteins, though being recruited to ICLs by FANCD2, can promote MMC resistance in a FA-pathway-independent manner (Yamamoto et al., 2011; Zhou et al., 2012). Furthermore, only partial epistasis of FANCD2 over CtIP could be explained by an additional role of CtIP upstream of FANCD2 or by the proposed role of FANCD2 in protecting stalled forks from degradation (Duquette et al., 2012; Schlacher et al., 2012). There is increasing evidence that arrested and unprotected replication forks frequently collapse and give rise to DSBs, which can then undergo resection and repair by HR (Couch et al., 2013). Accordingly, we observed enhanced ATM-dependent phosphorylation of CtIP and RPA2 in cells co-treated with MMC and ATR inhibitor, indicative of ongoing DSB resection (Fugger et al., 2013). In line with this, CtIP phosphorylation was reduced upon depletion of MUS81, an endonuclease implicated in the cleavage of stalled forks and DSB formation (Ciccia et al., 2008). Furthermore, CtIP-dependent processing of collapsed forks upon hydroxyurea treatment was recently reported to be beneficial for genome integrity in the absence of FANCM (Blackford et al., 2012). Therefore, we conclude that CtIP can partially suppress genomic instability in the absence of FANCD2, whereas, in FA-pathway-proficient cells, monoubiquitinated FANCD2 coordinates CtIP-mediated DNA-end resection during ICL repair.

EXPERIMENTAL PROCEDURES

Cell Culture and Transfection

U2OS, HEK293T, and HEK293 cells were grown in Dulbecco's modified Eagle's medium (DMEM) supplemented with 10% fetal calf serum (FCS), 100 U/ml penicillin, and 100 μg/ml streptomycin. U2OS clones stably expressing siRNA-resistant forms of GFP-CtIP were described previously (Sartori et al., 2007). FANCD2-deficient cells (PD20F) were obtained from Fanconi Anemia Research Foundation (FARF) and cultured in DMEM supplemented with 10% FCS and standard antibiotics. PD20F cells complemented with FANCD2 wild-type (FARF) or K561R (kindly provided by Josef Jiricny) were grown in standard medium supplemented with 1 μg/ml Puromycin. MRC5^{shCtIP} cells were grown in DMEM supplemented with 10% Tet system approved FCS, 100 U/ml penicillin, 100 μg/ml streptomycin, Blasticidin (5 μg/ml), and Zeocin (250 μg/ml). Plasmids were transfected either by using the standard calcium phosphate method or FuGENE 6 (Roche) according to manufacturer's instructions. Transfection of all siRNA oligos was done with 40 nM final concentration using Lipofectamine RNAiMAX (Invitrogen). Data for survival curves were generated by colony-formation assays as described previously (Sartori et al., 2007).

Triton Extraction

Isolation of Triton-insoluble (chromatin-enriched) fraction was performed as previously described (Peña-Diaz et al., 2012). In brief, cells were rinsed twice in cold PBS and incubated for 5 min on ice in preextraction buffer (25 mM HEPES [pH 7.4], 50 mM NaCl, 1 mM EDTA, 3 mM $MgCl_2$, 300 mM sucrose, 0.5% Triton X-100, and protease inhibitors). After buffer removal, adherent cellular material was harvested by scraping the cells into Laemmli buffer. The chromatin-enriched fraction was then heat denatured, sonicated, and analyzed by immunoblotting.

SUPPLEMENTAL INFORMATION

Supplemental Information includes Supplemental Experimental Procedures and six figures and can be found with this article online at http://dx.doi.org/10.1016/j.celrep.2014.03.069.

AUTHOR CONTRIBUTIONS

O.M. and A.A.S. designed the research. L.P.F. performed the laser microirradiation experiments, and H.A.B. helped with the ubiquitin binding assay. K.H. generated the inducible MRC5^{shCtIP} cell line. All other experiments were performed by O.M. with the help of C.A. and U.K. O.M. and A.A.S. analyzed the data and wrote the paper.

ACKNOWLEDGMENTS

We are very grateful to Minoru Takata and Junya Unno for providing reagents and for communicating results prior to publication. We thank Pavel Janscak for providing purified recombinant human CtIP protein and experimental advice. We are grateful to Agata Smogorzewska, Johan de Winter, Josef Jiricny, Matthias Peter, the Fanconi Anemia Research Fund, and Vertex Pharmaceuticals for providing reagents. We thank Josef Jiricny and Orlando Schärer for critical reading of the manuscript. This work was supported by grants from the Swiss National Science Foundation (31003A_135507 and PDFMP3-127523), the Promedica Stiftung, the Olga Mayenfisch Stiftung, and the Vontobel Foundation (to A.A.S.).

Received: August 30, 2013
Revised: March 4, 2014
Accepted: March 27, 2014
Published: May 1, 2014

REFERENCES

Adamo, A., Collis, S.J., Adelman, C.A., Silva, N., Horejsi, Z., Ward, J.D., Martinez-Perez, E., Boulton, S.J., and La Volpe, A. (2010). Preventing nonhomologous end joining suppresses DNA repair defects of Fanconi anemia. Mol. Cell *39*, 25–35.

Andreassen, P.R., D'Andrea, A.D., and Taniguchi, T. (2004). ATR couples FANCD2 monoubiquitination to the DNA-damage response. Genes Dev. *18*, 1958–1963.

Bienko, M., Green, C.M., Crosetto, N., Rudolf, F., Zapart, G., Coull, B., Kannouche, P., Wider, G., Peter, M., Lehmann, A.R., et al. (2005). Ubiquitin-binding domains in Y-family polymerases regulate translesion synthesis. Science *310*, 1821–1824.

Blackford, A.N., Schwab, R.A., Nieminuszczy, J., Deans, A.J., West, S.C., and Niedzwiedz, W. (2012). The DNA translocase activity of FANCM protects stalled replication forks. Hum. Mol. Genet. *21*, 2005–2016.

Bomar, M.G., Pai, M.-T., Tzeng, S.-R., Li, S.S.-C., and Zhou, P. (2007). Structure of the ubiquitin-binding zinc finger domain of human DNA Y-polymerase eta. EMBO Rep. *8*, 247–251.

Chapman, J.R., Taylor, M.R.G., and Boulton, S.J. (2012). Playing the end game: DNA double-strand break repair pathway choice. Mol. Cell *47*, 497–510.

Chapman, J.R., Barral, P., Vannier, J.-B., Borel, V., Steger, M., Tomas-Loba, A., Sartori, A.A., Adams, I.R., Batista, F.D., and Boulton, S.J. (2013). RIF1 is essential for 53BP1-dependent nonhomologous end joining and suppression of DNA double-strand break resection. Mol. Cell *49*, 858–871.

Ciccia, A., McDonald, N., and West, S.C. (2008). Structural and functional relationships of the XPF/MUS81 family of proteins. Annu. Rev. Biochem. *77*, 259–287.

Couch, F.B., Bansbach, C.E., Driscoll, R., Luzwick, J.W., Glick, G.G., Bétous, R., Carroll, C.M., Jung, S.Y., Qin, J., Cimprich, K.A., and Cortez, D. (2013). ATR phosphorylates SMARCAL1 to prevent replication fork collapse. Genes Dev. *27*, 1610–1623.

Deans, A.J., and West, S.C. (2011). DNA interstrand crosslink repair and cancer. Nat. Rev. Cancer *11*, 467–480.

Di Virgilio, M., Callen, E., Yamane, A., Zhang, W., Jankovic, M., Gitlin, A.D., Feldhahn, N., Resch, W., Oliveira, T.Y., Chait, B.T., et al. (2013). Rif1 prevents resection of DNA breaks and promotes immunoglobulin class switching. Science *339*, 711–715.

Please cite this article in press as: Murina et al., FANCD2 and CtIP Cooperate to Repair DNA Interstrand Crosslinks, Cell Reports (2014), http://dx.doi.org/10.1016/j.celrep.2014.03.069

Duquette, M.L., Zhu, Q., Taylor, E.R., Tsay, A.J., Shi, L.Z., Berns, M.W., and McGowan, C.H. (2012). CtIP is required to initiate replication-dependent interstrand crosslink repair. PLoS Genet. *8*, e1003050.

Escribano-Díaz, C., Orthwein, A., Fradet-Turcotte, A., Xing, M., Young, J.T.F., Tkáč, J., Cook, M.A., Rosebrock, A.P., Munro, M., Canny, M.D., et al. (2013). A cell cycle-dependent regulatory circuit composed of 53BP1-RIF1 and BRCA1-CtIP controls DNA repair pathway choice. Mol. Cell *49*, 872–883.

Fugger, K., Chu, W.K., Haahr, P., Kousholt, A.N., Beck, H., Payne, M.J., Hanada, K., Hickson, I.D., and Sørensen, C.S. (2013). FBH1 co-operates with MUS81 in inducing DNA double-strand breaks and cell death following replication stress. Nat Commun *4*, 1423.

Garcia-Higuera, I., Taniguchi, T., Ganesan, S., Meyn, M.S., Timmers, C., Hejna, J., Grompe, M., and D'Andrea, A.D. (2001). Interaction of the Fanconi anemia proteins and BRCA1 in a common pathway. Mol. Cell *7*, 249–262.

Hanada, K., Budzowska, M., Modesti, M., Maas, A., Wyman, C., Essers, J., and Kanaar, R. (2006). The structure-specific endonuclease Mus81-Eme1 promotes conversion of interstrand DNA crosslinks into double-strands breaks. EMBO J. *25*, 4921–4932.

Hofmann, K. (2009). Ubiquitin-binding domains and their role in the DNA damage response. DNA Repair (Amst.) *8*, 544–556.

Huertas, P., and Jackson, S.P. (2009). Human CtIP mediates cell cycle control of DNA end resection and double strand break repair. J. Biol. Chem. *284*, 9558–9565.

Joo, W., Xu, G., Persky, N.S., Smogorzewska, A., Rudge, D.G., Buzovetsky, O., Elledge, S.J., and Pavletich, N.P. (2011). Structure of the FANCI-FANCD2 complex: insights into the Fanconi anemia DNA repair pathway. Science *333*, 312–316.

Karanja, K.K., Cox, S.W., Duxin, J.P., Stewart, S.A., and Campbell, J.L. (2012). DNA2 and EXO1 in replication-coupled, homology-directed repair and in the interplay between HDR and the FA/BRCA network. Cell Cycle *11*, 3983–3996.

Kim, H., and D'Andrea, A.D. (2012). Regulation of DNA cross-link repair by the Fanconi anemia/BRCA pathway. Genes Dev. *26*, 1393–1408.

Knipscheer, P., Räschle, M., Smogorzewska, A., Enoiu, M., Ho, T.V., Schärer, O.D., Elledge, S.J., and Walter, J.C. (2009). The Fanconi anemia pathway promotes replication-dependent DNA interstrand cross-link repair. Science *326*, 1698–1701.

Kottemann, M.C., and Smogorzewska, A. (2013). Fanconi anaemia and the repair of Watson and Crick DNA crosslinks. Nature *493*, 356–363.

Kousholt, A.N., Fugger, K., Hoffmann, S., Larsen, B.D., Menzel, T., Sartori, A.A., and Sørensen, C.S. (2012). CtIP-dependent DNA resection is required for DNA damage checkpoint maintenance but not initiation. J. Cell Biol. *197*, 869–876.

Meetei, A.R., de Winter, J.P., Medhurst, A.L., Wallisch, M., Waisfisz, Q., van de Vrugt, H.J., Oostra, A.B., Yan, Z., Ling, C., Bishop, C.E., et al. (2003). A novel ubiquitin ligase is deficient in Fanconi anemia. Nat. Genet. *35*, 165–170.

Moldovan, G.L., and D'Andrea, A.D. (2009). How the fanconi anemia pathway guards the genome. Annu. Rev. Genet. *43*, 223–249.

Murfuni, I., Basile, G., Subramanyam, S., Malacaria, E., Bignami, M., Spies, M., Franchitto, A., and Pichierri, P. (2013). Survival of the replication checkpoint deficient cells requires MUS81-RAD52 function. PLoS Genet. *9*, e1003910.

Nakanishi, K., Cavallo, F., Perrouault, L., Giovannangeli, C., Moynahan, M.E., Barchi, M., Brunet, E., and Jasin, M. (2011). Homology-directed Fanconi anemia pathway cross-link repair is dependent on DNA replication. Nat. Struct. Mol. Biol. *18*, 500–503.

Nimonkar, A.V., Genschel, J., Kinoshita, E., Polaczek, P., Campbell, J.L., Wyman, C., Modrich, P., and Kowalczykowski, S.C. (2011). BLM-DNA2-RPA-MRN and EXO1-BLM-RPA-MRN constitute two DNA end resection machineries for human DNA break repair. Genes Dev. *25*, 350–362.

Pace, P., Mosedale, G., Hodskinson, M.R., Rosado, I.V., Sivasubramaniam, M., and Patel, K.J. (2010). Ku70 corrupts DNA repair in the absence of the Fanconi anemia pathway. Science *329*, 219–223.

Peña-Diaz, J., Bregenhorn, S., Ghodgaonkar, M., Follonier, C., Artola-Borán, M., Castor, D., Lopes, M., Sartori, A.A., and Jiricny, J. (2012). Noncanonical mismatch repair as a source of genomic instability in human cells. Mol. Cell *47*, 669–680.

Peterson, S.E., Li, Y., Wu-Baer, F., Chait, B.T., Baer, R., Yan, H., Gottesman, M.E., and Gautier, J. (2013). Activation of DSB processing requires phosphorylation of CtIP by ATR. Mol. Cell *49*, 657–667.

Plosky, B.S., Vidal, A.E., Fernández de Henestrosa, A.R., McLenigan, M.P., McDonald, J.P., Mead, S., and Woodgate, R. (2006). Controlling the subcellular localization of DNA polymerases iota and eta via interactions with ubiquitin. EMBO J. *25*, 2847–2855.

Reaper, P.M., Griffiths, M.R., Long, J.M., Charrier, J.-D., Maccormick, S., Charlton, P.A., Golec, J.M.C., and Pollard, J.R. (2011). Selective killing of ATM- or p53-deficient cancer cells through inhibition of ATR. Nat. Chem. Biol. *7*, 428–430.

Reczek, C.R., Szabolcs, M., Stark, J.M., Ludwig, T., and Baer, R. (2013). The interaction between CtIP and BRCA1 is not essential for resection-mediated DNA repair or tumor suppression. J. Cell Biol. *201*, 693–707.

Sartori, A.A., Lukas, C., Coates, J., Mistrik, M., Fu, S., Bartek, J., Baer, R., Lukas, J., and Jackson, S.P. (2007). Human CtIP promotes DNA end resection. Nature *450*, 509–514.

Sato, K., Ishiai, M., Toda, K., Furukoshi, S., Osakabe, A., Tachiwana, H., Takizawa, Y., Kagawa, W., Kitao, H., Dohmae, N., et al. (2012). Histone chaperone activity of Fanconi anemia proteins, FANCD2 and FANCI, is required for DNA crosslink repair. EMBO J. *31*, 3524–3536.

Schlacher, K., Wu, H., and Jasin, M. (2012). A distinct replication fork protection pathway connects Fanconi anemia tumor suppressors to RAD51-BRCA1/2. Cancer Cell *22*, 106–116.

Smogorzewska, A., Matsuoka, S., Vinciguerra, P., McDonald, E.R., 3rd, Hurov, K.E., Luo, J., Ballif, B.A., Gygi, S.P., Hofmann, K., D'Andrea, A.D., and Elledge, S.J. (2007). Identification of the FANCI protein, a monoubiquitinated FANCD2 paralog required for DNA repair. Cell *129*, 289–301.

Unno, J., Itaya, A., Taoka, M., Sato, K., Tomida, J., Sakai, W., Sugasawa, K., Ishiai, M., Ikura, T., Toshiaki, I., et al. (2014). FANCD2 binds CTIP and regulates DNA-end resection during DNA interstrand crosslink repair. Cell Rep. *7*, Published online May 1, 2014. http://dx.doi.org/10.1016/j.celrep.2014.04.005.

Wang, H., Shi, L.Z., Wong, C.C.L., Han, X., Hwang, P.Y.-H., Truong, L.N., Zhu, Q., Shao, Z., Chen, D.J., Berns, M.W., et al. (2013). The interaction of CtIP and Nbs1 connects CDK and ATM to regulate HR-mediated double-strand break repair. PLoS Genet. *9*, e1003277.

Yamamoto, K.N., Kobayashi, S., Tsuda, M., Kurumizaka, H., Takata, M., Kono, K., Jiricny, J., Takeda, S., and Hirota, K. (2011). Involvement of SLX4 in interstrand cross-link repair is regulated by the Fanconi anemia pathway. Proc. Natl. Acad. Sci. USA *108*, 6492–6496.

Yu, X., and Chen, J. (2004). DNA damage-induced cell cycle checkpoint control requires CtIP, a phosphorylation-dependent binding partner of BRCA1 C-terminal domains. Mol. Cell. Biol. *24*, 9478–9486.

Zhou, W., Otto, E.A., Cluckey, A., Airik, R., Hurd, T.W., Chaki, M., Diaz, K., Lach, F.P., Bennett, G.R., Gee, H.Y., et al. (2012). FAN1 mutations cause karyomegalic interstitial nephritis, linking chronic kidney failure to defective DNA damage repair. Nat. Genet. *44*, 910–915.

Zimmermann, M., Lottersberger, F., Buonomo, S.B., Sfeir, A., and de Lange, T. (2013). 53BP1 regulates DSB repair using Rif1 to control 5′ end resection. Science *339*, 700–704.

Cell Reports, Volume *7*
Supplemental Information

FANCD2 and CtIP Cooperate in the Repair of DNA Interstrand Crosslinks

Olga Murina, Christine von Aesch, Ufuk Karakus, Lorenza P. Ferretti, Hella A. Bolck, Kay Hänggi, and Alessandro A. Sartori

Supplemental Experimental Procedures

Plasmids.

The pcDNA3.1-based expression vectors for FLAG-FANCD2, GFP-FANCD2 and GFP-FANCD2 K561R were kindly provided by Minoru Takata (Kyoto University, Japan). Expression constructs for epitope-tagged CtIP were described previously (Steger et al., 2013). The pGEX-4T1 plasmids for bacterial expression of CtIP fragments were described previously (Sartori et al., 2007). CtIP 45-298 fragment was generated by introducing two stop codons in pGEX-4T1 CtIP 45-371. The pcDNA5-based GFP-SLX4 expression vector was a kind gift from Johan P. de Winter (VU University Medical Center, The Netherlands) (Stoepker et al., 2011). The pET23-based 6xHis-ubiquitin vector for bacterial expression was kindly provided by Matthias Peter (ETH Zurich, Switzerland). All CtIP and ubiquitin mutations were introduced by site-directed mutagenesis using Expand Long Template PCR System (Roche) and confirmed by sequencing. To generate an entry vector harboring shCtIP (target sequence: CGTCAGCCTTACAACGCAA (You et al., 2009)), annealed double-stranded DNA oligos were ligated into pENTR/HI/TO (Invitrogen). The lentiviral destination construct encoding shCtIP (pLenti4-shCtIP) was generated in an *in vitro* recombination reaction after transformation of bacteria with pENTR-shCtIP and pLenti4/DEST (Invitrogen).

siRNA sequences.

All siRNA duplexes were purchased from Microsynth AG, the sequences were as follows: Luciferase (CNTL; CGUACGCGGAAUACUUCGA), CtIP (CtIP-1; GCUAAAACAGGAACGAAUC) and CtIP-2 (UCCACAACAUAAUCCUAAU) (Sartori et al., 2007), FANCD2 (CAGAGUUUGCUUCACUCUCUA) (Kratz et al.,

2010), FANCA (CAGCGTTGAGATATCAAAGAT) (Kim et al., 2008), FAN1 (GUAAGGCUCUUUCAACGUA) (Kratz et al., 2010), NBS1 (GGAGGAAGAUGUCAAUGUUUU) (Yoo et al., 2009), SLX4 (AAACGUGAAUGAAGCAGAAUU) (Svendsen et al., 2009), MUS81 (CAGCCCUGGUGGAUCGAUA) (Neelsen et al., 2013), BRCA1 (GGAACCUGUCUCCACAAAG) (Bruun et al., 2003).

Lentivirus production.

Lentiviruses encoding either the Tet-Repressor protein (TetR) or shCtIP were generated in human 293FT cell line as previously described (Tiscornia et al., 2006). Briefly, 293FT cells were transfected with a lentiviral vector (pLenti6/TR or pLenti4-shCtIP) in combination with ViraPowerTM Packaging Mix using LipofectamineTM 2000 according to the manufacturers protocol (Invitrogen). Virus-containing supernatant was collected 72 h post-transfection and filtered through a sterile 0.45 μm low protein-binding filter (Millex-HV 0.45 μm PVDF, Millipore). The filtrated viral supernatant was aliquoted into 1.5 ml cryovials and stored at -80°C.

Generation of a stable MRC5 cell line with inducible shCtIP expression.

SV40-immortalized MRC5 cells were first transduced with viral supernatant harbouring pLenti6/TR and, 24 h later, infected with viral supernatant containing pLenti4/shCtIP. 48 h after the second transduction, cells were split at low confluency and grown in selection medium containing Blasticidin (5 μg/ml) and ZeocinTM (500 μg/ml) for 11 days. Antibiotic-resistant colonies were isolated, expanded and individual clones screened for doxycycline (DOX) -inducible expression of shCtIP by immunoblotting.

Generation of the stable U2OS cell lines expressing GFP-CtIP-S327A, -RRK/AAA or -RYIE/AAIA.

U2OS cells (40% confluent) were transfected with the pEGFP-C1 plasmid containing siRNA-resistant CtIP cDNA, harbouring corresponding mutations in the coding sequence, using FuGENE 6 (Roche). 24 h after transfection, standard medium was replaced with selection medium containing Genetecin® (G418, GIBCO, 500 μg/ml). The medium was replaced every 2-3 days and antibiotic-resistant colonies were isolated and screened for GFP-CtIP expression by both immunofluorescence microscopy and western blotting.

Immunofluorescence Microscopy

U2OS or MRC5^{shCtIP} cells grown on coverslips were either fixed directly in formaldehyde and permeabilized or pre-extracted for 5 min on ice before fixation in 4% formaldehyde (w/v) in PBS for 12 min as described previously (Sartori et al., 2007). After incubation with indicated primary and appropriate Alexa Fluor-488, -594 and -647 conjugated secondary antibodies (1:1'000) (Life Technologies), coverslips were mounted with Vectrashield® (Vector Laboratories) containing DAPI and sealed. Images were acquired on a Leica DMRB fluorescence microscope. Laser micro-irradiation was performed as described previously (Eid et al., 2010).

Metaphase spread analysis.

HEK293 cells were transfected with indicated siRNAs at a final concentration of 40 nM using Lipofectamine RNAiMax transfection reagent (Invitrogen). 48 hours later cells were either mock-treated or treated with MMC (25 ng/ml) for 20 hours. Prior to harvesting, cells were treated with Colcemid (Gibco) at a final concentration of 0.1

μg/ml for 1 hour. Then, cells were collected in a 15 ml Falcon tube and centrifuged at 200 g for 5 minutes. Cells were resuspended in 5 ml of a hypotonic KCl solution (0.075 M) and incubated for 10 minutes at 37°C. To fix the cells, 1 ml of fixing solution containing Methanol:Acetic acid (3:1) was added to the suspension, mixed and centrifuged at 200 g for 5 minutes. Then, cells were resuspended directly in fixing solution containing Methanol:Acetic acid (3:1), which was added dropwise, while gently vortexing, and spun down. This step was repeated twice. Finally, the cell pellet was resuspended in 0.5-1 ml Methanol:Acetic acid fixing solution depending on the density of the cell suspension. 20 μl (2 drops) of the cell suspension was dropped on a pre-wetted glass slide (45° tilted) from 30 cm distance. Slide was air-dried and DNA was stained with DAPI. Immunofluorescent images were acquired in the DAPI-channel using the Leica DMRB microscope with Leica DFC 360 FX camera and the Leica objective HCX PL AP0 100x.

To prepare metaphase spreads from MRC5^{shCtIP} cells, they were transfected with nontargeting or FANCD2 siRNA. 6 h after siRNA transfection, cells were cultivated in absence or presence of DOX (1 μg/ml) for 48 h. Cells were treated with MMC (20 ng/ml) for 20 h and with Colcemid at a final concentration of 0.1 μg/ml in the last 3 hours. Cells were harvested as described above.

Antibodies.

The primary antibodies used in this study are listed in a separate table below. Secondary HRP-conjugated anti-mouse and anti-rabbit antibodies were form GE-Healthcare and the HRP-conjugated anti-goat was from Santa Cruz Biotech. Alexa Fluor-488, -594, and -647-conjugated secondary antibodies were from Invitrogen.

Chemicals.

Mitomycin C (MMC), 8-Methoxypsoralen (8-MOP) and MG132 were purchased from Sigma. ATM inhibitor (KU-55933) was purchased from Tocris Bioscience. ATR inhibitor (VE-821) was provided by Vertex Pharmaceuticals (Abingdon, UK).

Immunoblotting, Immunoprecipitation, GST pulldown and Far-Western.

If not specified otherwise, cell extracts were prepared in Laemmli buffer (4% SDS, 20% glycerol, 120 mM Tris-HCl pH 6.8). Proteins were resolved by SDS–PAGE and transferred to nitrocellulose. Immunoblots were performed by using the appropriate antibodies and proteins visualized using the ECL detection system (Amersham).

For GST pulldown assays and immunoprecipitation assays, cells were lysed in either NP-40 extraction buffer (50 mM Tris-HCl, pH 7.5, 120 mM NaCl, 1 mM EDTA, 15 mM sodium pyrophosphate and 1 % NP-40 supplemented with phosphatase inhibitors (20 mM NaF, 1 mM sodium orthovanadate), protease inhibitors (1 mM benzamidine and 0.1 mM PMSF), deubiquitinase inhibitor (10 mM N-ethylmaleimide) and 10U Benzonase® (Roche)) or Triton X-100 buffer (50 mM Tris-HCl, pH 7.5, 200 mM NaCl, 1 mM EDTA, 0.2 % Triton X-100 supplemented with phosphatase, protease and deubiquitinase inhibitors) and clarified by centrifugation at 14000 rpm. GST pull-downs and immunoprecipitations were performed as described previously (Sartori et al., 2007). Far-western blot analysis was performed as described (Wu et al., 2007). Anti-GFP immunoprecipitates from HEK293T cells transfected with GFP-CtIP-wt or GFP-CtIP-ΔN were subjected to far-western analysis using recombinant HA-Ubiquitin (10 μg, Boston Biochem) as a probe followed by anti-HA immunoblotting.

Purification of recombinant human CtIP.

Insect Sf9 cells infected with FLAG-GST-CtIP-6H recombinant baculovirus were harvested 50 h after infection. The cell pellet was resuspended in lysis buffer (50 mM Tris-HCl, pH 7.5, 0.5 M NaCl, 0.1% NP-40, 10 % glycerol, 10 mM imidazole) supplemented with protease inhibitors (Roche). Cells were disrupted by douncer homogenization and cell debris was removed by centrifugation at 45K for 45 min at 4°C. Supernatant was filtered and loaded to Ni-NTA beads (Qiagen) overnight at 4°C. Beads were washed extensively with lysis buffer and lysis buffer supplemented with 60 mM imidazole and then protein was eluted using lysis buffer supplemented with 400 mM imidazole. Elution fractions were pooled, NaCl concentration was adjusted to 150 mM and loaded to heparin beads (GE Healthcare) for 90 min at 4°C. Heparin beads were washed with wash buffer (50 mM Tris-HCl, pH 7.5, 0.15 M NaCl, 0.1 % NP-40, 10 % glycerol) and proteins were eluted with elution buffer (50 mM Tris-HCl pH 7.5, 1 M NaCl, 0.1% NP-40, 10% glycerol). Elution fractions were pooled and dialyzed against dialysis buffer (50 mM Tris-HCl, pH 7.5, 0.15 M NaCl, 20% glycerol), aliquoted and stored at -80°C.

***In vitro* protein interaction.**

To analyze *in vitro* protein interaction between CtIP and FANCD2, GFP-FANCD2 wild-type or K561R mutant transiently expressed in HEK293T cells were immunoprecipitated with the anti-GFP antibody, coupled to Protein-A Sepharose beads (GE Healthcare) for 2 h at 4°C and immunocomplexes were stringently washed four times with NTEN buffer (0.5% NP- 40, 0.1 mM EDTA, 20 mM Tris-HCl, pH 7.4, 1 M NaCl). 0.5 μg of recombinant human FLAG-GST-CtIP-6His purified from Sf9 insect cells were incubated either alone or with GFP-fusion FANCD2 immunocomplexes bound to Protein-A Sepharose beads for 2 h at 4°C in 1 ml

TEN100 buffer (0.1 mM EDTA, 20 mM Tris-HCl, pH 7.4, 100 mM NaCl, 200 µg/ml BSA). Immunocomplexes were washed four times with NTEN350 buffer (0.5% NP-40, 0.1 mM EDTA, 20 mM Tris-HCl, pH 7.4, 350 mM NaCl), boiled in SDS-sample buffer and analyzed by SDS-PAGE followed by immunoblotting.

To analyze *in vitro* protein interaction between CtIP and ubiquitin, recombinant human FLAG-GST-CtIP-6His (0.2 µg) was incubated either alone or together with recombinant HA-Ubiquitin (5 µg, Boston Biochem) for 2 h at 4 C in the following buffer (20 mM HEPES, pH 7.5, 150 mM NaCl, 1 mM EDTA, 1 mM EGTA, 25 nM NaF, 1% Triton-X-100, 10% glycerol, 10 µM ZnCl2, 200 µg/ml BSA supplemented with EDTA-free protease inhibitor cocktail). The samples were subjected to immunoprecipitation using anti-HA antibody. Immunocomplexes were washed four times with NTEN250 buffer (0.5% NP-40, 0.1 mM EDTA, 20 mM Tris-HCl, pH 7.4, 250 mM NaCl), boiled in SDS-sample buffer and analyzed by immunoblotting.

***In vitro* Ubiquitin-binding assay.**

pET23-6xHis-ubiquitin wt vector (His-Ub wt, kind gift from Matthias Peter), I44A mutant or empty vector were grown in BL21-CodonPlus(DE3)-RIL Escherichia coli (Invitrogen) and protein expression was induced upon addition of 1 mM IPTG for 4 h at 37 °C. Proteins were solubilized in the lysis buffer containing 50 mM Tris-HCl, pH 7.5, 300 mM NaCl, 1 mM EDTA, 10 % glycerol, 1 % Triton X-100 and 20 mM imidazole supplemented with 1 mM DTT, 1 mM PMSF and EDTA-free protease inhibitor cocktail (Roche). His-Ub proteins were coupled to Ni-NTA Agarose (Qiagen), washed three times with lysis buffer supplemented with 500 mM NaCl and additional 20 mM imidazole, once with TEN100 buffer (20 mM Tris-HCl, pH 7.4, 0.1 mM EDTA and 100 mM NaCl) and incubated in TEN100 buffer supplemented with 1

mg/ml BSA for 30 min at 4 °C. Next, His-Ub proteins bound to Ni-NTA Agarose were incubated either with 1 mg of HeLa nuclear extract or with 1 mg of HEK293T lysates transiently expressing GFP-CtIP or GFP-CtIP-ΔN for 2 h at 4 °C in 1 ml of cell lysis buffer (20 mM HEPES, pH 7.5, 150 mM NaCl, 1 mM EDTA, 1 mM EGTA, 25 nM NaF, 1% Triton-X-100, 10% glycerol, 10 μM ZnCl2, supplemented with phosphatase inhibitors (20 mM NaF) and EDTA-free protease inhibitor cocktail). Beads were then washed once with NTEN300 buffer (0.5% NP-40, 0.1 mM EDTA, 20 mM Tris-HCl, pH 7.4, 300 mM NaCl), transferred to a new tube, washed another three times with NTEN300 and once with TEN100 buffer. Complexes were boiled in SDS sample buffer and analyzed by SDS–PAGE followed by immunoblotting.

***In Situ* Proximity Ligation Assay.**

In situ proximity ligation assay (PLA) in combination with immunofluorescence confocal microscopy was performed using Duolink II Detection Kit with anti-Mouse PLUS and anti-Rabbit MINUS PLA Probes, according to the manufacturer's instructions (Olink Bioscience) (Söderberg et al., 2006).

CellTiter-Blue® Cell Viability assay.

U2OS clones stably expressing siRNA-resistant forms of GFP-CtIP or MRC5^{shCtIP} cells were transfected with indicated siRNA. 48 hours post-transfection cells were seeded in triplicates at a density of 500 cells/well in 96 well plate. 24 h later cells were continuously treated with indicated doses of MMC and grown for 5 days at 37°C. To measure cell viability, CellTiter-Blue® reagent (Promega) was added on the last day, cells were incubated at 37°C for 4 h, and then fluorescence was measured at 560/590 nm.

PUVA treatment.

U2OS cells were incubated in PBS containing 10 μg/ml 8-MOP (Sigma) for 30 min. After incubation, cells were exposed to 10 kJ/m2 UV-A (365 nM, Vilber Lourmat Bio-Link BLX Crosslinker) in the presence of 8-MOP. Post-treatment PBS was removed and fresh media was added. At the indicated timepoints cells were harvested and proteins were analyzed by immunoblotting.

Supporting Table: Primary antibodies

Antibody target	Species	Supplier/Reference	Application*
pATM S1981	rabbit	2152-1 (Epitomics)	IB
ATR (N-19)	goat	sc-1887 (Santa Cruz)	IB
BRCA1 (D-9)	mouse	sc-6954 (Santa Cruz)	IB
BrdU	mouse	RPN202 (GE Healthcare)	IF
CHK1 (G-4)	mouse	sc-8408 (Santa Cruz)	IB
pCHK1 S345	rabbit	2341(Cell Signaling)	IB
CtIP (14-1)	mouse	gift from Richard Baer	IF
CtIP	rabbit	A300-488A (Bethyl)	IF (in situ PLA)
CtIP (D-4)	mouse	sc-271339 (Santa Cruz)	IB
ERCC1 (FL-297)	rabbit	sc-10785 (Santa Cruz)	IB
FAN1	sheep	gift from John Rouse	IB
FANCA	rabbit	A301-980A (Bethyl)	IB
FANCD2 (FI17)	mouse	sc-20022 (Santa Cruz)	IB and IF (in situ PLA)
FANCD2	rabbit	ab2187 (Abcam)	IF
FLAG	mouse	F3165 (Sigma)	IB
GFP	rabbit	ab290 (Abcam)	IP
GFP	mouse	sc-9996 (Santa Cruz)	IB
HA	mouse	sc-7392 (Santa Cruz)	IB and IP
γH2AX (20E3)	rabbit	9718 (Cell Signaling)	IB and IF
KAP1 pS824	rabbit	A300-767A (Bethyl)	IB
MRE11 (12D7)	mouse	GTX70212 (GeneTex)	IB
MUS81	mouse	M1445 (Sigma)	IB
NBS1 (1D7)	mouse	GTX70224 (GeneTex)	IB
Pol η	rabbit	ab17725 (Abcam)	IB
RIF1	rabbit	A300-569A (Bethyl)	IF
RPA2 (Ab-3)	mouse	NA19L (Calbiochem)	IB and IF
pRPA S4/S8	rabbit	A300-245A (Bethyl)	IB and IF
SLX4	rabbit	A302-270A (Bethyl)	IB
β-Tubulin (D-10)	mouse	sc-5274 (Santa Cruz)	IB
TFIIH p89 (S-19)	rabbit	sc-293 (Santa Cruz)	IB

*IB: Immunoblot, IF: Immunofluorescence, IP: Immunoprecipitation

SUPPLEMENTARY FIGURE LEGENDS

Figure S1 (related to Figure 1). CtIP localizes to ICL lesions in a FANCD2-dependent but NBS1- and SLX4-independent manner.

(**A**) U2OS cells were transfected with non-targeting (CNTL), CtIP or FANCD2 siRNA. 48 h after transfection, cells were treated for 24 h with mitomycin C (MMC) and survival was determined after eight days by colony formation. Data are presented as the mean ± SD (N=3). (**B**) Representative images of metaphase spreads from cells described in (C) after treatment with MMC (25 ng/ml) for 20 h. Selected chromosomal aberrations are displayed in higher magnifications. (**C**) U2OS cells were transfected with indicated siRNAs. 48 h after transfection, cells were treated for 24 h with MMC (120 ng/ml) and total and chromatin-bound proteins were analyzed by immunoblotting. (**D**) U2OS cells were transfected with different CtIP siRNAs. 48 h after transfection, cells were treated as in (C) and total proteins were analyzed by immunoblotting. Signal intensities of FANCD2 isoforms were quantified using Image J software and L/S indicates the ratio of monoubiquitinated (L) to non-monoubiquitinated (S) FANCD2. (**E**) U2OS cells were grown in absence (-) or presence (+) of 10 μg/ml 8-MOP for 30 min prior to UVA exposure and harvested at the indicated time points after PUVA treatment. RPA2 and P-RPA2 represent non-modified and hyperphosphorylated forms of RPA2, respectively. (**F,G**) U2OS cells were transfected with the indicated siRNAs. 48 h after transfection, cells were either mock-treated (-) or treated with PUVA and released for 4 h. Total and chromatin-bound proteins were analyzed by immunoblotting using the indicated antibodies. (**H**) FANCD2-mutant human fibroblasts (PD20F) and PD20F cells stably expressing either wild-type FANCD2 (wt) or the K561R mutant were grown on coverslips, mock-treated or treated as in (C), pre-extracted, fixed and co-immunostained for CtIP and γH2AX. (**I**) U2OS cells grown on coverslips were pre-treated for 2 h with DMSO or MG-132 (20 μM) and then treated with MMC (500 ng/ml) for 4 h.

Cells were pre-extracted, fixed and co-immunostained for CtIP and γH2AX. (**J,K**) U2OS cells were transfected with indicated siRNAs. 48 h after transfection, cells were treated as in (C) and total and chromatin-bound proteins were analyzed by immunoblotting. The arrow indicates a non-specific band detected by the anti-SLX4 antibody. In (C, D, F, G, J and K), the asterisks indicate hyperphosphorylated CtIP. In (C, F, G and J), D2 and D2-Ub represent non-ubiquitinated and monoubiquitinated forms of FANCD2, respectively. In (C, F, G, J, and K), TFIIH and CHK1 were used as loading controls for chromatin-enriched and soluble proteins, respectively. In (H and I), graphs show the percentage of γH2AX-foci positive cells displaying more than 10 CtIP foci. For each condition at least 100 cells were scored. Data are presented as the mean ± SD (N=2). In (H and I) scale bar, 10 μm.

Figure S2 (related to Figure 2). FANCD2 and CtIP promote resection during ICL repair.

(**A**) U2OS cells were treated with MMC (120 ng/ml) for the indicated time points and whole cell lysates were analyzed by immunoblotting. (**B**) U2OS cells were transfected with the indicated siRNAs. 48 h after siRNA transfection, cells were either mock-treated (-) or treated with PUVA, released for 2 and 4 h and harvested for immunoblot analysis. (**C-E**) U2OS cells were transfected with indicated siRNAs. 48 h after siRNA transfection, cells grown on coverslips were treated for 24 h with MMC (120 ng/ml), pre-extracted, fixed and either co-immunostained for RPA2 and RPA2-pS4/S8 (C), γH2AX and BrdU (D), or immunostained for RIF1 (E). Scale bar, 10 μm. (**F**) U2OS cells transfected with CtIP siRNA, were co-transfected with siRNA-resistant GFP-tagged CtIP wild-type (wt), T847A or S327A mutant CtIP 24 h post-siRNA transfection. 48 h post-siRNA transfection, cells were analyzed by immunoblotting prior to MMC treatment. (**G**) HEK293T cells were transfected with the indicated pEGFP-C1 expression vectors. After 48 h, cells were lysed in NP-40 buffer and

whole cell extracts (4 mg) were analyzed by immunoblotting before (Input) and after immunoprecipitation (IP) using anti-GFP antibody. Ponceau staining is shown to indicate the amounts of immunoglobulins (IgG) used in the IPs. (**H**) U2OS cells stably expressing empty vector (e.v.) or siRNA-resistant GFP-tagged wild-type CtIP (wt), T847A, or S327A mutant CtIP were transfected with CtIP siRNA for 72 h and whole cell extracts were analyzed by western blotting. (**I**) Same cells as in (H) were either mock-treated or continuously treated with MMC and the survival was determined after 5 days using the CellTiter-Blue® Cell Viability assay. Data are presented as the mean ± SD (N≥3).

Figure S3 (related to Figure 3). FANCD2-CtIP interaction requires FANCA but not SLX4 or FAN1.

(**A**) HEK293T cells were co-transfected with GFP-FANCD2 together with either empty vector or FLAG-CtIP. 48 h after transfection, cells were lysed in NP40 buffer and whole cell extracts were analyzed by immunoblotting before (Input) and after immunoprecipitation (IP) using anti-FLAG M2 affinity resin. Ponceau staining is shown to indicate the amounts of immunoglobulins (IgG) used in the IPs. (**B**) Coomassie-stained gel of recombinant FLAG-GST-CtIP-6His (0.5 µg) purified from Sf9 insect cells. (**C**) U2OS cells were transfected with indicated siRNAs. 48 h after siRNA transfection, cells were lysed and whole cell extracts were analyzed by immunoblotting. (**D**) Detection of endogenous CtIP-FANCD2 complexes by *in* situ PLA. Same cells as in (C) grown on coverslips were treated for 24 h with MMC (120 ng/ml) and pre-extracted prior to fixation. After incubation with antibodies against CtIP alone or against both CtIP and FANCD2, protein-protein interactions were detected using a fluorescently labeled probe (PLA-613). Scale bar, 20 µm. (**E**) Recombinant His-tagged ubiquitin (rHis-Ub) was immobilized on Ni-NTA agarose beads and incubated with whole cell extracts from HEK293T cells expressing GFP-SLX4 (*left*) or GFP-CtIP (*right*). Inputs

and precipitated bead fractions from the pull-downs were subjected to immunoblotting with anti-GFP antibody. Ponceau staining is shown to indicate the amounts of His-Ubiquitin used in the pull-down assays. (**F**) His alone (-) or recombinant wt and I44A mutant ubiquitin (rHis-Ub) coupled to Ni-NTA agarose beads were incubated with HeLa nuclear extracts (NE). Input and precipitated bead fractions from the pull-downs were subjected to immunoblotting. Ponceau staining is shown to indicate the amounts of rHis-Ub used in the pull-down assay.

Figure S4 (related to Figure 4). Identification and functional characterization of CtIP mutants impaired in FANCD2 interaction.

(**A**) Multiple sequence alignment of the putative FANCD2-interacting region in CtIP orthologs (amino acids 160-298) was performed using Clustal W (www.ebi.ac.uk/Tools/msa). PDSP, RRK, RYxE and ILV motifs are highlighted in black boxes. Other, highly conserved amino acid residues are marked in bold typeface. R177Q and Y186C represent two cancer-associated CtIP mutations recorded in the Catalogue of Somatic Mutations in Cancer (COSMIC*)* database (www.cancer.sanger.ac.uk). (**B**) U2OS cells were transfected with CtIP siRNA and after 24 h co-transfected with the indicated siRNA-resistant GFP-tagged CtIP constructs. 48 h post-siRNA transfection, cells grown on coverslips were treated for 24 h with MMC (120 ng/ml), fixed and immunostained for RIF1. Graphs show the percentage of GFP-positive cells displaying more than 10 GFP-CtIP foci and the percentage of GFP-positive cells displaying more than 10 RIF1 foci, respectively. For each condition at least 100 cells were scored. Data are presented as the mean ± SEM (N=2). (**C**) Same cells as in (B) were analyzed by immunoblotting. (**D**) U2OS cells stably expressing siRNA-resistant GFP-CtIP-wt, GFP-CtIP-RRK/AAA, or GFP-CtIP-RYIE/AAIA were transfected with CtIP siRNA and treated as in (D). 15 min after irradiation, cells were fixed, immunostained for γH2AX and analyzed by fluorescence microscopy. (**E**) U2OS cells stably expressing siRNA-resistant GFP-CtIP-wt

were transfected with indicated siRNAs. 24 h after siRNA transfection, cells grown on coverslips were sensitized with BrdU (10 μM) for 24 h prior to laser microirradiation. 30 min after irradiation, cells were fixed, co-immunostained for FANCD2 and γ-H2AX and analyzed by fluorescence microscopy. (**F**) Recombinant His-tagged ubiquitin (rHis-Ub) was immobilized on Ni-NTA agarose beads and incubated with whole cell extracts from HEK293T cells depleted of endogenous CtIP and expressing GFP-CtIP-wt or GFP-CtIP-ΔN (deleted of CtIP amino acids 153-322). Inputs and precipitated bead fractions from the pull-downs were subjected to immunoblotting with anti-GFP antibody. Ponceau staining is shown to indicate the amounts of rHis-Ub used in the pull-down assays. (**G**) Anti-GFP immunoprecipitates from HEK293T cells transfected with GFP-CtIP-wt or GFP-CtIP-ΔN were subjected to far-western analysis using recombinant HA-Ubiquitin as a probe followed by anti-HA immunoblotting. Ponceau staining is shown to indicate the amounts of proteins transferred onto the nitrocellulose membrane. In (B, D and E) scale bar, 5 μm.

Figure S5 (related to Figure 5). Analysis of CtIP/FANCD2 and CtIP/BRCA1 double-deficient cells in response to MMC treatment.

(**A**) FANCD2-deficient cells (PD20F) and PD20F stably expressing wild-type FANCD2 (D2) transfected with indicated siRNAs. 48 h post-siRNA transfection, cells were treated with the indicated doses of MMC for 24 h and survival was determined after eight days by colony formation. Data are presented as the mean ± SEM (N=3) (*left*). The same cells were analyzed by immunoblotting (*right*). (**B**) $MRC5^{shCtIP}$ cells were transfected with indicated siRNAs. 6 h post-siRNA transfection, cells were cultivated in the absence or presence of doxycycline (DOX, 1 μg/ml) for 48 h. Cells grown on coverslips were treated for 24 h with MMC (120 ng/ml), pre-extracted, fixed and immunostained for RIF1. Scale bar, 10 μm. (**C**) Representative images of metaphase spreads from cells described in (B) after treatment with

MMC (20 ng/ml) for 20 h. Selected radial chromosomes are displayed in higher magnifications. (**D**) MRC5^{shCtIP} cells were transfected with indicated siRNAs. 6 h post-siRNA transfection, cells were cultivated in the absence or presence of doxycycline (DOX, 1 µg/ml) for 48 h. Cells were continuously treated with the indicated doses of MMC and the survival was determined after 5 days using the CellTiter-Blue® Cell Viability assay. Data are presented as the mean ± SD (N=3) (*left*). The same cells were analyzed by immunoblotting (*right*).

Figure S6. CtIP-mediated resection counteracts ICL-induced DNA damage in a FANCD2-dependent and -independent manner.

Replication fork stalling at ICLs triggers activation of the ATR kinase resulting in monoubiquitination and stable association of the FANCD2-FANCI complex on chromatin. Monoubiquitinated FANCD2 recruits FAN1 and SLX4-associated nucleases to coordinate ICL incision giving rise to DSB intermediates. Translesion synthesis (TLS) polymerases bypass the unhooked crosslink and nucleotide excision repair (NER) removes the remaining adducts. Monoubiquitinated FANCD2 interacts with CtIP, thereby tethering it to damaged chromatin to ensure proper coordination of ICL processing and DNA-end resection. Once the DSB is formed, CtIP is phosphorylated by ATM kinase and promotes resection, thus initiating homologous recombination (HR), and, concomitantly antagonizing non-homologous end joining (NHEJ). In the absence of FANCD2, or in case of impaired activation of the FA-pathway, persistent ICLs trigger the conversion of stalled replication forks into DSBs, a process that is at least partially dependent on the endonucleolytic activity of MUS81. Also in this case, CtIP-dependent resection commits cells to error-free repair of DSBs, thus preserving genome stability in response to ICL damage.

Murina. Figure S1

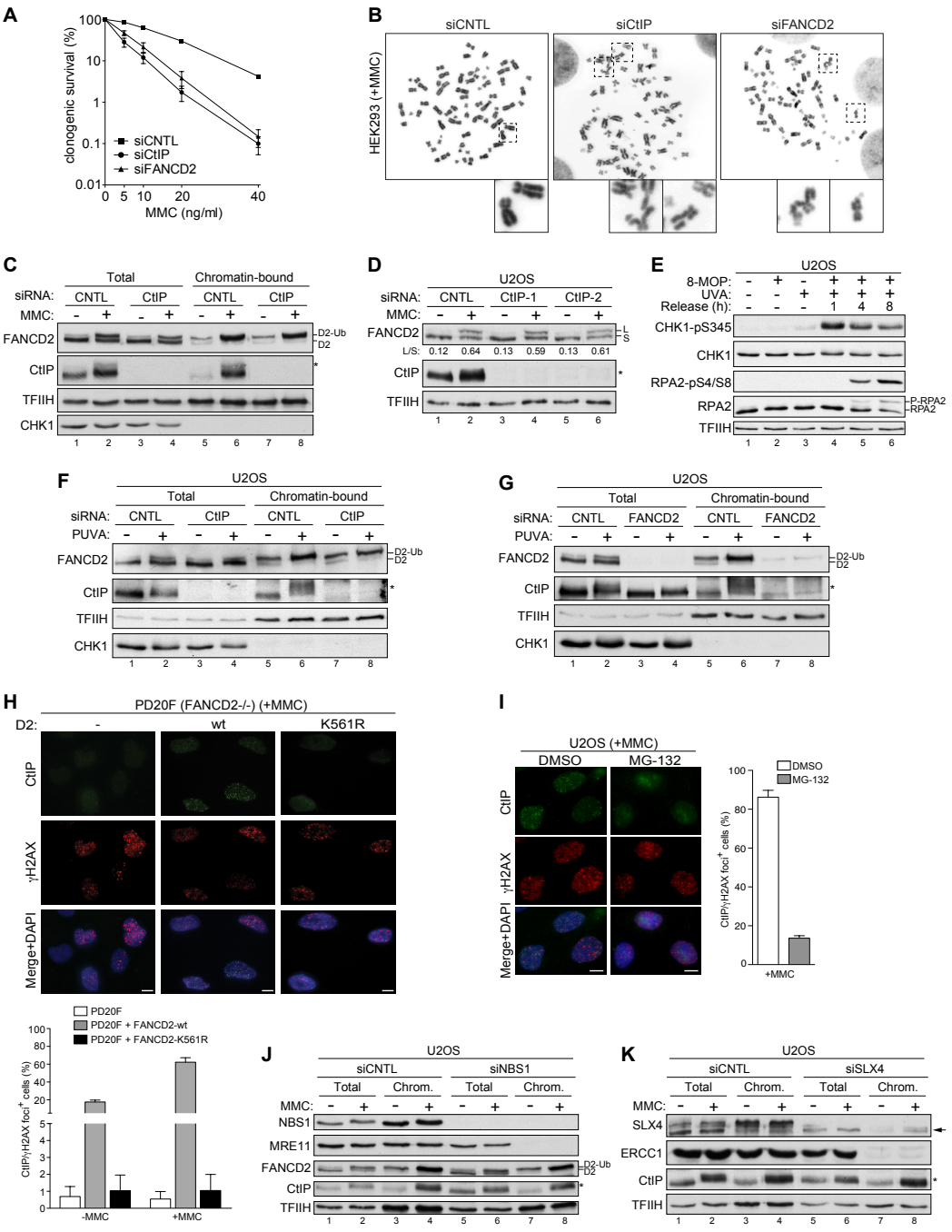

Murina. Figure S2

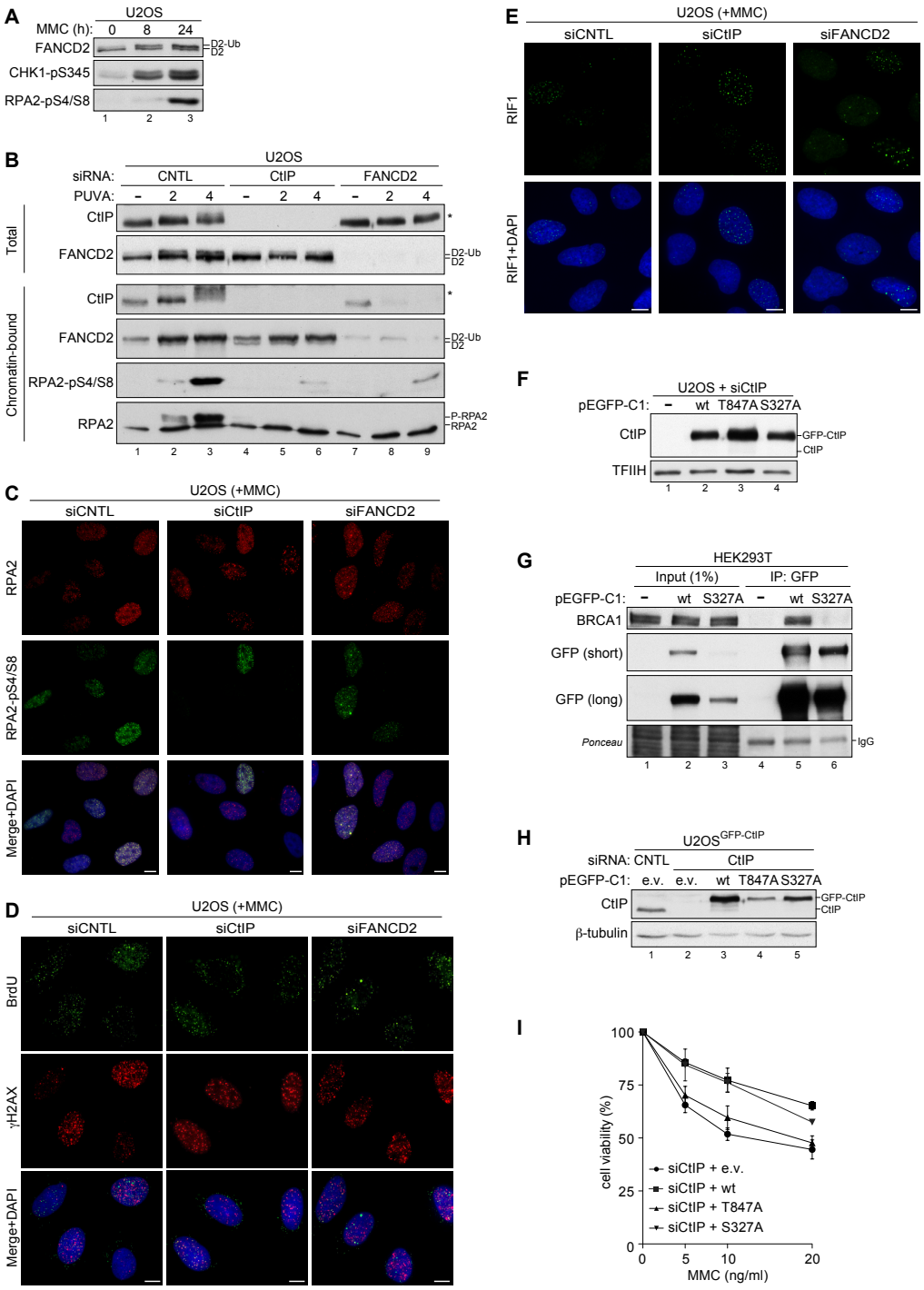

Murina. Figure S3

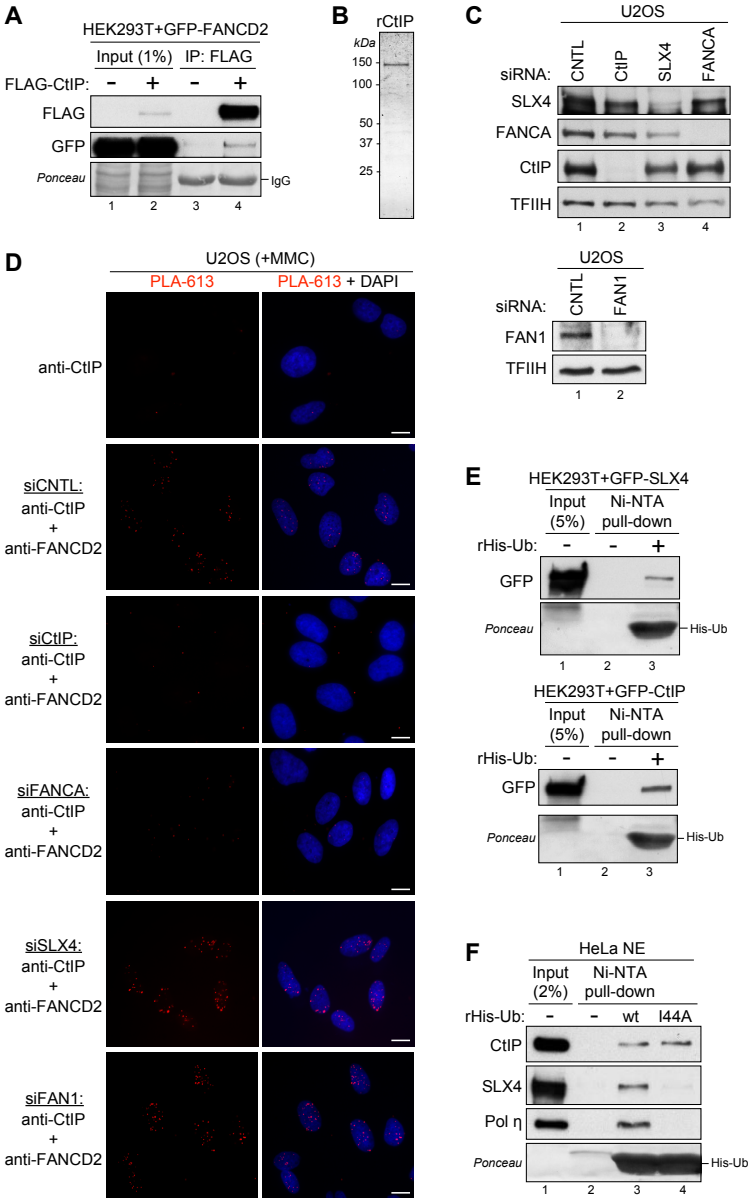

Murina. Figure S4

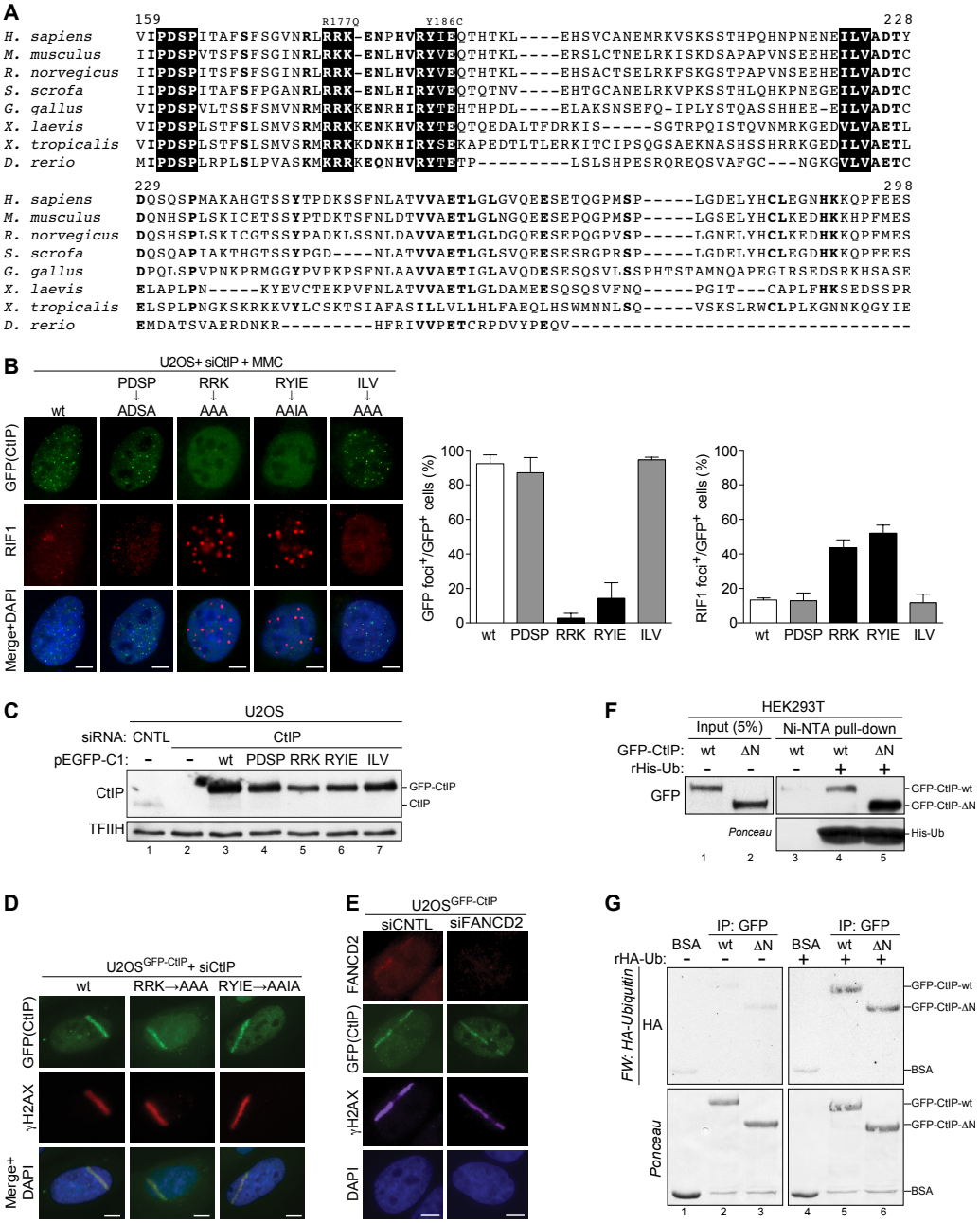

Murina. Figure S5

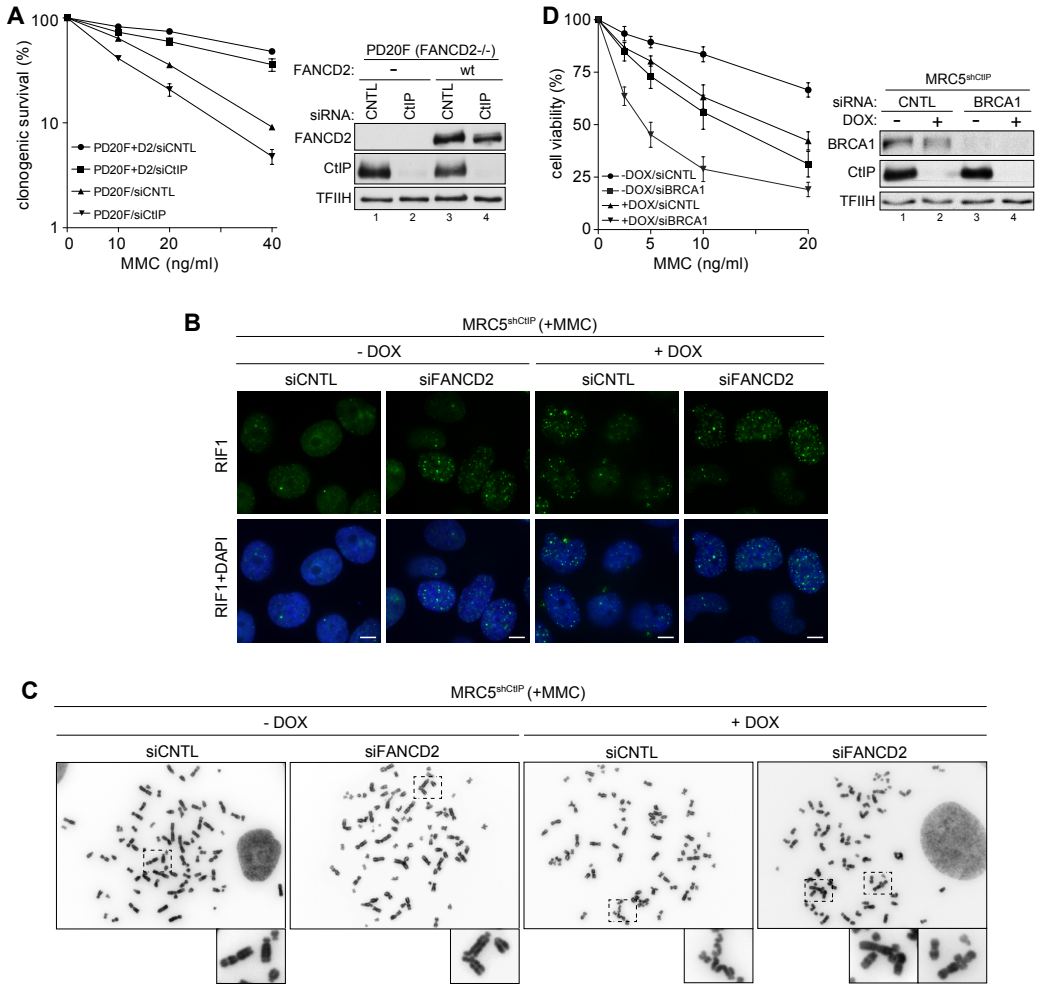

Murina. Figure S6

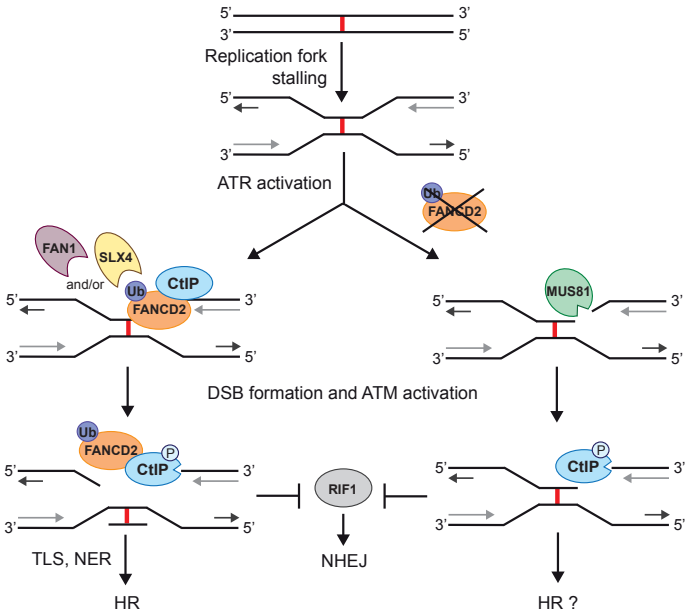

Supplemental References

Bruun, D., Folias, A., Akkari, Y., Cox, Y., Olson, S., and Moses, R. (2003). siRNA depletion of BRCA1, but not BRCA2, causes increased genome instability in Fanconi anemia cells. DNA Repair (Amst.) *2*, 1007–1013.

Eid, W., Steger, Martin, El-Shemerly, M., Ferretti, L.P., Peña-Diaz, J., König, C., Valtorta, E., Sartori, A.A., and Ferrari, S. (2010). DNA end resection by CtIP and exonuclease 1 prevents genomic instability. EMBO Rep. *11*, 962–968.

Kim, J.M., Kee, Y., Gurtan, A., and D'Andrea, A.D. (2008). FA core complex moves to chromatin. *111*, 4837–4838.

Kratz, K., Schöpf, B., Kaden, S., Sendoel, A., Eberhard, R., Lademann, C., Cannavo, E., Sartori, A.A., Hengartner, M.O., and Jiricny, J. (2010). Deficiency of FANCD2-associated nuclease KIAA1018/FAN1 sensitizes cells to interstrand crosslinking agents. Cell *142*, 77–88.

Neelsen, K.J., Zanini, I.M.Y., Herrador, R., and Lopes, M. (2013). Oncogenes induce genotoxic stress by mitotic processing of unusual replication intermediates. The Journal of Cell Biology *200*, 699–708.

Sartori, A.A., Lukas, C., Coates, J., Mistrik, M., Fu, S., Bartek, J., Baer, R., Lukas, J., and Jackson, S.P. (2007). Human CtIP promotes DNA end resection. Nature *450*, 509–514.

Söderberg, O., Gullberg, M., Jarvius, M., Ridderstråle, K., Leuchowius, K.-J., Jarvius, J., Wester, K., Hydbring, P., Bahram, F., Larsson, L.-G., et al. (2006). Direct observation of individual endogenous protein complexes in situ by proximity ligation. Nat. Methods *3*, 995–1000.

Steger, Martin, Murina, O., Hühn, D., Ferretti, L.P., Walser, R., Hänggi, K., Lafranchi, L., Neugebauer, C., Paliwal, S., Janscak, P., et al. (2013). Prolyl Isomerase PIN1 Regulates DNA Double-Strand Break Repair by Counteracting DNA End Resection. Mol Cell *50*, 333–343.

Stoepker, C., Hain, K., Schuster, B., Hilhorst-Hofstee, Y., Rooimans, M.A., Steltenpool, J., Oostra, A.B., Eirich, K., Korthof, E.T., Nieuwint, A.W.M., et al. (2011). SLX4, a coordinator of structure-specific endonucleases, is mutated in a new Fanconi anemia subtype. Nat Genet *43*, 138–141.

Svendsen, J.M., Smogorzewska, A., Sowa, M.E., O'Connell, B.C., Gygi, S.P., Elledge, S.J., and Harper, J.W. (2009). Mammalian BTBD12/SLX4 assembles a Holliday junction resolvase and is required for DNA repair. Cell *138*, 63–77.

Tiscornia, G., Singer, O., and Verma, I.M. (2006). Production and purification of lentiviral vectors. Nat Protoc *1*, 241–245.

Wu, Y., Li, Q., and Chen, X.-Z. (2007). Detecting protein-protein interactions by Far western blotting. Nat Protoc *2*, 3278–3284.

Yoo, H.Y., Kumagai, A., Shevchenko, A., Shevchenko, A., and Dunphy, W.G.

(2009). The Mre11-Rad50-Nbs1 complex mediates activation of TopBP1 by ATM. Mol. Biol. Cell *20*, 2351–2360.

You, Z., Shi, L.Z., Zhu, Q., Wu, P., Zhang, Y.-W., Basilio, A., Tonnu, N., Verma, I.M., Berns, M.W., and Hunter, T. (2009). CtIP Links DNA Double-Strand Break Sensing to Resection. Mol Cell *36*, 954–969.

3.2. Functional characterization of human RAD50S mutants in the DNA damage response

Establishing human cell lines stably expressing *RAD50* transgenes

A specific class of separation-of-function RAD50 point mutations, called rad50S, that led to the defects in meiosis, was first isolated in budding yeast and later described in fission yeast and mice [90,98,101,309]. However, the mechanisms underlying RAD50S phenotypes are still unknown. In order to investigate the functions of human *RAD50S*, we introduced the K22M mutation, corresponding to the *rad50-R20M* 'S' allele in *S. cerevisiae*, into a retroviral plasmid encoding wild-type (wt) *RAD50* cDNA [90]. The retroviral constructs containing *RAD50-wt* and *RAD50-K22M* cDNA were then used to complement an immortalized RAD50-deficient fibroblast cell line (F239). The F239 cell line was derived from a patient carrying hypomorphic mutations in both the maternal and the paternal *RAD50* alleles resulting in low levels of unstable RAD50 protein [47]. At first, we verified the expression levels of the individual MRN subunits in the stable cell lines. As expected, analysis of patient-derived F239 cells revealed extremely low level of RAD50 that was detected as a weak band corresponding to a larger RAD50 variant by western blotting (Figure 10A, lane 1). Both *RAD50-wt* and *RAD50-K22M*-complemented F239 cells displayed similar expression levels of RAD50 as well as increased MRE11 and NBS1 protein levels, indicating successful restoration of the MRN complex (Figure 10A, lane 2 and 3). Furthermore, we observed a rescue of the impaired nuclear localization of MRE11 compared to the parental F239 cells (Figure 10B).

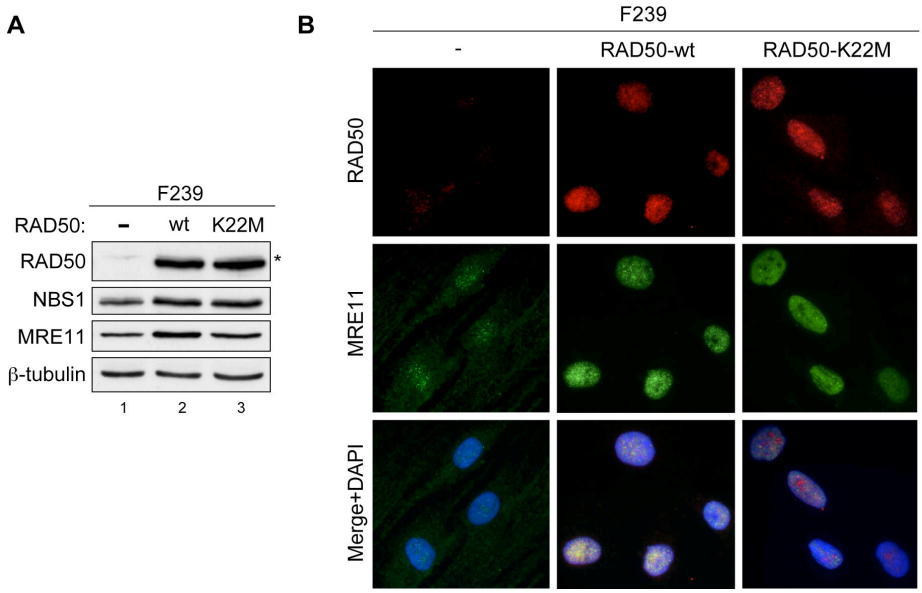

Figure 10. Analysis of RAD50, MRE11 and NBS1 expression levels in RAD50-wt- and -K22M-complemented F239 cell lines. (**A**) RAD50-deficient cell line (F239) and F239 cells stably expressing RAD50-wt or -K22M mutant proteins were lysed and subjected to western blot analysis. (**B**) Same cells as in (A) were grown on coverslips, fixed and co-immunostained for RAD50 and MRE11. The asterisk indicates a larger RAD50 variant in patient-derived F239 cells.

We also analyzed the potential impact of RAD50S mutation on the integrity of the MRN complex. Immunoprecipitation of MRE11 from F239 cells stably expressing either RAD50-wt or RAD50-K22M mutant demonstrated that the RAD50S mutation does not significantly alter the stoichiometry of the MRN complex (Figure 11).

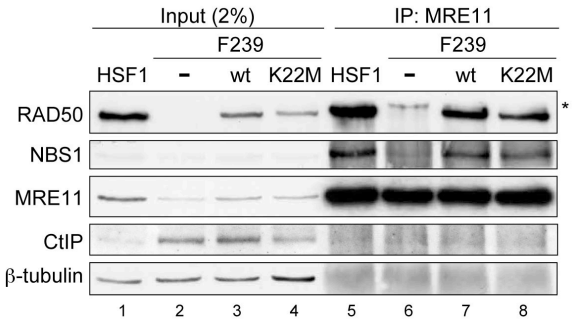

Figure 11. RAD50-K22M does not alter MRN complex formation. Normal human skin fibroblast cell line (HSF1), F239 and F239 cells expressing either RAD50-wt or -K22M mutant were lysed in RIPA buffer and whole cell extracts were subjected to immunoprecipitation using anti-MRE11 antibody. The asterisk indicates a larger RAD50 variant in patient-derived F239 cells detected in the anti-MRE11 immunoprecipitates.

DNA damage signaling and repair in cells expressing RAD50-K22M

In response to DSBs, MRN is required for the activation of ATM and downstream ATM-dependent signaling events [77,79]. RAD50-deficient cells displayed defective recruitment of both MRE11 and NBS1 to sites of IR-induced DSBs, thus leading to impaired ATM activation, radiosensitivity and chromosomal instability [47]. Thus, we next investigated whether complementation of F239 cells with RAD50 would restore MRE11 nuclear foci formation and ATM activation after irradiation. Indeed, we observed IR-induced RAD50 and MRE11 foci both in cells expressing RAD50-wt and -K22M mutant (Figure 12A). Furthermore, stable expression of RAD50 in F239 cells restored ATM autophosphorylation at serine 1981, a marker for ATM activation, to a similar level as compared to RAD50-proficient skin fibroblasts [18] (Figure 12B). Taken together, these data indicate successful complementation of RAD50-deficient cells and suggest that RAD50S (K22M) is proficient in promoting IR-induced activation of ATM.

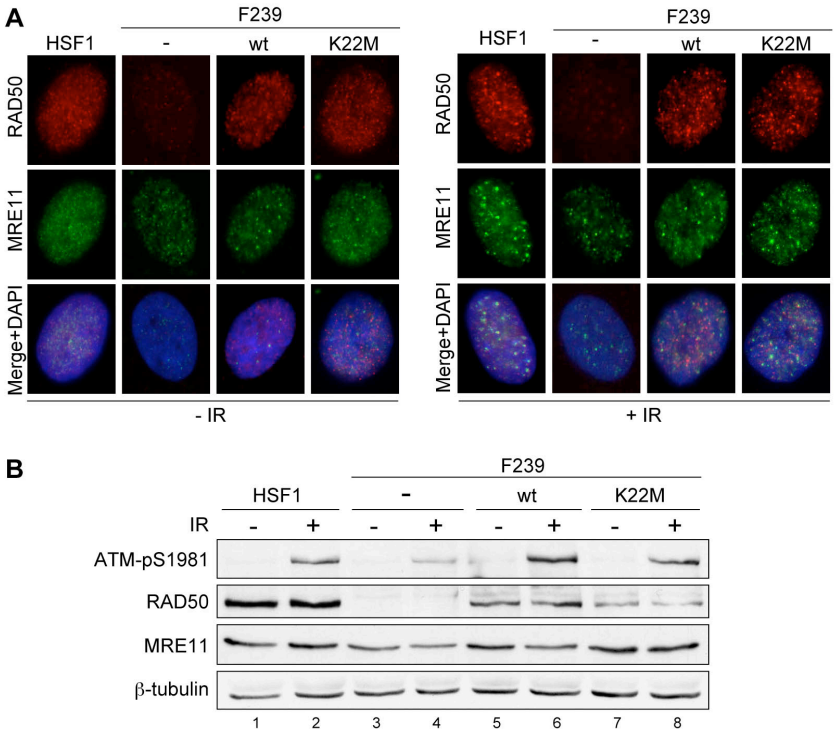

Figure 12. RAD50-K22M does not abrogate IR-induced MRN foci and ATM activation. (**A**) Normal human skin fibroblasts (HSF1), RAD50-deficient cell line (F239) and F239 cell line complemented with either *RAD50-wt* or *-K22M* mutant transgenes were grown on coverslips, pre-extracted before and 30 min after irradiation (5 Gy), fixed and co-immunostained for RAD50 and MRE11. (**B**) Same cells as in (A) were harvested for western blot analysis.

It was shown that mouse embryonic fibroblasts (MEFs) carrying *Rad50S* alleles display hypersensitivity to camptothecin (CPT) and etoposide (ETOP), inhibitors of topoisomerase I and II (Top I and Top II), respectively, indicative of defects in the repair of topoisomerase-mediated DNA damage [102]. To address the impact of RAD50S mutation on the processing of stabilized topoisomerase cleavage complexes in human cells, we analysed the sensitivity of complemented F239 cell lines to CPT and ETOP. Remarkably, while wild-type RAD50 restored the CPT and ETOP hypersensitivity of patient-derived F239 cells, RAD50-K22M cells exhibited increased sensitivity to both drugs (Figures 13A and 13B). Moreover, similar to Rad50S MEFs, human RAD50-K22M cells were slightly more sensitive to CPT- than to ETOP-induced damage [102]. Importantly, cells complemented with RAD50-K22M were only mildly sensitive to bleomycin, a radiomimetic drug inducing DSBs that are free of protein-DNA adducts [310], indicating a specific defect in the repair of topoisomerase-associated DNA damage in RAD50S mutant cells (Figure 13C).

We also noticed that proliferation of RAD50-deficient cells was strongly impaired compared to RAD50-proficient fibroblasts HSF1 (Figure 14). However, complementation with RAD50-wt or RAD50-K22M did not restore the reduced growth rate of F239 patient cells. Since RAD50 deficiency is associated with an increased spontaneous chromosomal instability [47], we speculated that mutations that have accumulated in cultured patient cells are most likely the cause of this slow growth phenotype which could not be rescued by re-expression of RAD50 protein.

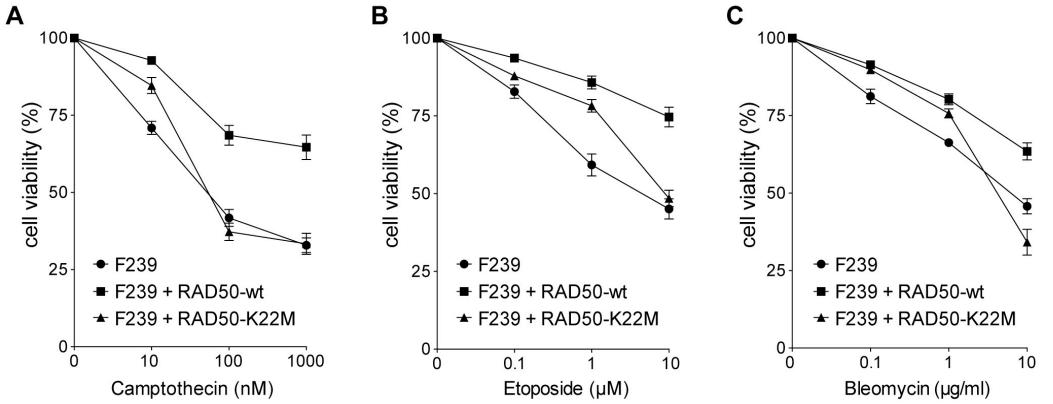

Figure 13. RAD50-K22M mutation confers camptothecin and etoposide hypersensitivity but only mild sensitivity to bleomycin. RAD50-deficient F239 cells (F239) and F239 cells expressing RAD50-wt or -K22M mutant were either mock-treated or continuously treated with indicated doses of camptothecin (**A**), etoposide (**B**) or bleomycin (**C**). Sensitivity was determined 5 days after treatment by CellTiter-Blue® Cell Viability assay. Data represent the mean ± SEM (N ≥ 3).

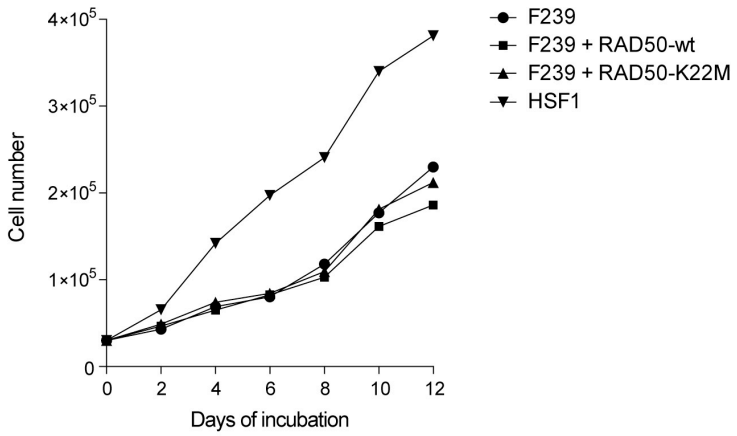

Figure 14. Growth curve of normal human skin fibroblasts (HSF1), F239 cells and F239 cells expressing either RAD50-wt or -K22M mutant. Cells were seeded in 6-well plates at a density of 3×10^4 cells per well and trypsinized every 48 h for cell number counting by a hemocytometer.

To address the mechanism underlying CPT hypersensitivity of human RAD50S cells, we examined whether DSB signaling is altered in F239 cells expressing RAD50-K22M mutant by analyzing the phosphorylation status of prominent DDR factors after CPT treatment. Taking into account the reduced proliferation rate of F239 cells, we incubated them with CPT, which is an S-phase specific drug, for 24 hours in order to increase the amount of S-phase cells exposed to DNA damage. Interestingly, K22M cells exhibited diminished CHK1 phosphorylation at serine 345, implying impaired ATR activation (Figure 15). Collaborative action of the MRN complex and Ctp1, the fission yeast orthologue of human CtIP, was reported to be involved in the removal of covalently

bound Top I complexes that are stabilized by CPT [98]. Moreover, MRN in conjunction with CtIP was shown to be required for the initiation of DNA-end resection and subsequent HR repair events in human cells [118]. We therefore analyzed RPA2 phosphorylation at serine 4 and serine 8, a marker for resection, in our cell lines and observed that resection was only partially restored in presence of the RAD50-K22M mutant (Figure 15). We also examined CtIP protein levels in complemented cell lines but did not detect any changes on western blots, thus excluding the possibility that impaired DNA-end resection in RAD50-K22M is related to reduced CtIP stability (Figure 15).

To substantiate our findings regarding a potential DSB processing defect caused by RAD50S mutation, we monitored CPT-induced RPA and RAD51 foci formation in our cell lines. Although we could not detect any major changes in the localization of RPA2 at sites of DSBs, RAD51 foci formation was diminished in cells expressing RAD50-K22M compared to cells complemented with RAD50-wt, indicative of impaired DNA-end resection and HR (Figure 16). Collectively, our data suggest that human RAD50-K22M does not affect MRN-dependent signaling and repair in response to IR but elicits a separation-of-function phenotype, exhibiting defects in the repair of DSBs caused by DNA topoisomerase poisons.

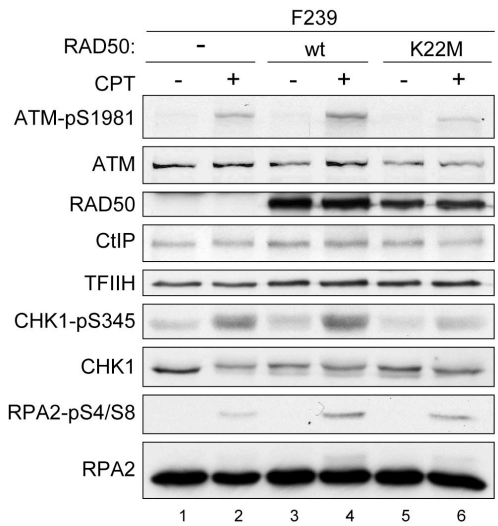

Figure 15. RAD50-K22M results in impaired ATR-mediated signaling in response to camptothecin. RAD50-deficient F239 cells and F239 cells complemented with RAD50-wt or -K22M mutant were either mock-treated or treated with camptothecin (CPT, 100 nM) for 24 h and then harvested for immunoblot analysis.

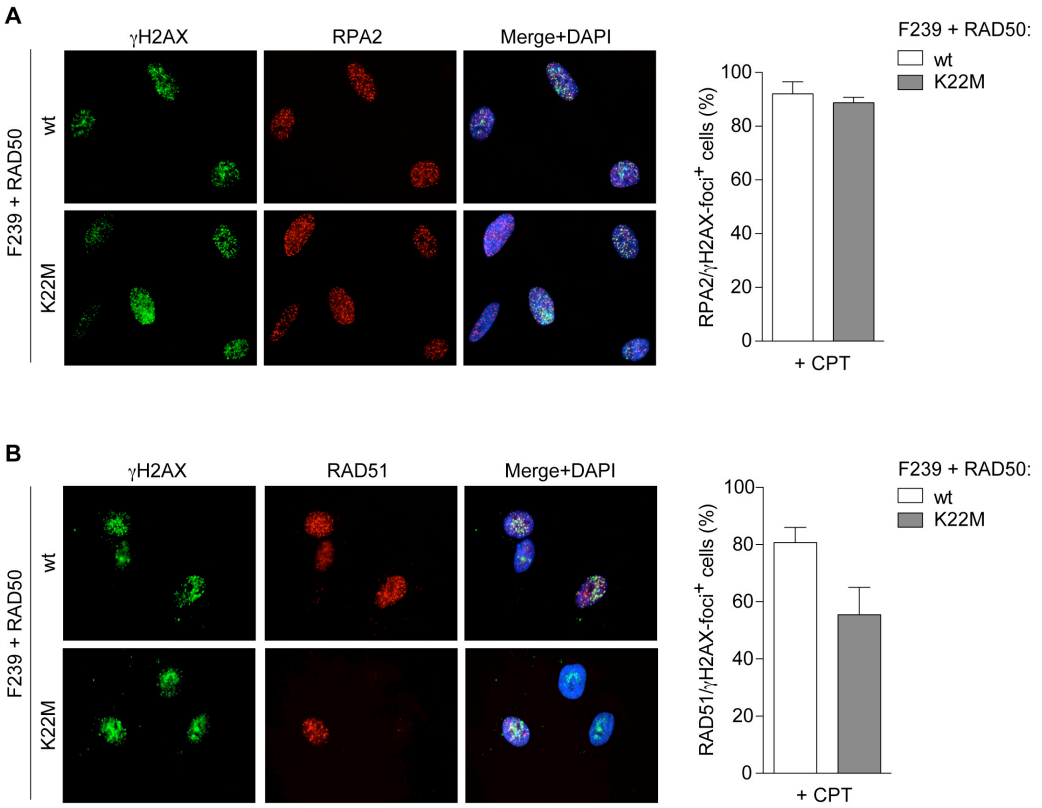

Figure 16. RAD51 foci formation is impaired in RAD50-K22M mutant cells. RAD50-deficient F239 cells and F239 cells complemented with RAD50-wt or -K22M mutant were grown on coverslips, treated with camptothecin (CPT, 100 nM) for 24 h, pre-extracted, fixed and co-immunostained for γH2AX and RPA2 (**A**) or RAD51 (**B**). Graphs show the percentage of γH2AX-foci positive cells displaying more than ten RPA2 (A) or RAD51 (B) foci. For each condition at least 100 cells were scored and data are presented as the mean ± SEM (N=2).

Characterization of F239 cells stably expressing *RAD50-R83I*, a second *'S'* allele

To determine whether impaired repair of topoisomerase-induced DNA damage is a general feature of cells expressing *RAD50S* mutants, we established an additional cell line stably expressing *RAD50-R83I,* corresponding to a second '*S*' allele in *S. cerevisiae*, *rad50-K81I* [90]. Although RAD50-R83I expression was reduced compared to RAD50-wt and K22M, increased stability of MRE11 confirmed successful restoration of the MRN complex in the R83I cell line (Figure 17A). Moreover, hypersensitivity to CPT of RAD50-R83I cells was comparable to that of K22M cells, indicating that defective processing of covalently bound Top I-DNA complexes is a general feature of cells expressing *RAD50S* alleles (Figure 17B). However, further experiments are needed to establish the pathological function of RAD50S in human cells.

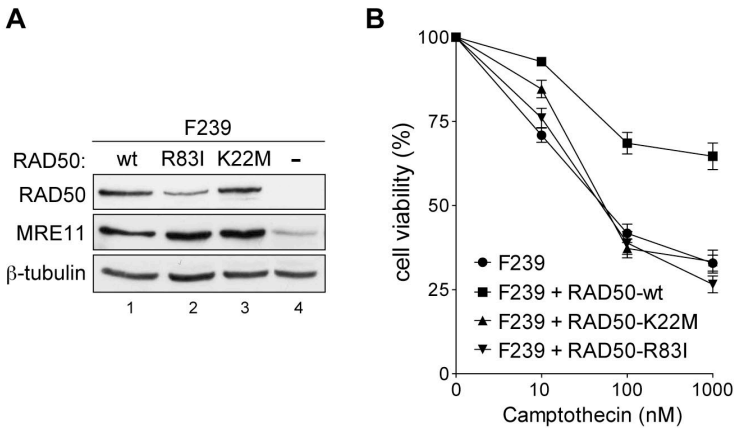

Figure 17. RAD50-R83I expression restores MRE11 levels but not camptothecin resistance. (**A**) RAD50-deficient F239 cells (F239) and F239 cells expressing RAD50-wt, -K22M or -R83I mutant were harvested for western blot analysis. (**B**) Same cells as in (A) were either mock-treated or continuously treated with indicated doses of camptothecin. Sensitivity was determined 5 days after treatment by CellTiter-Blue® Cell Viability assay. Data represent the mean ± SEM (N ≥ 3).

Investigating RAD50S functions at the molecular level

Based on the available structural and genetic data of RAD50, we speculated that RAD50S mutations may negatively affect the interaction between the MRN complex and CtIP, which would be consistent with a defect in DSB repair. We first examined the interaction between MRN and CtIP by co-immunoprecipitation experiments in the established cell lines. However, we could not detect CtIP in complex with MRN when we immunoprecipitated MRE11 from whole cell extracts (Figure 11). We thus used an alternative approach and addressed whether RAD50 directly interacts with CtIP *in vitro*. Furthermore, to test whether 'S' mutations may interfere with RAD50-CtIP association, we expressed GST-tagged RAD50 fragments (wt, K22M and R83I) containing the N-terminal globular domain of RAD50 (1-172 aa) in bacteria and analyzed their ability to pull-down CtIP from HeLa nuclear extracts. Interestingly, we observed that the binding of CtIP to both RAD50S mutants was reduced compared to RAD50-wt, indicating that RAD50 may indeed physically interact with CtIP and that K22M and R83I mutations weaken the interaction (Figure 18). Structural analysis revealed that MR exists as a heterotetramer (M2R2) *in vivo* [52]. However, the absence of both RAD50 and MRE11 in the pull-down samples suggests that the GST-RAD50 fragment does not interact with the MR complex and, thus, that CtIP binding is not mediated by the endogenous MRN complex.

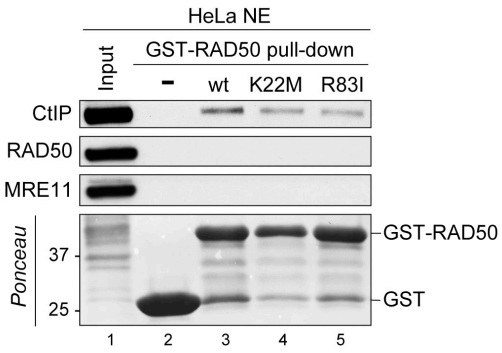

Figure 18. RAD50S mutations impair RAD50-CtIP interaction. GST-fusions proteins were coupled to glutathione sepharose beads and incubated with HeLa nuclear extract (NE). The precipitates were thoroughly washed and analysed by western blotting using indicated antibodies.

Impact of RAD50S mutations on homology-directed repair

Besides analyzing cellular phenotypes of cells expressing *RAD50S* mutant alleles, we addressed the potential impact of RAD50S mutations on the efficiency of homology-directed repair (HDR) using a HEK293-based GFP reporter assay [311]. The stably integrated DR-GFP reporter cassette consists of a full-length GFP gene (SceGFP) harboring a recognition site for the rare cutting endonuclease *I-SceI* and an internal GFP fragment (iGFP) (Figure 19A). Using the iGFP fragment as a template, repair of the *I-SceI*-generated DSB by homologous recombination leads to the restoration of a functional GFP gene, thus resulting in GFP-positive cells that are counted by flow cytometry. To test the effect of RAD50S mutants on HDR, we generated FLAG-tagged *RAD50-K22M* and *RAD50-R83I* expression constructs by site-directed mutagenesis of the plasmid harboring *RAD50-wt* cDNA. We also made a double *K22M/R83I* mutant that so far has never been described in either yeast or mammalian systems. Expression of K22M and K22M/R83I mutants resulted in a significant increase in HDR compared to the RAD50-wt protein, while expression of the R83I single mutant had no impact on the frequency of repair (Figure 19B). Given that *I-SceI* induces "clean" DSBs free of protein-DNA adducts, these data imply that RAD50S mutations do not impair processing of such DSBs and may even increase overall HDR efficiency. However, the experiments were performed in the presence of endogenous RAD50 protein that may attenuate the effect of RAD50S mutations on HDR. Therefore, alternative approaches such as the use of siRNA-resistant RAD50 expression constructs in RAD50-depleted HEK293 DR-GFP cells or an integration of the DR-GFP substrate directly in the established F239 cell lines are required to verify the effect of RAD50S mutants on HDR.

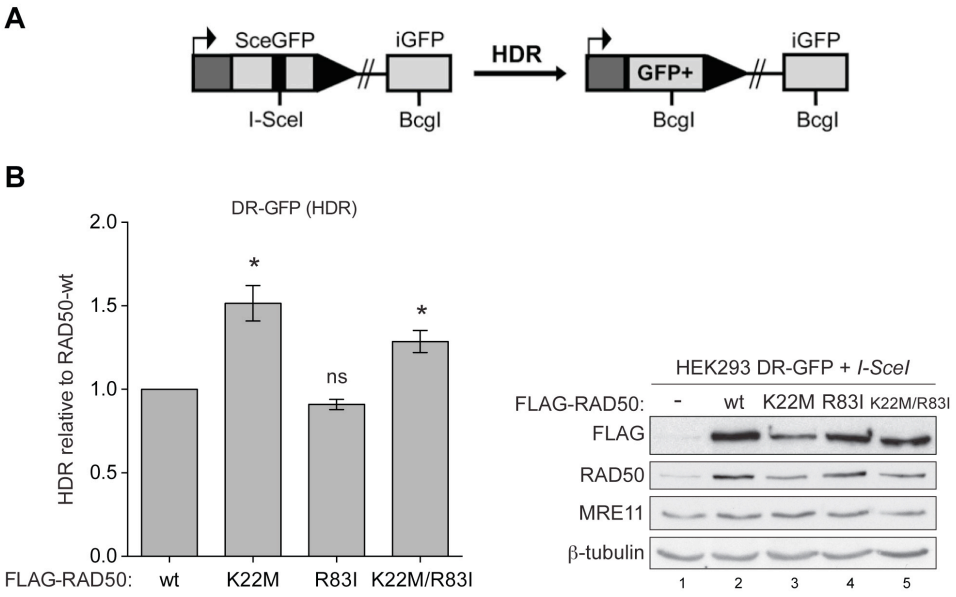

Figure 19. Analysis of RAD50S mutants with respect to homology-directed repair. (**A**) Scheme of the DR-GFP reporter along with the homology-directed repair (HDR) product that results in GFP-positive cells. (**B**) HEK293 DR-GFP cells were co-transfected with the *I-SceI* expression plasmid together with indicated FLAG-RAD50 plasmids and harvested after 48 h for flow cytometry (*left panel*) and immunoblot analysis (*right panel*). Data is represented as mean ± SEM (N=3), p values were calculated using paired t-test: *p < 0.05, ns (not significant).

Addressing the genetic interaction between RAD50 and CtIP in *Schizosaccharomyces pombe* (in collaboration with Dr. Edgar Hartsuiker and Dr. Rolf Kraehenbuehl, Bangor University, Wales, UK)

Nbs1 was shown to directly bind to phosphorylated Ctp1, the fission yeast ortholog of human CtIP, via its FHA domain, thereby promoting the recruitment of Ctp1 to DSBs and HR [66,70]. Remarkably, overexpression of Ctp1 rescued the DNA damage sensitivity of *nsb1-s10* and *nbs1 (R27A)* mutant strains harboring the functionally disruptive mutations in the FHA domain of Nbs1, but not of an *nbs1* null mutant [66,72]. These data suggested that overexpression of Ctp1 can circumvent the repair defects of Nbs1 mutant impaired in Ctp1 binding. Based on these observations, we hypothesized that overexpression of Ctp1 might also suppress the DNA damage sensitivity of a rad50S mutant strain. Therefore, we established collaboration with Dr. Edgar Hartsuiker and Dr. Rolf Kraehenbuehl (Bangor University, Wales, UK), experts in studying the role of the MRN complex in *S. pombe*. As expected, *rad50S (K81I)* mutant was hypersensitive to CPT, though to a lesser extent than *ctp1Δ, rad50Δ* or *ctp1Δ rad50Δ* strains [98] (Figure

20). Ctp1 overexpression restored CPT-hypersensitivity of *ctp1Δ* strain confirming the functionality of the expressed construct. However, overexpression of Ctp1 neither suppressed CPT-hypersensitivity of *rad50S* nor of *rad50Δ*. Importantly, Ctp1 expression specifically hindered the growth of strains lacking the functional Rad50 already in absence of exogenous damage, thus precluding the analysis of genetic interaction between Rad50S and Ctp1 in response to CPT. It is plausible that highly overexpressed Ctp1 lacks proper regulation that might be, at least partially, MRN-dependent. To reduce the adverse effect of strong Ctp1 expression on the cell proliferation, Ctp1 could be driven by a weaker promoter or the analysis could be performed in *ctp1Δ rad50S* background to decrease the levels of Ctp1 since the growth of *ctp1Δ rad50Δ* strain was improved compared to *rad50Δ* upon Ctp1 overexpression.

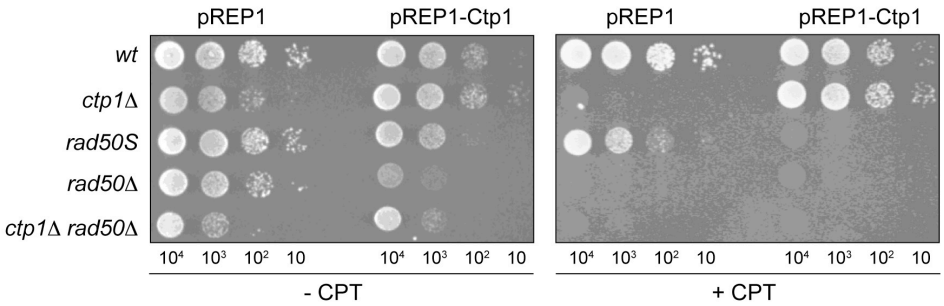

Figure 20. Analysis of RAD50S hypersensitivity to CPT upon Ctp1 overexpression in *S. pombe*. Indicated strains were transformed with a multicopy plasmid, pREP1, expressing Ctp1, or with an empty control plasmid. Replicates of serial dilutions of the indicated strains were spotted on control medium (*left panel*) or medium supplemented with 2.5 μM CPT (*right panel*) and grown at 30°C.

4. DISCUSSION

4.1. FANCD2 and CtIP cooperate to repair DNA interstrand crosslinks

Faithful repair of DNA interstrand crosslinks (ICLs) requires a complex cascade of signalling and repair events. Upon replication fork stalling in the vicinity of the ICL, ATR activation facilitates monoubiquitination of the FANCD2-FANCI (FANCD2-I) heterodimer by the FA core complex, a multi-subunit E3 ubiquitin ligase [12]. Monoubiquitinated FANCD2-I is targeted to damaged chromatin to coordinate subsequent ICL repair events, including incision of the crosslink and translesion synthesis [312]. Once a DSB intermediate is formed, FANCD2 is thought to regulate replication-coupled HR through its association with downstream FA proteins such as BRCA2/FANCD1 and PALB2/FANCN [12]. One of the critical steps of HR is DNA-end resection, however, its role in the context of ICL repair has been poorly characterized. Therefore, in the first part of my thesis, we investigated the functional interplay between DNA-end resection and the FA pathway in ICL repair by focusing on CtIP, a key factor of the resection and HR machinery.

We show that upon treatment of cells with ICL-inducing agents, monoubiquitinated FANCD2 tethers CtIP to damaged chromatin through a physical interaction with CtIP. This situation is reminiscent of the FAN1 nuclease, which is also recruited to ICL lesions by a direct interaction with monoubiquitinated FANCD2 [253,255,256]. However, in contrast to FAN1 implicated in ICL incision, our data strongly supports a key role for CtIP in the resection of DSBs generated during ICL repair. Indeed, we observed that ICL-induced RPA2 hyperphosphorylation and BrdU focus formation, both markers for single-stranded DNA regions, were reduced in CtIP-depleted cells. Furthermore, cells lacking FANCD2 displayed very similar phenotypes, indicating an unanticipated role for FANCD2 in promoting DNA-end resection. DSB intermediates are formed following the incision of the crosslink by SLX4-associated endonucleases and FAN1 [231]. Remarkably, depletion of SLX4 or FAN1 did not interfere with CtIP localization to damaged chromatin, suggesting that CtIP is recruited to ICLs before they get processed. However, as the precise mechanism of ICL incision has not yet been elucidated in detail and, potentially, there is a lot of redundancy between ICL processing enzymes, we cannot

completely exclude the possibility that CtIP is only recruited after DSB intermediates have been generated [237]. Of note, chronic MMC treatment that we applied has some limitations regarding the analysis of protein recruitment to ICL damage and is more conclusive with regards to the stable association or retention of proteins at the damage sites. One of the methods to address the sequential recruitment of the proteins to ICLs include generation of local damage by treatment of cells with psoralen followed by photoactivation with UVA laser (PUVA) and subsequent single cell analysis by immunofluorescence microscopy [313]. Alternatively, cells can be irradiated with UVA in the presence of psoralen and harvested at different time points for the analysis of protein recruitment to damaged chromatin [243]. We analyzed CtIP chromatin association in PUVA-treated cells and observed a time-dependent increase in levels of chromatin-bound CtIP. Furthermore, depletion of FANCD2 impaired CtIP localization to PUVA-induced lesions, thus confirming that FANCD2 anchors CtIP to the sites of ICL damage.

FANCD2 monoubiquitination is commonly used as readout to define which FA proteins act upstream of FANCD2 and hence participate in damage signaling, or are downstream and therefore are more likely to directly contribute to ICL repair [314]. Though FANCD2 monoubiquitination still efficiently occurred in cells lacking CtIP, we noticed slightly reduced levels of monoubiquitinated FANCD2 on damaged chromatin. CtIP has been recently implicated in the initiation of ICL repair at stalled forks prior to monoubiquitination of FANCD2 and ICL incision [308]. However, the effect of CtIP depletion on monoubiquitination of FANCD2 was only partial and not comparable to the reduction observed in absence of FA core complex or ATR kinase activity [247,250]. We thus suggest that CtIP is not required for FANCD2 monoubiquitination during ICL repair, but its lack leads to a negative feedback loop reducing FA pathway activation, which is similar to the effect observed in cells lacking XPF-ERCC1 complex [249].

FANCD2 as well as FA core proteins have been reported to directly regulate nucleases involved in ICL incision and TLS polymerases [231]. We therefore proposed that FANCD2 may tether CtIP to damaged chromatin to ensure that DNA-end resection and HR takes place at the right place and at the right time. Consistent with this idea, and together with the fact that DNA-end resection prevents NHEJ, the FA pathway has already been implicated in NHEJ inhibition [301,302,315]. For instance, FANCD2/I has been reported to possess nucleosome-assembly *in vitro*, which may sterically impede the access of the NHEJ machinery to DNA termini [315]. We observed that cells lacking

either CtIP or FANCD2 exhibited increased radial chromosome formation and RIF1 foci following MMC treatment, indicative of enhanced NHEJ activity. Remarkably, CtIP mutants impaired in FANCD2-binding also demonstrated elevated RIF1 foci, implicating a critical function of the CtIP-FANCD2 complex in resection and, thus, suppression of NHEJ. In analogy of the MRN-CtIP partnership involved in the processing of CPT-induced DSBs, the FANCD2-CtIP complex may cooperate in ICL processing. Interestingly, few reports have indicated that both Sae2, the yeast homologue of CtIP, and FANCD2 possess intrinsic endo- and exonuclease activities, respectively [142,302].

To restrict DNA-end resection to S/G2 phases, CtIP is 'activated' by CDK-mediated phosphorylation on several residues including S327 and T847 [120,131]. Remarkably, phosphorylation of CtIP on T847 appears to be a universal mechanism regulating CtIP function in resection, since ICL repair was impaired in CtIP-T847A mutant cells, displaying increased MMC-induced RIF1 foci and MMC hypersensitivity. On the other hand, phosphorylation of CtIP on S327, a prerequisite for CtIP-BRCA1 complex formation, turned out to be dispensable for the repair of ICLs. Consistent with our findings, isogenic mouse embryonic fibroblast cell lines expressing either Ctip-S326A mutant or Ctip wild-type displayed comparable levels of MMC hypersensitivity and chromosomal stability [132]. In contrast, however, it was shown that CtIP-BRCA1 interaction is required to suppress IR-induced RIF1 foci and plays an important role in the repair of topoisomerase-mediated DNA damage, indicating that further investigations are needed to clarify the significance of the CtIP-BRCA1 complex in DNA repair [132,133,152].

While CtIP acts with the MRN complex in the initial short-range resection of DSBs, subsequent long-range resection requires additional helicases and nucleases such as BLM, DNA2, or EXO1 [141,145]. FANCD2 was reported to interact with DNA2 and BLM, however the functional significance of these interactions has not been investigated [304,307]. To further define the role of FANCD2 in the regulation of DNA-end resection further, it would be important to address the relative contribution of these factors during ICL repair. The MRN complex is also required for the full activation of ATM kinase that in turn phosphorylates various target proteins including CtIP [73,74,78]. Remarkably, we noticed that CtIP is phosphorylated upon ICL-induced damage in an ATM-dependent manner. Interestingly, the efficient recruitment of CtIP to laser-induced DSBs was reported to require ATM kinase activity and a "damage recruitment (DR) motif" in the

middle part of CtIP [74] (see Figure 4). The authors proposed that ATM-dependent phosphorylation of CtIP unmasks the DR motif, which then mediates CtIP damage recruitment through its direct binding to the DSBs [74]. Based on our data, recruitment of CtIP to ICLs requires FANCD2, but still takes place upon ATM inhibition, implying that the DR motif of CtIP might play a minor role for its recruitment to crosslinks. Furthermore, the two short FANCD2-binding motifs that we identified within CtIP are located outside the DR region, indicating that DR motif is not sufficient for tethering CtIP to ICL-damaged chromatin. Emphasizing the potential differential regulation of CtIP following induction of ICLs compared to laser-induced DSBs, we show that FANCD2 is dispensable for CtIP localization at damage sites generated by laser micro-irradiation. Thus, the role of ATM-mediated phosphorylation of CtIP in the context of ICL repair still remains to be elucidated, but it may be required to facilitate resection function of CtIP after ICLs have been processed into DSBs similar to the classical HR pathway [73,74]. Notably, CtIP was also reported to undergo phosphorylation by ATR kinase in response to DSBs [134]. Given the major role of ATR-mediated signaling in processing of ICL-induced damage, it will be worth investigating the impact of ATR-dependent phosphorylation on CtIP in ICL repair.

Using a combined bioinformatics and experimental approach, we discovered two motifs in the N-terminus of CtIP (RRK (177-179 aa) and RYIE (185-188 aa)) required for FANCD2 binding, localization to MMC-induced foci and crosslink resistance. As these motifs reside in a highly conserved stretch of twelve amino acids, it is reasonable to think that they constitute a single interaction domain. However, the disruption of these motifs reduces CtIP-FANCD2 interaction without abolishing it, suggesting the involvement of additional regions in CtIP positioned outside the 177-188 aa stretch that can mediate the interaction. Interestingly, although CtIP and FANCD2 form a complex in unperturbed conditions, MMC treatment dramatically increase the interaction of CtIP with FANCD2 (*in situ* PLA), indicating that FANCD2 monoubiquitination may facilitate complex formation. The latter is akin to the situation with the FAN1 nuclease which binds monoubiquitinated FANCD2 through its ubiquitin-binding zinc finger (UBZ) domain [253-256]. Although bioinformatics analysis failed to predict any motifs resembling known UBDs in CtIP, we observed that CtIP directly interacts with ubiquitin *in vitro*. Moreover, CtIP was still able to recognize a mutant form of ubiquitin (I44A) that impairs most of the known UBD-mediated interactions [282,316]. Due to the structural and functional diversity of already characterized UBDs and the continuously increasing

number of newly identified ubiquitin-binding motifs, it is plausible that CtIP recognize ubiquitin by a unique novel mechanism [317,318]. Remarkably, a CtIP mutant lacking both FANCD2-interacting motifs was still proficient in ubiquitin binding. We thus speculate that CtIP may employ a dual mode of recognizing monoubiquitinated FANCD2, mediated by the RRK-RYIE motifs and a 'cryptic' ubiquitin-binding domain. Consequently, FANCD2-CtIP interaction may be reinforced by the ability of CtIP to recognize ubiquitin. Similar mechanism has been described for the recognition of monoubiquitinated PCNA by TLS polymerases such as Pol η or Pol ι that bind modified PCNA via both PIP-box and UBDs to provide a more specific interaction [282,316]. Alternatively, CtIP may recognize ubiquitin-moiety of other ubiquitinated DDR proteins localized on chromatin, and hence enhance its chromatin association [319]. Clearly, further investigations are needed to determine the role of CtIP-ubiquitin interaction in the DDR.

FANCD2 conformation is dynamic and can undergo changes upon DNA binding or monoubiquitination [320-322]. Thus, it is also reasonable to think that such structural changes in FANCD2 might expose the CtIP-binding surface on FANCD2 and thus stimulate CtIP-FANCD2 complex formation. According to our data, CtIP was still able to interact with a FANCD2-K561R mutant, albeit with lower efficiency compare to wild-type FANCD2, implying that CtIP may bind to a region other than the stretch containing monoubiquitinated lysine on FANCD2. Interestingly, FANCD2 contains a conserved acidic EDGE motif in its C-terminus which may be involved in protein-protein interactions [323]. Similar to cells lacking CtIP, cells expressing an EDGE mutant of FANCD2 are proficient in FANCD2 monoubiquitination and foci formation, but are hypersensitive to MMC, suggesting that this region is involved in the repair process downstream and independent of FANCD2 monoubiquitination [323]. It would be interesting to test whether the observed phenotype is caused by the impaired interaction between CtIP and FANCD2-EDGE mutant.

We noticed that CtIP mutants impaired in FANCD2-binding failed to form MMC-induced foci, but were still recruited to DNA damage sites generated by laser microirradiation, implying that FANCD2 promotes CtIP localization only to a subset of DNA lesions. Very recently, it has been reported that FANCD2 is required for the recruitment of CtIP to stalled and collapsed replication forks as well as to IR-induced lesions [324]. These data suggest that CtIP is recruited to chromatin in a FANCD2-

dependent manner both during DNA replication and DSB repair. However, given that the overall HR defect of cells lacking FANCD2 is milder that the one of CtIP-depleted cells, it is likely that FANCD2 specifically regulates CtIP-mediated DNA-end resection during HR repair of replication-associated DSBs, but plays a less significant role in the repair of other types of DSBs [118,247]. To address this question, it would be beneficial to analyze the recruitment of our CtIP mutants compromised in FANCD2-binding in response to different kinds of DNA damage and examine their ability to promote DNA-end resection and HR using reporter assays.

CtIP has been shown to interact with two tumor suppressor proteins: retinoblastoma and BRCA1 [108-110]. FANCD2 is also a tumor suppressor and besides cancer susceptibility of FA patients caused by mutations in FANCD2, loss or decrease in FANCD2 protein levels is associated with the development of sporadic cancers in non-FA patients [229,325]. Thus, based on our data, FANCD2 is the third tumor suppressor protein interacting with CtIP. Remarkably, R177Q and Y186C are two cancer-associated missense mutations in human CtIP recorded in the COSMIC database that map exactly to the region responsible for FANCD2 interaction, suggesting that CtIP-FANCD2 complex formation may be directly implicated in tumor suppression. Generation of mice expressing mutant CtIP and monitoring them for tumor development may be a valuable approach to assess the role of the CtIP-FANCD2 interaction in tumor suppression.

Interestingly, we repeatedly observed residual CtIP levels on chromatin in FANCD2-depleted and PD20F FANCD2-deficient cells, implying that small amounts of CtIP bind to chromatin independently of FANCD2 and thus may promote DNA-end resection in absence of FANCD2. Indeed, depletion of CtIP in cells lacking FANCD2 aggravates the phenotypes such as MMC hypersensitivity and aberrant NHEJ activity of cells lacking either factor alone, indicating that CtIP supports genome integrity in a FA-deficient background. Consistent with our findings, there is increasing evidence for FA-pathway independent functions of proteins that are otherwise recruited to ICLs by FANCD2. Increased crosslink sensitivity has been shown for FAN1-deficient patient cells depleted of FANCD2, indicating that FAN1, despite its direct association with monoubiquitinated FANCD2, can participate in the processing of ICLs in the absence of the FA pathway [326]. Likewise, enhanced MMC and cisplatin sensitivity was reported for chicken DT40 cells lacking both FA pathway and FAN1 or another FANCD2-interacting protein SLX4 [257,327]. Alternatively, only partial epistasis of CtIP and FANCD2 can result from additional role of FANCD2 in protecting stalled forks from degradation or, conversely,

by the recently proposed role of CtIP in resection upstream of FANCD2 [251,308]. Similarly, we observed non-epistatic relationships between CtIP and BRCA1 in the repair of ICL damage. BRCA1 is a multifunctional DDR protein that participates in various cellular processes, including HR and checkpoint control [205]. Furthermore, BRCA1 was reported to function independently of HR in crosslink repair by promoting optimal FANCD2 accumulation at the sites of ICL-induced damage [303]. Thus, we conclude that enhanced MMC sensitivity of CtIP/BRCA1-double depleted is probably caused by non-overlapping functions of two proteins in ICL repair, supporting the idea that CtIP-mediated DNA-end resection is important to alleviate the toxic effects of ICL damage in the absence of proficient FA/BRCA signaling pathway.

ICL-stalled replication forks frequently collapse into DSBs that can undergo resection and repair by HR or get misrepaired by NHEJ giving rise to chromosomal aberrations [234,265,328]. Accordingly, we observed that co-treatment of cells with MMC and a small molecule ATR inhibitor triggered increased formation of DSBs and enhanced ATM-dependent phosphorylation of CtIP and RPA2, indicative of elevated DNA-end resection [329]. Consequently, depletion of MUS81, an endonuclease implicated in the cleavage of stalled forks and DSB formation, significantly reduced CtIP phosphorylation, further supporting the role of CtIP in the resection of aberrant replication-associated DSBs [262,265]. Notably, it has been shown that HU-stalled forks collapse into DSBs upon ATR inhibition via SLX4-dependent endonuclease cleavage [330]. Given that SLX4 is a scaffold protein for several endonucleases such as XPF, MUS81 and SLX1, it would be interesting to test whether SLX4 depletion gives a stronger defect than depletion of MUS81 alone in cleavage of ICL-stalled forks in ATR-inhibited cells, and whether it further reduces CtIP phosphorylation. Remarkably, and in line with our data, CtIP-dependent processing of collapsed forks upon HU treatment was demonstrated to be beneficial for genome integrity and cellular survival in the absence of the FANCM translocase [331].

In summary, our findings highlight the complex interplay between CtIP-mediated DNA-end resection and the FA pathway and demonstrate that monoubiquitinated FANCD2 coordinates CtIP-dependent resection during ICL repair. Furthermore, they reveal the crucial role of CtIP in preserving genome integrity in response to ICL damage.

4.2. Characterization of human RAD50S mutants in the DNA damage response

In the second part of my thesis, we investigated molecular aspects of DNA-end resection in human cells by examining the phenotypes of separation-of-function (S) mutations in RAD50, a subunit of the MRN complex. Several studies highlighted the critical role of the MRN complex both in the removal of covalently attached proteins from DNA termini and in promoting DNA-end resection [41]. The most detailed evidence for the function of the MRN complex in this process came from analysis of meiosis in yeast [332]. The MRX complex is required for the clearance of meiosis-specific topoisomerase-like transferase Spo11 that remains covalently attached to 5'-ends after induction of the break [61,87]. Certain *Rad50* mutations that blocked Spo11 cleavage, but did not show any strong mitotic repair defects, were isolated more than 20 years ago and named "S" mutations for the separation of meiotic and mitotic functions [90]. The existence of such "S" mutations indicated the requirement of some specific functions of the MRN complex in meiosis. However, these mutations were not extensively characterized in budding yeast. Instead RAD50S mutations were modelled and analysed in fission yeast and mouse, but the molecular mechanisms underlying RAD50S phenotypes are still unclear [100]. Here, we provide the first phenotypic characterization of RAD50S mutations in human cells. Most of our analysis has been performed for human RAD50-K22M mutation since it is the only "S" mutation examined in mice [101]. Similar to the *RAD50S* alleles in *S. pombe* and mice, human *RAD50S* alleles caused cellular hypersensitivity to topoisomerase I and II inhibitors, CPT and ETOP [98,101-103]. These inhibitors stabilize topoisomerase I and II cleavage complexes leading to blocked DNA ends [97]. Consequently, these complexes have to be released from DNA to allow further DNA-end processing and repair. We observed a slight reduction in phosphorylated form of RPA2 in RAD50-K22M cells in response to CPT indicative of a DNA-end resection defect. The impairment of resection can be caused by the delay in the initial removal of Top I cleavage complexes from DNA or in the progression of DNA-end resection *per se*. Analysis of *Rad50S* alleles in fission yeast suggested that they might be defective in both Top I and Top II removal [98,99]. It will be interesting to check whether human RAD50S mutations demonstrate a similar defect. One of the approaches to address this question is to use DNA-linked protein detection (DLPD) assay that analyzes the presence of topoisomerases covalently bound to the DNA [333]. If this is the case, then the molecular mechanism of the removal of covalently attached protein complexes from DNA impaired

by RAD50S appears to be universal between different organisms. Notably, our preliminary data demonstrate reduced RAD51 foci formation in RAD50-K22M cells upon CPT treatment, suggesting a defect in HR. It is plausible that due to faulty DNA-end resection formation of RAD51 nucleoprotein filament is also compromised or delayed in these cells. Time course experiments will help to answer whether the appearance of CPT-induced RAD51 foci is delayed in RAD50S background.

The RPA-coated ssDNA arising from 5'-3' end resection of DSBs triggers activation of ATR-CHK1-mediated signaling, thus the MRN complex has been implicated in the ATR activation due to its role in resection [41]. We also noticed impaired CHK1 phosphorylation on S345 in RAD50S cells, indicative of attenuated ATR activation. Since the decrease in CHK1 phosphorylation is more profound in RAD50-K22M mutant cells than in RAD50-deficient parental cell line, it is tempting to speculate that RAD50S might impair some specific functions of the MRN complex required for ATR activation. Recently, several groups reported a direct contribution of the MRN complex to ATR-CHK1 activation via recruitment of TopBP1 in response to replication stress [334-336]. Further studies are required to establish if human RAD50S mutations indeed lead to a dominant negative phenotype in regards of ATR activation. Whereas there is no strong evidence for the impact of RAD50S mutations on ATR activation in other species, constitutive ATM-dependent signaling was reported for RAD50S alleles in mice and budding yeast [103,104]. However, we did not observe any significant changes in activation of ATM kinase as measured by autophosphorylation on S1981 in human RAD50-K22M cells. The unprocessed DNA damage accumulating in Rad50S background as evident from increased spontaneous chromosomal instability was proposed to be a trigger of chronic ATM activation and was further exacerbated by CPT treatment [101]. Thus, the analysis of chromosomal aberrations in human RAD50S cells in both unperturbed and CPT-treated cells can be useful to address the potential defects of RAD50S mutations in repair.

The integrity of the MRN complex is essential for the proper DNA-end resection and DDR [88]. However, RAD50-K22M mutation did not significantly alter the stability of the MRN complex. Moreover, RAD50S cells were proficient in MRN foci formation and activation of ATM kinase in response to IR, further confirming the functionality of the MRN complex. Remarkably, RAD50S mutations did not show any defect in the repair of *I-SceI*-induced "clean" DSBs that are free of protein-DNA adducts as measured by the

DR-GFP reporter assay. In addition, RAD50-K22M cells were only mildly sensitivity to bleomycin that induces DSBs, which also do not contain any proteins trapped to DNA ends. Therefore, these data suggest that RAD50-K22M mutation does not impede the ability of the MRN complex to repair DSBs *per se*, but specifically impairs processing of toxic protein-DNA adducts, implying the separation-of-function phenotype of human RAD50S mutation. In line with our observations, *RAD50S* alleles in fission yeast and mice did not show any profound sensitivity to the DSB-inducing agents except of Top I and Top II poisons [98,101-103].

It is still unclear why RAD50S mutant cells are predominantly hypersensitive to DNA topoisomerase poisons. Intriguingly, cells lacking CtIP, a partner of the MRN complex required for DNA-end resection, also demonstrate hypersensitivity to CPT and ETOP, but only mild sensitivity to IR [118,120]. Given that RAD50S mutations cluster on a surface patch predicted to form a conserved protein-protein interaction site and that cells lacking CtIP are phenotypically similar to cells expressing *RAD50S* mutant allele, we hypothesized that the MRN-CtIP interaction might be impaired by RAD50S mutations [52,118]. CtIP has been already reported to interact with individual subunits of the MRN complex [118,127]. However, we could not co-immunoprecipitate CtIP together with the MRE11 from whole cell lysates, probably due to the low abundance of CtIP protein. Indeed, when we used HeLa nuclear extracts that are enriched for nuclear proteins, we succeeded in detection of CtIP interaction with recombinantly expressed N-terminal part of RAD50. Remarkably, the presence of either RAD50S mutations, K22M or R83I, reduced this interaction. Though the interaction between CtIP and RAD50 was expected, the binding region on RAD50 has not been mapped so far [127]. We provide evidence that CtIP can interact with N-terminus of RAD50 and that RAD50S mutations impair CtIP-RAD50 association. Nevertheless, it still remains to be tested whether additional regions on RAD50 can mediate its binding to CtIP.

The collaborative action of the MRN complex and CtIP is required for DNA-end resection in different eukaryotes, however the molecular basis of DNA-end resection seems to be slightly distinct [141]. In budding yeast, resection is carried out by the MRX complex together with Sae2, which possesses intrinsic endonuclease activity [142]. However, no similar activity has been yet reported for any Sae2/CtIP orthologues from different species. On the other hand, Sae2 does not physically interact with the MRX complex, whereas human CtIP directly associates with MRN and stimulates its endonuclease activity [118,143]. Endonuclease activity of the MRN-CtIP (i.e. MRX-Sae2

in *S. cerevisiae*) complex is particularly important for the repair of the DSBs blocked by a protein adduct. In this case, endonuclease activity is required to create nicks in DNA flanking the DSB ends that allows subsequent resection by exonucleases [62]. Given that impairment of MRN-CtIP association by RAD50S mutations may interfere with the endonuclease activity of the complex, it is likely to impede the processing of toxic protein-DNA adducts. However, further biochemical analysis of RAD50S mutations is required to substantiate this hypothesis.

Fission yeast Ctp1 is more similar to CtIP than Sae2 in terms of its function in DNA-end resection [71,98]. Although biochemical data of Ctp1 interaction with RAD50 in *S. pombe* is missing, Ctp1 was shown to directly bind to Nbs1 in a phosphorylation-dependent manner [66,70]. Based on our preliminary *in vitro* data showing that RAD50S weakens CtIP binding, it is possible that a comparable interaction defect can be observed for Rad50S mutations in fission yeast. Besides pull-down experiments, a valuable approach to address the interaction between two proteins is to analyze the suppression of repair defects of the mutant protein by overexpression of its interaction partner [66,72]. However, we did not observe a rescue of CPT sensitivity in rad50S mutant strains by Ctp1 overexpression. Moreover, Ctp1 overexpression in fission yeast turned out to be detrimental for cell viability. Therefore, additional analysis is needed to address the interaction between CtIP/Ctp1 and RAD50 as well as the effect of RAD50S mutations on the CtIP-RAD50 complex formation. Importantly, retention of proteins at DSBs can influence subsequent repair steps [62,137]. Since the MRN complex and CtIP most likely act together on damaged chromatin, it will also be informative to explore the chromatin association of these factor in RAD50 wild-type and RAD50S background both in unperturbed and damaged cells.

Collectively, our data indicate that RAD50S mutations in human cells cause a defect in the repair of DSBs induced by DNA topoisomerase poisons and suggest that the underlying molecular mechanisms is associated with impaired interaction between RAD50 and CtIP.

5. CONCLUSIONS AND PROSPECTIVES

DNA repair mechanisms are essential for any organism to maintain the genome integrity and guarantee survival. DNA-end resection represents a major restriction point during DSB repair because it irreversibly commits cells to HR and counteracts NHEJ, thereby controlling the balance between the two pathways. Inappropriate repair of DSBs is a major source of gross chromosomal aberrations that can trigger carcinogenesis. Therefore, a detailed mechanistic understanding of how DNA-end resection is executed and how it is interconnected with other DNA repair mechanisms is of unquestioned relevance for cancer biology. Although a substantial progress has been made in the last decades in identifying new players of DNA-end resection, the functional significance of their genetic and biochemical interactions is still largely elusive.

The main focus of this thesis was on the human CtIP protein, an evolutionarily conserved DNA-end resection factor. We establish that CtIP is essential for the faithful repair of ICLs and that its DNA-end resection function is orchestrated by FANCD2, which tethers CtIP to damaged chromatin. Remarkably, this coordination is mainly achieved by a direct physical interaction between CtIP and FANCD2. Thus, our study is the first to demonstrate a critical role of a CtIP-FANCD2 complex during ICL repair. Given that FANCD2-deficient cells are impaired not only in ICL repair but also in HR, further analysis has to reveal whether the coordination of CtIP functions by FANCD2 represents a more general regulatory mechanism for DNA-end resection. We also provide evidence that CtIP binds to ubiquitin, indicating that CtIP may specifically interact with ubiquitinated substrates. However, based on our data, CtIP seems to employ a rather unique mode of ubiquitin recognition that does not involve any of the known ubiquitin-binding domains. Given the importance of ubiquitination in various DNA damage signaling and repair pathways, further work to establish the mechanism and the role of CtIP-ubiquitin interaction appears to be rewarding.

To date, 16 *Fanconi Anemia* (FA) complementation groups have been identified, but the molecular basis in some FA individuals is still unresolved. We find that depletion of CtIP leads to increased sensitivity to ICL-inducing agents and elevated chromosomal rearrangements, two key hallmarks of FA cells. However, no mutations in *CtIP* have so far been reported in unclassified FA patients and it still remains to be elucidated whether *CtIP* is a *FA* gene.

New insights into the functional interplay between FA and HR repair pathways are also of considerable medical relevance. Epigenetic silencing and somatic mutations with subsequent loss of heterozygosity of *FA* genes in non-FA patients are reported to be one of the frequent triggers of tumorigenesis [229,337]. Referring to the concept of synthetic lethality, inactivation of compensatory pathways such as intact cell cycle checkpoints and HR was shown to be particularly deleterious for these cells, and hence may significantly broaden the therapeutic strategies to selectively target FA-deficient tumors [338-340]. We observe that CtIP depletion enhances the cytotoxicity of MMC in FA-pathway deficient cells. Thus, one could foresee that targeted inhibition of CtIP function or possibly its interaction with FANCD2 might potentiate chemotherapy that is based on ICL-inducing agents. However, due to the current lack of structural and biochemical data of CtIP, the generation of potent small molecule inhibitors will take some time. Thorough investigation of the DNA-end resection machinery, its interactome and regulation are areas of future interest that will extend our understanding of the DNA damage response mechanisms and their clinical applications.

6. MATERIALS AND METHODS

FANCD2 and CtIP cooperate to repair DNA interstrand crosslinks

Please find Materials and Methods in the manuscript (section 3.1.).

Functional characterization of human RAD50S mutants in the DNA damage response

Cell lines and tissue culture

RAD50-deficient (F239) cells immortalized with human telomerase reverse transcriptase (hTERT) were grown in DMEM supplemented with 15% fetal calf serum, 100 U/ml penicillin and 100 μg/ml streptomycin as described previously [47]. F239 cells expressing *RAD50* transgenes were maintained in the above medium supplemented with 500 μg/ml of Geneticin (G418, GIBCO). The amphotropic Phoenix packaging cells, DR-GFP HEK293 cells and hTERT-immortalized human skin fibroblasts (HSF1) were grown in DMEM medium, 10% fetal calf serum, 100 U/ml penicillin and 100 μg/ml streptomycin. All cells were maintained at 37°C with 6% CO2.

Plasmids

The pCLNXS retroviral expression vector containing full-length, wild-type human *RAD50* cDNA was kindly provided by Yaniv Lerenthal (Tel Aviv University, Israel) and described previously [47]. The pcDNA3.1-based expression vector harboring FLAG-tagged *RAD50* cDNA was a kind gift from Martin F. Lavin (University of Queensland, Australia) [341]. The pGEX-4T1-RAD50 plasmid containing N-terminal domain of RAD50 (1-172 amino acids) was constructed by cloning polymerase chain reaction (PCR) product into pGEX-4T1 vector (Amersham) using EcoRI and XhoI restriction enzymes (New England Biolabs). RAD50S mutations were introduced by site-directed mutagenesis using Expand Long Template PCR System (Roche) and the following primers: RAD50-K22M forward 5'-GACAAAGATA**T**GCAAATTATCACTTTCTTCAGC-3', RAD50-K22M reverse 5'-GTGATAATTTGC**A**TATCTTTGTCCTCTATTCCA-3'; RAD50-R83I forward 5'-AGCCCAGATT**AT**TCTGCAATTTCGTGATGTCAAT-3', RAD50-R83I reverse 5'-

CGAAATTGCAGAA**T**AATCTGGGCTCTCACATCTGT-3'. All constructs were verified by DNA sequencing.

Retroviral production

Retroviruses encoding *RAD50* transgenes were generated in amphotropic Phoenix packaging cell line as described previously [342]. Briefly, Phoenix cells plated in 100 mm tissue culture dishes and grown for 24 h were transfected with 10 µg of retroviral pCLNXS plasmids bearing *RAD50* transgenes using standard calcium phosphate method. 10 h later medium was replaced. Virus-containing supernatant was collected 48 h post-transfection and filtered through a sterile 0.45 µm low protein-binding filter (Millex-HV 0.45 µm PVDF, Millipore). The filtrated viral supernatant was immediately used for infection or aliquoted into 1.5 ml cryovials and stored at -80°C.

Generation of stable F239 cell lines expressing *RAD50* transgenes

The parental RAD50-deficient F239 fibroblasts were transduced with viral supernatant that harbored pCLNXS vectors containing *RAD50* transgenes. Polybrene was added to a final concentration of 8 µg/ml and cells were incubated at 37°C. 24 h later medium was replaced. 48 h after transduction F239 cells were split and grown in selection medium containing 500 µg/ml of Geneticin (G418, GIBCO). Antibiotic-resistant bulk cell lines were established within 6 weeks. The expression levels of *RAD50* transgenes were analyzed by immunobloting.

Immunofluorescence microscopy

F239 parental cells and F239 cells expressing *RAD50* transgenes grown on coverslips were either fixed directly in formaldehyde and permeabilized or pre-extracted to remove non-chromatin bound proteins for 5 min on ice before fixation in 4% formaldehyde (w/v) in PBS for 12 min as described previously [118]. After washing with PBS, coverslips were blocked in PBS with 3% fetal calf serum for 1 h. Following incubation with indicated primary and appropriate Alexa Fluor-488 and -594 conjugated secondary antibodies (1:1'000), coverslips were mounted with Vectrashield® (Vector Laboratories) containing DAPI and sealed. Images were acquired on a Leica DMRB fluorescence microscope.

Immunoblotting and Immunoprecipitation

If not specified otherwise, cell extracts were prepared in Laemmli buffer (4% SDS, 20% glycerol, 120 mM Tris-HCl pH 6.8). Proteins were resolved by SDS–PAGE and transferred to nitrocellulose (GE Healthcare). Immunoblots were performed by using the appropriate primary and secondary antibodies. Proteins were visualized using the ECL detection system (Amersham).

For immunoprecipitation assays, cells were lysed in RIPA buffer (50 mM Tris-HCl, pH 7.4, 1% NP-40, 0.25% Na-deoxycholate, 150 mM NaCl, 1 mM EDTA and 0.1% SDS) supplemented with phosphatase inhibitors (20 mM NaF, 1 mM sodium orthovanadate) and protease inhibitors (1 mM benzamidine and 0.1 mM PMSF). Extracts were clarified by centrifugation at 14'000 rpm. Immunoprecipitating anti-MRE11 antibodies were added to the supernatant and incubated at 4°C overnight (O/N). After additional 2 h incubation with Protein A Sepharose beads (GE Healthcare), precipitated immunocomplexes were washed four times in lysis buffer (containing 0.5% NP-40, without SDS), boiled in SDS sample buffer and loaded on an SDS-polyacrylamide gel. Proteins were analyzed by immunoblotting, as described above.

GST pull-down assay

GST-RAD50 fusion constructs were grown in BL21 (DE3) *Escherichia coli* (Invitrogen) and proteins were expressed by incubation at 16°C for 20 h after the addition of 100 mM IPTG (AppliChem). Proteins were purified from soluble extracts with glutathione Sepharose 4 fast flow beads (GE Healthcare). GST fusion proteins bound to glutathione beads were mixed with 1 mg of HeLa nuclear extract pretreated with 1 mM ATP at 30°C for 30 min and incubated for 2 h at 4°C in 1 ml of IP buffer (20 mM HEPES-KOH, pH 7.5, 0.2 mM EDTA, 100 mM KCl, 0.5 mM PMSF, 0.5 mM DTT). Beads were then washed four times with NTEN150 buffer (0.05% NP-40, 0.1 mM EDTA, 20 mM Tris-HCl, pH 7.4, 150 mM NaCl) and twice with TEN100 (20 mM Tris-HCl, pH 7.4, 0.1 mM EDTA and 100 mM NaCl). Samples were boiled in SDS sample buffer and analyzed by SDS-PAGE followed by immunoblotting.

Antibodies

The primary antibodies are indicated in Table 2. Secondary HRP-conjugated anti-mouse and anti-rabbit antibodies were form GE-Healthcare. Alexa Fluor-488 and -594-conjugated secondary antibodies were from Invitrogen.

Table 2. Primary antibodies.

Antibody target	Species	Supplier/Reference	Application*
ATM (2C1)	mouse	GTX70103 (GeneTex)	IB
pATM S1981	rabbit	2152-1 (Epitomics)	IB
CHK1 (G-4)	mouse	sc-8408 (Santa Cruz)	IB
pCHK1 S345	rabbit	2341(Cell Signaling)	IB
CtIP (D-4)	mouse	sc-271339 (Santa Cruz)	IB
FLAG	mouse	F3165 (Sigma)	IB
γH2AX (JBW301)	mouse	05-636 (Millipore)	IF
γH2AX (20E3)	rabbit	9718 (Cell Signaling)	IF
MRE11 (12D7)	mouse	GTX70212 (GeneTex)	IB and IF
MRE11	rabbit	NB100-142 (Novus)	IP
NBS1 (1D7)	mouse	GTX70224 (GeneTex)	IB
RAD50 (13B3)	mouse	GTX70228 (GeneTex)	IB and IF
RAD51 (H-92)	rabbit	sc-8349 (Santa Cruz)	IF
RPA2 (Ab-3)	mouse	NA19L (Calbiochem)	IB and IF
pRPA S4/S8	rabbit	A300-245A (Bethyl)	IB
β-Tubulin (D-10)	mouse	sc-5274 (Santa Cruz)	IB
TFIIH p89 (S-19)	rabbit	sc-293 (Santa Cruz)	IB

*IB: Immunoblot, IF: Immunofluorescence, IP: Immunoprecipitation

Chemicals

Camptothecin (CPT), etoposide (ETOP) and bleomycin were purchased from Sigma.

Ionizing radiation

Exposure to ionizing radiation was carried out with a Faxitron X-ray machine (Faxitron X-ray).

Proliferation assay

HSF1, F239 and F239 cells expressing *RAD50* transgenes were seeded in duplicates at a density of 3×10^4 cells per well in 6-well plates and grown under standard conditions. Cells were trypsinized every 48 h for cell number counting by a hemocytometer under microscope during 12 days.

CellTiter-Blue® Cell Viability assay

F239 parental cells and F239 cells expressing *RAD50* transgenes were seeded in triplicates at a density of 1'500 and 3'000 cells/well in 96 well plate. 24 h later cells were continuously treated with the indicated doses of camptothecin, etoposide or bleomycin and grown for 5 days at 37°C. CellTiter-Blue® reagent (Promega, 20 µl/well) was added on the last day, cells were incubated at 37°C for 4 h, and then fluorescence was measured at 560/590 nm.

Homology-directed repair (HDR) reporter assay

HDR repair efficiency was measured in DR-GFP HEK293 cell line as described previously [311]. In brief, cells were co-transfected with 0.6 µg of pcDNA3.1 vector or 0.6 µg of *I-SceI* expression plasmid (pCBASce) together with 0.6 µg of indicated FLAG-tagged RAD50 constructs using 2.4 µl of JetPrime (Polyplus). 4 h after *I-SceI* transfection, the media was replaced. 48 h later cells were analyzed for GFP expression by flow cytometry on a CyAn ADP 9 (Dako).

Yeast Strains and Techniques

Standard procedures, media for propagation and genetic manipulations and *S. pombe* strains used for sensitivity assays were described previously [98,343]. Briefly, indicated strains transformed with a multicopy expression vector pREP1 either empty or carrying $Ctp1^{+}$ were spotted as serial dilutions on control medium or medium containing 2.5 µM CPT and grown for 4 days at 30°C.

Statistics

Statistical analyses were carried out using unpaired, two-tailed t tests. p values expressed as $*p < 0.05$ were considered significant. ns indicates that the difference between the two groups is not significant.

7. REFERENCES

1. Hoeijmakers JH. Genome maintenance mechanisms for preventing cancer. Nature. 2001 May 17;411(6835):366–74.
2. De Bont R, van Larebeke N. Endogenous DNA damage in humans: a review of quantitative data. Mutagenesis. 2004 May;19(3):169–85.
3. Schär P. Spontaneous DNA damage, genome instability, and cancer--when DNA replication escapes control. Cell. 2001 Feb 9;104(3):329–32.
4. Ciccia A, Elledge SJ. The DNA damage response: making it safe to play with knives. Mol. Cell. 2010 Oct 22;40(2):179–204.
5. Hoeijmakers JHJ. DNA damage, aging, and cancer. N. Engl. J. Med. 2009 Oct 8;361(15):1475–85.
6. Bartek J, Lukas J, Bartkova J. DNA damage response as an anti-cancer barrier: damage threshold and the concept of 'conditional haploinsufficiency'. Cell Cycle. 2007 Oct 1;6(19):2344–7.
7. Robertson AB, Klungland A, Rognes T, Leiros I. DNA repair in mammalian cells: Base excision repair: the long and short of it. Cell. Mol. Life Sci. 2009 Mar;66(6):981–93.
8. Jiricny J. The multifaceted mismatch-repair system. Nat. Rev. Mol. Cell Biol. 2006 May;7(5):335–46.
9. Schärer OD. Nucleotide excision repair in eukaryotes. Cold Spring Harb Perspect Biol. 2013 Oct;5(10):a012609.
10. Chapman JR, Taylor MRG, Boulton SJ. Playing the end game: DNA double-strand break repair pathway choice. Mol. Cell. 2012 Aug 24;47(4):497–510.
11. Prakash S, Johnson RE, Prakash L. Eukaryotic translesion synthesis DNA polymerases: specificity of structure and function. Annu. Rev. Biochem. 2005;74:317–53.
12. Kim H, D'Andrea AD. Regulation of DNA cross-link repair by the Fanconi anemia/BRCA pathway. Genes Dev. 2012 Jul 1;26(13):1393–408.
13. Rouse J, Jackson SP. Interfaces between the detection, signaling, and repair of DNA damage. Science. 2002 Jul 26;297(5581):547–51.
14. Jackson SP, Bartek J. The DNA-damage response in human biology and disease. Nature. 2009 Oct 22;461(7267):1071–8.
15. Cimprich KA, Cortez D. ATR: an essential regulator of genome integrity. Nat. Rev. Mol. Cell Biol. 2008 Aug;9(8):616–27.
16. Shiloh Y. ATM and related protein kinases: safeguarding genome integrity. Nat. Rev. Cancer. 2003 Mar;3(3):155–68.
17. Rupnik A, Lowndes NF, Grenon M. MRN and the race to the break. Chromosoma. 2010 Apr;119(2):115–35.
18. Bakkenist CJ, Kastan MB. DNA damage activates ATM through intermolecular autophosphorylation and dimer dissociation. Nature. 2003 Jan

30;421(6922):499–506.

19. Burma S, Chen BP, Murphy M, Kurimasa A, Chen DJ. ATM phosphorylates histone H2AX in response to DNA double-strand breaks. J. Biol. Chem. 2001 Nov 9;276(45):42462–7.

20. Matsuoka S, Ballif BA, Smogorzewska A, McDonald ER, Hurov KE, Luo J, et al. ATM and ATR substrate analysis reveals extensive protein networks responsive to DNA damage. Science. 2007 May 25;316(5828):1160–6.

21. Falck J, Mailand N, Syljuåsen RG, Bartek J, Lukas J. The ATM-Chk2-Cdc25A checkpoint pathway guards against radioresistant DNA synthesis : Article : Nature. Nature. 2001 Apr 12;410(6830):842–7.

22. Chehab NH, Malikzay A, Appel M, Halazonetis TD. Chk2/hCds1 functions as a DNA damage checkpoint in G(1) by stabilizing p53. Genes Dev. 2000 Feb 1;14(3):278–88.

23. Karlsson-Rosenthal C, Millar JBA. Cdc25: mechanisms of checkpoint inhibition and recovery. Trends Cell Biol. 2006 Jun;16(6):285–92.

24. Malumbres M, Barbacid M. Cell cycle, CDKs and cancer: a changing paradigm. Nat. Rev. Cancer. 2009 Mar;9(3):153–66.

25. Wold MS. Replication protein A: a heterotrimeric, single-stranded DNA-binding protein required for eukaryotic DNA metabolism. Annu. Rev. Biochem. 1997;66:61–92.

26. Cortez D, Guntuku S, Qin J, Elledge SJ. ATR and ATRIP: partners in checkpoint signaling. Science. 2001 Nov 23;294(5547):1713–6.

27. Zou L, Elledge SJ. Sensing DNA damage through ATRIP recognition of RPA-ssDNA complexes. Science. 2003 Jun 6;300(5625):1542–8.

28. Zhao H, Piwnica-Worms H. ATR-mediated checkpoint pathways regulate phosphorylation and activation of human Chk1. Mol. Cell. Biol. 2001 Jul;21(13):4129–39.

29. Liu Q, Guntuku S, Cui XS, Matsuoka S, Cortez D, Tamai K, et al. Chk1 is an essential kinase that is regulated by Atr and required for the G(2)/M DNA damage checkpoint. Genes Dev. 2000 Jun 15;14(12):1448–59.

30. Kastan MB, Bartek J. Cell-cycle checkpoints and cancer. Nature. 2004 Nov 18;432(7015):316–23.

31. Huen MSY, Chen J. The DNA damage response pathways: at the crossroad of protein modifications. Cell Res. 2008 Jan;18(1):8–16.

32. Hanahan D, Weinberg RA. Hallmarks of cancer: the next generation. Cell. 2011 Mar 4;144(5):646–74.

33. Negrini S, Gorgoulis VG, Halazonetis TD. Genomic instability--an evolving hallmark of cancer. Nat. Rev. Mol. Cell Biol. 2010 Mar;11(3):220–8.

34. McGranahan N, Burrell RA, Endesfelder D, Novelli MR, Swanton C. Cancer chromosomal instability: therapeutic and diagnostic challenges. EMBO Rep. 2012 Jun;13(6):528–38.

35. Lengauer C, Kinzler KW, Vogelstein B. Genetic instability in colorectal

cancers. Nature. 1997 Apr 10;386(6625):623–7.

36. Loeb LA. Mutator phenotype may be required for multistage carcinogenesis. Cancer Res. 1991 Jun 15;51(12):3075–9.

37. Halazonetis TD, Gorgoulis VG, Bartek J. An oncogene-induced DNA damage model for cancer development. Science. 2008 Mar 7;319(5868):1352–5.

38. Bartkova J, Horejsi Z, Koed K, Krämer A, Tort F, Zieger K, et al. DNA damage response as a candidate anti-cancer barrier in early human tumorigenesis. Nature. 2005 Apr 14;434(7035):864–70.

39. Williams RS, Williams JS, Tainer JA. Mre11-Rad50-Nbs1 is a keystone complex connecting DNA repair machinery, double-strand break signaling, and the chromatin template. Biochem. Cell Biol. 2007 Aug;85(4):509–20.

40. Williams GJ, Lees-Miller SP, Tainer JA. Mre11-Rad50-Nbs1 conformations and the control of sensing, signaling, and effector responses at DNA double-strand breaks. DNA Repair (Amst.). 2010 Dec 10;9(12):1299–306.

41. Stracker TH, Petrini JHJ. The MRE11 complex: starting from the ends. Nat. Rev. Mol. Cell Biol. 2011 Feb;12(2):90–103.

42. Xiao Y, Weaver DT. Conditional gene targeted deletion by Cre recombinase demonstrates the requirement for the double-strand break repair Mre11 protein in murine embryonic stem cells. Nucleic Acids Research. 1997 Aug 1;25(15):2985–91.

43. Luo G, Yao MS, Bender CF, Mills M, Bladl AR, Bradley A, et al. Disruption of mRad50 causes embryonic stem cell lethality, abnormal embryonic development, and sensitivity to ionizing radiation. Proc. Natl. Acad. Sci. U.S.A. 1999 Jun 22;96(13):7376–81.

44. Zhu J, Petersen S, Tessarollo L, Nussenzweig A. Targeted disruption of the Nijmegen breakage syndrome gene NBS1 leads to early embryonic lethality in mice. Curr. Biol. 2001 Jan 23;11(2):105–9.

45. Carney JP, Maser RS, Olivares H, Davis EM, Le Beau M, Yates JR, et al. The hMre11/hRad50 protein complex and Nijmegen breakage syndrome: linkage of double-strand break repair to the cellular DNA damage response. Cell. 1998 May 1;93(3):477–86.

46. Varon R, Vissinga C, Platzer M, Cerosaletti KM, Chrzanowska KH, Saar K, et al. Nibrin, a novel DNA double-strand break repair protein, is mutated in Nijmegen breakage syndrome. Cell. 1998 May 1;93(3):467–76.

47. Waltes R, Kalb R, Gatei M, Kijas AW, Stumm M, Sobeck A, et al. Human RAD50 deficiency in a Nijmegen breakage syndrome-like disorder. Am. J. Hum. Genet. 2009 May;84(5):605–16.

48. Stewart GS, Maser RS, Stankovic T, Bressan DA, Kaplan MI, Jaspers NG, et al. The DNA double-strand break repair gene hMRE11 is mutated in individuals with an ataxia-telangiectasia-like disorder. Cell. 1999 Dec 10;99(6):577–87.

49. Taylor AMR, Groom A, Byrd PJ. Ataxia-telangiectasia-like disorder (ATLD)-its clinical presentation and molecular basis. DNA Repair (Amst.). 2004 Aug;3(8-9):1219–25.

50. Lamarche BJ, Orazio NI, Weitzman MD. The MRN complex in double-strand break repair and telomere maintenance. FEBS Lett. 2010 Sep 10;584(17):3682–95.

51. Hopfner KP, Karcher A, Shin DS, Craig L, Arthur LM, Carney JP, et al. Structural biology of Rad50 ATPase: ATP-driven conformational control in DNA double-strand break repair and the ABC-ATPase superfamily. Cell. 2000 Jun 23;101(7):789–800.

52. Hopfner KP, Karcher A, Craig L, Woo TT, Carney JP, Tainer JA. Structural biochemistry and interaction architecture of the DNA double-strand break repair Mre11 nuclease and Rad50-ATPase. Cell. 2001 May 18;105(4):473–85.

53. de Jager M, van Noort J, van Gent DC, Dekker C, Kanaar R, Wyman C. Human Rad50/Mre11 is a flexible complex that can tether DNA ends. Mol. Cell. 2001 Nov;8(5):1129–35.

54. Hopfner K-P, Craig L, Moncalian G, Zinkel RA, Usui T, Owen BAL, et al. The Rad50 zinc-hook is a structure joining Mre11 complexes in DNA recombination and repair. Nature. 2002 Aug 1;418(6897):562–6.

55. He J, Shi LZ, Truong LN, Lu C-S, Razavian N, Li Y, et al. Rad50 zinc hook is important for the Mre11 complex to bind chromosomal DNA double-stranded breaks and initiate various DNA damage responses. J. Biol. Chem. 2012 Sep 14;287(38):31747–56.

56. Wiltzius JJW, Hohl M, Fleming JC, Petrini JHJ. The Rad50 hook domain is a critical determinant of Mre11 complex functions. Nat. Struct. Mol. Biol. 2005 May;12(5):403–7.

57. Hohl M, Kwon Y, Galván SM, Xue X, Tous C, Aguilera A, et al. The Rad50 coiled-coil domain is indispensable for Mre11 complex functions. Nat. Struct. Mol. Biol. 2011 Oct;18(10):1124–31.

58. Williams RS, Moncalian G, Williams JS, Yamada Y, Limbo O, Shin DS, et al. Mre11 dimers coordinate DNA end bridging and nuclease processing in double-strand-break repair. Cell. 2008 Oct 3;135(1):97–109.

59. Paull TT, Gellert M. The 3‘ to 5’ exonuclease activity of Mre 11 facilitates repair of DNA double-strand breaks. Mol. Cell. 1998 Jun;1(7):969–79.

60. Trujillo KM, Yuan SS, Lee EY, Sung P. Nuclease activities in a complex of human recombination and DNA repair factors Rad50, Mre11, and p95. J. Biol. Chem. 1998 Aug 21;273(34):21447–50.

61. Usui T, Ohta T, Oshiumi H, Tomizawa J, Ogawa H, Ogawa T. Complex formation and functional versatility of Mre11 of budding yeast in recombination. Cell. 1998 Nov 25;95(5):705–16.

62. Garcia V, Phelps SEL, Gray S, Neale MJ. Bidirectional resection of DNA double-strand breaks by Mre11 and Exo1. Nature. 2011 Nov 10;479(7372):241–4.

63. Shibata A, Moiani D, Arvai AS, Perry J, Harding SM, Genois M-M, et al. DNA Double-Strand Break Repair Pathway Choice Is Directed by Distinct MRE11 Nuclease Activities. Mol. Cell. 2013 Dec 3.

64. Moreno-Herrero F, de Jager M, Dekker NH, Kanaar R, Wyman C, Dekker C.

Mesoscale conformational changes in the DNA-repair complex Rad50/Mre11/Nbs1 upon binding DNA. Nature. 2005 Sep 15;437(7057):440–3.

65. van der Linden E, Sanchez H, Kinoshita E, Kanaar R, Wyman C. RAD50 and NBS1 form a stable complex functional in DNA binding and tethering. Nucleic Acids Research. 2009 Apr;37(5):1580–8.

66. Lloyd J, Chapman JR, Clapperton JA, Haire LF, Hartsuiker E, Li J, et al. A supramodular FHA/BRCT-repeat architecture mediates Nbs1 adaptor function in response to DNA damage. Cell. 2009 Oct 2;139(1):100–11.

67. Becker E, Meyer V, Madaoui H, Guerois R. Detection of a tandem BRCT in Nbs1 and Xrs2 with functional implications in the DNA damage response. Bioinformatics. 2006 Jun 1;22(11):1289–92.

68. Hari FJ, Spycher C, Jungmichel S, Pavic L, Stucki M. A divalent FHA/BRCT-binding mechanism couples the MRE11-RAD50-NBS1 complex to damaged chromatin. EMBO Rep. 2010 May;11(5):387–92.

69. Spycher C, Miller ES, Townsend K, Pavic L, Morrice NA, Janscak P, et al. Constitutive phosphorylation of MDC1 physically links the MRE11-RAD50-NBS1 complex to damaged chromatin. The Journal of Cell Biology. 2008 Apr 21;181(2):227–40.

70. Williams RS, Dodson GE, Limbo O, Yamada Y, Williams JS, Guenther G, et al. Nbs1 flexibly tethers Ctp1 and Mre11-Rad50 to coordinate DNA double-strand break processing and repair. Cell. 2009 Oct 2;139(1):87–99.

71. Limbo O, Chahwan C, Yamada Y, de Bruin RAM, Wittenberg C, Russell P. Ctp1 is a cell-cycle-regulated protein that functions with Mre11 complex to control double-strand break repair by homologous recombination. Mol. Cell. 2007 Oct 12;28(1):134–46.

72. Akamatsu Y, Murayama Y, Yamada T, Nakazaki T, Tsutsui Y, Ohta K, et al. Molecular characterization of the role of the Schizosaccharomyces pombe nip1+/ctp1+ gene in DNA double-strand break repair in association with the Mre11-Rad50-Nbs1 complex. Mol. Cell. Biol. 2008 Jun;28(11):3639–51.

73. Wang H, Shi LZ, Wong CCL, Han X, Hwang PY-H, Truong LN, et al. The interaction of CtIP and Nbs1 connects CDK and ATM to regulate HR-mediated double-strand break repair. PLoS Genet. 2013;9(2):e1003277.

74. You Z, Shi LZ, Zhu Q, Wu P, Zhang Y-W, Basilio A, et al. CtIP links DNA double-strand break sensing to resection. Mol. Cell. 2009 Dec 25;36(6):954–69.

75. Eid W, Steger M, El-Shemerly M, Ferretti LP, Peña-Diaz J, König C, et al. DNA end resection by CtIP and exonuclease 1 prevents genomic instability. EMBO Rep. 2010 Dec;11(12):962–8.

76. Desai-Mehta A, Cerosaletti KM, Concannon P. Distinct functional domains of nibrin mediate Mre11 binding, focus formation, and nuclear localization. Mol. Cell. Biol. 2001 Mar;21(6):2184–91.

77. Falck J, Coates J, Jackson SP. Conserved modes of recruitment of ATM, ATR and DNA-PKcs to sites of DNA damage. Nature. 2005 Mar 31;434(7033):605–11.

78. You Z, Chahwan C, Bailis J, Hunter T, Russell P. ATM activation and its recruitment to damaged DNA require binding to the C terminus of Nbs1. Mol. Cell. Biol. 2005 Jul;25(13):5363–79.

79. Uziel T, Lerenthal Y, Moyal L, Andegeko Y, Mittelman L, Shiloh Y. Requirement of the MRN complex for ATM activation by DNA damage. EMBO J. 2003 Oct 15;22(20):5612–21.

80. Lammens K, Bemeleit DJ, Möckel C, Clausing E, Schele A, Hartung S, et al. The Mre11:Rad50 structure shows an ATP-dependent molecular clamp in DNA double-strand break repair. Cell. 2011 Apr 1;145(1):54–66.

81. Deshpande RA, Williams GJ, Limbo O, Williams RS, Kuhnlein J, Lee J-H, et al. ATP-driven Rad50 conformations regulate DNA tethering, end resection, and ATM checkpoint signaling. EMBO J. 2014 Feb 3.

82. Möckel C, Lammens K, Schele A, Hopfner K-P. ATP driven structural changes of the bacterial Mre11:Rad50 catalytic head complex. Nucleic Acids Research. 2012 Jan;40(2):914–27.

83. Lim HS, Kim JS, Park YB, Gwon GH, Cho Y. Crystal structure of the Mre11-Rad50-ATPγS complex: understanding the interplay between Mre11 and Rad50. Genes Dev. 2011 May 15;25(10):1091–104.

84. Majka J, Alford B, Ausio J, Finn RM, McMurray CT. ATP hydrolysis by RAD50 protein switches MRE11 enzyme from endonuclease to exonuclease. J. Biol. Chem. 2012 Jan 20;287(4):2328–41.

85. Borde V. The multiple roles of the Mre11 complex for meiotic recombination. Chromosome Res. 2007;15(5):551–63.

86. Keeney S, Giroux CN, Kleckner N. Meiosis-specific DNA double-strand breaks are catalyzed by Spo11, a member of a widely conserved protein family. Cell. 1997 Feb 7;88(3):375–84.

87. Keeney S, Neale MJ. Initiation of meiotic recombination by formation of DNA double-strand breaks: mechanism and regulation. Biochem. Soc. Trans. 2006 Aug;34(Pt 4):523–5.

88. Mimitou EP, Symington LS. DNA end resection: many nucleases make light work. DNA Repair (Amst.). 2009 Sep 2;8(9):983–95.

89. Keeney S. Spo11 and the Formation of DNA Double-Strand Breaks in Meiosis. Genome Dyn Stab. 2008 Jan 1;2:81–123.

90. Alani E, Padmore R, Kleckner N. Analysis of wild-type and rad50 mutants of yeast suggests an intimate relationship between meiotic chromosome synapsis and recombination. Cell. 1990 May 4;61(3):419–36.

91. Clerici M, Mantiero D, Lucchini G, Longhese MP. The Saccharomyces cerevisiae Sae2 protein promotes resection and bridging of double strand break ends. J. Biol. Chem. 2005 Nov 18;280(46):38631–8.

92. McKee AH, Kleckner N. A general method for identifying recessive diploid-specific mutations in Saccharomyces cerevisiae, its application to the isolation of mutants blocked at intermediate stages of meiotic prophase and characterization of a new gene SAE2. Genetics. 1997 Jul;146(3):797–816.

93. Prinz S, Amon A, Klein F. Isolation of COM1, a new gene required to complete meiotic double-strand break-induced recombination in Saccharomyces cerevisiae. Genetics. 1997 Jul;146(3):781–95.

94. Neale MJ, Pan J, Keeney S. Endonucleolytic processing of covalent protein-linked DNA double-strand breaks. Nature. 2005 Aug 18;436(7053):1053–7.

95. Deng C, Brown JA, You D, Brown JM. Multiple endonucleases function to repair covalent topoisomerase I complexes in Saccharomyces cerevisiae. Genetics. 2005 Jun;170(2):591–600.

96. Champoux JJ. DNA topoisomerases: structure, function, and mechanism. Annu. Rev. Biochem. 2001;70:369–413.

97. Pommier Y, Leo E, Zhang H, Marchand C. DNA topoisomerases and their poisoning by anticancer and antibacterial drugs. Chem. Biol. 2010 May 28;17(5):421–33.

98. Hartsuiker E, Neale MJ, Carr AM. Distinct requirements for the Rad32(Mre11) nuclease and Ctp1(CtIP) in the removal of covalently bound topoisomerase I and II from DNA. Mol. Cell. 2009 Jan 16;33(1):117–23.

99. Hartsuiker E, Mizuno K, Molnar M, Kohli J, Ohta K, Carr AM. Ctp1CtIP and Rad32Mre11 nuclease activity are required for Rec12Spo11 removal, but Rec12Spo11 removal is dispensable for other MRN-dependent meiotic functions. Mol. Cell. Biol. 2009 Apr;29(7):1671–81.

100. Usui T, Petrini JHJ, Morales M. Rad50S alleles of the Mre11 complex: questions answered and questions raised. Exp. Cell Res. 2006 Aug 15;312(14):2694–9.

101. Bender CF, Sikes ML, Sullivan R, Huye LE, Le Beau MM, Roth DB, et al. Cancer predisposition and hematopoietic failure in Rad50(S/S) mice. Genes Dev. 2002 Sep 1;16(17):2237–51.

102. Morales M, Liu Y, Laiakis EC, Morgan WF, Nimer SD, Petrini JHJ. DNA damage signaling in hematopoietic cells: a role for Mre11 complex repair of topoisomerase lesions. Cancer Res. 2008 Apr 1;68(7):2186–93.

103. Morales M, Theunissen J-WF, Kim CFB, Kitagawa R, Kastan MB, Petrini JHJ. The Rad50S allele promotes ATM-dependent DNA damage responses and suppresses ATM deficiency: implications for the Mre11 complex as a DNA damage sensor. Genes Dev. 2005 Dec 15;19(24):3043–54.

104. Usui T, Ogawa H, Petrini JH. A DNA damage response pathway controlled by Tel1 and the Mre11 complex. Mol. Cell. 2001 Jun;7(6):1255–66.

105. Schaeper U, Subramanian T, Lim L, Boyd JM, Chinnadurai G. Interaction between a cellular protein that binds to the C-terminal region of adenovirus E1A (CtBP) and a novel cellular protein is disrupted by E1A through a conserved PLDLS motif. J. Biol. Chem. 1998 Apr 10;273(15):8549–52.

106. Molloy DP, Barral PM, Bremner KH, Gallimore PH, Grand RJ. Structural determinants outside the PXDLS sequence affect the interaction of adenovirus E1A, C-terminal interacting protein and Drosophila repressors with C-terminal binding protein. Biochim. Biophys. Acta. 2001 Mar 9;1546(1):55–70.

107. Quinlan KGR, Verger A, Kwok A, Lee SHY, Perdomo J, Nardini M, et al. Role of the C-terminal binding protein PXDLS motif binding cleft in protein interactions and transcriptional repression. Mol. Cell. Biol. 2006 Nov;26(21):8202–13.

108. Wong AK, Ormonde PA, Pero R, Chen Y, Lian L, Salada G, et al. Characterization of a carboxy-terminal BRCA1 interacting protein. Oncogene. 1998 Nov 5;17(18):2279–85.

109. Yu X, Wu LC, Bowcock AM, Aronheim A, Baer R. The C-terminal (BRCT) domains of BRCA1 interact in vivo with CtIP, a protein implicated in the CtBP pathway of transcriptional repression. J. Biol. Chem. 1998 Sep 25;273(39):25388–92.

110. Fusco C, Reymond A, Zervos AS. Molecular cloning and characterization of a novel retinoblastoma-binding protein. Genomics. 1998 Aug 1;51(3):351–8.

111. Chen P-L, Liu F, Cai S, Lin X, Li A, Chen Y, et al. Inactivation of CtIP leads to early embryonic lethality mediated by G1 restraint and to tumorigenesis by haploid insufficiency. Mol. Cell. Biol. 2005 May;25(9):3535–42.

112. Vilkki S, Launonen V, Karhu A, Sistonen P, Västrik I, Aaltonen LA. Screening for microsatellite instability target genes in colorectal cancers. J. Med. Genet. 2002 Nov;39(11):785–9.

113. Bilbao C, Ramírez R, Rodríguez G, Falcón O, León L, Díaz-Chico N, et al. Double strand break repair components are frequent targets of microsatellite instability in endometrial cancer. Eur. J. Cancer. 2010 Oct;46(15):2821–7.

114. Soria-Bretones I, Sáez C, Ruíz-Borrego M, Japón MA, Huertas P. Prognostic value of CtIP/RBBP8 expression in breast cancer. Cancer Med. 2013 Dec;2(6):774–83.

115. Wu M, Soler DR, Abba MC, Nunez MI, Baer R, Hatzis C, et al. CtIP silencing as a novel mechanism of tamoxifen resistance in breast cancer. Mol. Cancer Res. 2007 Dec;5(12):1285–95.

116. Liu F, Lee W-H. CtIP activates its own and cyclin D1 promoters via the E2F/RB pathway during G1/S progression. Mol. Cell. Biol. 2006 Apr;26(8):3124–34.

117. You Z, Bailis JM. DNA damage and decisions: CtIP coordinates DNA repair and cell cycle checkpoints. Trends Cell Biol. 2010 Jul;20(7):402–9.

118. Sartori AA, Lukas C, Coates J, Mistrik M, Fu S, Bartek J, et al. Human CtIP promotes DNA end resection. Nature. 2007 Nov 22;450(7169):509–14.

119. Huertas P, Cortés-Ledesma F, Sartori AA, Aguilera A, Jackson SP. CDK targets Sae2 to control DNA-end resection and homologous recombination. Nature. 2008 Oct 2;455(7213):689–92.

120. Huertas P, Jackson SP. Human CtIP mediates cell cycle control of DNA end resection and double strand break repair. J. Biol. Chem. 2009 Apr 3;284(14):9558–65.

121. Kousholt AN, Fugger K, Hoffmann S, Larsen BD, Menzel T, Sartori AA, et al. CtIP-dependent DNA resection is required for DNA damage checkpoint maintenance but not initiation. The Journal of Cell Biology. 2012 Jun 25;197(7):869–76.

122. Qvist P, Huertas P, Jimeno S, Nyegaard M, Hassan MJ, Jackson SP, et al. CtIP Mutations Cause Seckel and Jawad Syndromes. PLoS Genet. 2011 Oct;7(10):e1002310.

123. Dubin MJ, Stokes PH, Sum EYM, Williams RS, Valova VA, Robinson PJ, et al. Dimerization of CtIP, a BRCA1- and CtBP-interacting protein, is mediated by an N-terminal coiled-coil motif. J. Biol. Chem. 2004 Jun 25;279(26):26932–8.

124. Wang H, Shao Z, Shi LZ, Hwang PY-H, Truong LN, Berns MW, et al. CtIP protein dimerization is critical for its recruitment to chromosomal DNA double-stranded breaks. J. Biol. Chem. 2012 Jun 15;287(25):21471–80.

125. Gu B, Chen P-L. Expression of PCNA-binding domain of CtIP, a motif required for CtIP localization at DNA replication foci, causes DNA damage and activation of DNA damage checkpoint. Cell Cycle. 2009 May 1;8(9):1409–20.

126. Chen L, Nievera CJ, Lee AY-L, Wu X. Cell cycle-dependent complex formation of BRCA1.CtIP.MRN is important for DNA double-strand break repair. J. Biol. Chem. 2008 Mar 21;283(12):7713–20.

127. Yuan J, Chen J. N terminus of CtIP is critical for homologous recombination-mediated double-strand break repair. J. Biol. Chem. 2009 Nov 13;284(46):31746–52.

128. Yu X, Baer R. Nuclear localization and cell cycle-specific expression of CtIP, a protein that associates with the BRCA1 tumor suppressor. J. Biol. Chem. 2000 Jun 16;275(24):18541–9.

129. Yun MH, Hiom K. CtIP-BRCA1 modulates the choice of DNA double-strand-break repair pathway throughout the cell cycle. Nature. 2009 May 21;459(7245):460–3.

130. Germani A, Prabel A, Mourah S, Podgorniak M-P, Di Carlo A, Ehrlich R, et al. SIAH-1 interacts with CtIP and promotes its degradation by the proteasome pathway. Oncogene. 2003 Dec 4;22(55):8845–51.

131. Yu X, Chen J. DNA damage-induced cell cycle checkpoint control requires CtIP, a phosphorylation-dependent binding partner of BRCA1 C-terminal domains. Mol. Cell. Biol. 2004 Nov;24(21):9478–86.

132. Reczek CR, Szabolcs M, Stark JM, Ludwig T, Baer R. The interaction between CtIP and BRCA1 is not essential for resection-mediated DNA repair or tumor suppression. The Journal of Cell Biology. 2013 May 27;201(5):693–707.

133. Escribano-Díaz C, Orthwein A, Fradet-Turcotte A, Xing M, Young JTF, Tkáč J, et al. A cell cycle-dependent regulatory circuit composed of 53BP1-RIF1 and BRCA1-CtIP controls DNA repair pathway choice. Mol. Cell. 2013 Mar 7;49(5):872–83.

134. Peterson SE, Li Y, Wu-Baer F, Chait BT, Baer R, Yan H, et al. Activation of DSB processing requires phosphorylation of CtIP by ATR. Mol. Cell. 2013 Feb 21;49(4):657–67.

135. Steger M, Murina O, Hühn D, Ferretti LP, Walser R, Hänggi K, et al. Prolyl Isomerase PIN1 Regulates DNA Double-Strand Break Repair by Counteracting DNA End Resection. Mol. Cell. 2013 May 9;50(3):333–43.

136. Kaidi A, Weinert BT, Choudhary C, Jackson SP. Human SIRT6 promotes DNA end resection through CtIP deacetylation. Science. 2010 Sep 10;329(5997):1348–53.

137. Symington LS, Gautier J. Double-strand break end resection and repair pathway choice. Annu. Rev. Genet. 2011;45:247–71.

138. Pierce AJ, Hu P, Han M, Ellis N, Jasin M. Ku DNA end-binding protein modulates homologous repair of double-strand breaks in mammalian cells. Genes Dev. 2001 Dec 15;15(24):3237–42.

139. Kass EM, Jasin M. Collaboration and competition between DNA double-strand break repair pathways. FEBS Lett. 2010 Sep 10;584(17):3703–8.

140. Wu D, Topper LM, Wilson TE. Recruitment and dissociation of nonhomologous end joining proteins at a DNA double-strand break in Saccharomyces cerevisiae. Genetics. 2008 Mar;178(3):1237–49.

141. Huertas P. DNA resection in eukaryotes: deciding how to fix the break. Nat. Struct. Mol. Biol. 2010 Jan;17(1):11–6.

142. Lengsfeld BM, Rattray AJ, Bhaskara V, Ghirlando R, Paull TT. Sae2 is an endonuclease that processes hairpin DNA cooperatively with the Mre11/Rad50/Xrs2 complex. Mol. Cell. 2007 Nov 30;28(4):638–51.

143. Nicolette ML, Lee K, Guo Z, Rani M, Chow JM, Lee SE, et al. Mre11-Rad50-Xrs2 and Sae2 promote 5' strand resection of DNA double-strand breaks. Nat. Struct. Mol. Biol. 2010 Dec;17(12):1478–85.

144. Shim EY, Chung W-H, Nicolette ML, Zhang Y, Davis M, Zhu Z, et al. Saccharomyces cerevisiae Mre11/Rad50/Xrs2 and Ku proteins regulate association of Exo1 and Dna2 with DNA breaks. EMBO J. 2010 Oct 6;29(19):3370–80.

145. Nimonkar AV, Genschel J, Kinoshita E, Polaczek P, Campbell JL, Wyman C, et al. BLM-DNA2-RPA-MRN and EXO1-BLM-RPA-MRN constitute two DNA end resection machineries for human DNA break repair. Genes Dev. 2011 Feb 15;25(4):350–62.

146. Gravel S, Chapman JR, Magill C, Jackson SP. DNA helicases Sgs1 and BLM promote DNA double-strand break resection. Genes Dev. 2008 Oct 15;22(20):2767–72.

147. Mimitou EP, Symington LS. Sae2, Exo1 and Sgs1 collaborate in DNA double-strand break processing. Nature. 2008 Oct 9;455(7214):770–4.

148. Aylon Y, Liefshitz B, Kupiec M. The CDK regulates repair of double-strand breaks by homologous recombination during the cell cycle. EMBO J. 2004 Dec 8;23(24):4868–75.

149. Ira G, Pellicioli A, Balijja A, Wang X, Fiorani S, Carotenuto W, et al. DNA end resection, homologous recombination and DNA damage checkpoint activation require CDK1. Nature. 2004 Oct 21;431(7011):1011–7.

150. Yu X, Fu S, Lai M, Baer R, Chen J. BRCA1 ubiquitinates its phosphorylation-dependent binding partner CtIP. Genes Dev. 2006 Jul 1;20(13):1721–6.

151. Buis J, Stoneham T, Spehalski E, Ferguson DO. Mre11 regulates CtIP-

dependent double-strand break repair by interaction with CDK2. Nat. Struct. Mol. Biol. 2012 Feb;19(2):246–52.

152. Nakamura K, Kogame T, Oshiumi H, Shinohara A, Sumitomo Y, Agama K, et al. Collaborative action of Brca1 and CtIP in elimination of covalent modifications from double-strand breaks to facilitate subsequent break repair. PLoS Genet. 2010 Jan;6(1):e1000828.

153. Ferretti LP, Lafranchi L, Sartori AA. Controlling DNA-end resection: a new task for CDKs. Front Genet. 2013;4:99.

154. Wyman C, Kanaar R. DNA double-strand break repair: all's well that ends well. Annu. Rev. Genet. 2006;40:363–83.

155. Yeeles JTP, Poli J, Marians KJ, Pasero P. Rescuing Stalled or Damaged Replication Forks. Cold Spring Harb Perspect Biol. 2013 May 1;5(5):a012815–5.

156. Barnes DE. DNA damage: air-breaks? Curr. Biol. 2002 Apr 2;12(7):R262–4.

157. Soulas-Sprauel P, Rivera-Munoz P, Malivert L, Le Guyader G, Abramowski V, Revy P, et al. V(D)J and immunoglobulin class switch recombinations: a paradigm to study the regulation of DNA end-joining. Oncogene. 2007 Dec 10;26(56):7780–91.

158. Jasin M, Rothstein R. Repair of strand breaks by homologous recombination. Cold Spring Harb Perspect Biol. 2013 Nov;5(11):a012740.

159. Chiruvella KK, Liang Z, Wilson TE. Repair of double-strand breaks by end joining. Cold Spring Harb Perspect Biol. 2013 May;5(5):a012757.

160. Zhuang J, Jiang G, Willers H, Xia F. Exonuclease function of human Mre11 promotes deletional nonhomologous end joining. J. Biol. Chem. 2009 Oct 30;284(44):30565–73.

161. Truong LN, Li Y, Shi LZ, Hwang PY-H, He J, Wang H, et al. Microhomology-mediated End Joining and Homologous Recombination share the initial end resection step to repair DNA double-strand breaks in mammalian cells. Proc. Natl. Acad. Sci. U.S.A. 2013 May 7;110(19):7720–5.

162. Rothkamm K, Krüger I, Thompson LH, Löbrich M. Pathways of DNA double-strand break repair during the mammalian cell cycle. Mol. Cell. Biol. 2003 Aug;23(16):5706–15.

163. Lieber MR. The mechanism of double-strand DNA break repair by the nonhomologous DNA end-joining pathway. Annu. Rev. Biochem. 2010;79:181–211.

164. Dynan WS, Yoo S. Interaction of Ku protein and DNA-dependent protein kinase catalytic subunit with nucleic acids. Nucleic Acids Research. 1998 Apr 1;26(7):1551–9.

165. Beucher A, Birraux J, Tchouandong L, Barton O, Shibata A, Conrad S, et al. ATM and Artemis promote homologous recombination of radiation-induced DNA double-strand breaks in G2. EMBO J. 2009 Nov 4;28(21):3413–27.

166. Mladenov E, Iliakis G. Induction and repair of DNA double strand breaks: the increasing spectrum of non-homologous end joining pathways. Mutat. Res. 2011

Jun 3;711(1-2):61–72.

167. Meek K, Dang V, Lees-Miller SP. DNA-PK: the means to justify the ends? Adv. Immunol. 2008;99:33–58.

168. Shrivastav M, De Haro LP, Nickoloff JA. Regulation of DNA double-strand break repair pathway choice. Cell Res. 2008 Jan;18(1):134–47.

169. Chan DW, Chen BP-C, Prithivirajsingh S, Kurimasa A, Story MD, Qin J, et al. Autophosphorylation of the DNA-dependent protein kinase catalytic subunit is required for rejoining of DNA double-strand breaks. Genes Dev. 2002 Sep 15;16(18):2333–8.

170. Ding Q, Reddy YVR, Wang W, Woods T, Douglas P, Ramsden DA, et al. Autophosphorylation of the catalytic subunit of the DNA-dependent protein kinase is required for efficient end processing during DNA double-strand break repair. Mol. Cell. Biol. 2003 Aug;23(16):5836–48.

171. Uematsu N, Weterings E, Yano K-I, Morotomi-Yano K, Jakob B, Taucher-Scholz G, et al. Autophosphorylation of DNA-PKCS regulates its dynamics at DNA double-strand breaks. The Journal of Cell Biology. 2007 Apr 23;177(2):219–29.

172. Moshous D, Callebaut I, de Chasseval R, Corneo B, Cavazzana-Calvo M, Le Deist F, et al. Artemis, a novel DNA double-strand break repair/V(D)J recombination protein, is mutated in human severe combined immune deficiency. Cell. 2001 Apr 20;105(2):177–86.

173. Ma Y, Pannicke U, Schwarz K, Lieber MR. Hairpin opening and overhang processing by an Artemis/DNA-dependent protein kinase complex in nonhomologous end joining and V(D)J recombination. Cell. 2002 Mar 22;108(6):781–94.

174. Goodarzi AA, Yu Y, Riballo E, Douglas P, Walker SA, Ye R, et al. DNA-PK autophosphorylation facilitates Artemis endonuclease activity. EMBO J. 2006 Aug 23;25(16):3880–9.

175. Coquelle N, Havali-Shahriari Z, Bernstein N, Green R, Glover JNM. Structural basis for the phosphatase activity of polynucleotide kinase/phosphatase on single- and double-stranded DNA substrates. Proc. Natl. Acad. Sci. U.S.A. 2011 Dec 27;108(52):21022–7.

176. Nick McElhinny SA, Havener JM, Garcia-Diaz M, Juárez R, Bebenek K, Kee BL, et al. A gradient of template dependence defines distinct biological roles for family X polymerases in nonhomologous end joining. Mol. Cell. 2005 Aug 5;19(3):357–66.

177. Ramsden DA, Asagoshi K. DNA polymerases in nonhomologous end joining: are there any benefits to standing out from the crowd? Environ. Mol. Mutagen. 2012 Dec;53(9):741–51.

178. Mladenov E, Iliakis G. The Pathways of Double-Strand Break Repair. intechopen.com. InTech; 2011.

179. Karanam K, Kafri R, Loewer A, Lahav G. Quantitative live cell imaging reveals a gradual shift between DNA repair mechanisms and a maximal use of HR in mid S phase. Mol. Cell. 2012 Jul 27;47(2):320–9.

180. Sung P, Krejci L, Van Komen S, Sehorn MG. Rad51 recombinase and recombination mediators. J. Biol. Chem. 2003 Oct 31;278(44):42729–32.

181. Zhang F, Ma J, Wu J, Ye L, Cai H, Xia B, et al. PALB2 links BRCA1 and BRCA2 in the DNA-damage response. Curr. Biol. 2009 Mar 24;19(6):524–9.

182. Sy SMH, Huen MSY, Chen J. PALB2 is an integral component of the BRCA complex required for homologous recombination repair. Proc. Natl. Acad. Sci. U.S.A. 2009 Apr 28;106(17):7155–60.

183. Shivji MKK, Mukund SR, Rajendra E, Chen S, Short JM, Savill J, et al. The BRC repeats of human BRCA2 differentially regulate RAD51 binding on single- versus double-stranded DNA to stimulate strand exchange. Proc. Natl. Acad. Sci. U.S.A. 2009 Aug 11;106(32):13254–9.

184. Thorslund T, McIlwraith MJ, Compton SA, Lekomtsev S, Petronczki M, Griffith JD, et al. The breast cancer tumor suppressor BRCA2 promotes the specific targeting of RAD51 to single-stranded DNA. Nat. Struct. Mol. Biol. 2010 Oct;17(10):1263–5.

185. Lok BH, Carley AC, Tchang B, Powell SN. RAD52 inactivation is synthetically lethal with deficiencies in BRCA1 and PALB2 in addition to BRCA2 through RAD51-mediated homologous recombination. Oncogene. 2013 Jul 25;32(30):3552–8.

186. Masson JY, Tarsounas MC, Stasiak AZ, Stasiak A, Shah R, McIlwraith MJ, et al. Identification and purification of two distinct complexes containing the five RAD51 paralogs. Genes Dev. 2001 Dec 15;15(24):3296–307.

187. Chun J, Buechelmaier ES, Powell SN. Rad51 paralog complexes BCDX2 and CX3 act at different stages in the BRCA1-BRCA2-dependent homologous recombination pathway. Mol. Cell. Biol. 2013 Jan;33(2):387–95.

188. Barber LJ, Youds JL, Ward JD, McIlwraith MJ, O'Neil NJ, Petalcorin MIR, et al. RTEL1 maintains genomic stability by suppressing homologous recombination. Cell. 2008 Oct 17;135(2):261–71.

189. Johnson RD, Jasin M. Sister chromatid gene conversion is a prominent double-strand break repair pathway in mammalian cells. EMBO J. 2000 Jul 3;19(13):3398–407.

190. Bugreev DV, Mazina OM, Mazin AV. Rad54 protein promotes branch migration of Holliday junctions. Nature. 2006 Aug 3;442(7102):590–3.

191. Wu L, Hickson ID. The Bloom's syndrome helicase suppresses crossing over during homologous recombination. Nature. 2003 Dec 18;426(6968):870–4.

192. Cejka P, Plank JL, Bachrati CZ, Hickson ID, Kowalczykowski SC. Rmi1 stimulates decatenation of double Holliday junctions during dissolution by Sgs1-Top3. Nat. Struct. Mol. Biol. 2010 Nov;17(11):1377–82.

193. Wyatt HDM, Sarbajna S, Matos J, West SC. Coordinated actions of SLX1-SLX4 and MUS81-EME1 for Holliday junction resolution in human cells. Mol. Cell. 2013 Oct 24;52(2):234–47.

194. Castor D, Nair N, Declais A-C, Lachaud C, Toth R, MacArtney TJ, et al. Cooperative control of holliday junction resolution and DNA repair by the SLX1

and MUS81-EME1 nucleases. Mol. Cell. 2013 Oct 24;52(2):221–33.

195. Garner E, Kim Y, Lach FP, Kottemann MC, Smogorzewska A. Human GEN1 and the SLX4-associated nucleases MUS81 and SLX1 are essential for the resolution of replication-induced Holliday junctions. Cell Rep. 2013 Oct 17;5(1):207–15.

196. Brill SJ. Linking the Enzymes that Unlink DNA. Mol. Cell. 2013 Oct 24;52(2):159–60.

197. Fekairi S, Scaglione S, Chahwan C, Taylor ER, Tissier A, Coulon S, et al. Human SLX4 is a Holliday junction resolvase subunit that binds multiple DNA repair/recombination endonucleases. Cell. 2009 Jul 10;138(1):78–89.

198. Svendsen JM, Smogorzewska A, Sowa ME, O'Connell BC, Gygi SP, Elledge SJ, et al. Mammalian BTBD12/SLX4 assembles a Holliday junction resolvase and is required for DNA repair. Cell. 2009 Jul 10;138(1):63–77.

199. Muñoz IM, Hain K, Declais A-C, Gardiner M, Toh GW, Sanchez-Pulido L, et al. Coordination of structure-specific nucleases by human SLX4/BTBD12 is required for DNA repair. Mol. Cell. 2009 Jul 10;35(1):116–27.

200. Ip SCY, Rass U, Blanco MG, Flynn HR, Skehel JM, West SC. Identification of Holliday junction resolvases from humans and yeast. Nature. 2008 Nov 20;456(7220):357–61.

201. Lichten M, de Massy B. The impressionistic landscape of meiotic recombination. Cell. 2011 Oct 14;147(2):267–70.

202. Jackson SP, Durocher D. Regulation of DNA damage responses by ubiquitin and SUMO. Mol. Cell. 2013 Mar 7;49(5):795–807.

203. Moynahan ME, Chiu JW, Koller BH, Jasin M. Brca1 controls homology-directed DNA repair. Mol. Cell. 1999 Oct;4(4):511–8.

204. Li ML, Greenberg RA. Links between genome integrity and BRCA1 tumor suppression. Trends Biochem. Sci. 2012 Oct;37(10):418–24.

205. Roy R, Chun J, Powell SN. BRCA1 and BRCA2: different roles in a common pathway of genome protection. Nat. Rev. Cancer. 2012 Jan;12(1):68–78.

206. Bunting SF, Callén E, Wong N, Chen H-T, Polato F, Gunn A, et al. 53BP1 inhibits homologous recombination in Brca1-deficient cells by blocking resection of DNA breaks. Cell. 2010 Apr 16;141(2):243–54.

207. Bouwman P, Aly A, Escandell JM, Pieterse M, Bartkova J, van der Gulden H, et al. 53BP1 loss rescues BRCA1 deficiency and is associated with triple-negative and BRCA-mutated breast cancers. Nat. Struct. Mol. Biol. 2010 Jun;17(6):688–95.

208. Zimmermann M, de Lange T. 53BP1: pro choice in DNA repair. Trends Cell Biol. 2014 Feb;24(2):108–17.

209. Chapman JR, Barral P, Vannier J-B, Borel V, Steger M, Tomas-Loba A, et al. RIF1 is essential for 53BP1-dependent nonhomologous end joining and suppression of DNA double-strand break resection. Mol. Cell. 2013 Mar 7;49(5):858–71.

210. Di Virgilio M, Callén E, Yamane A, Zhang W, Jankovic M, Gitlin AD, et al.

Rif1 prevents resection of DNA breaks and promotes immunoglobulin class switching. Science. 2013 Feb 8;339(6120):711–5.

211. Zimmermann M, Lottersberger F, Buonomo SB, Sfeir A, de Lange T. 53BP1 regulates DSB repair using Rif1 to control 5' end resection. Science. 2013 Feb 8;339(6120):700–4.

212. Feng L, Fong K-W, Wang J, Wang W, Chen J. RIF1 counteracts BRCA1-mediated end resection during DNA repair. J. Biol. Chem. 2013 Apr 19;288(16):11135–43.

213. Panier S, Boulton SJ. Double-strand break repair: 53BP1 comes into focus. Nat. Rev. Mol. Cell Biol. 2014 Jan;15(1):7–18.

214. Callén E, Di Virgilio M, Kruhlak MJ, Nieto-Soler M, Wong N, Chen H-T, et al. 53BP1 mediates productive and mutagenic DNA repair through distinct phosphoprotein interactions. Cell. 2013 Jun 6;153(6):1266–80.

215. Muñoz IM, Jowsey PA, Toth R, Rouse J. Phospho-epitope binding by the BRCT domains of hPTIP controls multiple aspects of the cellular response to DNA damage. Nucleic Acids Research. 2007;35(16):5312–22.

216. Escribano-Díaz C, Durocher D. DNA repair pathway choice--a PTIP of the hat to 53BP1. EMBO Rep. 2013 Aug;14(8):665–6.

217. Fradet-Turcotte A, Canny MD, Escribano-Díaz C, Orthwein A, Leung CCY, Huang H, et al. 53BP1 is a reader of the DNA-damage-induced H2A Lys 15 ubiquitin mark. Nature. 2013 Jul 4;499(7456):50–4.

218. Chapman JR, Sossick AJ, Boulton SJ, Jackson SP. BRCA1-associated exclusion of 53BP1 from DNA damage sites underlies temporal control of DNA repair. J. Cell. Sci. 2012 Aug 1;125(Pt 15):3529–34.

219. Shao G, Lilli DR, Patterson-Fortin J, Coleman KA, Morrissey DE, Greenberg RA. The Rap80-BRCC36 de-ubiquitinating enzyme complex antagonizes RNF8-Ubc13-dependent ubiquitination events at DNA double strand breaks. Proc. Natl. Acad. Sci. U.S.A. 2009 Mar 3;106(9):3166–71.

220. Reid LJ, Shakya R, Modi AP, Lokshin M, Cheng J-T, Jasin M, et al. E3 ligase activity of BRCA1 is not essential for mammalian cell viability or homology-directed repair of double-strand DNA breaks. Proc. Natl. Acad. Sci. U.S.A. 2008 Dec 30;105(52):20876–81.

221. Goodarzi AA, Jeggo P, Löbrich M. The influence of heterochromatin on DNA double strand break repair: Getting the strong, silent type to relax. DNA Repair (Amst.). 2010 Dec 10;9(12):1273–82.

222. Ziv Y, Bielopolski D, Galanty Y, Lukas C, Taya Y, Schultz DC, et al. Chromatin relaxation in response to DNA double-strand breaks is modulated by a novel ATM- and KAP-1 dependent pathway. Nat. Cell Biol. 2006 Aug;8(8):870–6.

223. Geuting V, Reul C, Löbrich M. ATM Release at Resected Double-Strand Breaks Provides Heterochromatin Reconstitution to Facilitate Homologous Recombination. PLoS Genet. 2013 Aug;9(8):e1003667.

224. Ryan RF, Schultz DC, Ayyanathan K, Singh PB, Friedman JR, Fredericks WJ,

et al. KAP-1 corepressor protein interacts and colocalizes with heterochromatic and euchromatic HP1 proteins: a potential role for Krüppel-associated box-zinc finger proteins in heterochromatin-mediated gene silencing. Mol. Cell. Biol. 1999 Jun;19(6):4366–78.

225. Goodarzi AA, Kurka T, Jeggo PA. KAP-1 phosphorylation regulates CHD3 nucleosome remodeling during the DNA double-strand break response. Nat. Struct. Mol. Biol. 2011 Jul;18(7):831–9.

226. Goodarzi AA, Noon AT, Deckbar D, Ziv Y, Shiloh Y, Löbrich M, et al. ATM signaling facilitates repair of DNA double-strand breaks associated with heterochromatin. Mol. Cell. 2008 Jul 25;31(2):167–77.

227. Costelloe T, Louge R, Tomimatsu N, Mukherjee B, Martini E, Khadaroo B, et al. The yeast Fun30 and human SMARCAD1 chromatin remodellers promote DNA end resection. Nature. 2012 Sep 27;489(7417):581–4.

228. Rowbotham SP, Barki L, Neves-Costa A, Santos F, Dean W, Hawkes N, et al. Maintenance of silent chromatin through replication requires SWI/SNF-like chromatin remodeler SMARCAD1. Mol. Cell. 2011 May 6;42(3):285–96.

229. Deans AJ, West SC. DNA interstrand crosslink repair and cancer. Nat. Rev. Cancer. 2011 Jul;11(7):467–80.

230. McHugh PJ, Spanswick VJ, Hartley JA. Repair of DNA interstrand crosslinks: molecular mechanisms and clinical relevance. Lancet Oncol. 2001 Aug;2(8):483–90.

231. Clauson C, Schärer OD, Niedernhofer L. Advances in understanding the complex mechanisms of DNA interstrand cross-link repair. Cold Spring Harb Perspect Biol. 2013 Oct;5(10):a012732.

232. Brooks PJ, Zakhari S. Acetaldehyde and the genome: Beyond nuclear DNA adducts and carcinogenesis. Environ. Mol. Mutagen. 2014 Mar;55(2):77–91.

233. Stone MP, Cho Y-J, Huang H, Kim H-Y, Kozekov ID, Kozekova A, et al. Interstrand DNA cross-links induced by alpha,beta-unsaturated aldehydes derived from lipid peroxidation and environmental sources. Acc. Chem. Res. 2008 Jul;41(7):793–804.

234. Moldovan G-L, D'Andrea AD. How the fanconi anemia pathway guards the genome. Annu. Rev. Genet. 2009;43:223–49.

235. Akkari YM, Bateman RL, Reifsteck CA, Olson SB, Grompe M. DNA replication is required To elicit cellular responses to psoralen-induced DNA interstrand cross-links. Mol. Cell. Biol. 2000 Nov;20(21):8283–9.

236. Rothfuss A, Grompe M. Repair kinetics of genomic interstrand DNA cross-links: evidence for DNA double-strand break-dependent activation of the Fanconi anemia/BRCA pathway. Mol. Cell. Biol. 2004 Jan;24(1):123–34.

237. Kottemann MC, Smogorzewska A. Fanconi anaemia and the repair of Watson and Crick DNA crosslinks. Nature. 2013 Jan 17;493(7432):356–63.

238. Auerbach AD. A test for Fanconi's anemia. Blood. 1988 Jul;72(1):366–7.

239. Räschle M, Knipscheer P, Knipsheer P, Enoiu M, Angelov T, Sun J, et al. Mechanism of replication-coupled DNA interstrand crosslink repair. Cell. 2008

Sep 19;134(6):969–80.

240. Kim JM, Kee Y, Gurtan A, D'Andrea AD. Cell cycle-dependent chromatin loading of the Fanconi anemia core complex by FANCM/FAAP24. Blood. 2008 May 15;111(10):5215–22.

241. Ciccia A, Ling C, Coulthard R, Yan Z, Xue Y, Meetei AR, et al. Identification of FAAP24, a Fanconi anemia core complex protein that interacts with FANCM. Mol. Cell. 2007 Feb 9;25(3):331–43.

242. Singh TR, Saro D, Ali AM, Zheng X-F, Du C-H, Killen MW, et al. MHF1-MHF2, a histone-fold-containing protein complex, participates in the Fanconi anemia pathway via FANCM. Mol. Cell. 2010 Mar 26;37(6):879–86.

243. Huang M, Kim JM, Shiotani B, Yang K, Zou L, D'Andrea AD. The FANCM/FAAP24 complex is required for the DNA interstrand crosslink-induced checkpoint response. Mol. Cell. 2010 Jul 30;39(2):259–68.

244. Wang LC, Gautier J. The Fanconi anemia pathway and ICL repair: implications for cancer therapy. Crit. Rev. Biochem. Mol. Biol. 2010 Oct;45(5):424–39.

245. Hodson C, Walden H. Towards a molecular understanding of the fanconi anemia core complex. Anemia. 2012;2012:926787.

246. Garcia-Higuera I, Taniguchi T, Ganesan S, Meyn MS, Timmers C, Hejna J, et al. Interaction of the Fanconi anemia proteins and BRCA1 in a common pathway. Mol. Cell. 2001 Feb;7(2):249–62.

247. Smogorzewska A, Matsuoka S, Vinciguerra P, McDonald ER, Hurov KE, Luo J, et al. Identification of the FANCI protein, a monoubiquitinated FANCD2 paralog required for DNA repair. Cell. 2007 Apr 20;129(2):289–301.

248. Meetei AR, Yan Z, Wang W. FANCL replaces BRCA1 as the likely ubiquitin ligase responsible for FANCD2 monoubiquitination. Cell Cycle. 2004 Feb;3(2):179–81.

249. Bhagwat N, Olsen AL, Wang AT, Hanada K, Stuckert P, Kanaar R, et al. XPF-ERCC1 participates in the Fanconi anemia pathway of cross-link repair. Mol. Cell. Biol. 2009 Dec;29(24):6427–37.

250. Andreassen PR, D'Andrea AD, Taniguchi T. ATR couples FANCD2 monoubiquitination to the DNA-damage response. Genes Dev. 2004 Aug 15;18(16):1958–63.

251. Schlacher K, Wu H, Jasin M. A distinct replication fork protection pathway connects Fanconi anemia tumor suppressors to RAD51-BRCA1/2. Cancer Cell. 2012 Jul 10;22(1):106–16.

252. Taniguchi T, Garcia-Higuera I, Andreassen PR, Gregory RC, Grompe M, D'Andrea AD. S-phase-specific interaction of the Fanconi anemia protein, FANCD2, with BRCA1 and RAD51. Blood. 2002 Oct 1;100(7):2414–20.

253. Kratz K, Schöpf B, Kaden S, Sendoel A, Eberhard R, Lademann C, et al. Deficiency of FANCD2-associated nuclease KIAA1018/FAN1 sensitizes cells to interstrand crosslinking agents. Cell. 2010 Jul 9;142(1):77–88.

254. Liu T, Ghosal G, Yuan J, Chen J, Huang J. FAN1 acts with FANCI-FANCD2 to promote DNA interstrand cross-link repair. Science. 2010 Aug

6;329(5992):693–6.

255. MacKay C, Declais A-C, Lundin C, Agostinho A, Deans AJ, MacArtney TJ, et al. Identification of KIAA1018/FAN1, a DNA repair nuclease recruited to DNA damage by monoubiquitinated FANCD2. Cell. 2010 Jul 9;142(1):65–76.

256. Smogorzewska A, Desetty R, Saito TT, Schlabach M, Lach FP, Sowa ME, et al. A genetic screen identifies FAN1, a Fanconi anemia-associated nuclease necessary for DNA interstrand crosslink repair. Mol. Cell. 2010 Jul 9;39(1):36–47.

257. Yamamoto KN, Kobayashi S, Tsuda M, Kurumizaka H, Takata M, Kono K, et al. Involvement of SLX4 in interstrand cross-link repair is regulated by the Fanconi anemia pathway. Proc. Natl. Acad. Sci. U.S.A. 2011 Apr 19;108(16):6492–6.

258. Nijman SMB, Huang TT, Dirac AMG, Brummelkamp TR, Kerkhoven RM, D'Andrea AD, et al. The deubiquitinating enzyme USP1 regulates the Fanconi anemia pathway. Mol. Cell. 2005 Feb 4;17(3):331–9.

259. Cohn MA, Kowal P, Yang K, Haas W, Huang TT, Gygi SP, et al. A UAF1-containing multisubunit protein complex regulates the Fanconi anemia pathway. Mol. Cell. 2007 Dec 14;28(5):786–97.

260. Kim JM, Parmar K, Huang M, Weinstock DM, Ruit CA, Kutok JL, et al. Inactivation of murine Usp1 results in genomic instability and a Fanconi anemia phenotype. Dev. Cell. 2009 Feb;16(2):314–20.

261. Huang J, Liu S, Bellani MA, Thazhathveetil AK, Ling C, de Winter JP, et al. The DNA Translocase FANCM/MHF Promotes Replication Traverse of DNA Interstrand Crosslinks. Mol. Cell. 2013 Nov 7;52(3):434–46.

262. Ciccia A, McDonald N, West SC. Structural and functional relationships of the XPF/MUS81 family of proteins. Annu. Rev. Biochem. 2008;77:259–87.

263. Chen XB, Melchionna R, Denis CM, Gaillard PH, Blasina A, Van de Weyer I, et al. Human Mus81-associated endonuclease cleaves Holliday junctions in vitro. Mol. Cell. 2001 Nov;8(5):1117–27.

264. Gaillard P-HL, Noguchi E, Shanahan P, Russell P. The endogenous Mus81-Eme1 complex resolves Holliday junctions by a nick and counternick mechanism. Mol. Cell. 2003 Sep;12(3):747–59.

265. Hanada K, Budzowska M, Modesti M, Maas A, Wyman C, Essers J, et al. The structure-specific endonuclease Mus81-Eme1 promotes conversion of interstrand DNA crosslinks into double-strands breaks. EMBO J. 2006 Oct 18;25(20):4921–32.

266. Hanada K, Budzowska M, Davies SL, van Drunen E, Onizawa H, Beverloo HB, et al. The structure-specific endonuclease Mus81 contributes to replication restart by generating double-strand DNA breaks. Nat. Struct. Mol. Biol. 2007 Nov;14(11):1096–104.

267. Kirschner K, Melton DW. Multiple roles of the ERCC1-XPF endonuclease in DNA repair and resistance to anticancer drugs. Anticancer Res. 2010 Sep;30(9):3223–32.

268. Orelli B, McClendon TB, Tsodikov OV, Ellenberger T, Niedernhofer LJ,

Schärer OD. The XPA-binding domain of ERCC1 Is Required for Nucleotide Excision Repair but Not Other DNA Repair Pathways. jbc.org.

269. Bogliolo M, Schuster B, Stoepker C, Derkunt B, Su Y, Raams A, et al. Mutations in ERCC4, encoding the DNA-repair endonuclease XPF, cause Fanconi anemia. Am. J. Hum. Genet. 2013 May 2;92(5):800–6.

270. Stoepker C, Hain K, Schuster B, Hilhorst-Hofstee Y, Rooimans MA, Steltenpool J, et al. SLX4, a coordinator of structure-specific endonucleases, is mutated in a new Fanconi anemia subtype. Nat. Genet. 2011 Feb;43(2):138–41.

271. Crossan GP, van der Weyden L, Rosado IV, Langevin F, Gaillard P-HL, McIntyre RE, et al. Disruption of mouse Slx4, a regulator of structure-specific nucleases, phenocopies Fanconi anemia. Nat. Genet. 2011 Feb;43(2):147–52.

272. Kim Y, Lach FP, Desetty R, Hanenberg H, Auerbach AD, Smogorzewska A. Mutations of the SLX4 gene in Fanconi anemia. Nat. Genet. 2011 Feb;43(2):142–6.

273. Fisher LA, Bessho M, Bessho T. Processing of a psoralen DNA interstrand cross-link by XPF-ERCC1 complex in vitro. J. Biol. Chem. 2008 Jan 18;283(3):1275–81.

274. Kumaresan KR, Hwang M, Thelen MP, Lambert MW. Contribution of XPF functional domains to the 5‘ and 3’ incisions produced at the site of a psoralen interstrand cross-link. Biochemistry. 2002 Jan 22;41(3):890–6.

275. Trujillo JP, Mina LB, Pujol R, Bogliolo M, Andrieux J, Holder M, et al. On the role of FAN1 in Fanconi anemia. Blood. 2012 Jul 5;120(1):86–9.

276. Wang AT, Sengerová B, Cattell E, Inagawa T, Hartley JM, Kiakos K, et al. Human SNM1A and XPF-ERCC1 collaborate to initiate DNA interstrand cross-link repair. Genes Dev. 2011 Sep 1;25(17):1859–70.

277. Chang DJ, Cimprich KA. DNA damage tolerance: when it's OK to make mistakes. Nat. Chem. Biol. 2009 Feb;5(2):82–90.

278. Moldovan G-L, Pfander B, Jentsch S. PCNA, the maestro of the replication fork. Cell. 2007 May 18;129(4):665–79.

279. Hoege C, Pfander B, Moldovan G-L, Pyrowolakis G, Jentsch S. RAD6-dependent DNA repair is linked to modification of PCNA by ubiquitin and SUMO. Nature. 2002 Sep 12;419(6903):135–41.

280. Watanabe K, Tateishi S, Kawasuji M, Tsurimoto T, Inoue H, Yamaizumi M. Rad18 guides poleta to replication stalling sites through physical interaction and PCNA monoubiquitination. EMBO J. 2004 Oct 1;23(19):3886–96.

281. Guo C, Tang T-S, Bienko M, Parker JL, Bielen AB, Sonoda E, et al. Ubiquitin-binding motifs in REV1 protein are required for its role in the tolerance of DNA damage. Mol. Cell. Biol. 2006 Dec;26(23):8892–900.

282. Bienko M, Green CM, Crosetto N, Rudolf F, Zapart G, Coull B, et al. Ubiquitin-binding domains in Y-family polymerases regulate translesion synthesis. Science. 2005 Dec 16;310(5755):1821–4.

283. Hicks JK, Chute CL, Paulsen MT, Ragland RL, Howlett NG, Guéranger Q, et al. Differential roles for DNA polymerases eta, zeta, and REV1 in lesion bypass of

intrastrand versus interstrand DNA cross-links. Mol. Cell. Biol. 2010 Mar;30(5):1217–30.

284. Sonoda E, Okada T, Zhao GY, Tateishi S, Araki K, Yamaizumi M, et al. Multiple roles of Rev3, the catalytic subunit of polzeta in maintaining genome stability in vertebrates. EMBO J. 2003 Jun 16;22(12):3188–97.

285. Sharma S, Canman CE. REV1 and DNA polymerase zeta in DNA interstrand crosslink repair. Environ. Mol. Mutagen. 2012 Dec;53(9):725–40.

286. Guo C, Fischhaber PL, Luk-Paszyc MJ, Masuda Y, Zhou J, Kamiya K, et al. Mouse Rev1 protein interacts with multiple DNA polymerases involved in translesion DNA synthesis. EMBO J. 2003 Dec 15;22(24):6621–30.

287. Hara K, Hashimoto H, Murakumo Y, Kobayashi S, Kogame T, Unzai S, et al. Crystal structure of human REV7 in complex with a human REV3 fragment and structural implication of the interaction between DNA polymerase zeta and REV1. J. Biol. Chem. 2010 Apr 16;285(16):12299–307.

288. Acharya N, Johnson RE, Prakash S, Prakash L. Complex formation with Rev1 enhances the proficiency of Saccharomyces cerevisiae DNA polymerase zeta for mismatch extension and for extension opposite from DNA lesions. Mol. Cell. Biol. 2006 Dec;26(24):9555–63.

289. Leung JWC, Wang Y, Fong K-W, Huen MSY, Li L, Chen J. Fanconi anemia (FA) binding protein FAAP20 stabilizes FA complementation group A (FANCA) and participates in interstrand cross-link repair. Proc. Natl. Acad. Sci. U.S.A. 2012 Mar 20;109(12):4491–6.

290. Kim H, Yang K, Dejsuphong D, D'Andrea AD. Regulation of Rev1 by the Fanconi anemia core complex. Nat. Struct. Mol. Biol. 2012 Feb;19(2):164–70.

291. Howlett NG, Taniguchi T, Olson S, Cox B, Waisfisz Q, De Die-Smulders C, et al. Biallelic inactivation of BRCA2 in Fanconi anemia. Science. 2002 Jul 26;297(5581):606–9.

292. Reid S, Schindler D, Hanenberg H, Barker K, Hanks S, Kalb R, et al. Biallelic mutations in PALB2 cause Fanconi anemia subtype FA-N and predispose to childhood cancer. Nat. Genet. 2007 Feb;39(2):162–4.

293. Liu Y, Tarsounas M, O'regan P, West SC. Role of RAD51C and XRCC3 in genetic recombination and DNA repair. J. Biol. Chem. 2007 Jan 19;282(3):1973–9.

294. Vaz F, Hanenberg H, Schuster B, Barker K, Wiek C, Erven V, et al. Mutation of the RAD51C gene in a Fanconi anemia-like disorder. Nat. Genet. 2010 May;42(5):406–9.

295. Sommers JA, Rawtani N, Gupta R, Bugreev DV, Mazin AV, Cantor SB, et al. FANCJ uses its motor ATPase to destabilize protein-DNA complexes, unwind triplexes, and inhibit RAD51 strand exchange. J. Biol. Chem. 2009 Mar 20;284(12):7505–17.

296. Litman R, Peng M, Jin Z, Zhang F, Zhang J, Powell S, et al. BACH1 is critical for homologous recombination and appears to be the Fanconi anemia gene product FANCJ. Cancer Cell. 2005 Sep;8(3):255–65.

297. Long DT, Räschle M, Joukov V, Walter JC. Mechanism of RAD51-dependent

DNA interstrand cross-link repair. Science. 2011 Jul 1;333(6038):84–7.

298. Hashimoto Y, Ray Chaudhuri A, Lopes M, Costanzo V. Rad51 protects nascent DNA from Mre11-dependent degradation and promotes continuous DNA synthesis. Nat. Struct. Mol. Biol. 2010 Nov;17(11):1305–11.

299. Nakanishi K, Cavallo F, Perrouault L, Giovannangeli C, Moynahan ME, Barchi M, et al. Homology-directed Fanconi anemia pathway cross-link repair is dependent on DNA replication. Nat. Struct. Mol. Biol. 2011 Apr;18(4):500–3.

300. Nakanishi K, Yang Y-G, Pierce AJ, Taniguchi T, Digweed M, D'Andrea AD, et al. Human Fanconi anemia monoubiquitination pathway promotes homologous DNA repair. Proc. Natl. Acad. Sci. U.S.A. 2005 Jan 25;102(4):1110–5.

301. Adamo A, Collis SJ, Adelman CA, Silva N, Horejsi Z, Ward JD, et al. Preventing nonhomologous end joining suppresses DNA repair defects of Fanconi anemia. Mol. Cell. 2010 Jul 9;39(1):25–35.

302. Pace P, Mosedale G, Hodskinson MR, Rosado IV, Sivasubramaniam M, Patel KJ. Ku70 corrupts DNA repair in the absence of the Fanconi anemia pathway. Science. 2010 Jul 9;329(5988):219–23.

303. Bunting SF, Callén E, Kozak ML, Kim JM, Wong N, López-Contreras AJ, et al. BRCA1 functions independently of homologous recombination in DNA interstrand crosslink repair. Mol. Cell. 2012 Apr 27;46(2):125–35.

304. Pichierri P, Franchitto A, Rosselli F. BLM and the FANC proteins collaborate in a common pathway in response to stalled replication forks. EMBO J. 2004 Aug 4;23(15):3154–63.

305. Hirano S, Yamamoto K, Ishiai M, Yamazoe M, Seki M, Matsushita N, et al. Functional relationships of FANCC to homologous recombination, translesion synthesis, and BLM. EMBO J. 2005 Jan 26;24(2):418–27.

306. Nakanishi K, Taniguchi T, Ranganathan V, New HV, Moreau LA, Stotsky M, et al. Interaction of FANCD2 and NBS1 in the DNA damage response. Nat. Cell Biol. 2002 Dec;4(12):913–20.

307. Karanja KK, Cox SW, Duxin JP, Stewart SA, Campbell JL. DNA2 and EXO1 in replication-coupled, homology-directed repair and in the interplay between HDR and the FA/BRCA network. Cell Cycle. 2012 Nov 1;11(21):3983–96.

308. Duquette ML, Zhu Q, Taylor ER, Tsay AJ, Shi LZ, Berns MW, et al. CtIP is required to initiate replication-dependent interstrand crosslink repair. PLoS Genet. 2012;8(11):e1003050.

309. Young JA, Schreckhise RW, Steiner WW, Smith GR. Meiotic recombination remote from prominent DNA break sites in S. pombe. Mol. Cell. 2002 Feb;9(2):253–63.

310. Povirk LF, Han YH, Steighner RJ. Structure of bleomycin-induced DNA double-strand breaks: predominance of blunt ends and single-base 5' extensions. Biochemistry. 1989 Jul 11;28(14):5808–14.

311. Bennardo N, Cheng A, Huang N, Stark JM. Alternative-NHEJ is a mechanistically distinct pathway of mammalian chromosome break repair. PLoS Genet. 2008 Jun;4(6):e1000110.

312. Knipscheer P, Räschle M, Smogorzewska A, Enoiu M, Ho TV, Schärer OD, et al. The Fanconi anemia pathway promotes replication-dependent DNA interstrand cross-link repair. Science. 2009 Dec 18;326(5960):1698–701.

313. Thazhathveetil AK, Liu S-T, Indig FE, Seidman MM. Psoralen conjugates for visualization of genomic interstrand cross-links localized by laser photoactivation. Bioconjug. Chem. 2007 Mar;18(2):431–7.

314. Moldovan G-L, D'Andrea AD. FANCD2 hurdles the DNA interstrand crosslink. Cell. 2009 Dec 24;139(7):1222–4.

315. Sato K, Ishiai M, Toda K, Furukoshi S, Osakabe A, Tachiwana H, et al. Histone chaperone activity of Fanconi anemia proteins, FANCD2 and FANCI, is required for DNA crosslink repair. EMBO J. 2012 Aug 29;31(17):3524–36.

316. Bomar MG, Pai M-T, Tzeng S-R, Li SS-C, Zhou P. Structure of the ubiquitin-binding zinc finger domain of human DNA Y-polymerase eta. EMBO Rep. 2007 Mar;8(3):247–51.

317. Husnjak K, Dikic I. Ubiquitin-binding proteins: decoders of ubiquitin-mediated cellular functions. Annu. Rev. Biochem. 2012;81:291–322.

318. Hofmann K. Ubiquitin-binding domains and their role in the DNA damage response. DNA Repair (Amst.). 2009 Apr 5;8(4):544–56.

319. Cohn MA, D'Andrea AD. Chromatin recruitment of DNA repair proteins: lessons from the fanconi anemia and double-strand break repair pathways. Mol. Cell. 2008 Nov 7;32(3):306–12.

320. Longerich S, Kwon Y, Tsai M-S, Hlaing AS, Kupfer GM, Sung P. Regulation of FANCD2 and FANCI monoubiquitination by their interaction and by DNA. Nucleic Acids Research. 2014 Mar 12.

321. Joo W, Xu G, Persky NS, Smogorzewska A, Rudge DG, Buzovetsky O, et al. Structure of the FANCI-FANCD2 complex: insights into the Fanconi anemia DNA repair pathway. Science. 2011 Jul 15;333(6040):312–6.

322. Sato K, Toda K, Ishiai M, Takata M, Kurumizaka H. DNA robustly stimulates FANCD2 monoubiquitylation in the complex with FANCI. Nucleic Acids Research. 2012 May;40(10):4553–61.

323. Montes de Oca R, Andreassen PR, Margossian SP, Gregory RC, Taniguchi T, Wang X, et al. Regulated interaction of the Fanconi anemia protein, FANCD2, with chromatin. Blood. 2005 Feb 1;105(3):1003–9.

324. Yeo JE, Lee EH, Hendrickson E, Sobeck A. CtIP mediates replication fork recovery in a FANCD2-regulated manner. Hum. Mol. Genet. 2014 Mar 4.

325. Barroso E, Milne RL, Fernández LP, Zamora P, Arias JI, Benítez J, et al. FANCD2 associated with sporadic breast cancer risk. Carcinogenesis. 2006 Sep;27(9):1930–7.

326. Zhou W, Otto EA, Cluckey A, Airik R, Hurd TW, Chaki M, et al. FAN1 mutations cause karyomegalic interstitial nephritis, linking chronic kidney failure to defective DNA damage repair. Nat. Genet. 2012 Aug;44(8):910–5.

327. Yoshikiyo K, Kratz K, Hirota K, Nishihara K, Takata M, Kurumizaka H, et al. KIAA1018/FAN1 nuclease protects cells against genomic instability induced by

interstrand cross-linking agents. Proc. Natl. Acad. Sci. U.S.A. 2010 Dec 14;107(50):21553–7.

328. Sobeck A, Stone S, Costanzo V, de Graaf B, Reuter T, de Winter J, et al. Fanconi anemia proteins are required to prevent accumulation of replication-associated DNA double-strand breaks. Mol. Cell. Biol. 2006 Jan;26(2):425–37.

329. Fugger K, Chu WK, Haahr P, Kousholt AN, Beck H, Payne MJ, et al. FBH1 co-operates with MUS81 in inducing DNA double-strand breaks and cell death following replication stress. Nat Commun. 2013;4:1423.

330. Couch FB, Bansbach CE, Driscoll R, Luzwick JW, Glick GG, Bétous R, et al. ATR phosphorylates SMARCAL1 to prevent replication fork collapse. Genes Dev. 2013 Jul 15;27(14):1610–23.

331. Blackford AN, Schwab RA, Nieminuszczy J, Deans AJ, West SC, Niedzwiedz W. The DNA translocase activity of FANCM protects stalled replication forks. Hum. Mol. Genet. 2012 May 1;21(9):2005–16.

332. Longhese MP, Bonetti D, Manfrini N, Clerici M. Mechanisms and regulation of DNA end resection. EMBO J. 2010 Sep 1;29(17):2864–74.

333. Hartsuiker E. Detection of covalent DNA-bound Spo11 and topoisomerase complexes. Methods Mol. Biol. 2011;745:65–77.

334. Duursma AM, Driscoll R, Elias JE, Cimprich KA. A role for the MRN complex in ATR activation via TOPBP1 recruitment. Mol. Cell. 2013 Apr 11;50(1):116–22.

335. Lee J, Dunphy WG. The Mre11-Rad50-Nbs1 (MRN) complex has a specific role in the activation of Chk1 in response to stalled replication forks. Mol. Biol. Cell. 2013 May;24(9):1343–53.

336. Shiotani B, Nguyen HD, Håkansson P, Maréchal A, Tse A, Tahara H, et al. Two distinct modes of ATR activation orchestrated by Rad17 and Nbs1. Cell Rep. 2013 May 30;3(5):1651–62.

337. Taniguchi T, D'Andrea AD. Molecular pathogenesis of Fanconi anemia: recent progress. Blood. 2006 Jun 1;107(11):4223–33.

338. Kennedy RD, D'Andrea AD. DNA repair pathways in clinical practice: lessons from pediatric cancer susceptibility syndromes. J. Clin. Oncol. 2006 Aug 10;24(23):3799–808.

339. Chen CC, Kennedy RD, Sidi S, Look AT, D'Andrea A. CHK1 inhibition as a strategy for targeting Fanconi Anemia (FA) DNA repair pathway deficient tumors. Mol. Cancer. 2009;8:24.

340. Shaheen M, Allen C, Nickoloff JA, Hromas R. Synthetic lethality: exploiting the addiction of cancer to DNA repair. Blood. 2011 Jun 9;117(23):6074–82.

341. Gatei M, Jakob B, Chen P, Kijas AW, Becherel OJ, Gueven N, et al. ATM protein-dependent phosphorylation of Rad50 protein regulates DNA repair and cell cycle control. J. Biol. Chem. 2011 Sep 9;286(36):31542–56.

342. Swift S, Lorens J, Achacoso P, Nolan GP. Rapid production of retroviruses for efficient gene delivery to mammalian cells using 293T cell-based systems. Curr Protoc Immunol. 2001 May;Chapter 10:Unit10.17C.

343. Moreno S, Klar A, Nurse P. Molecular genetic analysis of fission yeast Schizosaccharomyces pombe. Meth. Enzymol. 1991;194:795–823.

8. ACKNOWLEDGEMENTS

First and foremost I would like to thank my supervisor Prof. Alessandro A. Sartori for giving me the opportunity to do my PhD in his laboratory. I am very grateful for all his valuable advice, support and for the excellent supervision he provided me.

I would also like to acknowledge all the present and past members of the Sartori laboratory for creating the perfect working atmosphere. Especially, I would like to thank Christine and Ufuk who contributed significantly to my work and Lorenza for the fruitful scientific discussions. Many thanks to Hella for assistance in my project and for writing the german summary. I would also like to acknowledge Martin for his help, particularly in the beginning of my PhD, and Kay for his contribution to the manuscript on the role of CtIP in ICL repair.

I would also like to sincerely thank my Thesis Committee members: Prof. Massimo Lopes, Prof. Primo Leo Schär and Dr. Manuel Stucki for critical discussions and scientific advice during my PhD.

Further I would like to express my gratitude to all the members of IMCR for providing exciting scientific exchanges and sharing reagents. I am grateful to Prof. Josef Jiricny for running such a great institute as IMCR and for his valuable suggestions.

Thanks to the Cancer Biology PhD program where I made some good friends.

I would also like to acknowledge my family, especially my mother for her support and encouragement. Last but not least I would like to thank Vadim for always being there for me and for all the discussions and fun we had together.

9. CURRICULUM VITAE

Surname	**MURINA**
Name	**Olga**
Date of birth	22nd June 1985
Nationality	Russian

Education

08/2009 – present	**PhD**, Cancer Biology PhD program, Laboratory of Prof. Dr. Alessandro A. Sartori, Institute of Molecular Cancer Research, University of Zurich, Switzerland.
09/2006 – 12/2008	**Master of Science in Biology**, *cum laude*, Saint-Petersburg State University, Russia.
09/2002 – 07/2006	**Bachelor of Science in Biology**, *cum laude*, Saint-Petersburg State University, Russia.
09/1999 – 06/2002	**Certificate of secondary (complete) general education**, Academic Gymnasium of Saint-Petersburg State University, Russia.

Relevant research experience

08/2009 – present	**Graduate studies,** Laboratory of Prof. Dr. Alessandro A. Sartori, Institute of Molecular Cancer Research, University of Zurich, Switzerland. Supervisor: Prof. Dr. Alessandro A. Sartori. Title: Molecular and cellular aspects of DNA-end resection by human CtIP.
09/2006 – 12/2008	**Master's thesis,** Laboratory of Physiological Genetics, Department of Genetics and Breeding, Faculty of Biology and Soil Sciences, Saint-Petersburg State University, Russia. Supervisor: Prof. Dr. Galina A. Zhouravleva. Title: Identification of genes influencing *sup45* nonsense mutants' viability in yeast *Saccharomyces cerevisiae*.
09/2003 – 06/2006	**Undergraduate research work,** Laboratory of Physiological Genetics, Department of Genetics and Breeding, Faculty of Biology and Soil Sciences, Saint-Petersburg State University, Russia. Supervisor: Prof. Dr. Galina A. Zhouravleva. Title: Search for genes influencing translation termination in yeast *Saccharomyces cerevisiae*.

Teaching experience

2012 – 2013	Supervision of a Master student, Laboratory of Prof. Dr. A. A. Sartori
2009 and 2010	Teaching assistant, Practical Block course "Genome Instability and Molecular Cancer Research" for Master students, University of Zurich

Publications

- **Murina O**, von Aesch C, Karakus U, Ferretti LP, Bolck HA, Hänggi K, Sartori AA. FANCD2 and CtIP cooperate to repair DNA interstrand crosslinks // *Cell Reports. 2014 May 22;7(4):1030-8.*

- Adelman CA, Lolo RL, Birkbak NJ, **Murina O**, Matsuzaki K, Horejsi Z, Parmar K, Borel V, Skehel JM, Stamp G, D'Andrea A, Sartori AA, Swanton C, Boulton SJ. HELQ promotes RAD51 paralogue-dependent repair to avert germ cell loss and tumorigenesis. // *Nature 2013 Oct 17;502(7471):381-4.*

- Steger M, **Murina O**, Hühn D, Ferretti LP, Walser R, Hänggi K, Lafranchi L, Neugebauer C, Paliwal S, Janscak P, Gerrits B, Del Sal G, Zerbe O, Sartori AA. Prolyl isomerase PIN1 regulates DNA double-strand break repair by counteracting DNA end resection // *Mol Cell. 2013 May 9;50(3):333-43.*

Presentations at Scientific Conferences

- FEBS DNA Repair Workshop: "NER and interstrand crosslink repair - from molecules to man", Smolenice Castle, Slovakia (June 9-13, 2013). Short talk and poster presentation: "CtIP associates with FANCD2 to promote faithful recombinational repair of DNA interstrand crosslinks".

- Keystone Symposia Conference on "X6: Genome Instability and DNA Repair", Banff, Canada (March 3-8, 2013). Poster presentation: "CtIP associates with FANCD2 to prime homology-directed repair of DNA interstrand crosslinks".

- 1st Swiss Meeting on "Genome Stability and Chromatin Dynamics", Weggis, Switzerland (May 30 - June 1, 2012). Poster presentation: "Diverse functions of CtIP in the repair of DNA interstrand crosslinks".

- Abcam Conference on "Maintenance of Genome Stability", Nassau, Bahamas (March 5-8, 2012). Poster presentation: "Investigating the function of human RAD50S mutants in the DNA damage response".

10. APPENDIX

10.1. Prolyl Isomerase PIN1 Regulates DNA Double-Strand Break Repair by Counteracting DNA End Resection

Martin Steger, **Olga Murina**, Daniela Huehn, Lorenza P. Ferretti, Reto Walser, Kay Haenggi, Lorenzo Lafranchi, Christine Neugebauer, Shreya Paliwal, Pavel Janscak, Bertran Gerrits, Giannino Del Sal, Oliver Zerbe and Alessandro A. Sartori

article published in Molecular Cell, 2013

I contributed the Figures 6A-B, S2G, S7A and performed the DR-GFP reporter assays in HEK293 and U2OS cells displayed in Fig. 1B-C, S2A and S7G.

Molecular Cell
Article

Prolyl Isomerase PIN1 Regulates DNA Double-Strand Break Repair by Counteracting DNA End Resection

Martin Steger,[1] Olga Murina,[1] Daniela Hühn,[1] Lorenza P. Ferretti,[1] Reto Walser,[2] Kay Hänggi,[1] Lorenzo Lafranchi,[1] Christine Neugebauer,[1] Shreya Paliwal,[1] Pavel Janscak,[1] Bertran Gerrits,[3] Giannino Del Sal,[4,5] Oliver Zerbe,[2] and Alessandro A. Sartori[1,*]
[1]Institute of Molecular Cancer Research
[2]Institute of Organic Chemistry
[3]Functional Genomics Center Zurich
University of Zurich, Winterthurerstrasse 190, CH-8057 Zürich, Switzerland
[4]Laboratorio Nazionale CIB, Area Science Park, Padriciano 99, 34149 Trieste, Italy
[5]Department of Life Sciences, University of Trieste, 34100 Trieste, Italy
*Correspondence: sartori@imcr.uzh.ch
http://dx.doi.org/10.1016/j.molcel.2013.03.023

SUMMARY

The regulation of DNA double-strand break (DSB) repair by phosphorylation-dependent signaling pathways is crucial for the maintenance of genome stability; however, remarkably little is known about the molecular mechanisms by which phosphorylation controls DSB repair. Here, we show that PIN1, a phosphorylation-specific prolyl isomerase, interacts with key DSB repair factors and affects the relative contributions of homologous recombination (HR) and nonhomologous end-joining (NHEJ) to DSB repair. We find that PIN1-deficient cells display reduced NHEJ due to increased DNA end resection, whereas resection and HR are compromised in PIN1-overexpressing cells. Moreover, we identify CtIP as a substrate of PIN1 and show that DSBs become hyperresected in cells expressing a CtIP mutant refractory to PIN1 recognition. Mechanistically, we provide evidence that PIN1 impinges on CtIP stability by promoting its ubiquitylation and subsequent proteasomal degradation. Collectively, these data uncover PIN1-mediated isomerization as a regulatory mechanism coordinating DSB repair.

INTRODUCTION

In response to DNA double-strand breaks (DSBs), cells initiate an elaborate signaling cascade known as the DNA damage response (DDR) to maintain genomic integrity (Jackson and Bartek, 2009). The DDR coordinates cell-cycle checkpoints and DNA repair or—if the damage cannot be repaired—triggers specialized programs such as apoptosis and senescence (Ciccia and Elledge, 2010). DSBs are the most cytotoxic lesions that are induced by ionizing radiation (IR) and DNA topoisomerase II poisons, such as etoposide (ETOP) and doxorubicin (Jackson and Bartek, 2009). They also frequently arise during S phase when replication forks encounter persistent single-strand breaks that are caused by camptothecin (CPT), a DNA topoisomerase I poison, or poly(ADP-ribose) polymerase (PARP) inhibitors (Pommier, 2006; Rouleau et al., 2010). Although DSBs are suitable substrates for both homologous recombination (HR) and nonhomologous end-joining (NHEJ), DSBs resulting from replication fork collapse are preferentially repaired by HR, whereas those induced by IR and ETOP are mostly addressed by NHEJ (Helleday, 2010; Shibata et al., 2011). It has been shown that NHEJ largely contributes to genomic instability and cytotoxicity in HR-defective cells treated with CPT or PARP inhibitors (Adachi et al., 2004; Eid et al., 2010; Patel et al., 2011). In contrast, HR is able to compensate to some degree for the repair of IR-induced DSBs in NHEJ mutant cells during late S/G2 phase (Beucher et al., 2009; Shibata et al., 2011).

HR is a rather slow, multistep repair process restricted to S/G2 phase when the intact sister chromatid is available to allow error-free repair (Heyer et al., 2010). Briefly, HR requires 5′ to 3′ nucleolytic degradation of DSB ends to generate long stretches of single-stranded DNA (ssDNA) - a mechanism generally described as DNA end resection. In vertebrates, DNA end resection is initiated by the collaborative action of the MRE11-RAD50-NBS1 (MRN) complex together with CtIP (Sartori et al., 2007). Subsequently, EXO1 and BLM are involved in long-range resection exposing long 3′ ssDNA tails that are immediately coated with RPA (Gravel et al., 2008). Finally, BRCA2 promotes the exchange of RPA with RAD51, allowing ssDNA-RAD51 nucleoprotein filaments to carry out homology search and DNA strand invasion (Heyer et al., 2010). In contrast, NHEJ occurs with faster kinetics and functions throughout the cell cycle (Shibata et al., 2011). Besides cell-cycle stage and DSB complexity, the division of labor between the two DSB repair pathways was shown to depend on the chromatin state around the lesion (Goodarzi et al., 2010). Mechanistically, however, DNA end resection is the key determinant of DSB repair pathway choice, because it prevents repair by NHEJ and commits cells to HR (Chapman et al., 2012).

Besides ATM-mediated phosphorylation of substrates at S/T-Q motifs in response to DSBs, phosphorylation at S/T-P

motifs is another major signaling mechanism in the regulation of cell-cycle progression and various stress responses (Matsuoka et al., 2007; Bennetzen et al., 2010). Enzymes responsible for S/T-P phosphorylation belong to a large family of proline-directed protein kinases, including cyclin-dependent kinases (CDKs) and mitogen-activated protein kinases (MAPKs) (Ubersax and Ferrell, 2007). Strikingly, CDK activity is required for DNA end resection and HR (Aylon et al., 2004; Ira et al., 2004; Huertas et al., 2008). However, it is currently unclear how, mechanistically, phosphorylation affects DSB repair pathway choice. Interestingly, a subset of proteins phosphorylated at S/T-P motifs exist in two different configurations, namely as *cis* and *trans* isoforms. The intrinsically slow interconversion between these two forms can be catalyzed by PIN1, which specifically binds phosphorylated S/T-P motifs through its WW domain and catalyzes *cis/trans* isomerization through its peptidylprolyl isomerase (PPIase) domain (Yaffe et al., 1997). In this way, PIN1 acts as a molecular switch to control the function of several proteins, including cell-cycle regulators and transcription factors, but so far has not been linked to DNA repair processes (Liou et al., 2011).

Here, we report that PIN1 interacts with prominent DSB repair factors including 53BP1, BRCA1-BARD1, and CtIP. Using immortalized and cancer cell lines, we find that PIN1 overexpression attenuates HR, while PIN1 depletion reduces NHEJ as a result of increased DNA end resection. We further demonstrate that PIN1-mediated isomerization of CtIP requires CtIP phosphorylation at two conserved S/T-P motifs (S276 and T315) and show that CDK2 activity is required for PIN1-CtIP interaction. We report that cells expressing a phosphomutant form of CtIP (CtIP-2A) deficient in PIN1 interaction exhibit hyperresection phenotypes similar to PIN1-deficient cells. Finally, we provide evidence that PIN1 negatively regulates CtIP protein stability by promoting CtIP polyubiquitylation and subsequent proteasomal degradation. Altogether, our findings uncover a key role for the prolyl isomerase PIN1 in controlling CtIP-dependent DNA end resection and, consequently, DSB repair.

RESULTS

PIN1 Isomerase Is Involved in the Regulation of DSB Repair

The importance of S/T-P phosphorylation in the regulation of DSB repair and the fact that PIN1 modulates the function of proteins phosphorylated at S/T-P motifs through proline isomerization prompted us to examine whether PIN1 interacts with DSB repair proteins. To this end, we performed pull-down experiments with recombinant GST-tagged PIN1, followed by mass spectrometry (MS) analysis. Besides known PIN1 substrates and many potentially novel PIN1 interaction partners, we identified several prominent DDR factors implicated in DSB repair, including BRCA1, 53BP1, and CtIP (see Figure S1 and Table S1 available online). Since all these factors were shown to be involved in DSB repair pathway choice, we examined whether PIN1 affects the repair of DSB by NHEJ or HR using cell lines bearing EJ5-GFP or DR-GFP reporter cassettes, respectively (Bennardo et al., 2008). Depletion of PIN1 decreased NHEJ frequencies to levels similar to those achieved by depleting key NHEJ factors such as XRCC4 and 53BP1 (Figure 1A) (Bunting et al., 2010). Conversely, we observed a slight but statistically significant increase in HR efficiency upon PIN1 depletion in both HEK293 and U2OS DR-GFP cells, while CtIP depletion resulted in a strong reduction in HR, as expected (Figure 1B and Figure S2A) (Sartori et al., 2007; Bennardo et al., 2008). Based on these observations, we speculated that high levels of PIN1 could interfere with HR. Indeed, transient overexpression of PIN1 caused a significant decrease in the HR reporter signal, without affecting the cell-cycle distribution (Figure 1C and Figure S2B). Importantly, the negative effect of PIN1 on HR was dependent on both substrate recognition and isomerization, as overexpression of a phospho-binding mutant (W34A) or a catalytic mutant (C113A) diminished HR to a lesser extent (1.4- and 2.0-fold, respectively) compared to wild-type (WT) (3.1-fold) (Figure 1C).

Next, we examined whether DSB signaling is altered in U2OS cells depleted for PIN1 by analyzing the phosphorylation status of prominent DDR factors after ETOP treatment. Interestingly, knockdown of PIN1 caused a marked increase in RPA2 hyperphosphorylation, indicative of increased ssDNA formation, but did not alter cell-cycle distribution profiles (Figure 1D, Figures S2C and S2D) (Sartori et al., 2007; Kousholt et al., 2012). Moreover, in agreement with increased rates of DNA end resection, we found that PIN1-depleted cells were more resistant to CPT than control-depleted cells, a phenotype which is reminiscent of NHEJ-deficient cells (Figure S2E) (Adachi et al., 2004; Eid et al., 2010; Shibata et al., 2011).

To further investigate whether loss of PIN1 indeed compromises NHEJ, we used pulsed-field gel electrophoresis (PFGE) to monitor the efficiency of *Pin1* knockout mouse embryonic fibroblasts (MEFs) in repairing ETOP-induced DSBs. *Pin1*$^{-/-}$ MEFs displayed both increased RPA2 phosphorylation and slower repair kinetics compared to PIN1-complemented cells, indicative of a defect in NHEJ caused by increased DNA resection (Figure 1E and Figure S2F). Consistent with impaired DNA end resection, we detected a clear reduction in IR-induced phosphorylation of RPA2 at S4/S8 after transient overexpression of PIN1-wt compared to mock-transfected cells or to cells overexpressing PIN1-W34A (Figure 1F and Figure S2G). Since we have identified the DNA end resection factor CtIP in our screen for PIN1 interactors (Figure S1), we addressed whether CtIP could be responsible for the observed hyperresection phenotype of PIN1-deficient cells. To this end, we depleted PIN1, CtIP, or both factors together from U2OS cells and monitored RPA foci formation in response to ETOP treatment as readout for DSB resection (Figure 1G and Figure S2H). As expected, approximately 25% of control-depleted cells exhibited RPA foci, and their formation was strictly CtIP dependent (Helleday, 2010; Shibata et al., 2011). Furthermore, and consistent with increased RPA2 phosphorylation, depletion of PIN1 led to an almost 2-fold increase in RPA-foci-positive cells. Remarkably, this increase was entirely dependent on CtIP, suggesting that PIN1 limits the resection activity of CtIP. Similarly, codepletion of CtIP partially rescued the NHEJ defect in PIN1-depleted HEK293 EJ5-GFP reporter cells, further demonstrating that PIN1 promotes NHEJ by counteracting CtIP-dependent DNA resection (Figure 1H). The fact that

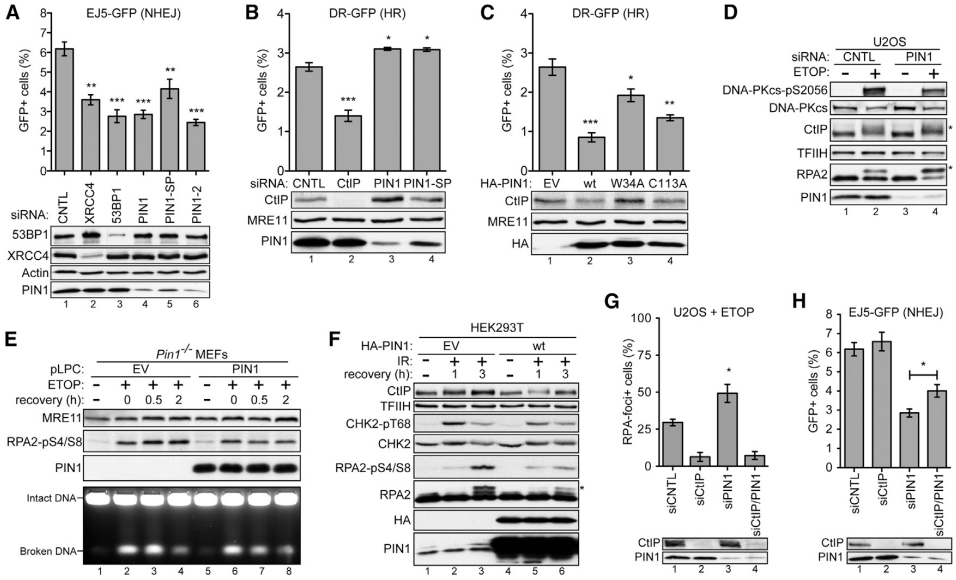

Figure 1. PIN1 Regulates DSB Repair

(A) HEK293 EJ5-GFP cells were transfected with the indicated siRNAs. Two days later, cells were transfected with the I-SceI expression plasmid and harvested after 48 hr for flow cytometry and immunoblot analysis.

(B) HEK293 DR-GFP cells were transfected with the indicated siRNAs and further processed as in (A).

(C) HEK293 DR-GFP cells were cotransfected with the indicated HA-PIN1 variants together with the I-SceI plasmid and further processed as in (A).

(D) Control- or PIN1-depleted U2OS cells were treated with etoposide (ETOP, 20 μM) for 6 hr, and whole-cell extracts were analyzed by immunoblotting. Asterisks indicate hyperphosphorylated forms of CtIP and RPA2, respectively.

(E) *Pin1*$^{-/-}$ MEFs complemented with empty vector (EV, pLPC) or PIN1 were treated with ETOP (10 μM) for 2 hr and lysed at the indicated times after ETOP removal. Whole-cell extracts were analyzed by immunoblotting, and the amount of broken DNA was assessed by PFGE followed by ethidium bromide (EtBr) staining (see also Figure S2F for quantification of the PFGE signals).

(F) HEK293T cells were transfected with empty vector (EV, pcDNA3.1) or HA-PIN1-wt for 72 hr. Cells were irradiated (30 Gy) and whole-cell extracts were prepared at indicated times and analyzed by immunoblotting. Asterisk indicates hyperphosphorylated form of RPA2.

(G) Forty-eight hours after transfection with the indicated siRNAs, U2OS cells grown on coverslips were treated with ETOP (5 μM) for 1 hr, fixed, and coimmunostained for γ-H2AX and RPA2 (see also Figure S2H). In each sample at least 50 cells were scored. Graph shows the percentage of cells exhibiting more than 10 RPA foci/nuclei. Immunoblot analysis of the same samples is shown below.

(H) Shown is NHEJ assay and immunoblot analysis after transfection with the indicated siRNAs as in (A). In (A), (B), (C), (G), and (H), data are represented as mean ± SEM (n ≥ 3). See also Figure S2.

CtIP depletion did not fully restore NHEJ could be explained by the possibility that, besides restricting the function of CtIP in DNA end resection, PIN1 may facilitate NHEJ through alternative mechanisms. For instance, we have identified 53BP1 and BRCA1 as putative PIN1 substrates (Figure S1), both playing key roles in the regulation of DSB repair pathway choice (Bunting et al., 2010).

PIN1 Interacts with CtIP Phosphorylated at Two S/T-P Motifs

To confirm the result of our MS analysis, suggesting that PIN1 and CtIP form a complex, we subjected whole-cell extracts from U2OS cells or from U2OS cells stably expressing GFP-tagged CtIP to GST-PIN1 pull-down assays. We found that both endogenous CtIP and GFP-CtIP interact with PIN1-wt but not with the PIN1-W34A mutant, indicating that the interaction is mediated by phosphorylation (Figure 2A). Consistently, treatment of extracts with λ-phosphatase prior to GST-PIN1 pull-down completely abolished the interaction with CtIP (Figures S3A and S3B). Next, we verified whether endogenous PIN1-CtIP complexes exist in cells by performing proximity ligation assays (in situ PLA), an elegant method to detect protein-protein interactions in situ (Söderberg et al., 2006). As shown in Figure 2B, we detected robust PLA signals in most of the cells, demonstrating interaction between PIN1 and CtIP. Moreover, we repeatedly observed more PLA signals per nucleus in EdU-positive cells than in EdU-negative cells, indicative of an increased PIN1-CtIP interaction during S phase (Figure 2B and Figure S3C).

Human CtIP contains in total 12 S/T-P motifs that could be targeted by proline-directed kinases (Figure S3D). To identify which of these motifs are recognized by PIN1, we tested the binding of PIN1 to a panel of serine/threonine to alanine point mutants of CtIP in a series of GST pull-down experiments

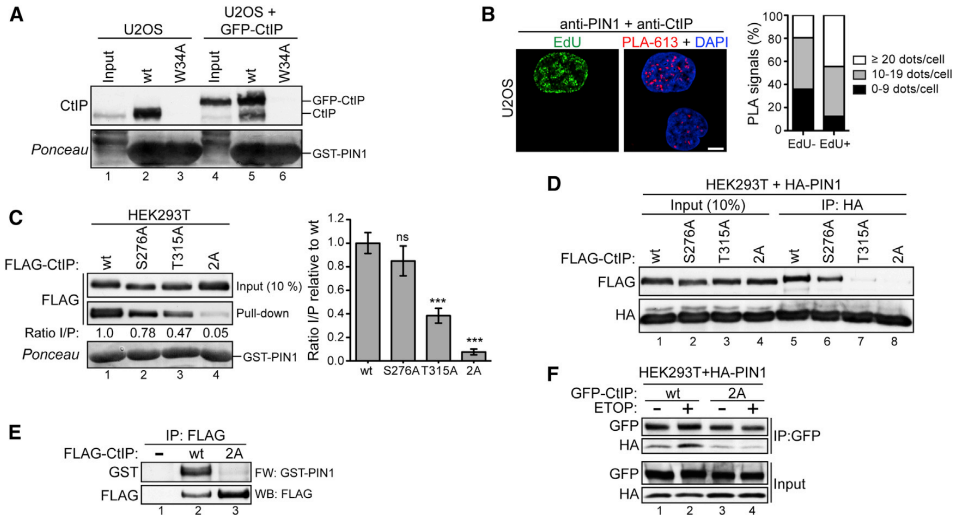

Figure 2. PIN1 Interacts with CtIP through Phosphorylated S/T-P Motifs

(A) GST-PIN1-wt or -W34A fusion proteins were immobilized on glutathione-Sepharose beads and incubated with whole-cell extracts from either U2OS cells (lanes 1–3) or U2OS cells stably expressing GFP-CtIP (lanes 4–6). Inputs and precipitated bead fractions from the pull-downs were subjected to immunoblotting with anti-CtIP antibodies.

(B) (Left) Detection of endogenous PIN1-CtIP complexes by in situ proximity ligation assay (PLA). U2OS cells were pulse labeled with 5′-ethynyl-2′-deoxyuridine (EdU, 10 μM) for 15 min, fixed, and incubated with antibodies against PIN1 and CtIP prior to detection of protein-protein interactions using a fluorescently labeled probe (PLA-613). Nuclei were visualized by DAPI staining, and EdU incorporation was detected according to the manufacturer's instructions (see also Figure S3C). (Right) Quantification of the PLA signals/cell. For both conditions, PLA signals from at least 50 cells were enumerated. Scale bar, 5 μm.

(C) (Left) GST-PIN1 pull-down assay using extracts of HEK293T cells expressing indicated FLAG-tagged versions of CtIP. The band intensities were quantified using ImageJ and represented as input/pull-down (I/P) ratios. (Right) Data are represented as mean values of densitometric quantification ± SEM ($n \geq 5$).

(D) HEK293T cells were cotransfected with HA-PIN1 and the indicated FLAG-CtIP plasmids. HA-PIN1 was immunoprecipitated from whole-cell extracts using anti-HA antibody, and immunocomplexes were analyzed by western blotting.

(E) Anti-FLAG immunoprecipitates from empty vector- or FLAG-CtIP-transfected HEK293T cells were subjected to far-western blotting using purified GST-PIN1 as a probe, followed by immunodetection with anti-GST antibody. After stripping, the same membrane was reprobed using anti-FLAG antibody.

(F) HEK293T cells were cotransfected with GFP-CtIP (wt and 2A) and HA-PIN1 for 48 hr before treatment with ETOP (10 μM) for 2 hr. Whole-cell extracts were analyzed by western blotting before (input) and after immunoprecipitation (IP) using anti-GFP antibody. See also Figure S3.

(Figures S3E–S3G). Our analysis revealed that PIN1-CtIP interaction is mainly mediated by T315 and is almost completely abolished in cells expressing a CtIP-S276A/T315A double mutant (CtIP-2A; Figure 2C). To corroborate these findings, we performed anti-HA immunoprecipitation experiments in HEK293T cells cotransfected with FLAG-CtIP and HA-PIN1 expression constructs. As expected, CtIP-wt did not interact with PIN1-W34A but was efficiently coprecipitated with PIN1-wt and PIN1-C113A (Figure S3H). Moreover, we were able to confirm that mutating either S276 or T315 to nonphosphorylatable alanine reduced the binding to PIN1, while PIN1-CtIP interaction is almost completely abolished in the CtIP-2A mutant (Figure 2D). In addition, far-western blot analysis indicated that this interaction is direct and that CtIP-T315 is more crucial for PIN1 binding than CtIP-S276 (Figure 2E and Figure S3I). Finally, we addressed whether PIN1-CtIP interaction is influenced by DNA damage and observed a slight increase in complex formation upon ETOP treatment, suggesting that CtIP phosphorylation at S276 and/or T315 may be induced upon DNA damage (Figure 2F).

CtIP-T315 Phosphorylation Promotes PIN1-CtIP Interaction

By examining the amino acid sequences surrounding S276 and T315, we noticed that both residues are highly conserved in mammals, suggesting that they are possibly targeted by proline-directed kinases in vivo (Figure S4A). In order to address whether T315 and S276 are indeed phosphorylated in vivo, we raised individual phospho-specific antibodies. As a first line of evidence, both phospho-antibodies recognized wt CtIP transiently overexpressed in cells, but not the corresponding alanine substitution mutants (Figure 3A). Second, we specifically detected CtIP-T315 after immunoprecipitating endogenous CtIP from HEK293T cells followed by immunoblotting with the anti-pT315 antibody, whereas the signal completely disappeared upon pretreatment of the extracts with λ-phosphatase (Figure 3B).

We next investigated whether CtIP-T315 phosphorylation increased after ETOP treatment but did not observe any significant changes in pT315 levels, suggesting that the enhanced binding of PIN1 to CtIP in presence of DNA damage (Figure 2F)

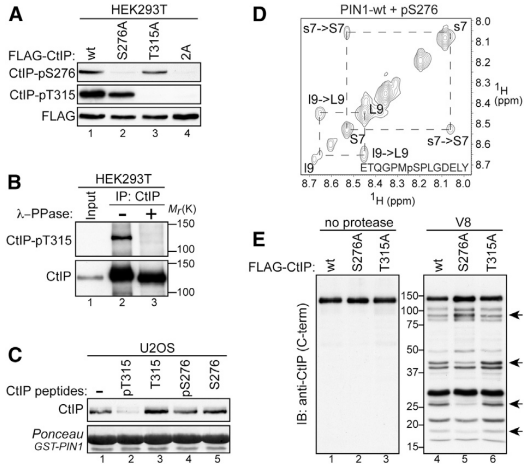

Figure 3. CtIP-T315 and CtIP-S276 Are Phosphorylated to Promote PIN1 Binding and *cis/trans* Isomerization

(A) Extracts from HEK293T cells transfected for 48 hr with the indicated FLAG-CtIP constructs were immunoblotted with either rabbit polyclonal antibodies raised against CtIP phosphopeptides or with anti-FLAG antibody.

(B) Extracts from HEK293T cells were treated with λ-PPase, immunoprecipitated using anti-CtIP antibody, and immunoblotted with the indicated antibodies.

(C) GST-PIN1 pull-down assays were performed using U2OS whole-cell extracts (0.5 mg) supplemented with the indicated CtIP peptides (80 μg).

(D) Shown is selected region of the two-dimensional ROESY spectra of the CtIP-pS276 peptide after incubation with purified, recombinant GST-PIN1.

(E) HEK293T cells were transfected with the indicated FLAG-CtIP constructs for 72 hr. CtIP proteins were purified using M2 magnetic beads, eluted with 3xFLAG peptides, digested with V8 protease, and analyzed by western blotting using anti-CtIP antibody. See also Figure S4 and Figure S5.

is mediated more by CtIP-S276 phosphorylation (Figure S4B). Finally, we were able to confirm the phosphorylation on T315 in vivo by MS analysis of CtIP immunoprecipitated from HEK293T cells (Figure S4C). To further substantiate our previous findings that pT315 is more crucial for PIN1 binding compared to pS276 (Figures 2C and 2D), we used synthetic CtIP phosphopeptides and examined their ability to compete for PIN1 binding in GST-PIN1 pull-down experiments. Remarkably, we found that increasing amounts of pT315 peptides completely abolished PIN1-CtIP interaction, whereas pS276 peptides and the nonphosphopeptides failed to do so, strongly suggesting that CtIP-pT315 is the preferred PIN1 binding site (Figure 3C and Figure S5A).

CtIP-S276 Phosphorylation Promotes CtIP Isomerization by PIN1

To determine whether PIN1 catalyzes *cis/trans* isomerization of the phosphorylated S/T-P motifs in CtIP, we applied nuclear magnetic resonance (NMR) spectroscopy to monitor exchange processes in the aforementioned CtIP phosphopeptides in the presence of recombinant PIN1 proteins (Wang et al., 2010). ROESY spectra of both phosphopeptides recorded in the absence of PIN1 were devoid of any crosspeaks that are indicative of an exchange process between the *cis* and *trans* species (data not shown). Importantly, upon addition of PIN1, we detected exchange crosspeaks in the spectrum of the CtIP-pS276 peptide, which were absent in the presence of a catalytically inactive mutant of PIN1 (C113A) and in the nonphosphorylated peptide (Figure 3D and Figures S5B–S5E). However, we could not detect any *cis/trans* isomerization signals in the CtIP-pT315 peptide (Figure S5F). Based on previously published data, we speculated that the presence of two consecutive proline residues in this peptide (pT-P-P) may hinder PIN1 isomerization (Lippens et al., 2007). Interestingly, we observed exchange crosspeaks in the ROESY spectrum of a modified CtIP-pT315 peptide in which the second proline was replaced with leucine (P317L; Figure S5G). In order to address whether PIN1 also isomerizes CtIP-pS276 in the setting of an intact CtIP protein, we performed limited proteolysis experiments using FLAG-CtIP purified from HEK293T cells (Stukenberg and Kirschner, 2001). In large agreement with our NMR data, V8 protease cleavage pattern of CtIP-S276A was clearly different compared to CtIP-wt and CtIP-T315A, indicating that pS276-P277 rather than pT315-P317 is isomerized in vivo (Figure 3E). Collectively, our findings support a model in which CtIP-pT315 is the major PIN1 docking site, whereas CtIP-pS276 serves as a PIN1 isomerization site.

CDK2 Activity Is Required for CtIP-T315 Phosphorylation

Next, we aimed at identifying the protein kinase(s) responsible for CtIP phosphorylation at S276 and T315 and, thus, for CtIP recognition by PIN1. Considering recent data showing that CtIP is targeted by CDKs, we examined whether CDK activity is required for CtIP-PIN1 interaction (Chapman et al., 2012). Interestingly, we found that a short treatment of cells with Roscovitine (a general CDK inhibitor), but not with RO-3306 (a selective CDK1 inhibitor), strongly reduced the binding of PIN1 to CtIP (Figure 4A and Figure S6A). Moreover, consistent with CtIP-T315 being the major PIN1 interaction site, cells treated with Roscovitine also displayed reduced phosphorylation of T315, while phosphorylation of S276 was not affected by CDK inhibition (Figures 4B and 4C). To further substantiate the role of CDKs in promoting CtIP-PIN1 interaction, we transiently expressed dominant-negative (dn) forms of CDK1, CDK2, and CDK4 in HEK293T cells and examined their effect on PIN1 binding to CtIP. As shown in Figure 4D, we observed the strongest reduction in CtIP-PIN1 complex formation in the absence of CDK2 activity, which did not affect cell-cycle distribution (Figure S6B). Furthermore, we found that overexpression of wt CDK2 resulted in a considerable increase in CtIP-PIN1 interaction (Figure S6C). Consistent with a role for CDK2 in the phosphorylation of T315, CtIP-pT315 levels steadily increased during S phase, peaked at late S/G2 phase, and were lowest in G1 (Figure S6D). From this data, we conclude that CDK2, by phosphorylating CtIP at T315, is predominantly responsible for the interaction between CtIP and PIN1.

CtIP-2A Phosphomutant Promotes Hyperresection of DSBs

To investigate the potential functions of CtIP isomerization at the cellular and molecular level, we generated stable U2OS cell

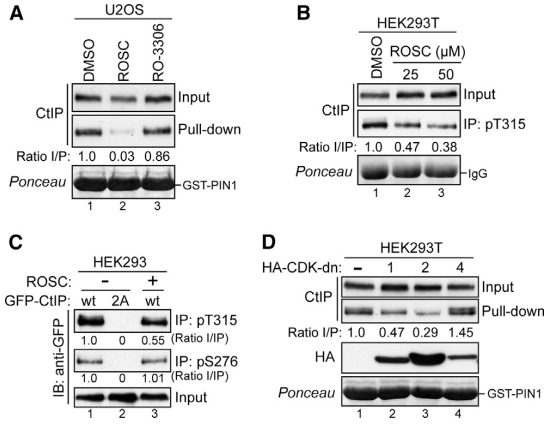

Figure 4. CtIP-PIN1 Interaction and CtIP-T315 Phosphorylation Require CDK2 Activity

(A) Extracts from U2OS cells treated for 2 hr with DMSO, R-Roscovitine (25 μM), or RO-3306 (25 μM) were subjected to GST-PIN1 pull-down assays.

(B) HEK293T cells were treated for 2 hr with DMSO or ROSC, and extracts were immunoblotted for CtIP before (input) and after immunoprecipitation (IP) using the anti-CtIP-pT315 antibody.

(C) HEK293 cells expressing GFP-CtIP (wt and 2A) were treated for 3 hr with either DMSO or ROSC (25 μM). After lysis, whole-cell extracts were immunoblotted for GFP either directly (input) or after immunoprecipitation (IP) with anti-pT315 or anti-pS276 antibodies.

(D) Extracts from HEK293T cells transfected with either pcDNA3.1 (–) or plasmids expressing HA-tagged dominant-negative (dn) mutants of CDK1, CDK2, and CDK4 for 48 hr were subjected to GST-PIN1 pull-down assays. The ratios of input versus pull-down (I/P; in A and D) and input versus IP (I/IP; in B and C) were quantified by densitometry using ImageJ. See also Figure S6.

clones that expressed siRNA-resistant GFP-tagged wt (GFP-CtIP-wt) or mutant CtIP in which both S276 and T315 were changed to nonphosphorylatable alanine (GFP-CtIP-2A) (Figures 5A and 5B). Importantly, the GFP-CtIP-2A mutant protein was still able to interact with BRCA1 and MRE11 (Figure S7A) and to localize to DSB-containing tracks generated by laser microirradiation (Figure 5C and Figure S7B). From this we concluded that PIN1 is required neither for CtIP complex formation with BRCA1 and MRN nor for CtIP recruitment to damaged chromatin that occurs exclusively in S/G2 cells (Sartori et al., 2007; Chen et al., 2008). Moreover, similar to PIN1 depletion, cells expressing CtIP-2A were slightly more CPT resistant than cells expressing CtIP-wt (Figure 5D and Figure S7C). However, the observed increase in CPT resistance could be, at least in part, due to higher expression levels of GFP-CtIP-2A compared to GFP-CtIP-wt (Figure 5A and Figure S7C). Strikingly, like PIN1-depleted cells, CtIP-2A mutant cells treated with ETOP displayed both increased RPA2 hyperphosphorylation and RPA foci formation, indicating higher rates of DSB resection (Figures 5E and 5F and Figure S7D). Since ETOP-induced DSBs are usually repaired with fast kinetics by classical NHEJ, and DNA end resection is known to counteract NHEJ, we speculated that NHEJ is compromised in CtIP-2A mutant cells (Shibata et al., 2011). To this end, we monitored the amount of broken DNA after ETOP treatment in both cell lines in the presence and absence of a DNA-PKcs inhibitor. Indeed, in both NHEJ-proficient and -deficient backgrounds, we found that CtIP-2A cells exhibited more DSBs than did CtIP-wt cells (Figure 5G and Figure S7E). This suggested that the DSB repair defect in CtIP-2A mutant cells is caused by hyperresection, thereby channeling repair into HR, which operates at slower kinetics compared to NHEJ. To further substantiate these findings, we measured the frequencies of HR and NHEJ in HEK293 GFP-reporter cells after transient transfection of CtIP-wt, CtIP-T847A, and CtIP-2A (Figures S7F–S7H). At first, overexpression of the CtIP-2A mutant coincided with a decrease in NHEJ, reflecting the fact that end resection precludes NHEJ usage. In contrast, however, CtIP-2A-expressing cells were as efficient in HR as cells expressing CtIP-wt, indicating that hyperresection may also negatively affect HR by promoting mutagenic types of homology-directed repair such as single-strand annealing (Bennardo et al., 2008). In fact, it was recently reported that depletion of DNA2, which promotes ''long-range'' resection, leads to increased HR using the same reporter cells (Karanja et al., 2012). Accordingly, the anticipated increase in HR due to hyperresection (e.g., in CtIP-2A cells) could be potentially outweighed by the fact that long-range resection hinders the restoration of a functional DR-GFP reporter gene.

Finally, we addressed whether PIN1 restricts CtIP-dependent DNA end resection particularly in late S/G2 phase when both HR and NHEJ are operable but most DSBs preferably undergo NHEJ (Shibata et al., 2011; Karanam et al., 2012). To this end, we exposed late S/G2 cells stably expressing either CtIP-wt or CtIP-2A to IR and measured the extent of DSB resection by monitoring the levels of hyperphosphorylated RPA2. Consistent with our previous results, we noted a significant increase in phosphorylated RPA2 in CtIP-2A mutant cells, indicative of enhanced resection (Figure 5H). Taken together, these results suggest that CtIP isomerization serves as a key regulatory mechanism restricting DSB resection in late S/G2 phase of the cell cycle.

PIN1 Controls CtIP Stability and Promotes Its Ubiquitylation

Prolyl isomerization by PIN1 was shown to play a crucial role in regulating the stability of many proteins (Liou et al., 2011). Interestingly, in many of our PIN1 depletion experiments, we have noticed increased CtIP protein levels (e.g., Figures 1B and 1D). Moreover, we repeatedly observed a reduction in the amount of CtIP after transient transfection of cells with PIN1-wt, but not with PIN1 mutants, particularly in the presence of DSBs (Figures 1C and 1F and Figure 6A). Thus, we speculated that PIN1 might indeed promote CtIP degradation. To address this idea, we treated cells expressing either CtIP-wt or CtIP-2A for 8 hr with MG132. Interestingly, by blocking the ubiquitin-proteasome pathway, we observed a more substantial increase in the levels of CtIP-wt (4.7-fold) compared to those of CtIP-2A (1.7-fold), indicating that PIN1 is at least partially responsible for CtIP degradation under these conditions (Figure 6B). Next, we exposed CtIP-wt- and CtIP-2A-expressing cells to ETOP and, at different time points after the removal of the drug, analyzed CtIP protein turnover by blocking de novo biosynthesis. Strikingly, CtIP-wt levels rapidly dropped after the recovery from ETOP, whereas CtIP-2A levels remained stable (Figure 6C and

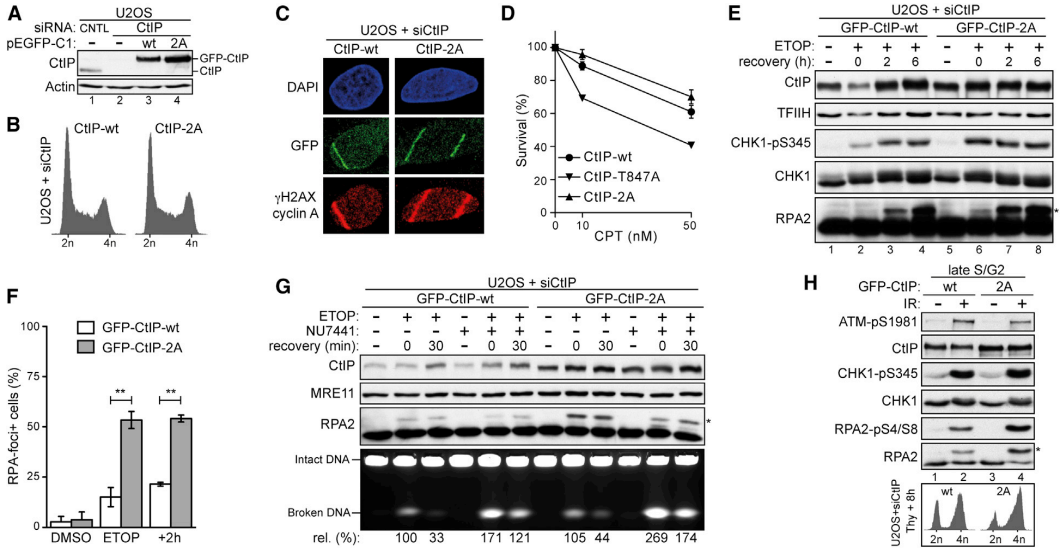

Figure 5. CtIP-2A Mutant Promotes Hyperresection of DSBs

(A) U2OS cells stably expressing siRNA-resistant GFP-tagged CtIP-wt and CtIP-2A or the empty vector (–) were transfected with CNTL or CtIP siRNA for 72 hr, and whole-cell extracts were analyzed by western blotting.

(B) The same cells as in (A) were analyzed by flow cytometry.

(C) The same cells as in (A) were sensitized with BrdU followed by laser microirradiation. After 30 min, cells were fixed, coimmunostained for γ-H2AX and cyclin A, and analyzed by fluorescence microscopy (see also Figure S7B).

(D) The same cells as in (A), including the resection-defective CtIP-T847A mutant, were transfected with CtIP siRNA for 72 hr and treated for 1 hr with either DMSO or low doses of CPT (see also Figure S7C). Survival was determined by colony formation. Data are represented as mean ± SEM (n = 3).

(E) The same cells as in (A) were treated with ETOP (5 μM) for 1 hr, released into drug-free medium for the indicated times, and analyzed by immunoblotting.

(F) The same cells as in (A) were treated with ETOP (5 μM) for 1 hr and were either immediately fixed or released into drug-free medium for 2 hr before fixation. After pre-extraction, cells were coimmunostained for RPA2 and γ-H2AX and analyzed by fluorescence microscopy (see also Figure S7D). For each condition at least 50 cells were scored. Graph shows the percentage of cells exhibiting more than 10 RPA foci per nuclei. Data are represented as mean ± SEM (n ≥ 2).

(G) The same cells as in (A) were treated with ETOP (10 μM) for 2 hr in the absence or presence of a DNA-PKcs inhibitor (NU7441, 10 μM). Cells were harvested either directly or at 30 min after the release into drug-free medium. Whole-cell extracts were analyzed by immunoblotting, and genomic DNA was analyzed by PFGE. DNA breakage in each lane was quantified using ImageJ and normalized against intact DNA. Relative amount of broken DNA in cells expressing GFP-CtIP-wt treated with ETOP was set to 100%.

(H) Same cells as in (A) were synchronized by a single thymidine block. Eight hours after the release from thymidine, cells enriched in S/G2 were irradiated at 30 Gy and, 2 hr later lysates were analyzed by immunoblotting. In (E), (G), and (H), the asterisk indicates the hyperphosphorylated form of RPA2. See also Figure S7.

Figure S8), further supporting the role of PIN1 in negatively regulating CtIP stability. Since polyubiquitylation is a requirement for proteasome-mediated protein degradation, we next addressed whether PIN1 may indeed facilitate CtIP ubiquitylation. To this end, we transfected His-Ubiquitin into HEK293 cell lines inducibly expressing GFP-CtIP and analyzed the level of CtIP polyubiquitylation after Ni-NTA pull-down (Figures 6D and 6E). Strikingly, CtIP ubiquitylation was largely abolished when PIN1 was efficiently depleted (Figure 6F). Moreover, the CtIP-2A mutant was less ubiquitylated compared to CtIP-wt (Figure 6G). Collectively, these results suggest that CtIP isomerization by PIN1 is a prerequisite for CtIP ubiquitylation and subsequent proteasomal degradation.

DISCUSSION

The PIN1 isomerase regulates a number of cellular processes but has so far not been connected to DNA repair (Liou et al., 2011). Here we report that human PIN1 interacts with key DSB repair factors and demonstrate that PIN1 is involved in the regulation of DSB repair. Our results point to a model in which PIN1 affects DSB repair by restricting DNA end resection through phosphorylation-dependent CtIP isomerization, which in turn controls CtIP stability (Figure 7). As a consequence of deregulated DNA end resection, we find that cells lacking PIN1 display reduced levels of NHEJ and potentially increased levels of mutagenic forms of homology-directed repair (e.g., single-strand annealing), while cells overexpressing PIN1 are compromised in error-free HR and repair DSBs more frequently by NHEJ. Since PIN1-mediated isomerization of p53 was shown to potentiate its activity in response to genotoxic stress, and based on the fact that p53 is a regulator of HR, our findings that PIN1 controls DSB repair pathway choice may specifically apply to cancer or immortalized cells that have lost p53 function (Zacchi et al., 2002; Zheng et al., 2002; Bertrand et al., 2004; Liou et al., 2011).

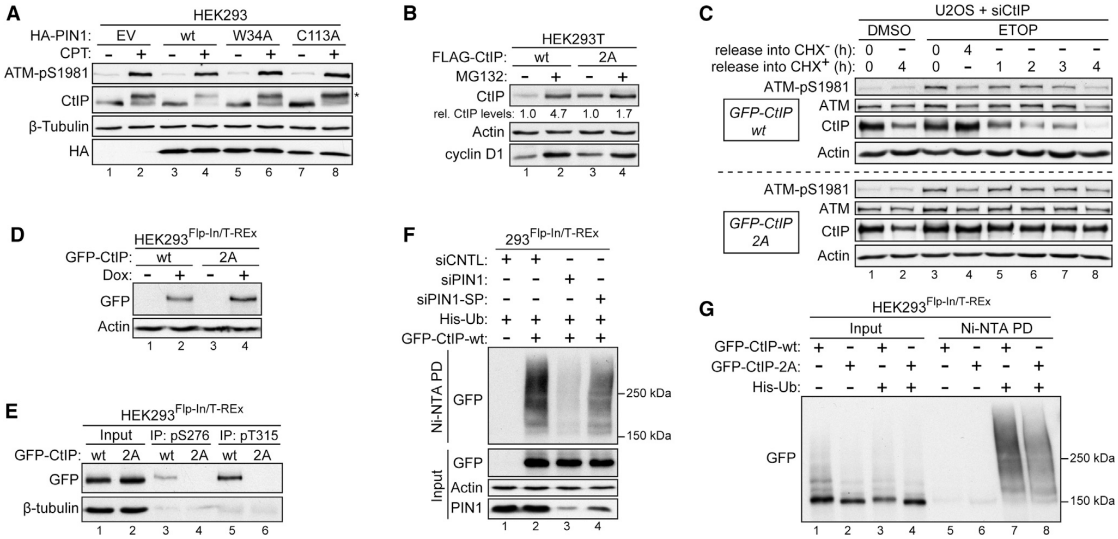

Figure 6. PIN1 Destabilizes CtIP by Promoting Its Ubiquitylation

(A) Two days after transfection with the indicated plasmids, HEK293 cells were treated with CPT (1 μM) for 2 hr and whole-cell extracts were analyzed by immunoblotting. Asterisk indicates hyperphosphorylated form of CtIP.

(B) HEK293T cells were transfected with either FLAG-CtIP-wt or FLAG-CtIP-2A. Eight hours after transfection, cells were splitted into two new plates. Twenty-four hours after plasmid transfection, cells were treated with MG132 (10 μM) for 8 hr and lysed for immunoblot analysis using the indicated antibodies. The signal intensities of CtIP bands were quantified by densitometric analysis using the ImageJ software and normalized to those of Actin. The values represent the relative increase in CtIP-wt and CtIP-2A levels upon MG132 treatment.

(C) Three days after transfection with CtIP siRNA, U2OS cells stably expressing siRNA-resistant GFP-CtIP (wt and 2A) were treated with DMSO or ETOP (10 μM). After 1 hr, cells were released into fresh medium supplemented with 200 μg/ml cycloheximide (CHX) or not for the indicated times, and lysates were analyzed by immunoblotting (see also Figure S8).

(D) HEK293/Flp-In/T-REx cells containing stably integrated GFP-CtIP constructs (wt and 2A) were cultivated in the absence or presence of doxycycline (Dox; 1 μg/ml) for 24 hr, and lysates were analyzed by immunoblotting.

(E) The same cells as in (D) were treated with Dox for 24 hr. After lysis, whole-cell extracts were analyzed by western blotting either directly (input) or after immunoprecipitation (IP) with the indicated anti-CtIP phospho-specific antibodies.

(F) Forty-eight hours after transfection with the indicated siRNAs, HEK293/Flp-In/T-REx cells were transfected with His-Ub, and the expression of GFP-CtIP-wt was simultaneously induced with Dox (except in lane 1). Eight hours after induction, cells were transfected with siRNA for a second time. Seventy-two hours after the first siRNA transfection, cells were treated with MG132 (20 μM) for 6 hr, followed by lysis in buffer containing guanidium-HCl. Ubiquitin conjugates were purified using Ni-NTA-agarose beads, eluted, and analyzed by western blotting using anti-GFP antibody.

(G) Thirty hours after transfection with His-Ub, Dox-induced HEK293/Flp-In/T-REx cells expressing either GFP-CtIP-wt or GFP-CtIP-2A were lysed in buffer containing guanidium-HCl and processed as in (F).

Besides restricting CtIP activity in DNA end resection, it is very tempting to speculate that PIN1 modulates DSB repair pathway choice through regulating the fate of other phosphoproteins. For example, based on our results and previously published data, it is very likely that PIN1 controls the function of 53BP1 and/or BRCA1: (1) we have identified both proteins in a proteomic screen for PIN1 interactors, (2) we find that depleting CtIP does not completely rescue the NHEJ defect in PIN1-deficient cells, (3) BRCA1 was shown to displace 53BP1 from DSBs to enable DNA resection by CtIP (Bunting et al., 2010), (4) PIN1 was very recently identified in a SILAC-based screen for 53BP1 interactors (Di Virgilio et al., 2013), and (5) both proteins are known to be phosphorylated at multiple S/T-P motifs, making them attractive targets for PIN1 (Jowsey et al., 2007; Johnson et al., 2009).

Regarding the mechanism of CtIP regulation by PIN1, we identify S276 and T315 as the two crucial S/T-P motifs mediating PIN1-CtIP interaction. Phosphorylated T315 emerges as the main docking site for PIN1, whereas pS276 is required for *cis/trans* isomerization. Furthermore, we find CDK2 to be the responsible kinase for the phosphorylation of T315. In contrast, phosphorylation of S276 turns out to be independent of CDK activity. In addition, we find that DNA damage stabilizes PIN1-CtIP interaction, but without upregulating T315 phosphorylation, suggesting that it is rather S276 phosphorylation that is induced by genotoxic stress. Interestingly, the amino acid sequence surrounding S276 matches the consensus motif for p38MAPK, a stress kinase reported to be activated by ATM and ATR in response to various DNA-damaging agents including DNA topoisomerase inhibitors (Manke et al., 2005; Reinhardt et al., 2007). Clearly, further investigations are needed to establish both the role of DNA damage in PIN1-mediated CtIP isomerization and the kinase responsible for S276 phosphorylation.

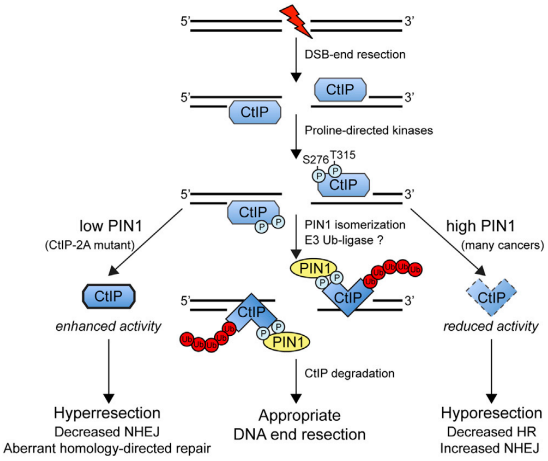

Figure 7. Hypothetical Model: How PIN1-Mediated CtIP Isomerization Controls DNA End Resection

During S/G2, CtIP together with other nucleases promotes the resection of DSBs. Following resection initiation, proline-directed kinases including CDK2 phosphorylate CtIP on T315 and S276, resulting in the binding of PIN1 to CtIP. PIN1-mediated isomerization of CtIP leads to CtIP ubiquitylation through an as-yet-unknown E3 ubiquitin ligase and subsequent CtIP degradation by the proteasome. This mechanism ensures an appropriate usage of DSB end resection. Consequently, cells with abrogated PIN1 function or inherently low PIN1 levels display reduced NHEJ and aberrant (error-prone) forms of homology-directed repair due to enhanced CtIP resection activity (hyperresection). In contrast, cells overexpressing PIN1 display reduced HR and increased NHEJ due to decreased CtIP resection activity (hyporesection). Therefore, we propose that PIN1 plays an important role in the regulation of DSB repair, particularly in late S and G2 phases of the cell cycle.

It also remains to be determined how, mechanistically, isomerization by PIN1 primes CtIP for polyubiquitylation and subsequent degradation. Interestingly, a similar regulatory mechanism involving CDK and PIN1 has recently been reported for hypoxia-induced PML degradation by a Cullin-3 (CUL3) E3 ubiquitin ligase. The authors of this study showed that phosphorylation of PML by CDK1/2 and PIN1-mediated isomerization promotes the recruitment of a CUL3-KLHL20 ubiquitin ligase to polyubiquitylate PML and trigger its degradation (Yuan et al., 2011). Alternatively, a SKP1-CUL1-F box protein (SCF)-type E3 ligase may be involved in CtIP ubiquitylation, since most F box proteins bind to a distinct sequence in their substrates, which typically needs to be phosphorylated (“phospho-degron”) (Silverman et al., 2012).

Ultimately, our findings that overexpression of PIN1 suppresses HR may have important therapeutic implications. For example, PIN1 overexpression, which is frequently found in cancers, may render those cells hypersensitive to PARP inhibition based on the concept of synthetic lethality, analogous to the situation described for BRCA mutant cancers (Bao et al., 2004; Rouleau et al., 2010; Bouwman and Jonkers, 2012). We anticipate that future studies investigating the role of PIN1 in the regulation of other DNA repair factors will provide further important clues to understand how PIN1 contributes to the maintenance of genome stability.

EXPERIMENTAL PROCEDURES

Cell Culture, siRNAs, and Plasmids

U2OS, HEK293T, *Pin1*$^{-/-}$ MEFs, and HEK293T retroviral packaging cells were grown in DMEM supplemented with 10% FCS, 100 U/ml penicillin, and 100 μg/ml streptomycin. The Flp-In T-REx HEK293 host cell line (Invitrogen) was maintained in medium supplemented with 10 μg/ml blasticidin and 300 μg/ml zeocin. Maintenance of the DR-GFP and EJ5-GFP HEK293 cell lines was done as described previously (Bennardo et al., 2008). U2OS clones stably expressing siRNA-resistant forms GFP-CtIP were generated as described previously and were cultured in DMEM supplemented with 10% FCS, standard antibiotics and 500 μg/ml G-418 (Sartori et al., 2007). Retroviral infection of *Pin1*$^{-/-}$ MEFs was carried out as described previously (Zacchi et al., 2002). IR was given using a Faxitron X-ray machine. Laser microirradiation was performed as described previously (Eid et al., 2010). Data for survival curves were generated by colony formation assays as described previously (Sartori et al., 2007). Transfection of siRNA oligos was done using Lipofectamine RNAiMAX (Invitrogen). All siRNA duplexes were purchased from Microsynth except the ON-TARGETplus SMARTpool for PIN1 (PIN1-SP [L-003291-00-0005] [Marcucci et al., 2011; Krishnan et al., 2012] Dharmacon), and the sequences (5′ to 3′) were as follows: luciferase (CNTL; CGUACGCGGAAUACUUCGA) (Sartori et al., 2007), CtIP (GCUAAAACAGGAACGAAUC) (Sartori et al., 2007), XRCC4 (AUAUGUUGGUGAACUGAGA) (Sartori et al., 2007), 53BP1 (CAGGACAGTCTTTCCACGAAT) (Meerang et al., 2011), PIN1-3′UTR (CCGU CACACAGUAUUUAUU), and PIN1-2 (GCUACAUCCAGAAGAUCAA) (Phan et al., 2007). All siRNA transfections were done with 40 nM final concentration of oligos. Plasmids were transfected by using either the standard calcium phosphate method or FuGene 6 (Roche) according to manufacturer’s instructions. The pGEX-4T3 plasmid for bacterial expression of recombinant GST-tagged PIN1 was a gift from Christopher Nelson (University of Victoria, Canada). The epitope-tagged expression vectors for human CtIP have been described previously (Yu et al., 2006; Sartori et al., 2007). The HA-tagged expression vectors for human PIN1 were described previously (Rustighi et al., 2009). The HA-tagged expression vectors for HA-CDK1-dn, HA-CDK4-dn, and HA-CDK2 (wt and dn) were purchased from Addgene (van den Heuvel and Harlow, 1993). The pcDNA3.1-6xHis-Ubiquitin plasmid was a gift from Matthias Peter (ETH Zurich, Switzerland). All PIN1 and CtIP point mutants were introduced by site-directed mutagenesis using Expand Long Template PCR System (Roche) and confirmed by sequencing.

Statistics

Statistical analyses were carried out using unpaired, two-tailed t tests. p values expressed as *$p < 0.05$, **$p < 0.005$, and ***$p < 0.0005$ were considered significant. ns indicates that the difference between the two groups is not significant.

SUPPLEMENTAL INFORMATION

Supplemental Information includes eight figures, one table, Supplemental Experimental Procedures, and Supplemental References and can be found with this article at http://dx.doi.org/10.1016/j.molcel.2013.03.023.

ACKNOWLEDGMENTS

We are very grateful to J. Stark (Department of Radiation Biology, Beckman Research Institute of City of Hope, Duarte, CA, USA) for EJ5-GFP and DR-GFP HEK293 and U2OS cell lines. We thank S. Ferrari and O. Schärer for critical reading of the manuscript. This work was supported by grants of the Swiss National Science Foundation (31003A-129747/1 to P.J. and 31003A_135507 to A.A.S.), the Promedica Stiftung (to A.A.S.), the Vontobel-Stiftung (to A.A.S.), and the “Forschungskredit” of the University of Zurich (54410102 to M.S.).

Received: October 2, 2012
Revised: February 2, 2013
Accepted: March 22, 2013
Published: April 25, 2013

REFERENCES

Adachi, N., So, S., and Koyama, H. (2004). Loss of nonhomologous end joining confers camptothecin resistance in DT40 cells. Implications for the repair of topoisomerase I-mediated DNA damage. J. Biol. Chem. *279*, 37343–37348.

Aylon, Y., Liefshitz, B., and Kupiec, M. (2004). The CDK regulates repair of double-strand breaks by homologous recombination during the cell cycle. EMBO J. *23*, 4868–4875.

Bao, L., Kimzey, A., Sauter, G., Sowadski, J.M., Lu, K.P., and Wang, D.-G. (2004). Prevalent overexpression of prolyl isomerase Pin1 in human cancers. Am. J. Pathol. *164*, 1727–1737.

Bennardo, N., Cheng, A., Huang, N., and Stark, J.M. (2008). Alternative-NHEJ is a mechanistically distinct pathway of mammalian chromosome break repair. PLoS Genet. *4*, e1000110. http://dx.doi.org/10.1371/journal.pgen.1000110.

Bennetzen, M.V., Larsen, D.H., Bunkenborg, J., Bartek, J., Lukas, J., and Andersen, J.S. (2010). Site-specific phosphorylation dynamics of the nuclear proteome during the DNA damage response. Mol. Cell. Proteomics *9*, 1314–1323.

Bertrand, P., Saintigny, Y., and Lopez, B.S. (2004). p53's double life: transactivation-independent repression of homologous recombination. Trends Genet. *20*, 235–243.

Beucher, A., Birraux, J., Tchouandong, L., Barton, O., Shibata, A., Conrad, S., Goodarzi, A.A., Krempler, A., Jeggo, P.A., and Löbrich, M. (2009). ATM and Artemis promote homologous recombination of radiation-induced DNA double-strand breaks in G2. EMBO J. *28*, 3413–3427.

Bouwman, P., and Jonkers, J. (2012). The effects of deregulated DNA damage signalling on cancer chemotherapy response and resistance. Nat. Rev. Cancer *12*, 587–598.

Bunting, S.F., Callén, E., Wong, N., Chen, H.-T., Polato, F., Gunn, A., Bothmer, A., Feldhahn, N., Fernandez-Capetillo, O., Cao, L., et al. (2010). 53BP1 inhibits homologous recombination in Brca1-deficient cells by blocking resection of DNA breaks. Cell *141*, 243–254.

Chapman, J.R., Taylor, M.R.G., and Boulton, S.J. (2012). Playing the end game: DNA double-strand break repair pathway choice. Mol. Cell *47*, 497–510.

Chen, L., Nievera, C.J., Lee, A.Y.-L., and Wu, X. (2008). Cell cycle-dependent complex formation of BRCA1.CtIP.MRN is important for DNA double-strand break repair. J. Biol. Chem. *283*, 7713–7720.

Ciccia, A., and Elledge, S.J. (2010). The DNA damage response: making it safe to play with knives. Mol. Cell *40*, 179–204.

Di Virgilio, M., Callen, E., Yamane, A., Zhang, W., Jankovic, M., Gitlin, A.D., Feldhahn, N., Resch, W., Oliveira, T.Y., Chait, B.T., et al. (2013). Rif1 prevents resection of DNA breaks and promotes immunoglobulin class switching. Science *339*, 711–715.

Eid, W., Steger, M., El-Shemerly, M., Ferretti, L.P., Peña-Diaz, J., König, C., Valtorta, E., Sartori, A.A., and Ferrari, S. (2010). DNA end resection by CtIP and exonuclease 1 prevents genomic instability. EMBO Rep. *11*, 962–968.

Goodarzi, A.A., Jeggo, P., and Löbrich, M. (2010). The influence of heterochromatin on DNA double strand break repair: Getting the strong, silent type to relax. DNA Repair (Amst.) *9*, 1273–1282.

Gravel, S., Chapman, J.R., Magill, C., and Jackson, S.P. (2008). DNA helicases Sgs1 and BLM promote DNA double-strand break resection. Genes Dev. *22*, 2767–2772.

Helleday, T. (2010). Homologous recombination in cancer development, treatment and development of drug resistance. Carcinogenesis *31*, 955–960.

Heyer, W.-D., Ehmsen, K.T., and Liu, J. (2010). Regulation of homologous recombination in eukaryotes. Annu. Rev. Genet. *44*, 113–139.

Huertas, P., Cortés-Ledesma, F., Sartori, A.A., Aguilera, A., and Jackson, S.P. (2008). CDK targets Sae2 to control DNA-end resection and homologous recombination. Nature *455*, 689–692.

Ira, G., Pellicioli, A., Balijja, A., Wang, X., Fiorani, S., Carotenuto, W., Liberi, G., Bressan, D., Wan, L., Hollingsworth, N.M., et al. (2004). DNA end resection, homologous recombination and DNA damage checkpoint activation require CDK1. Nature *431*, 1011–1017.

Jackson, S.P., and Bartek, J. (2009). The DNA-damage response in human biology and disease. Nature *461*, 1071–1078.

Johnson, N., Cai, D., Kennedy, R.D., Pathania, S., Arora, M., Li, Y.-C., D'Andrea, A.D., Parvin, J.D., and Shapiro, G.I. (2009). Cdk1 participates in BRCA1-dependent S phase checkpoint control in response to DNA damage. Mol. Cell *35*, 327–339.

Jowsey, P., Morrice, N.A., Hastie, C.J., McLauchlan, H., Toth, R., and Rouse, J. (2007). Characterisation of the sites of DNA damage-induced 53BP1 phosphorylation catalysed by ATM and ATR. DNA Repair (Amst.) *6*, 1536–1544.

Karanam, K., Kafri, R., Loewer, A., and Lahav, G. (2012). Quantitative live cell imaging reveals a gradual shift between DNA repair mechanisms and a maximal use of HR in mid S phase. Mol. Cell *47*, 320–329.

Karanja, K.K., Cox, S.W., Duxin, J.P., Stewart, S.A., and Campbell, J.L. (2012). DNA2 and EXO1 in replication-coupled, homology-directed repair and in the interplay between HDR and the FA/BRCA network. Cell Cycle *11*, 3983–3996.

Kousholt, A.N., Fugger, K., Hoffmann, S., Larsen, B.D., Menzel, T., Sartori, A.A., and Sørensen, C.S. (2012). CtIP-dependent DNA resection is required for DNA damage checkpoint maintenance but not initiation. J. Cell Biol. *197*, 869–876.

Krishnan, N., Lam, T.T., Fritz, A., Rempinski, D., O'Loughlin, K., Minderman, H., Berezney, R., Marzluff, W.F., and Thapar, R. (2012). The prolyl isomerase Pin1 targets stem-loop binding protein (SLBP) to dissociate the SLBP-histone mRNA complex linking histone mRNA decay with SLBP ubiquitination. Mol. Cell. Biol. *32*, 4306–4322.

Liou, Y.-C., Zhou, X.Z., and Lu, K.P. (2011). Prolyl isomerase Pin1 as a molecular switch to determine the fate of phosphoproteins. Trends Biochem. Sci. *36*, 501–514.

Lippens, G., Landrieu, I., and Smet, C. (2007). Molecular mechanisms of the phospho-dependent prolyl cis/trans isomerase Pin1. FEBS J. *274*, 5211–5222.

Manke, I.A., Nguyen, A., Lim, D., Stewart, M.Q., Elia, A.E.H., and Yaffe, M.B. (2005). MAPKAP kinase-2 is a cell cycle checkpoint kinase that regulates the G2/M transition and S phase progression in response to UV irradiation. Mol. Cell *17*, 37–48.

Marcucci, R., Brindle, J., Paro, S., Casadio, A., Hempel, S., Morrice, N., Bisso, A., Keegan, L.P., Del Sal, G., and O'Connell, M.A. (2011). Pin1 and WWP2 regulate GluR2 Q/R site RNA editing by ADAR2 with opposing effects. EMBO J. *30*, 4211–4222.

Matsuoka, S., Ballif, B.A., Smogorzewska, A., McDonald, E.R., 3rd, Hurov, K.E., Luo, J., Bakalarski, C.E., Zhao, Z., Solimini, N., Lerenthal, Y., et al. (2007). ATM and ATR substrate analysis reveals extensive protein networks responsive to DNA damage. Science *316*, 1160–1166.

Meerang, M., Ritz, D., Paliwal, S., Garajova, Z., Bosshard, M., Mailand, N., Janscak, P., Hübscher, U., Meyer, H., and Ramadan, K. (2011). The ubiquitin-selective segregase VCP/p97 orchestrates the response to DNA double-strand breaks. Nat. Cell Biol. *13*, 1376–1382.

Patel, A.G., Sarkaria, J.N., and Kaufmann, S.H. (2011). Nonhomologous end joining drives poly(ADP-ribose) polymerase (PARP) inhibitor lethality in homologous recombination-deficient cells. Proc. Natl. Acad. Sci. USA *108*, 3406–3411.

Phan, R.T., Saito, M., Kitagawa, Y., Means, A.R., and Dalla-Favera, R. (2007). Genotoxic stress regulates expression of the proto-oncogene Bcl6 in germinal center B cells. Nat. Immunol. *8*, 1132–1139.

Pommier, Y. (2006). Topoisomerase I inhibitors: camptothecins and beyond. Nat. Rev. Cancer *6*, 789–802.

Reinhardt, H.C., Aslanian, A.S., Lees, J.A., and Yaffe, M.B. (2007). p53-deficient cells rely on ATM- and ATR-mediated checkpoint signaling through the p38MAPK/MK2 pathway for survival after DNA damage. Cancer Cell *11*, 175–189.

Rouleau, M., Patel, A., Hendzel, M.J., Kaufmann, S.H., and Poirier, G.G. (2010). PARP inhibition: PARP1 and beyond. Nat. Rev. Cancer *10*, 293–301.

Rustighi, A., Tiberi, L., Soldano, A., Napoli, M., Nuciforo, P., Rosato, A., Kaplan, F., Capobianco, A., Pece, S., Di Fiore, P.P., and Del Sal, G. (2009).

The prolyl-isomerase Pin1 is a Notch1 target that enhances Notch1 activation in cancer. Nat. Cell Biol. *11*, 133–142.

Sartori, A.A., Lukas, C., Coates, J., Mistrik, M., Fu, S., Bartek, J., Baer, R., Lukas, J., and Jackson, S.P. (2007). Human CtIP promotes DNA end resection. Nature *450*, 509–514.

Shibata, A., Conrad, S., Birraux, J., Geuting, V., Barton, O., Ismail, A., Kakarougkas, A., Meek, K., Taucher-Scholz, G., Löbrich, M., and Jeggo, P.A. (2011). Factors determining DNA double-strand break repair pathway choice in G2 phase. EMBO J. *30*, 1079–1092.

Silverman, J.S., Skaar, J.R., and Pagano, M. (2012). SCF ubiquitin ligases in the maintenance of genome stability. Trends Biochem. Sci. *37*, 66–73.

Söderberg, O., Gullberg, M., Jarvius, M., Ridderstråle, K., Leuchowius, K.-J., Jarvius, J., Wester, K., Hydbring, P., Bahram, F., Larsson, L.-G., and Landegren, U. (2006). Direct observation of individual endogenous protein complexes in situ by proximity ligation. Nat. Methods *3*, 995–1000.

Stukenberg, P.T., and Kirschner, M.W. (2001). Pin1 acts catalytically to promote a conformational change in Cdc25. Mol. Cell *7*, 1071–1083.

Ubersax, J.A., and Ferrell, J.E., Jr. (2007). Mechanisms of specificity in protein phosphorylation. Nat. Rev. Mol. Cell Biol. *8*, 530–541.

van den Heuvel, S., and Harlow, E. (1993). Distinct roles for cyclin-dependent kinases in cell cycle control. Science *262*, 2050–2054.

Wang, Y., Liu, C., Yang, D., Yu, H., and Liou, Y.-C. (2010). Pin1At encoding a peptidyl-prolyl cis/trans isomerase regulates flowering time in Arabidopsis. Mol. Cell *37*, 112–122.

Yaffe, M.B., Schutkowski, M., Shen, M., Zhou, X.Z., Stukenberg, P.T., Rahfeld, J.U., Xu, J., Kuang, J., Kirschner, M.W., Fischer, G., et al. (1997). Sequence-specific and phosphorylation-dependent proline isomerization: a potential mitotic regulatory mechanism. Science *278*, 1957–1960.

Yu, X., Fu, S., Lai, M., Baer, R., and Chen, J. (2006). BRCA1 ubiquitinates its phosphorylation-dependent binding partner CtIP. Genes Dev. *20*, 1721–1726.

Yuan, W.-C., Lee, Y.-R., Huang, S.-F., Lin, Y.-M., Chen, T.-Y., Chung, H.-C., Tsai, C.-H., Chen, H.-Y., Chiang, C.-T., Lai, C.-K., et al. (2011). A Cullin3-KLHL20 Ubiquitin ligase-dependent pathway targets PML to potentiate HIF-1 signaling and prostate cancer progression. Cancer Cell *20*, 214–228.

Zacchi, P., Gostissa, M., Uchida, T., Salvagno, C., Avolio, F., Volinia, S., Ronai, Z., Blandino, G., Schneider, C., and Del Sal, G. (2002). The prolyl isomerase Pin1 reveals a mechanism to control p53 functions after genotoxic insults. Nature *419*, 853–857.

Zheng, H., You, H., Zhou, X.Z., Murray, S.A., Uchida, T., Wulf, G., Gu, L., Tang, X., Lu, K.P., and Xiao, Z.-X.J. (2002). The prolyl isomerase Pin1 is a regulator of p53 in genotoxic response. Nature *419*, 849–853.

Molecular Cell, Volume *50*

Supplemental Information

Prolyl Isomerase PIN1 Regulates DNA Double-Strand Break Repair by Counteracting DNA End Resection

Martin Steger, Olga Murina, Daniela Hühn, Lorenza P. Ferretti, Reto Walser, Kay Hänggi, Lorenzo Lafranchi, Christine Neugebauer, Shreya Paliwal, Pavel Janscak, Bertran Gerrits, Giannino Del Sal, Oliver Zerbe, and Alessandro A. Sartori

Supplemental Information Inventory

Figure S1 (related to Figure 1). Mass spectrometry analysis of PIN1 interacting proteins
In this analysis we have discovered potentially novel PIN1 substrates, some of them involved in the DNA damage response including BRCA1, 53BP1 and CtIP.

Figure S2 (related to Figure 1). PIN1 negatively regulates DNA end resection
Here we show that PIN1 depletion increases HR frequency, DNA end resection and resistance to camptothecin treatment in U2OS cells without altering cell cycle distribution. Furthermore, overexpression of PIN1 decreases DNA end resection, again without altering cell cycle distribution.

Figure S3 (related to Figure 2). Molecular characterization of the PIN1-CtIP interaction
In-depth molecular analysis of the PIN1-CtIP interaction using various different approaches.

Figure S4 (related to Figure 3). CtIP-T315 is phosphorylated in cells
A multiple alignment of CtIP homologs from different species indicates that the regions encompassing CtIP-S276 and CtIP-T315 are conserved in higher eukaryotes. We can detect T315 phosphorylation in cells by using a phospho-specific antibody raised against a synthetic CtIP phosphopeptide and by mass spectrometry.

Figure S5 (related to Figure 3). Analysis of CtIP-PIN1 interaction and CtIP *cis/trans* isomerization using synthetic CtIP phosphopeptides
Here we show that CtIP-pT315 is the major PIN1 interaction motif, while CtIP-pS276 phosphopeptide is isomerized by PIN1.

Figure S6 (related to Figure 4). CDK2 activity is required for CtIP-PIN1 interaction and CtIP-T315 phosphorylation
By treating cells with a CDK inhibitor, transfecting cells with a plasmid expressing a dominant-negative version of CDK2 and synchronization of cells, we show that CDK2 activity promotes CtIP-PIN1 interaction, most likely through direct phosphorylation of CtIP at T315.

Figure S7 (related to Figure 5). Increased DSB resection in cells expressing CtIP-2A
Cells expressing a mutant form of CtIP (S276A/T315A) that is refractory to PIN1-mediated isomerization exhibit increased resection of DSBs. In addition, transient expression of a CtIP-2A leads to reduced NHEJ in GFP reporter cells.

Figure S8 (related to Figure 6C). Increased half-life of the CtIP-2A mutant protein in presence of DNA damage
Quantification of GFP-CtIP-wt versus GFP-CtIP-2A protein levels in ETOP-treated U2OS cells in presence or absence of cycloheximide.

Table S1 (related to Figures 1 and S1). PIN-interacting proteins identified by pull-down experiments and mass spectrometry.

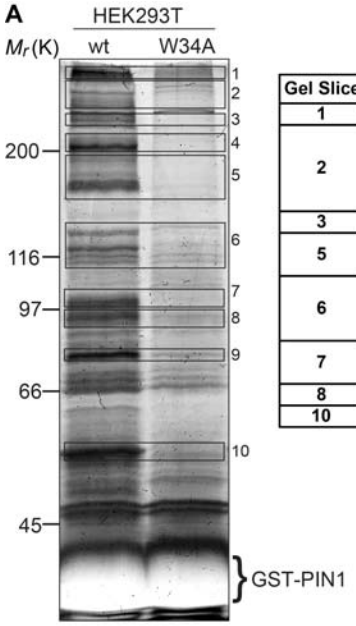

Gel Slice	Identified Protein	Acc No.	wt/W34A*	Pathways	References
1	MAP1A	P78559	53/0	Mitotic regulation	Endoh et al. 2011
2	SMRT	Q9Y618	41/0	Signal transduction	Stanya et al. 2008
	MDC1	Q14676	84/2	DSB repair	*this study*
	53BP1	Q12888	3/0	DSB repair	*this study*
	BRCA1	P38398	14/2	DSB repair	*this study*
3	SLX4	Q8IY92	45/5	DSB repair	*this study*
5	TOP2A	P11388	7/0	Mitotic regulation	Xu and Manley, 2007
	BLM	P54132	14/10	DSB repair	*this study*
6	PTIP	Q6ZW49	14/0	DSB repair	*this study*
	RB	P06400	13/0	Cell proliferation	Rizzolio et al. 2012
	CtIP	Q99708	2/0	DSB repair	*this study*
7	BARD1	Q99728	20/2	DSB repair	*this study*
	BCL6	P41182	1/0	Apoptosis	Phan et al. 2007
8	β-catenin	P35222	13/0	Cell proliferation	Ryo et al. 2001
10	p54nrb	Q15233	90/43	Mitotic regulation	Proteau et al. 2005

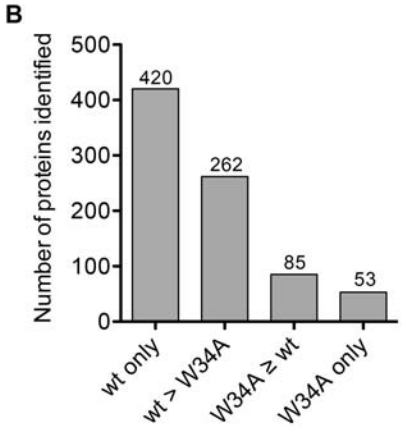

Figure S1 (related to Figure 1). Mass spectrometry analysis of PIN1 interacting proteins (**A**) HEK293T whole cell extracts (5 mg) were subjected to GST pulldown experiments using either wild-type PIN1 (wt) or a WW domain mutant of PIN1 (W34A), unable to interact with phosphorylated proteins, as baits. Isolated proteins were separated by SDS-PAGE. After silver staining, the indicated parts of the gel were excised and processed for mass spectrometry analysis. Examples of proteins identified in different gel slices are illustrated in a table (*total spectral counts identified with PIN1-wt and PIN1-W34A, respectively). (**B**) Graph summarizing the results obtained from the screen. For example, 420 proteins were identified only in PIN1-wt pulldowns, while 262 proteins were identified in which more unique peptides were recovered using wt PIN1 compared to W34A mutant. The entire data set including 820 proteins identified in the PIN1 pulldown screen is shown in Supplementary Table S1.

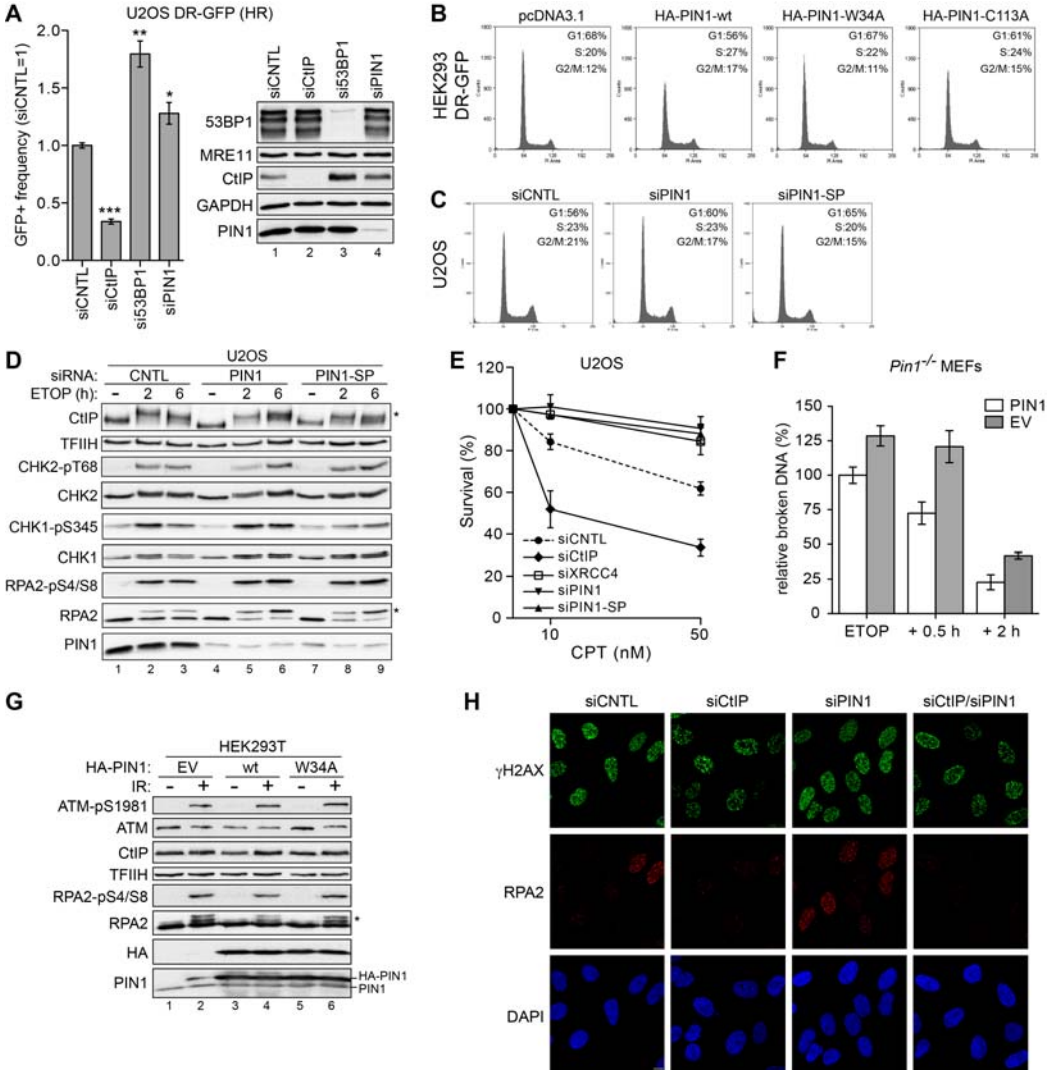

Figure S2 (related to Figure 1). PIN1 negatively regulates DNA end resection
(**A**) U2OS DR-GFP cells were transfected with the indicated siRNAs. At 48 h post-transfection, cells were transfected with the I-SceI expression plasmid and the GFP+ population was analyzed 72 h post-plasmid transfection. The percentage of GFP+ cells was determined for each condition and was normalized with the non-targeting (siCNTL) condition. Data are presented as the mean ± SEM (N=3). (**B**) HEK293 (DR-GFP) cells were transfected with the indicated plasmids for 96 h and analyzed by flow cytometry. (**C**) U2OS cells were transfected with the indicated siRNA oligos for 48 h and analyzed by flow cytometry prior to treatment. (**D**) Same cells as in (C) wer treated with DMSO (-) or etoposide (ETOP, 20 μM) for the indicated times. Whole cell extracts were subjected to SDS-PAGE followed by western blotting using the indicated antibodies (*hyperphosphorylated forms of CtIP and RPA2). (**E**) 48 h after transfection with the indicated siRNA oligonucleotides, U2OS cells were treated for 1 h with either DMSO or camptothecin (CPT) and survival was determined by colony formation. Data are presented as the mean ± SD (N=3). (**F**) Quantification of the PFGE signals shown in Figure 1E. DNA breakage in each lane was normalized against intact DNA. Relative amount of broken DNA in *Pin1*$^{-/-}$ MEFs complemented with PIN1 was set to 100%. Data are presented as the mean ± SEM (N=3). (**G**) HEK293T cells were transfected with the indicated plasmids (EV, pcDNA3.1) for 72 h and treated with 30 Gy of IR. Whole cell extracts were prepared after 3 h and analyzed by immunoblotting. (**H**) 48 h after transfection with the indicated siRNA oligos, U2OS cells grown on coverslips were treated for 1 h with 5 μM ETOP, fixed and co-immunostained for γ-H2AX and RPA2; nuclei were stained with DAPI (blue). Scale bar, 10 μm.

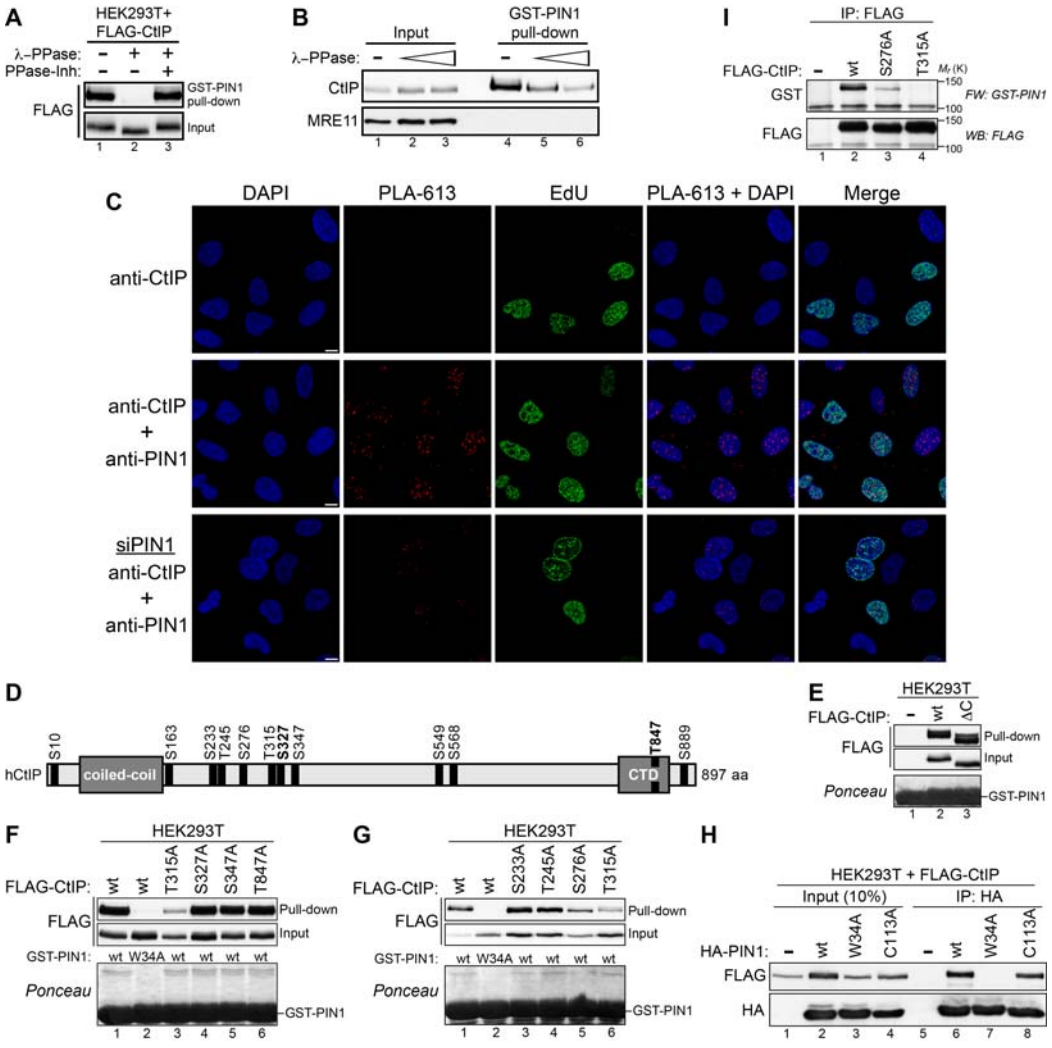

Figure S3 (related to Figure 2). Molecular characterization of the PIN1-CtIP interaction
(**A**) Lysates from HEK293T cells expressing FLAG-CtIP were mock-treated, treated with λ-PPase or treated with a combination of λ-PPase and phosphatase inhibitors (50 mM EDTA and 1 mM sodium orthovanadate) prior to GST-PIN1 pulldown. (**B**) U2OS whole cell extracts were treated with increasing concentrations of λ-PPase prior to GST-PIN1 pulldown. (**C**) Detection of endogenous PIN1-CtIP complexes by *in situ* PLA. Non-transfected or PIN1-depleted U2OS cells were pulse-labeled with EdU (10 μM) for 15 min prior to fixation. After incubation with antibodies against CtIP alone (upper panel) or against both CtIP and PIN1 (middle and lower panels), protein-protein interactions were detected using fluorescence labeled probes (PLA-613). EdU detection was carried out according to manufacturer's instructions and nuclei were stained with DAPI. Scale bars, 10 μm. (**D**) Schematic representation of human CtIP with conserved domains and putative S/T-P phosphorylation motifs. Coiled-coil domain and the conserved C-terminal domain (CTD) are indicated. S327 and T847, the two known S/T-P phosphorylation sites, are illustrated in bold. (**E-G**) GST-PIN1 pulldowns using whole cell extracts of HEK293T cells expressing wt or mutant versions of FLAG-CtIP. Ponceau staining is shown to illustrate that equal amounts of GST-PIN1-wt or -W34A were used. ΔC refers to a mutant of CtIP (aa 1-789) lacking the entire C-terminus. (**H**) HEK293T cells were transfected with either FLAG-CtIP alone (-) or together with different HA-PIN1 plasmids (wt, W34A or C113A). Whole cell extracts were subjected to co-immunoprecipitations using anti-HA antibodies before analysis by immunoblotting. (**I**) Anti-FLAG immunoprecipitates from HEK293T cells transfected with the indicated plasmids were subjected to far-western analysis using purified GST-PIN1 as a probe followed by anti-GST immunoblotting. After stripping the same membrane was reprobed using anti-FLAG antibody.

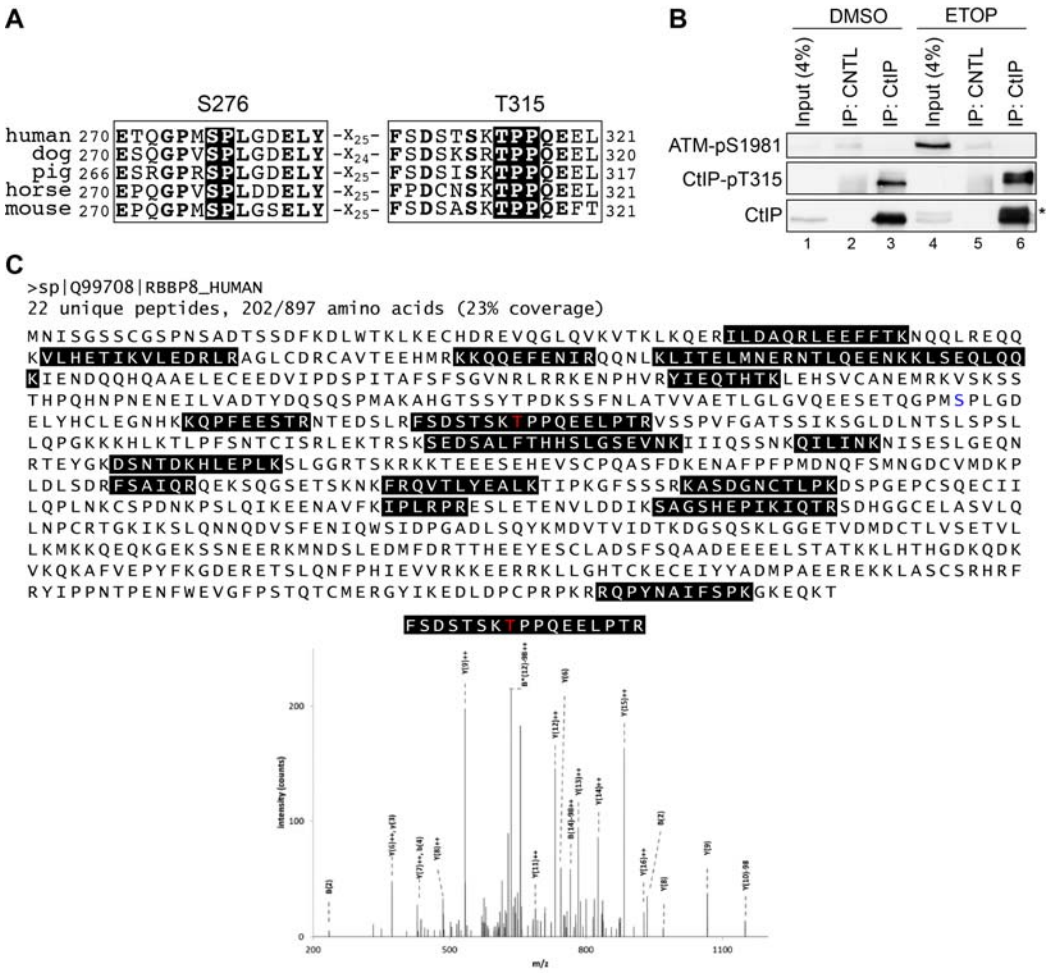

Figure S4 (related to Figure 3). CtIP-T315 is phosphorylated in cells
(**A**) Multiple sequence alignment of the CtIP region containing S276 and T315. (**B**) Extracts from HEK293T cells (5 mg) treated with either DMSO or ETOP (10 μM) for 2 h were immunoprecipitated using either a non-specific, rabbit antiserum or anti-CtIP antibodies and immunoblotted with the indicated antibodies. Asterisk indicates hyperphosphorylated form of CtIP. (**C**) CtIP immunoprecipitated from HEK293T cells was subjected to mass spectrometry (MS) analysis to map phosphorylation sites. In brief, CtIP tryptic peptides indicated by black boxes (covering 23 % of the CtIP sequence) were analyzed by by LC-MS-MS using a Thermo LTQ linear ion trap mass spectrometer. MS/MS spectra of the peptide containing T315 (highlighted in red) is shown below with the corresponding B and Y ions. T315 and S313 were identified as the two likeliest phosphorylation sites using the Mascot-Delta Score (MD-score) phospho-localization algorithm. Note that no peptides containing S276 (highlighted in blue) were covered by the analysis.

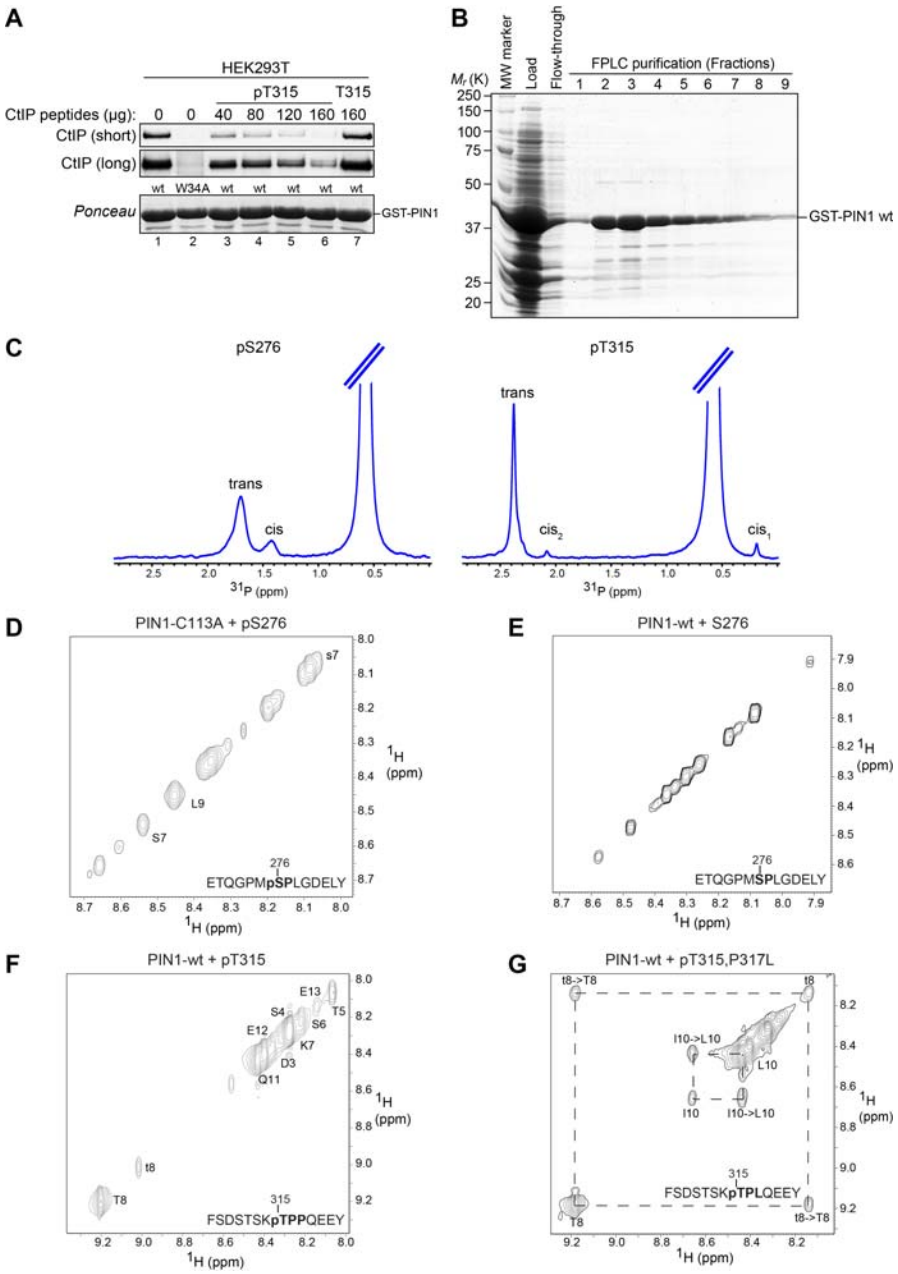

Figure S5 (related to Figure 3). Analysis of CtIP-PIN1 interaction and CtIP *cis/trans* isomerization using synthetic CtIP phosphopeptides

(**A**) GST-PIN1 pull-down assays were performed in HEK293T whole cell extracts (0.5 mg) supplemented with either increasing amounts of the CtIP-pT315 phosphopeptide or with the CtIP-T315 peptide (lane 7). (**B**) Purification of GST-PIN1-wt and -C113A (data not shown) from bacterial lysates using a GSTrap FF™ column connected to a FPLC™ System. Fractions eluted from the column by 10 mM glutathione were separated by SDS-PAGE and stained with Commassie Blue. (**C**) 31P{1H} spectra obtained from pS276 and pT315 peptides (2.4 mM) in 20 mM sodium phosphate (pH 6.8) at 25 °C. The ratios of *trans* to *cis* are 4 and approximately 16 for pS276 and pT315, respectively, as judged by the integrals under the peaks. Note the presence of two weak *cis* peaks in pT315 peptide due to the presence of two consecutive proline residues in +1 and +2 after the phospho-threonine. The strong, capped peak at 0.55 ppm in both spectra results from the phosphate buffer. (**D-G**) Selected region of the two-dimensional ROESY spectra of the indicated synthetic CtIP peptides in presence of recombinant GST-PIN1.

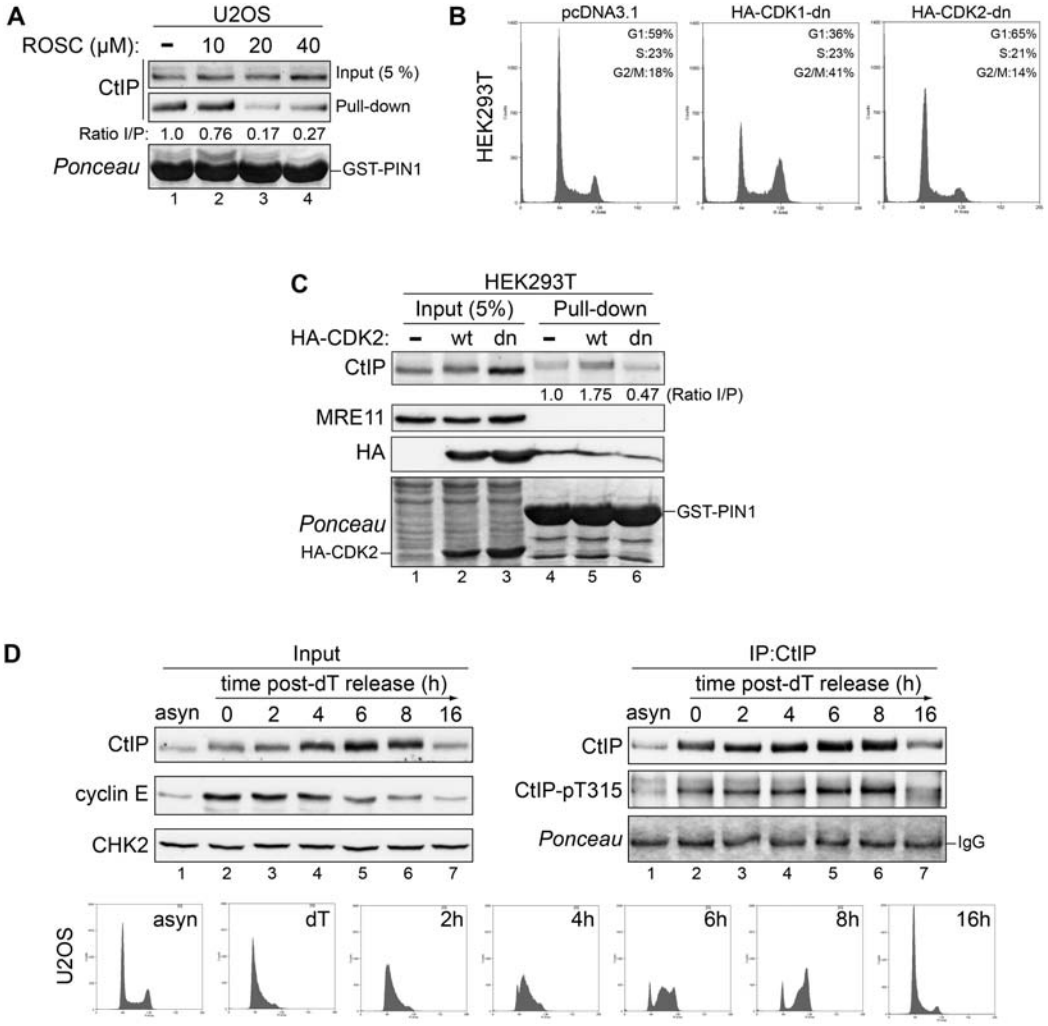

Figure S6 (related to Figure 4). CDK2 activity is required for CtIP-PIN1 interaction and CtIP-T315 phosphorylation

(**A**) Extracts from U2OS cells treated with increasing amounts of R-Roscovitine for 2 h were subjected to GST-PIN1 pull-down assays. The ratios of input versus pull-down (I/P) were quantified by densitometry using Image J. (**B**) HEK293T cells were transfected with either pcDNA3.1 or plasmids expressing HA-tagged dominant-negative (dn) mutant version of CDK1 and CDK2, respectively, and 48 h later analyzed by flow cytometry. (**C**) Extracts from HEK293T cells, transfected with pcDNA3.1 (-) or plasmids expressing HA-CDK2 (wt and dn) for 48 h, were subjected to GST-PIN1 pulldown assays. The ratios of input versus pull-down (I/P) were quantified by densitometry using Image J. (**D**) U2OS cells were synchronized by a double thymidine (dT) block. At the indicated time points after the release from thymidine, cells were either subjected to flow cytometry or lysed. Whole cell extracts were analyzed by western blotting either directly (input) or after immunoprecipitation (IP) with anti-CtIP antibodies.

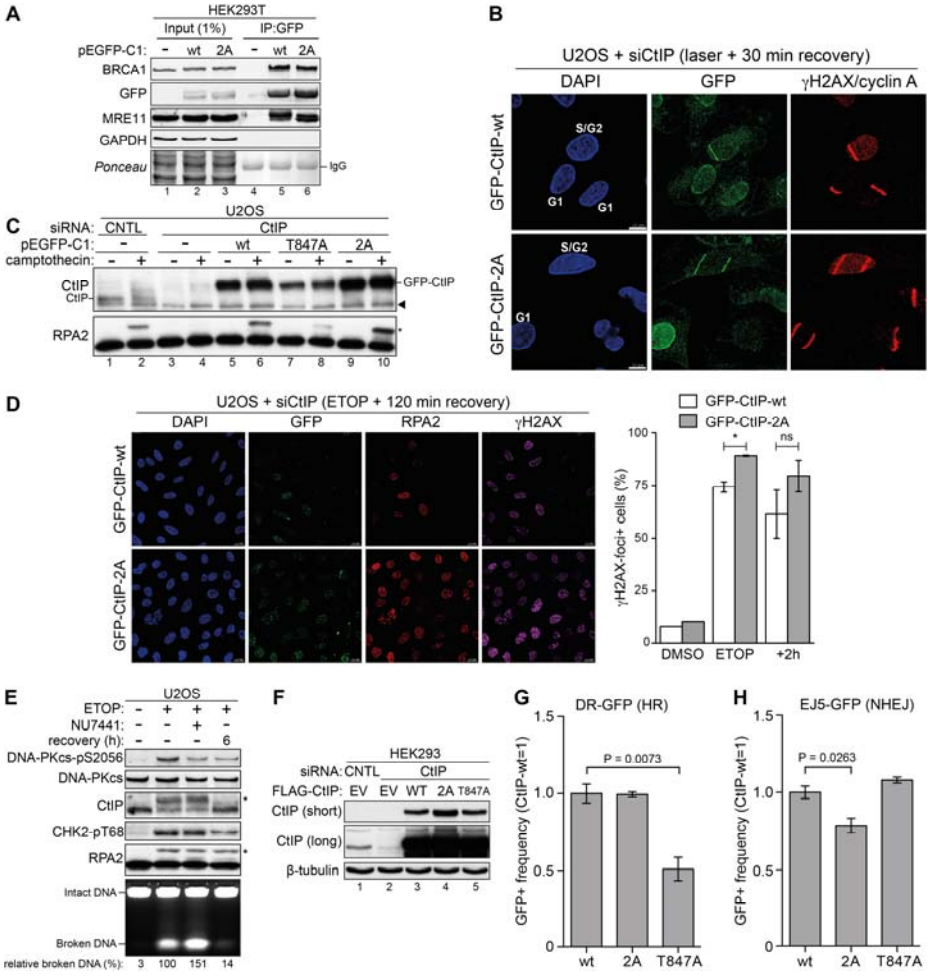

Figure S7 (related to Figure 5). Increased DSB resection in cells expressing CtIP-2A
(**A**) Extracts from HEK293T cells transfected with the indicated plasmids for 48 h were subjected to immunoprecipitation (IP) using anti-GFP antibody and analyzed by immunoblotting. (**B**) U2OS cells stably expressing siRNA-resistant GFP-CtIP constructs were transfected with CtIP siRNA and sensitized with BrdU. 30 minutes after laser microirradiation, cells were fixed, co-immunostained for γ-H2AX and cyclin A and analyzed by fluorescence microscopy. Note that only S/G2-phase cells have pan-nuclear cyclin A staining. Scale bars, 10 μm. (**C**) 72 h after siRNA transfection, U2OS cells stably expressing different GFP-tagged CtIP versions were treated with CPT (1 μM) for 2 h and lysates were analyzed by immunoblotting. Arrowhead indicates a nonspecific band; asterisk indicates hyperphosphorylated RPA2. (**D**) Same cells as in (B) were treated with ETOP (5 μM) for 1 h and released into drug-free medium for 2 h. Left, After pre-extraction, cells were fixed, co-immunostained for RPA2 and γ-H2AX and analyzed by fluorescence microscopy. Scale bars, 20 μm. Right, For each condition at least 50 cells were scored. Graph shows the percentage of nuclei exhibiting more than 10 γ-H2AX-foci. (**E**) U2OS cells were mock-treated (lane 1) or treated with ETOP (10 μM) for 2 h in the absence (lane 2) or presence (lane 3) of NU7441 (10 μM). Additionally, cells were released into drug-free medium for 6 h after ETOP treatment (lane 4). Lysates were analyzed by immunoblotting and genomic DNA was analysed by PFGE. Asterisks indicate hyperphosphorylated forms of CtIP and RPA2. (**F,G**) HEK293 DR-GFP cells were transfected with the indicated siRNAs for 48 h. Cells were then co-transfected with the I-SceI expression plasmid together with the indicated siRNA-resistant FLAG-CtIP constructs. After a second transfection with CtIP siRNA, CtIP expression and GFP+ population were analyzed 48 h post-I-SceI transfection by immunoblotting (F) and flow cytometry (G), respectively. The percentage of GFP+ cells was determined for each condition and was normalized with the CtIP-wt condition. (**H**) HEK293 EJ5-GFP cells were analyzed as in (G). Data in (D, G and H) are represented as mean ± SEM (N=3).

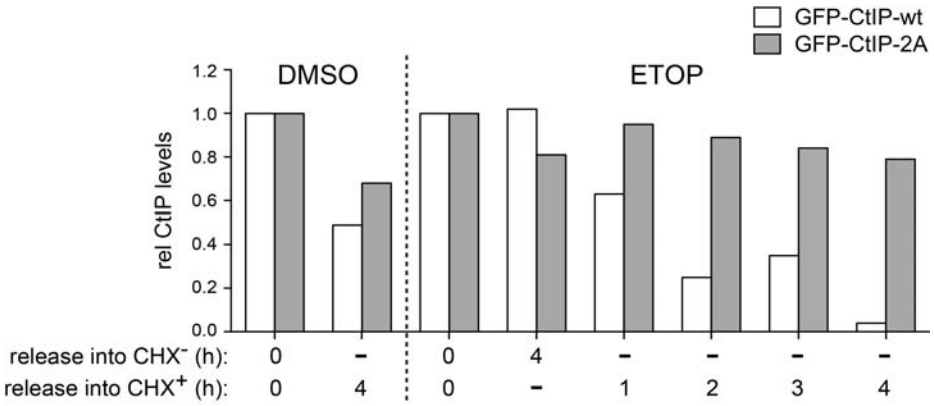

Figure S8 (related to Figure 6C). Increased half-life of the CtIP-2A mutant protein in presence of DNA damage

The signal intensities of CtIP bands from Figure 6C were quantified by densitometric analysis using the ImageJ software and normalized to those of Actin. The values represent the relative decrease in both GFP-CtIP-wt and GFP-CtIP-2A protein levels at different time points after CHX treatment in presence or absence of etoposide (ETOP).

SUPPLEMENTAL EXPERIMENTAL PROCEDURES

HR and NHEJ reporter assays.

DSB repair efficiency by HR and NHEJ was measured in DR-GFP and EJ5-GFP HEK293 cell lines as described previously (Bennardo et al., 2008; Meerang et al., 2011). In brief, 48 h after siRNA transfection, cells were either mock-transfected or transfected with 0.6 µg of an I-SceI expression plasmid (pCBASce) using 1.2 µl of JetPrime (Polyplus). 4 h after I-SceI transfection, the media was replaced, followed by a second transfection with siRNA oligos (15 nM). To measure the effect of PIN1 overexpression, cells were co-transfected with 0.6 µg of pCBASce together with 0.6 µg of pcDNA3-PIN1 using 2.4 µl of JetPrime (Polyplus). To measure the effect of CtIP overexpression, 48 h after siCtIP transfection, cells were co-transfected with 0.6 µg of pCBASce together with 0.2 µg of various FLAG-tagged CtIP constructs using 1.6 µl of JetPrime (Polyplus). 4 h after I-SceI transfection, the media was replaced, followed by a second transfection with siCtIP (15 nM). 48 h after after I-SceI transfection, cells were analyzed for GFP expression by flow cytometry on a CyAn ADP 9 (Dako). HR efficiency in U2OS DR-GFP cells was measured exactly as described previously (Muñoz et al., 2012).

Generation of stable HEK293/Flp-In/GFP-CtIP cell lines.

To generate cell lines able to express GFP-CtIP-wt and GFP-CtIP-2A in an inducible manner, Flp-In T-REx-293 cells (60% confluence) were transfected with a mixture containing the GFP-CtIP receptor cDNA in the pcDNA5/FRT/TO vector and the Flp recombinase cDNA in the pOG44 vector (ratio 1:9) using FuGene 6 transfection reagent (Roche) according to the manufacturer's instructions. Two days after transfection, cells were diluted 1:5 in 10-cm plates and the medium was supplemented with 100 µg/ml hygromycin. The medium was replaced every 2-3 days and cells were selected for approximately 2 weeks. Resistant colonies were pooled and cells were screened for GFP-CtIP expression by both immunofluorescence microscopy and western blotting. To induce expression of GFP-CtIP, cells were treated with 1 µg/ml doxycycline (Dox) for 24 h (see Figure 6D).

Antibodies.

The primary antibodies used in this study are listed in a separate table below. Rabbit polyclonal phospho-specific antibodies against CtIP-pS276 and CtIP-pT315 were produced by Eurogentec with synthetic phosphopeptides (KLH-coupled) corresponding to residues surrounding S276 (ETQGPMpSPLGDEL) and T315 (SDSTSKpTPPQEE) of human CtIP. Secondary HRP-conjugated anti-mouse and anti-rabbit antibodies were form GE-Healthcare and the HRP-conjugated anti-goat was from Santa Cruz Biotech. Alexa Fluor-488, -594, and -647-conjugated secondary antibodies were from Invitrogen.

Chemicals.

R-Roscovitine and RO-3306 were purchased from Calbiochem. Etoposide and camptothecin were purchased from SIGMA. DNA-PKcs inhibitor (NU7441) was purchased from Tocris Bioscience. EdU (5-ethynyl-2'-deoxyuridine) was from Invitrogen. MG132 was purchased from Sigma.

Immunoblotting, GST pulldown, Immunoprecipitation and Far-Western.

If not specified otherwise, cell extracts were prepared in Laemmli buffer (4% SDS, 20% glycerol, 120 mM Tris-HCl pH 6.8). Proteins were resolved by SDS–PAGE, transferred to nitrocellulose. Immunoblots were performed by using the appropriate antibodies and proteins visualised using the ECL detection system (Amersham).

For GST pulldown assays and immunoprecipitation assays, cells were lysed in either NP-40 extraction buffer (50 mM Tris-HCl, pH 7.5, 120 mM NaCl, 1 mM EDTA, 6 mM EGTA, 15 mM sodium pyrophosphate and 1 % NP-40 supplemented with phosphatase inhibitors (20 mM NaF, 1 mM sodium orthovanadate) and protease inhibitors (1 mM benzamidine and 0.1 mM PMSF)) or RIPA buffer (50 mM Tris-HCl, pH 7.4, 1 % NP-40, 0.25 % sodium deoxycholate, 150 mM NaCl, 1 mM EDTA and 0.1% SDS supplemented with phosphatase and protease inhibitors)) and clarified by centrifugation at 14000 rpm. For HA-PIN1 immunoprecipitations using anti-HA antibody, cells were lysed in modified NP-40 buffer (10 mM HEPES, pH 7.5, 250 mM NaCl, 0.1 % NP-40, 5 mM EDTA, 0.5 mM DTT and 0.05 % SDS supplemented with protease and phosphatase inhibitors). GST pull-downs and immunoprecipitations were

performed as described previously (Sartori et al., 2007). Far-western blot analysis was performed as described previously (Wu et al., 2007). Densitometric analysis of protein bands were performed using ImageJ.

In Situ Proximity Ligation Assay.

In situ proximity ligation assay (PLA) in combination with immunofluorescence confocal microscopy was performed using Duolink II Detection Kit with anti-Mouse PLUS and anti-Rabbit MINUS PLA Probes, according to the manufacturer's instructions (Olink Bioscience).

Pulsed field gel electrophoresis (PFGE).

A modified protocol for PFGE was carried out as described previously (Meerang et al., 2011). The gels were stained with ethidium bromide and analyzed using a CCD camera (BioRad).

Liquid chromatography-MS/MS analysis.

MS analysis was carried out as described previously (Zheng et al., 2009). In brief, Following GST-PIN1 pulldowns or CtIP immunoprecipitation using anti-CtIP antibody, proteins were separated by SDS-PAGE and stained with silver or colloidal commassie, respectively. Protein bands were in-gel digested with Trypsin Gold (Promega) according to standard procedures. The resulting peptides were further purified using C18-resin containing ZipTips according to manufacturer's instructions (Millipore) prior to LC-MS-MS analysis using a Thermo LTQ linear ion trap mass spectrometer. The precursor and fragment ion tolerances were set to 10 ppm and 0.8 Da, respectively. Iodoacetamide derivative of cysteine was specified in Mascot as a fixed modification. Oxidation of methionine and phosphorylation of serine, threonine and tyrosine were specified in Mascot as variable modifications. Scaffold (version Scaffold 3.3.1, Proteome Software Inc., Portland, OR) was used to validate MS/MS based peptide and protein identifications. Peptide identifications were accepted if they could be established at greater than 95.0% probability as specified by the Peptide Prophet algorithm (Nesvizhskii et al., 2003). Protein identifications were accepted if they could be established at greater than 99.0% probability and contained at least one identified peptide. Proteins that contained similar

peptides and could not be differentiated based on MS/MS analysis alone were grouped to satisfy the principles of parsimony.

Immunofluorescence Microscopy.

U2OS cells grown on cover slips were either fixed directly in formaldehyde and permeabilized or pre-extracted for 10 min on before fixation in 4% formaldehyde (w/v) in PBS for 12 min as described previously (Eid et al., 2010). After incubation with indicated primary and appropriate secondary antibodies, cover slips were mounted with Vectrashield® (Vector Laboratories) containing DAPI and sealed. Images were acquired on a Leica confocal SP2 fluorescence microscope.

Purification of GST-PIN1.

GST-fusion proteins of PIN1 were expressed in bacteria after induction by IPTG for 20 h at 16°C. After centrifugation, the bacterial pellet was resuspended in cold PBS supplemented with 0.2 % Triton X-100 and protease inhibitors (1 mM PMSF, 1 mM benzamidine and Roche protease inhibitor cocktail). After sonication and centrifugation, GST-PIN1 proteins were purified using a GSTrap fast-flow column according to manufacturer's instructions (GE Healthcare).

NMR spectroscopy analysis of CtIP peptides.

Phospho- and non-phospho-peptides corresponding to residues surrounding S276 (ETQGPM(p)SPLGDELY) and T315 (FSDSTSK(p)TPPQEEY and FSDSTSKpTPLQEEY, where proline 317 was replaced by leucine) of human CtIP were purchased from Bachem. Unless stated otherwise all NMR samples contained 2.4 mM solutions of the respective CtIP peptide in 20 mM sodium phosphate buffer at pH 6.5. To these solutions PIN1-wt or PIN1-C113A were added at a concentration of 30 μM. All ^{1}H-detected spectra were acquired on a Bruker AV-600 or AV-700 spectrometer equipped with triple-resonance cryoprobes. The ^{31}P spectra were recorded on a Bruker AV2-500 spectrometer equipped with a QNP cryoprobe. All NMR experiments were conducted at 298K, except when stated otherwise, and water suppression was achieved by presaturation. Resonance assignment was achieved based on

75 ms TOCSY, DQF-COSY and 110 ms ROESY spectra. All spectra were acquired with 2048 x 256 complex points, using a spectral width of 5400 Hz in both dimensions, 16 to 32 scans per increment and a 2 s interscan delay. ^{31}P-spectra were acquired with ^{1}H-decoupling, 512 scans per experiment and an interscan delay of 3 s.

V8 Protease Digestion of FLAG-CtIP

HEK293T cells were transfected with FLAG-CtIP plasmids for 72 h prior to lysis in NP-40 extraction buffer. FLAG-CtIP was immunoprecipitated from five milligrams of total protein lysates using FLAG-M2 magnetic beads. The beads were washed five times with TBS. FLAG-CtIP was eluted with 85 µl of TBS supplemented with 3xFLAG peptides for 1 h according to manufacturer's instructions (Sigma). The eluates (20 µl) were either mock-treated or incubated with 0.5 µg/ml of V8 protease (Sigma) for 30 min at 20°C. Samples were separated on SDS-PAGE, transferred to nitrocellulose membranes, and probed with anti-CtIP (Bethyl) and with anti-FLAG antibodies.

***In vivo* ubiquitylation assay**

Stable HEK293/Flp-In/GFP-CtIP cells were induced with Dox (1 µg/ml), simultaneously transfected with His-ubiquitin and were cultured for 24 h followed by MG132 treatment (20 µM) for 6 h. Cells were washed and scraped in 0.5 ml of ice-cold PBS. Five percent (5 %) of the cell suspension was used for direct Western blot analysis. The remaining cells (95 %) were lysed in buffer A (6 M guanidine-HCl, 0.1 M Na_2HPO_4/NaH_2PO_4, pH 8.0, 10 mM imidazole and 10 mM NEM). Lysates were incubated with Ni^{2+}-NTA agarose for 3 h at room temperature. The beads were washed three times with buffer A, twice with buffer A/TI (1 vol buffer A: 3 vol buffer TI [25 mM Tris-HCl, pH 6.8, and 20 mM imidazole]), and three times in buffer TI. Purified proteins were eluted by boiling the beads in 2 x sample buffer supplemented with 250 mM imidazole and then analyzed by western blotting.

Antibody target	Species	Supplier/Reference	Application*
ATM (2C1)	mouse	GTX70103 (GeneTex)	IB
pATM S1981	rabbit	2152-1 (Epitomics)	IB
α-Actin (I-19)	rabbit	sc-1616 (Santa Cruz)	IB
53BP1 (H-300)	rabbit	sc-22760 (Santa Cruz)	IB
CtIP (14-1)	mouse	gift from Richard Baer	IB
CtIP	rabbit	A300-488A (Bethyl)	IP
CtIP (D-4)	mouse	sc-271339 (Santa Cruz)	IB
CtIP (T-16)	goat	sc-5970 (Santa Cruz)	IP and IB
CHK1 (G4)	mouse	sc-8408 (Santa Cruz)	IB
pCHK1 S345	rabbit	2341(Cell Signaling)	IB
CHK2	rabbit	gift from Grant Stewart	IB
pCHK2 T68 (C13C1)	rabbit	2197P (Cell Signaling)	IB
Cyclin A (C-19)	rabbit	sc-596 (Santa Cruz)	IF
Cyclin D1	rabbit	RB-010 (NeoMarkers)	IB
pDNA-PKcs S2056	rabbit	ab18192 (Abcam)	IB
FLAG	mouse	F3165 (Sigma)	IP and IB
GAPDH	mouse	MAB374 (Millipore)	IB
GFP	rabbit	ab290 (Abcam)	IP and IB
GFP	mouse	sc-9996 (Santa Cruz)	IB
GST	mouse	A00865 (GenScript)	IB
HA	mouse	sc-7392 (Santa Cruz)	IP and IB
γH2AX (JBW301)	mouse	05-636 (Millipore)	IF
γH2AX (20E3)	rabbit	9718 (Cell Signaling)	IB and IF
MRE11	mouse	GTX70212 (GeneTex)	IB
MRE11	rabbit	NB100-142 (Novus)	IB
PIN1	rabbit	2136-1 (Epitomics)	IB and IF
PIN1	rabbit	600-401-A20 (Rockland)	IP
p53 (DO-1)	mouse	sc-126 (Santa Cruz)	IB
RAD51 (H-92)	rabbit	sc-8349 (Santa Cruz)	IB
RPA2 (Ab-3)	mouse	NA19L (Calbiochem)	IF and IB
RPA2 (9H8)	mouse	ab2175 (Abcam)	IB
pRPA S4/S8 (BL647)	rabbit	A300-245A (Bethyl)	IB
β-Tubulin (D-10)	mouse	sc-5274 (Santa Cruz)	IB
TFIIH p89 (S-19)	rabbit	sc-293 (Santa Cruz)	IB
XRCC4	rabbit	ab145 (Abcam)	IB

*IB: Immunoblot, IF: Immunofluorescence, IP: Immunoprecipitation

SUPPLEMENTAL REFERENCES

Bennardo, N., Cheng, A., Huang, N., and Stark, J.M. (2008). Alternative-NHEJ is a mechanistically distinct pathway of mammalian chromosome break repair. PLoS Genetics *4*, e1000110.

Eid, W., Steger, M., El-Shemerly, M., Ferretti, L.P., Peña-Diaz, J., König, C., Valtorta, E., Sartori, A.A., and Ferrari, S. (2010). DNA end resection by CtIP and exonuclease 1 prevents genomic instability. EMBO Rep. *11*, 962–968.

Meerang, M., Ritz, D., Paliwal, S., Garajova, Z., Bosshard, M., Mailand, N., Janscak, P., Hübscher, U., Meyer, H., and Ramadan, K. (2011). The ubiquitin-selective segregase VCP/p97 orchestrates the response to DNA double-strand breaks. Nat. Cell Biol. *13*, 1376–1382.

Muñoz, M.C., Laulier, C., Gunn, A., Cheng, A., Robbiani, D.F., Nussenzweig, A., and Stark, J.M. (2012). RING finger nuclear factor RNF168 is important for defects in homologous recombination caused by loss of the breast cancer susceptibility factor BRCA1. J. Biol. Chem. *287*, 40618–40628.

Nesvizhskii, A.I., Keller, A., Kolker, E., and Aebersold, R. (2003). A statistical model for identifying proteins by tandem mass spectrometry. Anal. Chem. *75*, 4646–4658.

Sartori, A.A., Lukas, C., Coates, J., Mistrik, M., Fu, S., Bartek, J., Baer, R., Lukas, J., and Jackson, S.P. (2007). Human CtIP promotes DNA end resection. Nature *450*, 509–514.

Wu, Y., Li, Q., and Chen, X.-Z. (2007). Detecting protein-protein interactions by Far western blotting. Nat Protoc *2*, 3278–3284.

Zheng, L., Kanagaraj, R., Mihaljevic, B., Schwendener, S., Sartori, A.A., Gerrits, B., Shevelev, I., and Janscak, P. (2009). MRE11 complex links RECQ5 helicase to sites of DNA damage. Nucleic Acids Res. *37*, 2645–2657.

10.2. HELQ promotes RAD51 paralogue-dependent repair to avert germ cell loss and tumorigenesis

Carrie A. Adelman, Rafal L. Lolo, Nicolai J. Birkbak, **Olga Murina**, Kenichiro Matsuzaki, Zuzana Horejsi, Kalindi Parmar, Valerie Borel, J. Mark Skehel, Gordon Stamp, Alan D'Andrea, Alessandro A. Sartori, Charles Swanton and Simon J. Boulton

article published in Nature, 2013

I contributed to this publication by performing the DR-GFP reporter assays in U2OS cells displayed in Fig. 4e and Extended Data Fig. 8b.

LETTER

doi:10.1038/nature12565

HELQ promotes RAD51 paralogue–dependent repair to avert germ cell loss and tumorigenesis

Carrie A. Adelman[1], Rafal L. Lolo[1], Nicolai J. Birkbak[2], Olga Murina[3], Kenichiro Matsuzaki[1], Zuzana Horejsi[1], Kalindi Parmar[4], Valérie Borel[1], J. Mark Skehel[5]†, Gordon Stamp[6], Alan D'Andrea[4], Alessandro A. Sartori[3], Charles Swanton[7,8] & Simon J. Boulton[1]

Repair of interstrand crosslinks (ICLs) requires the coordinated action of the intra-S-phase checkpoint and the Fanconi anaemia pathway, which promote ICL incision, translesion synthesis and homologous recombination (reviewed in refs 1, 2). Previous studies have implicated the 3′–5′ superfamily 2 helicase HELQ in ICL repair in *Drosophila melanogaster* (MUS301 (ref. 3)) and *Caenorhabditis elegans* (HELQ-1 (ref. 4)). Although *in vitro* analysis suggests that HELQ preferentially unwinds synthetic replication fork substrates with 3′ single-stranded DNA overhangs and also disrupts protein–DNA interactions while translocating along DNA[5,6], little is known regarding its functions in mammalian organisms. Here we report that HELQ helicase-deficient mice exhibit subfertility, germ cell attrition, ICL sensitivity and tumour predisposition, with *Helq* heterozygous mice exhibiting a similar, albeit less severe, phenotype than the null, indicative of haploinsufficiency. We establish that HELQ interacts directly with the RAD51 paralogue complex BCDX2 and functions in parallel to the Fanconi anaemia pathway to promote efficient homologous recombination at damaged replication forks. Thus, our results reveal a critical role for HELQ in replication-coupled DNA repair, germ cell maintenance and tumour suppression in mammals.

To examine the effect of HELQ deficiency in vertebrates, we generated a $Helq^{\Delta C}$-deficient mouse strain that is truncated at the carboxy terminus of HELQ (Fig. 1a, b and Extended Data Fig. 1a, b) and results in loss of detectable HELQ protein (Fig. 1d and Extended Data Fig. 1c). Although $Helq^{\Delta C/\Delta C}$ mice are viable (Fig. 1c), are born in normal Mendelian ratios and lack growth or developmental abnormalities (Extended Data Fig. 1d, e), breeding experiments with $Helq^{\Delta C/\Delta C}$ mutant pairs revealed a fertility defect. Eight heterozygous and 8 homozygous pairs were mated continuously for 5–6 months, resulting in 320 offspring in the case of heterozygotes (an average of 6.1 litters and 40 pups each) but only 38 pups in the case of homozygotes (1.4 litters and 4.7 pups per pair). Mating of mutants to control animals revealed that females contribute more to this phenotype than males (Fig. 1e).

Consistent with a fertility defect, $Helq^{\Delta C/\Delta C}$ testes were smaller than those of wild-type males (0.58% of body weight for wild type versus 0.38% for mutants (Fig. 1f)). Histological analysis of testes revealed many normal tubules but also regions of atrophy in the mutants (Fig. 1g and Extended Data Fig. 1g–l). Dysgenesis/atrophy was even more pronounced in $Helq^{\Delta C/\Delta C}$ ovaries (Fig. 1g and Extended Data Fig. 1f). A possible stem cell origin was investigated as no particular subset of spermatocytes appeared affected (Extended Data Fig. 1g–l). Indeed, $Helq^{\Delta C/\Delta C}$ adults had significantly fewer c-KIT (also known as KIT)$^{+}$ spermatogonia than controls (Extended Data Fig. 2a, b). As atrophy was not linked to ageing (Extended Data Fig. 2c), a developmental origin was examined; tubules from 5-day-old wild-type mice contained sixfold more spermatogonia than mutants (Fig. 1h), indicating that atrophic tubules in mutant adults may primarily arise from reduced spermatogonial stem cell pools during development.

The effect of HELQ deficiency during organismal ageing revealed that tumour-free survival was significantly reduced in *Helq* mutants (Fig. 1i and Extended Data Fig. 2d), with twice as many $Helq^{\Delta C/\Delta C}$ mice developing two or more primary tumours in comparison to controls (Fig. 1j). Ovarian tumours (resembling granulosa and other sex cord stromal tumours; Extended Data Fig. 3b–f) and pituitary adenomas (Extended Data Fig. 3g–j) were the most prominent tumour types in female mice, with incidences of 40% in the case of ovarian tumours and 30% in the case of pituitary tumours (Fig. 1k). Unexpectedly, $Helq^{+/\Delta C}$ heterozygous females also presented with ovarian pathology similar to that of younger mutant females (Extended Data Fig. 2d). Pathology included cystic (4 out of 7 mice) and dysgenic/atrophic (5 out of 7) ovaries with few or no maturing follicles (7 out of 7) and luteinized stroma (2 out of 7). $Helq^{+/\Delta C}$ heterozygous females also frequently displayed pituitary (5 out of 7 mice), Harderian gland (3 out of 7) and gastrointestinal (3 out of 7) adenomas, polyps and hyperplasias. Although these phenotypes are less severe than observed in the $Helq^{\Delta C/\Delta C}$ homozygous mice, the data reveal that loss of a single allele of *Helq* confers haploinsufficiency in mice.

The phenotype of $Helq^{\Delta C/\Delta C}$ mice is similar to that observed in mouse models of Fanconi anaemia[7]. Haematopoietic stem and progenitor cell (HSPC) defects and sensitivity to ICLs are also hallmarks of Fanconi anaemia and were therefore examined in *Helq* mutants. Although bone marrow HSPCs from $Helq^{\Delta C/\Delta C}$ mice exhibit hypersensitivity to the ICL agent mitomycin C (MMC; Extended Data Fig. 4a), $Helq^{\Delta C/\Delta C}$ HSPCs were not compromised in numbers (Extended Data Fig. 4b, c), proliferative capacity (Extended Data Fig. 4d, e) or engraftment (Extended Data Fig. 4f–i). HELQ-deficient cells exhibited hypersensitivity to replication blocking agents such as MMC and camptothecin (CPT; Fig. 2a, b), but not to ionizing radiation or ultraviolet radiation (Fig. 2c, d). $Helq^{\Delta C/\Delta C}$ cells also exhibited significantly more chromatid breaks and radial chromosomes than control cells upon treatment with mitomycin C (MMC; Fig. 2e, j). Silencing of *HELQ* by short interfering RNA (siRNA) in human cells resulted in similar phenotypes (Extended Data Fig. 4j).

To examine the phenotypic relationship between HELQ and the Fanconi anaemia pathway we generated $Helq^{\Delta C/\Delta C}$ $Fancd2^{-/-}$ double-mutant mice (the *Fancd2* strain is described in ref. 8). Double mutants were born in Mendelian ratios (Extended Data Fig. 4k) and growth and appearance were normal. Surprisingly, testes from double mutants were significantly smaller than single mutants and all tubules were atrophic, containing only Sertoli cells (Fig. 2f, g). Similarly, double-mutant cells exhibited greater sensitivity to MMC and CPT than either single-mutant (Fig. 2h, i) and spontaneous and MMC-induced chromosomal aberrations were significantly increased over the *Helq* single mutant

[1]DNA Damage Response Laboratory, London Research Institute, Cancer Research UK, Clare Hall, South Mimms EN6 3LD, UK. [2]Center for Biological Sequence Analysis, Technical University of Denmark, Lyngby 2800, Denmark. [3]Institute of Molecular Cancer Research, University of Zurich, Winterthurerstrasse 190, CH-8057 Zurich, Switzerland. [4]Department of Radiation Oncology, Dana Farber Cancer Institute, Boston, Massachusetts 02215, USA. [5]Protein Analysis and Proteomics Laboratory, London Research Institute, Cancer Research UK, Clare Hall, South Mimms EN6 3LD, UK. [6]Experimental Histopathology Laboratory, London Research Institute, Cancer Research UK, 44 Lincoln's Inn Fields, London WC2A 3LY, UK. [7]Translational Cancer Therapeutics Laboratory, London Research Institute, Cancer Research UK, 44 Lincoln's Inn Fields, London WC2A 3LY, UK. [8]UCL Cancer Institute, Huntley Street, London WC1E 6DD, UK. †Present address: Mass Spectrometry, Medical Research Council Laboratory of Molecular Biology, Hills Road, Cambridge CB2 0QH, UK.

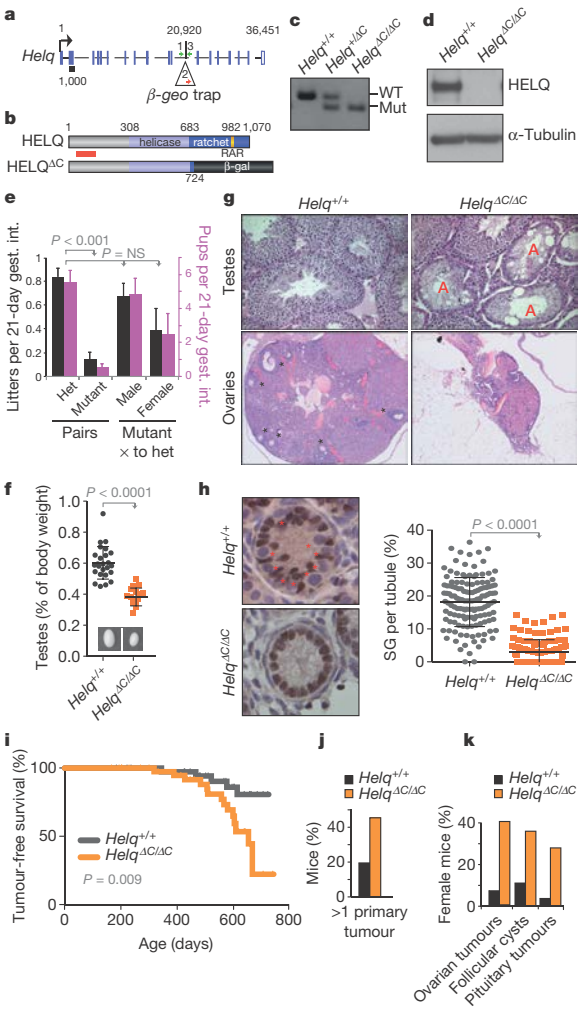

Figure 1 | A mouse model of HELQ deficiency. **a**, *Helq* genomic locus. Base pairs are indicated above. Introns are not to scale; exons are roughly to scale with black bar indicating 1 kilobase. Location of the *β-geo* gene trap and genotyping primers are shown. **b**, HELQ domain architecture: amino acids are indicated, red bar spans epitope recognized by the HELQ antibody used for western blotting. **c**, *Helq* genotype PCR. **d**, Lysates from ear fibroblasts of *Helq* mice probed for HELQ. **e**, The number of litters (black) and pups (pink) generated per 21-day gestational interval. **f**, *Helq* testis images and weights. **g**, Histological sections of *Helq* gonads. 'A' denotes atrophic tubules; asterisks denote developing ovarian follicles. **h**, Left, 5-day-old neonatal testes labelled with the Sertoli marker WT1 (brown) and haematoxylin (blue), to reveal spermatogonia (asterisks). Right, quantification of spermatogonia (SG). **i**, Epithelial and stromal tumour-free survival of *Helq* mice. **j**, **k**, Frequency of mice with two or more primary tumours (**j**) and female-specific pathology (**k**).

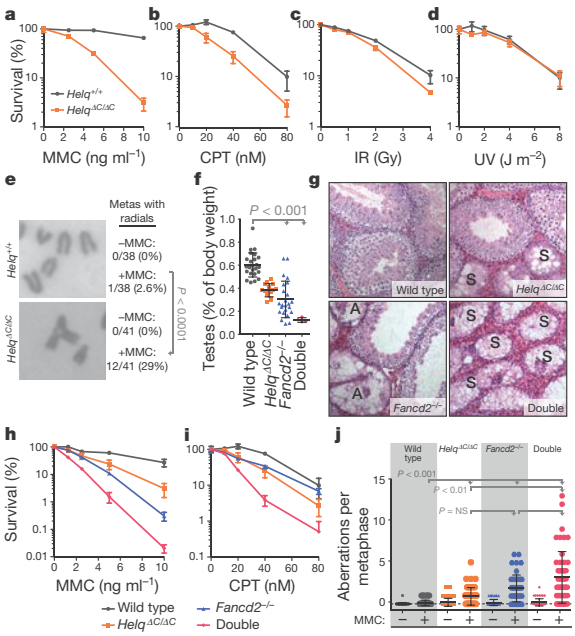

Figure 2 | *Helq* damage sensitivity and *Helq Fancd2* double-mutant phenotypes. **a**–**d**, Clonogenic survival assays of immortalized cells exposed to the indicated damaging agents. **e**, Metaphase chromosomes (metas) from immortalized cells treated with 5 ng ml^{-1} MMC for 16 h; frequency of metaphases with radials ± MMC are indicated. **f**, Testis weights of wild-type, *Helq* single- and *Helq Fancd2* double-mutant mice. **g**, Histological sections of testes. A, atrophic; S, Sertoli cell only. **h**, **i**, Clonogenic survival assays as in **a**. **j**, Metaphase aberrations from immortalized cells treated with or without 10 ng ml^{-1} MMC for 16 h.

(Fig. 2j). These results suggest that HELQ and FANCD2 act in parallel ICL repair pathways.

To gain insight into the function of HELQ during DNA repair, we performed proteomic analysis of proteins co-precipitated with Flag-tagged HELQ. Mass spectrometry revealed several checkpoint and DNA repair proteins, including the replication checkpoint kinase ATR, the single-stranded DNA binding protein RPA70 (also known as RPA1), the four components of the BCDX2 complex required for homologous recombination, and the FANCD2–FANCI heterodimer that functions in the Fanconi anaemia pathway (Fig. 3a, b and Extended Data Fig. 5a). Interaction partners identified by mass spectrometry were confirmed via immunoprecipitation/western blot (Fig. 3c). Reciprocal immunoprecipitation of RAD51C confirmed its association with Flag–HELQ (Fig. 3d), and endogenous HELQ was detected in RAD51C immunoprecipitates from 293T cells and vice versa (Fig. 3e). Recombinant BCDX2 proteins purified from either insect cells or bacteria also bound to purified Flag–HELQ but not to ALC1–Flag or Flag controls (Fig. 3f). Intriguingly, XRCC3, a component of the RAD51C–XRCC3 (CX3) RAD51 paralogue complex, was not detected by either mass spectrometry or western blotting of Flag–HELQ immunoprecipitates (Fig. 3c). Furthermore, HELQ was not found in reciprocal immunoprecipitates with endogenous XRCC3 (Extended Data Fig. 5c). These data indicate that HELQ interacts directly with the BCDX2 complex but not with the CX3 complex.

As ATR, RPA70, the BCDX2 complex and FANCD2–FANCI all respond to stalled replication forks, we examined the localization of green fluorescent protein-tagged HELQ (HELQ–GFP) expressed in NIH 3T3 cells[9]. Subcellular fractionation revealed that HELQ–GFP is enriched on chromatin in response to replication fork stalling with either MMC or aphidicolin, and this is compromised by ATR inhibition (Fig. 3g and Extended Data Fig. 5e–g).

To determine the possible underlying cause of the defect in HELQ-deficient cells we examined replication dynamics, indices of checkpoint activation, Fanconi anaemia pathway activation, double-stranded break (DSB) formation, and the integrity of homologous recombination. Replication fork extension rates in *Helq*$^{\Delta C/\Delta C}$ cells were significantly lower than in wild-type cells (Extended Data Fig. 6d, e) and this was exacerbated by treatment with CPT (Extended Data Fig. 6d). Replication

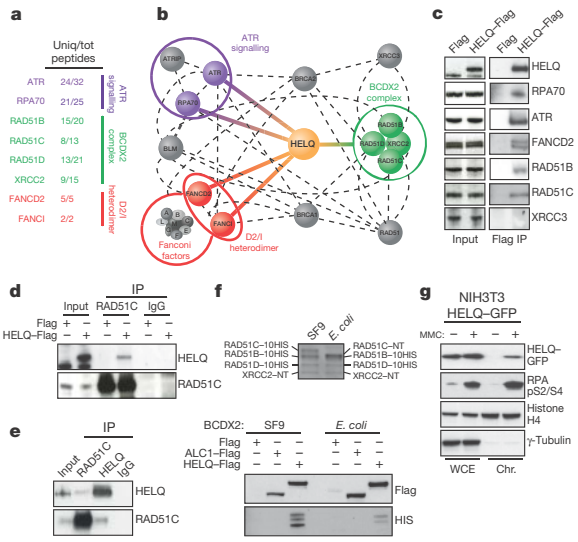

Figure 3 | HELQ interacts with DNA replication stress response factors. **a**, Unique and total peptides identified by mass spectroscopy analysis of HELQ–Flag co-immunoprecipitates isolated from 293 cells. **b**, HELQ interaction network based on the mass spectroscopy results (coloured lines) and reported interactions from BIOGRID, STRING and MINT databases (dashed lines). **c**, Western blots of input and Flag immunoprecipitates (IP) from HELQ–Flag and Flag control samples. **d**, Reciprocal immunoprecipitates of endogenous RAD51C with HELQ–Flag. **e**, Endogenous HELQ and RAD51C immunoprecipitates from 293T cells. **f**, Purified, His-tagged BCDX2 complexes (top) were incubated with Flag-complexed beads (bottom) to test for a direct interaction. Flag and ALC1–Flag are shown as negative controls. NT, non-transfected. **g**, Western blot analysis of whole cells extracts (WCE) and chromatin fractions (Chr) from NIH3T3 HELQ–GFP-expressing cells treated with or without 100 ng ml^{-1} MMC for 24 h.

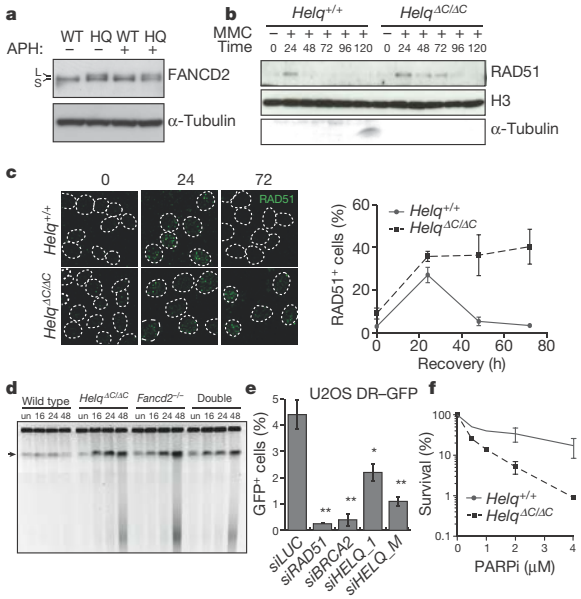

Figure 4 | HELQ influences DNA repair and homologous recombination efficiency. **a**, Lysates from immortalized mouse cells, grown under physiological O_2 and treated with or without 3 μM aphidicolin (APH) for 6 h, were probed for FANCD2. Wild-type (WT), HELQ-deficient (HQ), unmodified (S) and ubiquitinated (L) forms of FANCD2 were used. **b**, Chromatin fractions from immortalized mouse cells, probed for RAD51, histone H3 and α-tubulin at the indicated time points (hours) following treatment with or without 100 ng ml^{-1} MMC. **c**, Left, representative images of RAD51 focus formation in immortalized mouse cells at the indicated time points (hours) following treatment with 1 μM MMC. Right, quantification of RAD51 foci at the indicated time points. **d**, Pulsed field gel electrophoresis of genomic DNA from immortalized cells treated with or without 1 μM MMC for 1 h and recovered for the indicated number of hours. un, undamaged. Wells, intact DNA; arrow, band containing large chromosomal fragments (10–0.45 megabases); below the arrow, smaller fragments resolved by size. **e**, Homologous recombination frequencies in direct repeat (DR)–GFP reporter cells treated with the indicated siRNAs. *LUC*, luciferase. *$P<0.05$; **$P<0.001$. **f**, Clonogenic survival assays of immortalized mouse cells exposed to PARP inhibitor (PARPi). Error bars represent s.e.m.

fork tract asymmetry was also evident in mutants relative to controls indicative of increased fork stalling/collapse (Extended Data Fig. 6f, g).

Checkpoint activation as measured by phosphorylation of ATM, CHK1 and CHK2 (also known as CHEK1 and CHEK2, respectively) and γH2AX in response to DNA damage was unaffected by loss of HELQ in either mouse or human cells (Extended Data Fig. 7a–d). Furthermore, HELQ-deficient cells exhibited constitutive FANCD2 monoubiquitination, indicating that HELQ is dispensable for this modification (Fig. 4a). Assessment of RAD51 recruitment to damaged replication forks revealed that RAD51 is enriched on chromatin in response to MMC treatment in HELQ-deficient mouse and human cells (Fig. 4b and Extended Data Fig. 7e, 8a) and RAD51, RPA (also known as RPA1) and γH2AX accumulate in repair foci (Fig. 4c and Extended Data Fig. 7e–g). However, RAD51 and γH2AX persisted on chromatin and remained present in repair foci at later time points in HELQ-deficient mouse and human cells (Fig. 4b, c and Extended Data Fig. 7e, f), suggesting that the defect in the absence of HELQ occurs at a step downstream of RAD51 recruitment to damaged replication forks. Pulsed field gel electrophoresis revealed that DSBs form in *Helq* and *Fancd2* single and double mutant cells after MMC treatment, but that these lesions persist at later time points, indicating that DSBs induced at ICLs are not efficiently repaired (Fig. 4d). siRNA-induced depletion of HELQ resulted in a two- to threefold decrease in homologous recombination efficiency, implicating HELQ in promoting homologous recombination (Fig. 4e and Extended Data Fig. 8b). Furthermore, clonogenic survival of HELQ-deficient mouse and human cells were significantly compromised in response to poly-ADP ribose polymerase (PARP) inhibition, which is a hallmark of homologous recombination-deficient cells[10] (Fig. 4f and Extended Data Fig. 8c). It is notable that the HELQ interacting protein and BCDX2 complex factor, RAD51D, is also required for PARP inhibitor resistance[11].

In summary, our results uncover a critical role for HELQ in germ cell maintenance and tumour suppression in mammals, which we attribute to a role in replication-coupled DNA repair. The interaction between HELQ and the RAD51 paralogue BCDX2 complex may provide molecular insight into the HELQ phenotype and its role in tumorigenesis, as the BCDX2 complex functions to promote replication-coupled homologous recombination, RAD51C has been implicated in a Fanconi anaemia-like disorder[12], and mutations in RAD51B and RAD51D are associated with hereditary ovarian cancer in humans[11,13–18]. These findings suggest *HELQ* as a strong candidate for screening in human cancers and also explain why mutations in *D. melanogaster* homologues of HELQ, RAD51, and the two RAD51 paralogues (MUS301 (also known as SPN-C), SPN-A, SPN-B and SPN-D, respectively) confer a very similar phenotype[19]. Finally, our findings help to explain the prevalence of non-synonymous variants in *HELQ*, which are significantly associated with upper aerodigestive tract cancers, particularly amongst smokers[20]; and variants in *HELQ* associated with early menopause[21], which may reflect the germ cell defects and ovarian dysgenesis observed in HELQ-deficient mice.

METHODS SUMMARY

HELQ-deficient mice were generated from a commercially available embryonic stem cell clone (clone ID: RRF112, Bay Genomics, University of California, Davis). All strains were maintained on a mixed B6/129 background. Testes for histology were fixed in Bouin's solution and periodic acid-Schiff/haematoxylin stained; all other tissues were fixed in neutral buffered formalin and stained with haematoxylin and eosin. Bone marrow cells were collected and analysed by FACS, colony formation and transplantation as described previously[8,22,23]. HELQ–Flag, Flag, and ALC1–Flag cell lines were generated using the HEK293 Flp-In system according to the manufacturer's protocol (Invitrogen). HELQ–GFP-expressing NIH3T3 cells were generated according to the bacterial artificial chromosome recombineering method described previously[9]. Pulse field gel electrophoresis was carried out similar to the method described in ref. 24. Isolation of HELQ–Flag immunocomplexes entailed lysis of cells in the presence of benzonase to prevent non-specific DNA-bridging of proteins. Flag immunoprecipitates for mass spectrometry analysis were eluted by boiling in SDS–PAGE sample buffer and processed using standard methods. The Biological General Repository for Interaction Data sets (BioGRID, http://thebiogrid.org/), the Molecular INTeraction database (MINT, http://mint.bio.uniroma2.it/mint) and Search Tool for the Retrieval of Interacting Genes/Proteins database (STRING, http://string-db.org/) were used to compile the interaction network. For assays of *in vitro* binding to purified His-tagged BCDX2, Flag-tagged proteins were purified by washing immune-complexed beads four times with buffer containing 1 M NaCl. Purified Flag proteins were then incubated with recombinant BCDX2 complex, washed and eluted for analysis. Chromatin fractionation was carried out using modified versions of previously established methods[25,26]. For siRNA transfections of U2OS cells, cells were subjected to two rounds of reverse transfections using siGENOME siRNA and Dharmafect1 (Thermofisher) according to the manufacturer's protocol. Histology/immunohistochemistry, primary cell line derivation and immortalization, immunofluorescence, assays for clonogenic survival, metaphase aberrations, micronuclei and DNA combing were carried out using standard procedures.

Online Content Any additional Methods, Extended Data display items and Source Data are available in the online version of the paper; references unique to these sections appear only in the online paper.

Received 26 March; accepted 15 August 2013.
Published online 4 September 2013.

1. Kim, H. & D'Andrea, A. D. Regulation of DNA cross-link repair by the Fanconi anemia/BRCA pathway. *Genes Dev.* **26,** 1393–1408 (2012).
2. Kottemann, M. C. & Smogorzewska, A. Fanconi anaemia and the repair of Watson and Crick DNA crosslinks. *Nature* **493,** 356–363 (2013).
3. Boyd, J. B., Golino, M. D., Shaw, K. E., Osgood, C. J. & Green, M. M. Third-chromosome mutagen-sensitive mutants of *Drosophila melanogaster*. *Genetics* **97,** 607–623 (1981).
4. Muzzini, D. M., Plevani, P., Boulton, S. J., Cassata, G. & Marini, F. *Caenorhabditis elegans* POLQ-1 and HEL-308 function in two distinct DNA interstrand cross-link repair pathways. *DNA Repair* **7,** 941–950 (2008).
5. Richards, J. D. *et al.* Structure of the DNA repair helicase hel308 reveals DNA binding and autoinhibitory domains. *J. Biol. Chem.* **283,** 5118–5126 (2008).
6. Ward, J. D. *et al.* Overlapping mechanisms promote postsynaptic RAD-51 filament disassembly during meiotic double-strand break repair. *Mol. Cell* **37,** 157–158 (2010).
7. Parmar, K., D'Andrea, A. & Niedernhofer, L. J. Mouse models of Fanconi anemia. *Mutat. Res.* **668,** 133–140 (2009).
8. Parmar, K. *et al.* Hematopoietic stem cell defects in mice with deficiency of Fancd2 or Usp1. *Stem Cells* **28,** 1186–1195 (2010).
9. Poser, I. *et al.* BAC TransgeneOmics: a high-throughput method for exploration of protein function in mammals. *Nature Methods* **5,** 409–415 (2008).
10. Huehls, A. M., Wagner, J. M., Huntoon, C. J. & Karnitz, L. M. Identification of DNA repair pathways that affect the survival of ovarian cancer cells treated with a poly(ADP-ribose) polymerase inhibitor in a novel drug combination. *Mol. Pharmacol.* **82,** 767–776 (2012).
11. Loveday, C. *et al.* Germline mutations in *RAD51D* confer susceptibility to ovarian cancer. *Nature Genet.* **43,** 879–882 (2011).
12. Vaz, F. *et al.* Mutation of the *RAD51C* gene in a Fanconi anemia-like disorder. *Nature Genet.* **42,** 406–409 (2010).
13. Meindl, A. *et al.* Germline mutations in breast and ovarian cancer pedigrees establish *RAD51C* as a human cancer susceptibility gene. *Nature Genet.* **42,** 410–414 (2010).
14. Loveday, C. *et al.* Germline *RAD51C* mutations confer susceptibility to ovarian cancer. *Nature Genet.* **44,** 475–476 (2012).
15. Vuorela, M. *et al.* Further evidence for the contribution of the *RAD51C* gene in hereditary breast and ovarian cancer susceptibility. *Breast Cancer Res. Treat.* **130,** 1003–1010 (2011).
16. Pelttari, L. M. *et al. RAD51C* is a susceptibility gene for ovarian cancer. *Hum. Mol. Genet.* **20,** 3278–3288 (2011).
17. Wickramanyake, A. *et al.* Loss of function germline mutations in *RAD51D* in women with ovarian carcinoma. *Gynecol. Oncol.* **127,** 552–555 (2012).
18. Osher, D. J. *et al.* Mutation analysis of *RAD51D* in non-BRCA1/2 ovarian and breast cancer families. *Br. J. Cancer* **106,** 1460–1463 (2012).
19. González-Reyes, A., Elliott, H. & St Johnston, D. Oocyte determination and the origin of polarity in *Drosophila*: the role of the spindle genes. *Development* **124,** 4927–4937 (1997).
20. McKay, J. D. *et al.* A genome-wide association study of upper aerodigestive tract cancers conducted within the INHANCE consortium. *PLoS Genet.* **7,** e1001333 (2011).
21. Stolk, L. *et al.* Meta-analyses identify 13 loci associated with age at menopause and highlight DNA repair and immune pathways. *Nature Genet.* **44,** 260–268 (2012).
22. Ceccaldi, R. *et al.* Bone marrow failure in Fanconi anemia is triggered by an exacerbated p53/p21 DNA damage response that impairs hematopoietic stem and progenitor cells. *Cell Stem Cell* **11,** 36–49 (2012).
23. Ploemacher, R. E., van der Sluijs, J. P., van Beurden, C. A., Baert, M. R. & Chan, P. L. Use of limiting-dilution type long-term marrow cultures in frequency analysis of marrow-repopulating and spleen colony-forming hematopoietic stem cells in the mouse. *Blood* **78,** 2527–2533 (1991).
24. Hanada, K. *et al.* The structure-specific endonuclease Mus81–Eme1 promotes conversion of interstrand DNA crosslinks into double-strands breaks. *EMBO J.* **25,** 4921–4932 (2006).
25. Aygün, O., Svejstrup, J. & Liu, Y. A. RECQ5–RNA polymerase II association identified by targeted proteomic analysis of human chromatin. *Proc. Natl Acad. Sci. USA* **105,** 8580–8584 (2008).
26. Mirzoeva, O. K. & Petrini, J. H. DNA replication-dependent nuclear dynamics of the Mre11 complex. *Mol. Cancer Res.* **1,** 207–218 (2003).

Acknowledgements We wish to thank S. West for purified BCDX2 complexes and antibody reagents; O. Fernández-Capetillo for ATR inhibitors; D. Cox, G. Martin and H. Chapman for assistance with mouse breeding and maintenance; E. Nye, T. Bunting and B. Spencer-Dene for histopathology services; I. Rosewell for transgenic services; H. Flynn for mass spectrometry services; and M. Petalcorin for assistance with BAC recombineering. O.M. and A.A.S. are supported by grants of the Swiss National Science Foundation (PDFMP3_127523) and the Vontobel Foundation. The laboratory of A.D. is supported by National Institutes of Health grant R01-DK43889. The laboratories of S.J.B. and C.S. are funded by Cancer Research UK. The S.J.B. laboratory is also funded by a European Research Council advanced investigator grant (RecMitMei). S.J.B. is a Royal Society Wolfson Research Merit Award holder.

Author Contributions C.A.A., R.L.L. and S.J.B. designed the study, performed experiments and wrote the manuscript unless otherwise stated, G.S. performed mouse post-mortem analyses and advised on histopathology, O.M. and A.A.S. performed and supervised DR-GFP homologous recombination assays, K.M. performed RAD51 foci experiments, Z.H. performed human clonogenic survival assays, K.P. and A.D. performed and supervised mouse bone marrow experiments, V.B. assisted with mouse tumour watch monitoring, J.M.S. supervised mass spectrometry, N.J.B. and C.S. advised on experiments and manuscript revisions, and all authors contributed to revision of the manuscript.

Author Information Reprints and permissions information is available at www.nature.com/reprints. The authors declare no competing financial interests. Readers are welcome to comment on the online version of the paper. Correspondence and requests for materials should be addressed to S.J.B. (simon.boulton@cancer.org.uk).

METHODS

Mouse strains, maintenance, localization of genetrap, genotyping. All mice were housed and maintained according to the Home Office guidance outlined in the Animals Scientific Procedures Act. All strains were maintained on a mixed B6/129 background.

A commercially available embryonic stem cell clone (clone ID: RRF112, Bay Genomics, University of California, Davis) harbouring the trapped allele of *Helq* was obtained. The position of the *β-geo* gene trap cassette from the pGT0LxF vector was determined via splinkerette PCR[27] using a modified version of the method described in ref. 28. In brief, 3 μg genomic DNA from *Helq* gene-trapped embryonic stem cells was digested overnight at 37 °C with BfaI. Splinkerette primers were annealed in SuRE Buffer M (Roche) by heating to 95 °C, followed by cooling by 1 °C increments for 15 s each. A total of 40 pmol of the annealed splinkerette adaptor was ligated to 600 ng of BfaI-digested genomic DNA, followed by passage over a PCR purification column (Qiagen). The splinkerette-adapted genomic DNA was re-digested with BfaI for 1 h (eliminating potential background due to splinkerette ligation to partially digested genomic DNA fragments) and re-purified. Primary and nested PCRs were performed using genetrap- and splinkerette-specific primers, with 0.4% of the primary PCR used in the nested round. Nested PCR products were gel purified and sequenced using standard methods.

The *Helq*$^{\Delta C}$ mouse strain was generated using standard transgenic technology. For more background and discussion pertaining to this and other aspects of the manuscript, see elsewhere in the Methods and Extended Data. FANCD2-deficient mice were described previously[8]. Mice were identified using standard ear snip methods, and snips were used for genomic DNA preparation using the HotSHOT method[29] for use in genotype PCR. *Helq* wild-type, heterozygous and mutant mice were genotyped in a single reaction using the following primers: pGT0LxF_F2-CA GGGTTTTCCCAGTCACGAC (genetrap-specific primer), mHELQint11_F8-GT CCTTGTGCCCAAAGTACAG (wild-type-specific primer), mHELQint11_R5-CC TAGTGTGGCTTATCTCCTTCTTC (common primer). *Fancd2* mice were genotyped according to the previously described method[8].

Breedings to establish Mendelian ratios and fertility consisted of continuously mated, individually housed pairs. The *Helq Fancd2* double-mutant strain was established from mating of double heterozygous *Helq*$^{+/\Delta C}$ *Fancd2*$^{+/-}$ mice. Weights of *Helq* mice were measured weekly starting at 10 days post-partum. The tumour watch cohort was established using littermate controls wherever possible and mice were regularly monitored for signs of deterioration using a scoring system that will be described in a separate publication. Mice were euthanized before terminal end points were reached.

Statistics. For survival study, sample size was estimated using standard power calculation methods in order to measure a difference of 3–4 months in survival between mutant and control groups. For *Helq* and *Helq Fancd2* matings, deviations from expected Mendelian ratios were tested by Chi-squared analysis ($P > 0.25$ for both strains). For fertility analysis, the number of litters and pups were tested using Kruskal–Wallace analysis of variance. The Gaussian approximation of *P* values indicated that medians varied significantly between the groups ($P = 0.0019$ for litters, $P = 0.0014$ for pups). Dunn's multiple comparison post-test was used to compare specific sample pairs. Results of *P* value calculations for both litters and pups were the same, and are the values indicated on the graph ($P < 0.001$ for control versus mutant pairs, $P =$ not significant for control versus male or female mutant pairs). For wild-type versus *Helq* mutant testes weights, the Mann–Whitney test was used to analyse whether the weights differed between the two groups. Gaussian approximation was used for calculation of the indicated *P* value ($P < 0.0001$). For wild-type and *Helq* mutant testes weights versus age, linear regression was used to generate slopes of best-fit lines which were tested for deviation of slope from zero. R^2 and *P* values indicated on the graph demonstrate that although there is a correlation between reduced testes weight and age in wild-type mice ($P = 0.0091$), there is no correlation between testes weight and age for *Helq* mutants ($P = 0.78$). For spermatogonia numbers in wild-type versus *Helq* mutant neonatal testes, the Mann–Whitney test was used to analyse whether spermatogonia differed between the two groups. Gaussian approximation was used for calculation of the indicated *P* value ($P < 0.0001$). For MMC-induced metaphase aberrations in wild-type versus *Helq* mutant cell lines, the Mann–Whitney test was used to analyse whether radial chromosomes per metaphase differed between the two groups ($P < 0.0001$). For wild-type versus *Helq* and *Fancd2* single- and double-mutant testes weights, the Kruskal–Wallace analysis of variance test was used. Gaussian approximation of the *P* value indicated that medians varied significantly between the groups ($P < 0.0001$). Dunn's multiple comparison post-test was used to compare specific sample pairs. Results of *P* value calculations are indicated on the graph ($P < 0.001$ for both wild-type versus *Fancd2* single mutant and wild type versus *Helq Fancd2* double mutant). For MMC-induced metaphase aberrations in wild-type versus *Helq* and *Fancd2* single mutants and *Helq Fancd2* double mutants, the Kruskal–Wallace analysis of variance test was used. Gaussian approximation of the *P* value indicated medians varied significantly between the groups ($P < 0.0001$). Dunn's multiple comparison post-test was used to compare specific sample pairs. Results of *P* value calculations for MMC-damaged samples are indicated on the graph ($P < 0.001$ for wild-type versus single and double mutants, $P < 0.01$ for *Helq* mutants versus double mutants, and $P =$ not significant for *Helq* versus *Fancd2* single mutants and for *Fancd2* mutants versus double mutants). For HELQ–GFP chromatin recruitment upon ATR inhibitor treatment, Student's *t*-test was performed to determine whether the observed differences were statistically significant. For DNA combing of replication tracts from wild-type versus *Helq* mutant cells at atmospheric O_2, and tracts from wild-type, *Helq* and *Fancd2* single, and *Helq Fancd2* double mutants at physiological O_2, the Kruskal–Wallace analysis of variance test was used. Gaussian approximation of the *P* values indicated that medians varied significantly between the groups ($P < 0.0001$ for both experiments). Dunn's multiple comparison post-test was used to compare specific sample pairs. Results of *P* value calculations are indicated on the graphs ($P < 0.01$ for wild type versus *Helq* mutants and for undamaged versus CPT damaged *Helq* mutant cells; $P < 0.001$ for wild type versus single and double mutants). For wild type versus *Helq* mutant tumour watch, the Kaplan–Meier epithelial and stromal tumour-free survival curve was analysed with Mantel–Cox log-rank test for *P* value calculation ($P = 0.009$).

Histology, immunohistochemistry sample preparation and reagents. For all histology, samples were paraffin embedded and sectioned at 4 μm. Testes for histology were fixed in Bouin's solution, Periodic acid-Schiff stained and haematoxylin counter-stained; all other tissues, including post-mortem tissues for analysis of tumour watch cohort, were fixed in 10% neutral buffered formalin (NBF) and stained with haematoxylin and eosin.

Immunohistochemistry was carried out using standard methods. In brief, testes for immunohistochemistry were NBF fixed and sections from adult mice were processed for c-KIT staining by microwaving in 0.01 M citrate buffer, pH 6, to unmask antigens. After incubation with c-KIT primary antibodies (Dako A4502, 1:600), samples were incubated with biotinylated secondary antibody (Vector) followed by incubation with Avidin Biotin Complex (Vector); slides were developed in 3, 3′-diaminobenzidine (DAB) substrate (Vector) and counterstained in haematoxylin. Neonatal testis sections were similarly processed and labelled with antibodies against WT1 (Santa Cruz sc-192, 1:450).

Cell line derivation. Ear fibroblasts for primary and SV40 immortalized cultures were generated as follows: mice were euthanized and ear tissue was collected using sterile scissors, ear fragments were rinsed twice in 70% ethanol followed by two rinses in PBS supplemented with 100 μg ml^{-1} kanamycin. Tissue was transferred into 0.3 ml of protease solution (4 mg ml^{-1} each of collagenase D and dispase in DMEM; filter sterilized), and incubated at 37 °C for 45 min. In total, 1.5 ml DMEM containing 10% FBS, 1× glutamine and 5× antibiotic–antimycotic solution were added to protease solution containing ear fragments, and samples were incubated at 37 °C overnight. Cells were dissociated by pipetting, passed through a 40-μm mesh cell strainer, and plated in DMEM as above except using 1× antibiotic–antimycotic solution. Cells were passaged upon reaching confluence to five dishes, and upon reaching confluence, cells were frozen at passage 1 or used immediately for immortalization or experiments.

Fibroblasts were immortalized via transfection with a vector expressing SV40 large T antigen. Constitutively expressed HELQ–Flag, Flag, and ALC1–Flag cell lines were generated using the 293 Flp-In system according to the manufacturer's protocol (Invitrogen). NIH3T3 cells stably expressing GFP-tagged mouse HELQ (consisting of a bacterial artificial chromosome (BAC) containing the entire *Helq* promoter and genomic locus) were generated according to the BAC recombineering method described previously[9]. These and all other cell lines used in this study (293T, HeLa, NIH3T3 and U2OS) were grown in DMEM supplemented with 10% FBS and L-glutamine. Cells were grown in 5% CO_2 incubators at atmospheric O_2 concentrations (~21%) with noted exceptions where samples were cultured at physiological O_2 concentrations (~5%).

For HELQ–GFP transient transfections in HeLa cells (Extended Data Fig. 3d), human *HELQ* was cloned into the pcDNA6.2/C-EmGFP-DEST vector using Gateway technology (Invitrogen). The vector was transfected into HeLa cells with Lipofectamine 2000 using the manufacturer's protocol (Invitrogen). Live or paraformaldehyde (PFA)-fixed cells (fixed cells were counterstained with DAPI (4′,6-diamidino-2-phenylindole)) were visualized 48–96 h after transfection under epifluorescence using a Zeiss Axio Imager M1 microscope with an ORCA-ER camera (Hamamatsu), and images were acquired using the Volocity software (Improvision, Perkin Elmer).

Clonogenic survival, metaphase spreads, growth and micronuclei analyses. For all experiments, fibroblast lines established from littermates or siblings were used wherever possible. Experiments involving primary cells were conducted in physiological O_2 using cell lines of similar passage number.

For clonogenic survival assays, SV40 immortalized mouse ear fibroblasts and siRNA-treated U2OS cells were plated in triplicate on 10-cm dishes at clonal density, allowed to adhere for 8–16 h, and damage treatments administered (CPT medium was changed after 24 h). After 8–10 days of growth, plates were rinsed, fixed/stained in 20% ethanol/4% crystal violet (w/v), rinsed in distilled water and colonies tabulated. All results were normalized to untreated to adjust for plating efficiency and determine percentage survival. Survival experiments were carried out on at least two independent sets of mutant and control mouse cell lines, and in most cases cell lines were tested in at least two independent experiments. Similar results were obtained across all experiments and sets of cell lines.

For analysis of metaphase aberrations, SV40 immortalized cells were damaged as indicated and treated with colcemid (2×10^{-7} M) for 30 min, collected, swelled in hypotonic solution (0.075 M KCl) for 7 min at 37 °C, fixed and washed in ice-cold methanol-acetic acid (3:1), dropped on humid slides and briefly steamed over a 65 °C bath. Slides were dried, stained with Giemsa (Sigma) for 10 min, rinsed with distilled water, and coverslips were mounted (Permount, Fisher). For each sample ≥40 spreads were scored.

Growth kinetics of primary cells were determined using a modified 3T3 protocol to calculate cumulative population doublings. In brief, primary cells were collected, counted and 150,000 cells reseeded in triplicate 10-cm dishes every third day. Cumulative population doublings were calculated using the formula: $\log_{10}(n/n_0) \times 3.32$, in which n = number of cells collected after growth and n_0 = number of cells seeded. Similar growth kinetics were obtained for three different mutant and control mouse embryonic fibroblasts and embryonic fibroblast cell line pairs.

Micronuclei were examined by seeding SV40 immortalized embryonic fibroblasts in 6-well dishes containing glass coverslips. The following day, cells were fixed in 4% PFA and stained with DAPI. For each sample ≥100 cells were scored.

Bone marrow protocols, antibodies/reagents, analysis. Bone marrow cells were collected from 3–4-month-old control and *Helq*$^{\Delta C/\Delta C}$ mice and analysed for haematopoietic stem and progenitor cells (HSPCs) as described previously[8,22]. For LSK (lineage$^-$ Sca-1$^+$ c-Kit$^+$) staining, cells were stained in Hank's balanced salt solution containing 2% FBS and 10 mM HEPES buffer (Gibco) using biotinylated-anti-lineage antibody cocktail (anti-Mac1α, Gr-1, Ter119, CD3e, CD4 and CD8a), phycoerythrin (PE)-Cy-7-anti-Sca-1 antibody (clone E13-161.7), and APC-anti-c-Kit antibody (clone 2B8), followed by staining with PE-streptavidin secondary antibody (all primary and secondary antibodies from BD Biosciences). The samples were acquired using a BD FACSAria high-speed sorter.

For c.f.u.-c assays, bone marrow cells were seeded in 12-well plates at a density of 7×10^4 cells per well in mouse MethoCult medium M3434 (StemCell Technologies) and haematopoietic colonies (c.f.u.-c) were counted at 7–10 days after culture. c.f.u.-c assays were used to determine the survival of bone marrow in presence of MMC. To determine the *ex vivo* clonal growth of murine HSPCs, a cobblestone area-forming cell (CAFC) assay was performed by a limiting dilution analysis of bone marrow in micro-cultures using the bone marrow stromal cell line FBMD-1 (refs 8, 23). This assay quantifies a spectrum of haematopoietic cells that is well-validated to compare with other functional assays. Specifically, day-7 and day-14 CAFC correspond to early progenitor cells and to c.f.u.-spleen-day-12 cells, whereas the more primitive haematopoietic stem cells with long-term repopulating ability correspond to day-28 CAFC[23].

Bone marrow transplantation was performed as described previously[8]. In brief, bone marrow cells (5×10^5) from control or *Helq*$^{\Delta C/\Delta C}$ mice (CD45.2$^+$) were mixed with 2.5×10^5 bone marrow supporting cells from CD45.1$^+$ congenic mice and transplanted into lethally irradiated CD45.1$^+$ congenic recipient mice. The donor cell engraftment efficiency in the recipient mice, after 17 weeks post-transplant, was determined by staining peripheral blood leukocytes with FITC-labelled anti-CD45.2 (clone 104) antibody. The percentage of donor-derived T cells, B cells and myeloid cells was determined by co-staining with PE-labelled anti-CD3e (clone 145-2C11), anti-B220 (clone RA3-6B2) and anti-Mac-1/Gr-1 antibodies (clones M1/70 and RB6-8C5), respectively, and analysed on a FACScan instrument (Becton Dickinson). All antibodies were from BD Biosciences.

Mass spectrometry and proteomics. HELQ–Flag and Flag control cells were collected and lysed in benzonase lysis buffer (20 mM Tris-Cl, pH 7.5, 75 mM NaCl, 10% glycerol, 2 mM $MgCl_2$, 0.5% NP40, 30 U ml^{-1} benzonase, protease inhibitors). NaCl concentration was adjusted to 150 mM, EDTA to 3 mM and lysates were cleared by centrifugation. Supernatants were pre-cleared with Protein G agarose beads for 30 min at 4 °C. Pre-cleared lysates were incubated with anti-Flag affinity agarose resin (Sigma) for 4 h at 4 °C. Beads were washed five times with wash buffer (20 mM Tris-Cl, pH 7.5, 150 mM NaCl, 3 mM EDTA, 0.5% NP40) and once with PBS. Bound proteins were eluted by boiling in SDS–PAGE sample buffer and eluates were resolved on NuPAGE Bis-Tris gels (Invitrogen) and stained with Sypro Ruby (Invitrogen). Gel slices were excised and processed for mass spectrometry using the Janus automated liquid handling system (PerkinElmer). Peptides were analysed by nanoscale capillary liquid chromatography–electrospray ionization/multi-stage mass spectrometry (LC–ESI MS/MS), data were processed using Mascot Distiller (Matrix Science) and exported to Scaffold for viewing (Proteome Software).

The Biological General Repository for Interaction Data sets (BioGRID, http://thebiogrid.org/), the Molecular INTeraction database (MINT, http://mint.bio.uniroma2.it/mint), and Search Tool for the Retrieval of Interacting Genes/Proteins database (STRING, http://string-db.org/) were used to compile the protein interaction network.

Cell lysates, *in vitro* binding assay and fractionation for western blot analyses. All cell lines used in this study were short tandem repeat-profiled and tested for mycoplasma infection before use. All lysis buffers were supplemented with protease inhibitor cocktail (Roche) and phosphatase inhibitors (Sigma).

For validation of mass spectrometry data, HELQ–Flag- and Flag-expressing cells were used. (This was due to our inability to validate these interactions using endogenous HELQ, stemming from the fact that it is expressed at very low levels in most human cell lines, and no antibodies were found to reliably immunoprecipitate the human version. Validation using endogenous mouse HELQ was similarly hindered by a lack of reagents available for detection of the mouse RAD51 paralogues.) Cells were lysed in the presence of benzonase and 2 mg of total protein were immunoprecipitated with anti-Flag affinity resin as above. Beads were washed, bound proteins eluted with 1 × NuPAGE LDS sample buffer and analysed by western blot. Similar methods were employed using lysates prepared from 293T cells to examine endogenous HELQ or RAD51C coimmunoprecipitates.

For *in vitro* binding assays, HELQ–Flag, ALC1–Flag and Flag cells were lysed in the presence of benzonase and pre-cleared lysate was used for Flag immunoprecipitate as described above. Flag-immunocomplexed beads were then washed four times with a modified wash buffer containing 1 M NaCl to remove bound co-precipitates, and once with *in vitro* binding buffer (20 mM Tris-Cl, pH 7.5, 280 mM NaCl, 3 mM EDTA, 0.5% NP40). Washed beads were incubated with recombinant RAD51 paralogue BCDX2 complex (gift of S. West's laboratory) in binding buffer for 4 h at 4 °C and washed four times with the same buffer. Eluates were analysed by western blot.

GFP-tagged HELQ was stably expressed in NIH3T3 cells using a BAC recombineering method to C-terminally Flag/GFP-tag the BAC-containing full-length genomic *Helq*, which included the endogenous promoter. This allowed HELQ–GFP to be expressed at physiological levels.

For chromatin fractionation of embryonic fibroblasts and siRNA-treated U2OS cells, cells were treated with or without 3 μM aphidicolin for 6 h or with or without 1 mM MMC for 24 h, collected and fractionated using a modified version of the method described in ref. 26: pellets were re-suspended in CSK buffer (10 mM PIPES, pH 6.8, 100 mM NaCl, 300 mM sucrose, 3 mM $MgCl_2$, 1 mM EGTA, pH 7, 0.5% Triton X-100), incubated for 10 min on ice (a small fraction of this was removed and SDS–PAGE sample buffer was added to obtain WCEs), pelleted at low speed and supernatants reserved as soluble fraction. Pellets were washed in CSK buffer, and re-pelleted. Pellets were re-suspended in benzonase CSK buffer (10 mM PIPES, pH 7.5, 100 mM NaCl, 300 mM sucrose, 3 mM $MgCl_2$, 0.5% Triton X-100, 0.1 U μl^{-1} benzonase), lysates were incubated for 30 min at 37 °C, pelleted and supernatants reserved for chromatin fraction. Pellets were re-suspended in high-salt CSK (recipe as above except NaCl was added to 500 mM), lysates were incubated for 10 min on ice, cleared at high speed and supernatants pooled with benzonase CSK lysates to yield chromatin extracts[25]. In total, 25 μg of soluble and 10 μg of chromatin proteins were analysed by western blotting.

Western blot, immunoprecipitated antibodies/reagents and siRNA oligonucleotides. Precast NuPAGE Bis-Tris or Tris-acetate gels and electrophoresis system were by Invitrogen. Western blotting transfers were carried out in BioRad transblot chambers and all blots were blocked and probed in 5% milk-phosphate buffer saline triton X100 (PBST) with the exception of p-CHK1 blots, which were processed in 3% BSA-Tris buffered saline triton X100 (TBST). Mouse and rabbit horseradish peroxidase-conjugated secondary antibodies were from ThermoFisher, and signals were visualized with ECL western blotting detection reagent (Amersham) or SuperSignal West Femto reagent (Thermoscientific).

Antibodies used for western blot analysis: Flag (Sigma F1804, 1:2,000), HELQ (Santa Cruz 81095, 1:200), His (Clontech 631212, 1:2,000), PARP1 (Trevigen 4338-ML-50, 1:1,000), CHK1 (Sigma C9358, 1:500), S345-P-CHK1 (Cell Signalling 2348, 1:500), CHK2/p-CHK2 (Upstate 05-649, 1:400), ATM (Sigma A1106, 1:2,000), S1981-p-ATM (Cell signalling 4526, 1:1,000), histone H3 (Abcam 10799, 1:2,000), α-tubulin (Sigma T6199, 1:2,000), RAD51 (Santa Cruz 8349, 1:200), FANCD2 (Epitomics 2986-1, 1:1,000), γH2AX (Cell Signalling 2577, 1:1,000), RPA32 (Abcam 12F3.3, 1:1,000), BRCA2 (Santa Cruz 8326, 1:200), TFIIH p89 (Santa Cruz 293, 1:200). All RAD51 paralogue antibodies were a kind gift from S. West's laboratory, as described in ref. 30: RAD51B (IH3 mouse monoclonal antibody, 1:500), RAD51C (2H11 mouse monoclonal antibody, 1:500), RAD51D (5B3 mouse monoclonal

antibody, 1:400), XRCC2 (7B7 mouse monoclonal antibody, 1:400), XRCC3 (10F1 mouse monoclonal antibody, 1:400).

Antibodies used for immunoprecipitation: RAD51C (R68 rabbit antibody), XRCC3 (10F1 mouse monoclonal antibody), mouse IgG (Abcam 18413) and rabbit IgG (Abcam 46540) were used where appropriate as negative control immunoprecipitates.

siRNA oligonucleotides: *RAD51* (ref. 31) 5′-AAGGGAAUUAGUGAAGCCAAA-3′, *BRCA2* (ref. 32) 5′-AACAACAAUUACGAACCAAAC-3′. siRNA oligonucleotides used in DR–GFP and in *HELQ_1* (this study): 5′-GAAGGUCCAAUAUAAUU-3′, *HELQ_3* (this study): 5′-AAUGUGAGGUGAUUAAGAA-3′, *HELQ_M*[33]: 5′-CAAAGGAAGATTTCCTCCAACTAAA-3′, *HELQ-01*: 5′-GUUUGAAGAUUGCAACGAA-3′, *HELQ-03*: 5′-AAUGUGAGGUGAUUAAGAA-3′, *HELQ-04*: 5′-GGUAGAAGAGUUACUAAGA-3′, *HELQ-17*: 5′-GUUUGAAGAUUGCAACGAA-3′, *XRCC2*: 5′-CAGGGTACTACGCAAGCCT-3′, *XRCC3*: 5′-CAGAATTATTGCTGCAATT-3′, *RAD51C*: 5′-AAGAGAATGTCTCACAAAT-3′, *RAD51D*: 5′-CTGGGTGGAAATAAGCTTA-3′.

siRNA transfection and ATR inhibition. U2OS cells were subjected to two rounds of reverse transfections using siGENOME siRNA and Dharmafect1 (Thermofisher) according to the manufacturer's protocol. Thirty-six hours after the second transfection, cells were treated for 14 h with 3 μM aphidicolin. For ATR inhibition, 3 μM ATR inhibitor was added to cultures 30 min before aphidicolin treatment.

Immunofluorescence. Cells were first washed in PBS and then fixed with 2% PFA at room temperature (18 °C) for 15 min, and then washed three times in PBS. The fixed cells were further permeabilized with 3% BSA in PBS plus 0.1% Triton X-100 for 30 min at room temperature. Primary antibodies (RAD51; 1:500, RPA; 1:1,000, γH2AX) were added and incubated at 37 °C for 1 h. After washing with PBS plus 0.1% Triton X-100, secondary antibodies (provided by Jackson ImmunoResearch) were applied and incubated for 1 h in the dark. The stained coverslips were mounted with prolong Gold Antifade reagent (Invitrogen). Imaging was carried out using Axio Imager (Zeiss) or Axioplan 2 Imaging (Zeiss) microscope and analysed by Axiovision software (Zeiss).

Homologous recombination reporter assays. DSB repair efficiency by homologous recombination was measured in DR–GFP U2OS cells as described previously[34]. In brief, 48 h after the first round of siRNA transfection (40 nM) using Lipofectamine RNAiMAX (Invitrogen), cells were either mock-transfected (pcDNA3.1) or transfected with 0.6 μg of an I-SceI expression plasmid (pCBASce) together with siRNA (20 nM) using 3.6 μl of Lipofectamine 2000 (Invitrogen). The media was replaced 3 h after I-SceI transfection and cells were analysed for GFP expression by flow cytometry on a Cyan ADP (Dako) 72 h after I-SceI transfection. To confirm siRNA efficiency, western blotting was carried out on 50 μg of NP-40 lysates plus sonication run on 4–15% Precast SDS–PAGE gels (Bio-Rad).

DNA combing. Replication tracts were labelled for 20 min with 20 μM iododeoxyuridine (IdU) (in atmospheric O_2 experiments, cells were treated with or without 2.5 μM CPT for the final 15 min of IdU labelling to test replication fork stalling/restart), washed three times with PBS and labelled for 20 min with 200 μM chlorodeoxyuridine (CldU). Cells were washed, collected on ice, counted and embedded in agarose. Cells were digested in 2–3 changes of proteinase K buffer for 24 h at 50 °C. Plugs were washed for 5 × 10 min in Tris-EDTA followed by β-agarase digestion overnight at 42 °C. Genomic DNA was combed onto silanized coverslips (Genomic Vision) using a Molecular Combing System instrument (Genomic Vision), dried and stained using previously described methods[35]. Experiments were conducted on two separate sets of mutant and control cell lines with similar results obtained for both experiments.

Pulsed field gel electrophoresis analysis. Immortalized embryonic fibroblasts were treated with or without MMC for 1 h and then allowed to recover for 16–48 h. Cells were collected and processed for pulsed field gel electrophoresis (PFGE) analysis similar to previously described methods[24]. In brief, cell suspensions were placed on ice, cell numbers counted and equivalent cell numbers or each genotype were embedded in agarose plugs in duplicate. Cells were digested by incubating plugs in proteinase K overnight at 50 °C, plugs were washed 4 × 1 h, sealed with low-melting-point agarose into the well of a 1% agarose/0.5× Tris/borate/EDTA (TBE) pulsed field gel, and run for 24 h on a Gene Navigator PFGE apparatus (Amersham) using the following conditions: running temperature: 13 °C; running angle: 120° (hex electrode); connection setup: interpolation (phase 1 of 2: N/S 30 s, E/W 30 s, phase time 23 h; phase 2 of 2: N/S 5 s, E/W 5 s); power program: 180 V 15 min, 170 V 30 min, 160 V 1 h, 150 V 2 h, 140 V 4 h, 130 V 8 h, 120 V 7 h. Gels were post-stained with ethidium bromide and washed in 0.5 × TBE. PFGE was carried out on two independent sets of mutant and control cell lines and results were repeated two or more times for each set of cell lines. Similar results were obtained across all experiments and sets of cell lines.

27. Horn, C. *et al.* Splinkerette PCR for more efficient characterization of gene trap events. *Nature Genet.* **39,** 933–934 (2007).
28. Dupuy, A. J., Fritz, S. & Largaespada, D. A. Transposition and gene disruption in the male germline of the mouse. *Genesis* **30,** 82–88 (2001).
29. Truett, G. E. *et al.* Preparation of PCR-quality mouse genomic DNA with hot sodium hydroxide and tris (HotSHOT). *Biotechniques* **29,** 52–54 (2000).
30. Masson, J. Y., Stasiak, A. Z., Stasiak, A., Benson, F. E. & West, S. C. Complex formation by the human RAD51C and XRCC3 recombination repair proteins. *Proc. Natl Acad. Sci. USA* **98,** 8440–8446 (2001).
31. Kratz, K. *et al.* Deficiency of FANCD2-associated nuclease KIAA1018/FAN1 sensitizes cells to interstrand crosslinking agents. *Cell* **142,** 77–88 (2010).
32. Bruun, D. *et al.* siRNA depletion of BRCA1, but not BRCA2, causes increased genome instability in Fanconi anemia cells. *DNA Repair* **2,** 1007–1013 (2003).
33. Moldovan, G. L. *et al.* DNA polymerase POLN participates in cross-link repair and homologous recombination. *Mol. Cell. Biol.* **30,** 1088–1096 (2010).
34. Gunn, A. & Stark, J. M. I-SceI-based assays to examine distinct repair outcomes of mammalian chromosomal double strand breaks. *Methods Mol. Biol.* **920,** 379–391 (2012).
35. Seiler, J. A., Conti, C., Syed, A., Aladjem, M. I. & Pommier, Y. The intra-S-phase checkpoint affects both DNA replication initiation and elongation: single-cell and -DNA fiber analyses. *Mol. Cell. Biol.* **27,** 5806–5818 (2007).

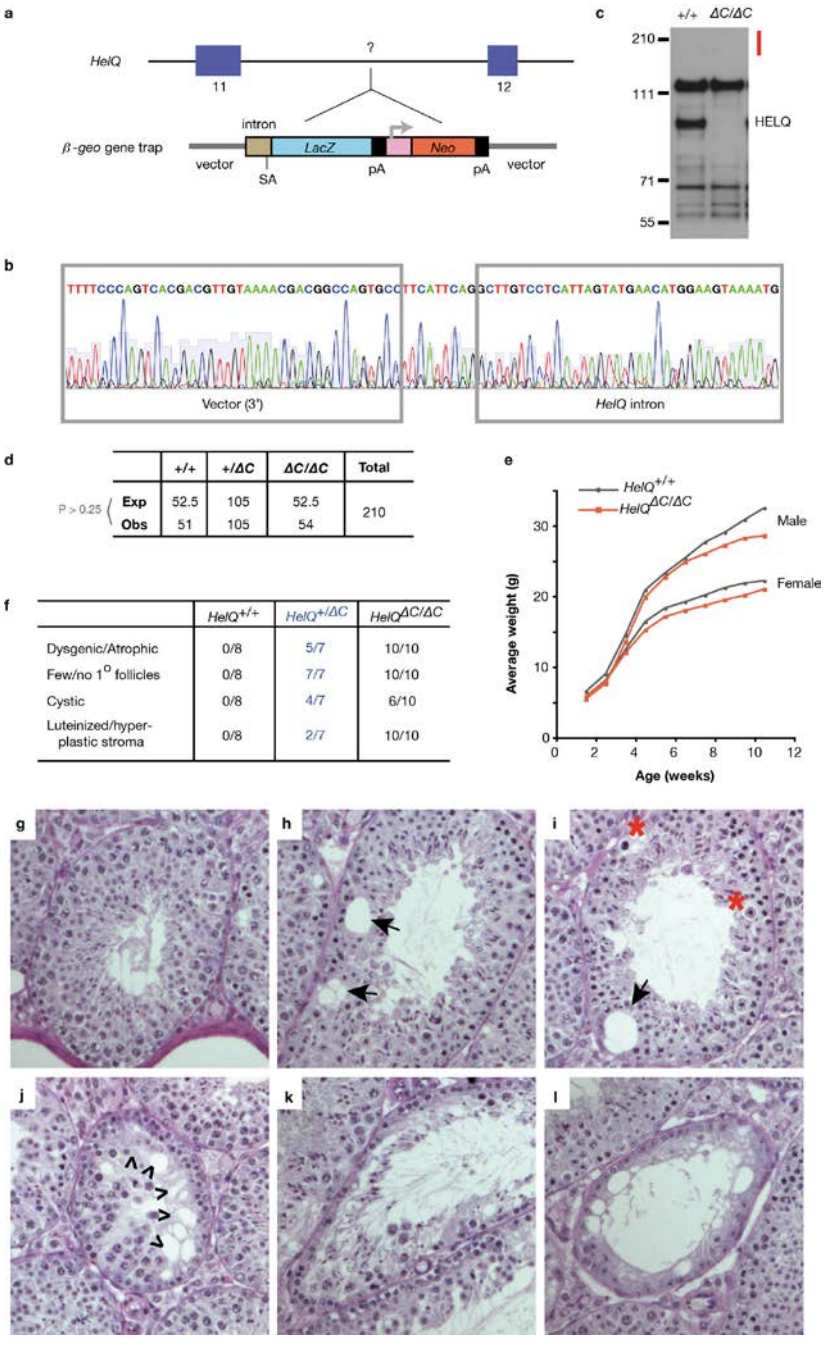

Extended Data Figure 1 | Allele and subfertility of HELQ deficiency. **a**, Schematic of the *β-geo* gene trap and its approximate location within the *Helq* genomic locus. **b**, Sequence and traces showing the exact location of the gene trap insertion as determined by sequencing of splinkerette PCR products. **c**, HELQ western blot from wild-type (+/+) and *Helq* mutant (ΔC/ΔC) mouse cells, showing loss of HELQ and absence of a HELQ–βgal fusion protein (which, if present, would be evident in the region of the blot marked with the red bar). **d**, Table of observed and expected Mendelian ratios calculated from heterozygous matings. Chi-squared analysis was used to test for deviation of observed from expected. **e**, Average weights of *Helq* mice tracked between 2 and 12 weeks of age. Means of 5–13 mice for each group are shown, and for clarity, s.d. is not plotted. Differences are not significant. **f**, Table of ovarian pathology in 30-week-old *Helq* control and mutant females (black text) and heterozygous females within the tumour watch study (blue text, 17–21 months old). **g–l**, Histological sections of testes from $Helq^{\Delta C/\Delta C}$ males showing various degrees of atrophy, including: normal tubules (**g**), mild atrophy (**h**, **i**), pockets of atrophy (arrows), pyknotic nuclei (asterisks); moderate atrophy (**j**, **k**), missing spermatogenic layer (arrowheads) and severe atrophy (**l**), with only Sertoli cells present.

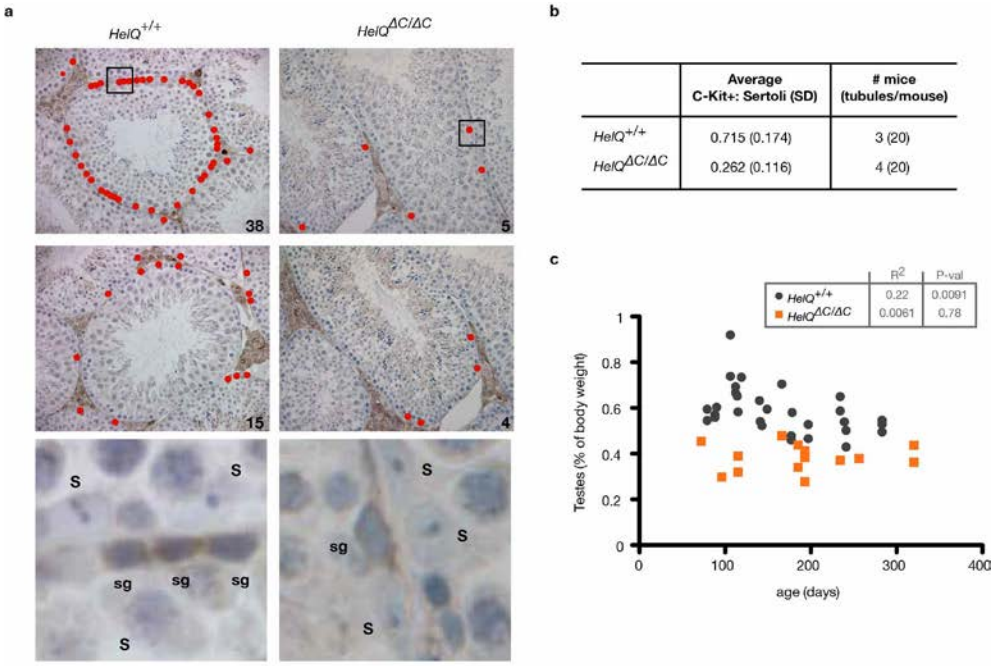

b

	Average C-Kit+: Sertoli (SD)	# mice (tubules/mouse)
$HelQ^{+/+}$	0.715 (0.174)	3 (20)
$HelQ^{\Delta C/\Delta C}$	0.262 (0.116)	4 (20)

d

		all mice		Female		Male	
		$HelQ^{+/+}$	$HelQ^{\Delta C/\Delta C}$	$HelQ^{+/+}$	$HelQ^{\Delta C/\Delta C}$	$HelQ^{+/+}$	$HelQ^{\Delta C/\Delta C}$
	mice in cohort	41	44	27	26	14	18
	total tumors (non-lymphoma)	34	63	16	43	18	21
	% with tumors (non-lymphoma)	46.3	63.6	37.0	69.2	64.3	55.6
	lymphoma	29.3	20.5	37.0	19.2	14.3	22.2
epithelial	lung tumor	17.1	13.6	11.1	7.7	28.6	22.2
epithelial	liver tumor	9.8	4.5	3.7	3.8	21.4	5.6
epithelial	harderian gland tumor	7.3	25.0	3.7	19.2	14.3	33.3
epithelial	other glandular tumors[1]	9.6	18.0	14.8	23.1	0	11.1
epithelial, Female specific	gastric tumor	19.5	29.5	11.1	26.9	35.7	33.3
epithelial, Female specific	pituitary tumor	-	-	3.7	28.0*	0	0
stromal, Female specific	ovarian tumor	-	-	7.4	40.0*	-	-
stromal	other tumors[2]	4.9	0	3.7	0	7.1	0

[1] including: salivary, thyroid, parathyroid, adrenal, mammary, and endometrial gland adenomas and cystic hyperplasias

[2] including: leiomyosarcoma, spindle cell sarcoma

* pituitary/ovaries not identified in 1 of 26 PMs, therefore tumor frequency calculated from 25 animals in the mutant cohort

Extended Data Figure 2 | HELQ-deficient germ cell and tumour phenotypes. **a**, Immunohistochemical analysis of adult testes labelled with the stem cell marker c-KIT$^+$ (brown) to highlight spermatogonia, and counterstained with haematoxylin to visualize remaining cells in the tubule (blue). Two representative images from wild-type (left) and mutant (right) mice are shown, with red circles indicating c-KIT$^+$ cells. The number of c-KIT$^+$ cells for each panel is indicated in the bottom right corner. Boxed regions in top panels are magnified in bottom panels to demonstrate staining. S, Sertoli cells; SG, c-KIT$^+$ spermatogonia. **b**, Tabulation of average c-KIT$^+$ cells per tubule normalized to the number of Sertoli cells. **c**, Testis weights plotted by mouse age in days. Linear regression used to generate slope of best-fit line; tested best-fit line for deviation of slope from 0: R^2 and P values are indicated, revealing no correlation between age and testes weight for *Helq* mutants. **d**, Table of tumour frequency and tumour spectrum of *Helq* mutant and control mice showing data for all mice, females, and males in the tumour watch cohort. 129/B6 background phenomena are coloured in grey text, *Helq* mutant-specific effects are in black, and female-specific pathology is highlighted in pink.

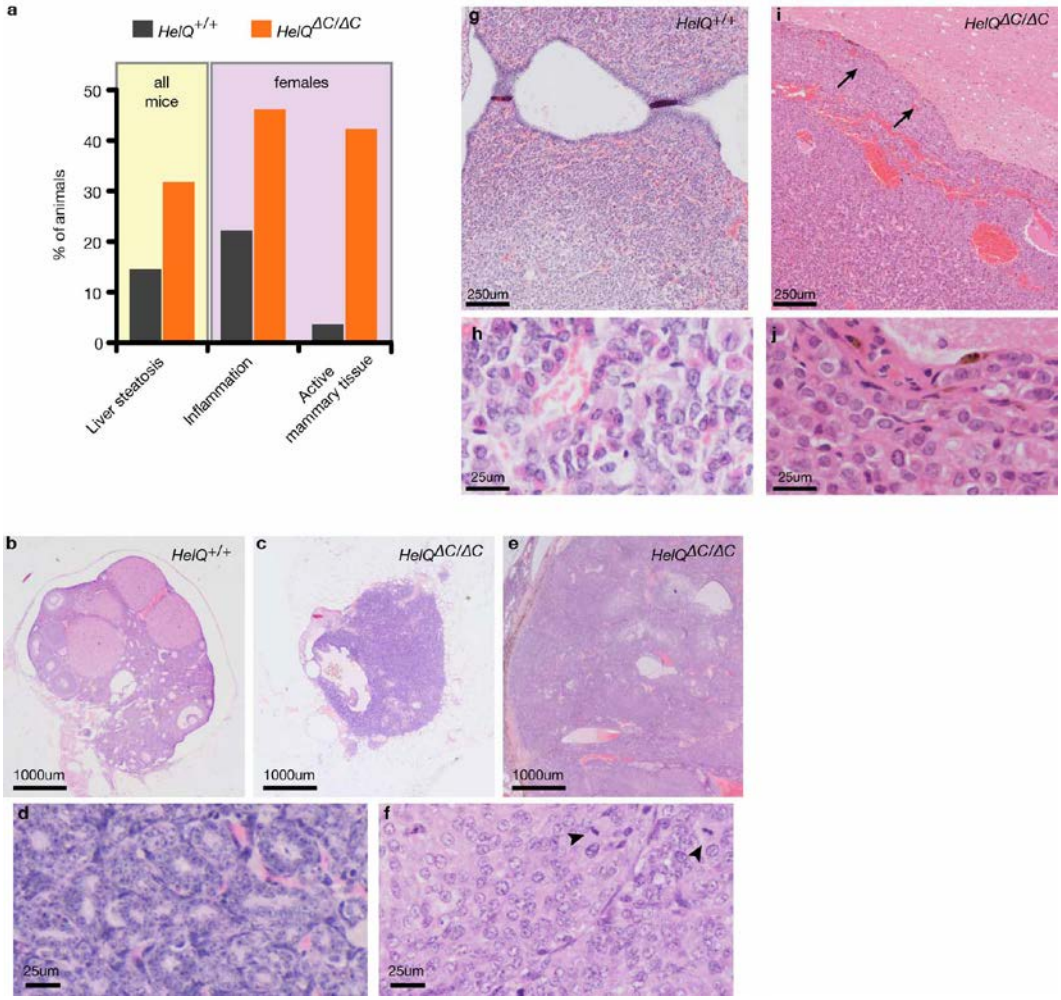

Extended Data Figure 3 | Tumour histology of HELQ deficiency. **a**, The frequency of liver steatosis in all mice, and inflammation and activated mammary tissue in female mice. **b**–**f**, Ovary sections showing normal wild-type ovary (**b**) and common ovarian pathology in mutant animals (**c**–**f**). Low-magnification (**c**) and high-magnification (**d**) images of dysgenic ovary from a *Helq* mutant exhibiting a sex cord stromal tumour containing tubular-like structures. Low-magnification (**e**) and high-magnification (**f**) images of large nodular granulosa cell tumour from a *Helq* mutant. Arrowheads indicate mitotic figures (**f**). **g**–**j**, Pituitary sections showing low-magnification (**g**) and high-magnification (**h**) images of normal wild-type pituitary. Low-magnification (**i**) and high-magnification (**j**) images of pituitary tumour from a *Helq* mutant mouse. Arrows indicate boundary where large, haemorrhagic pituitary adenoma compresses overlying brain (**h**).

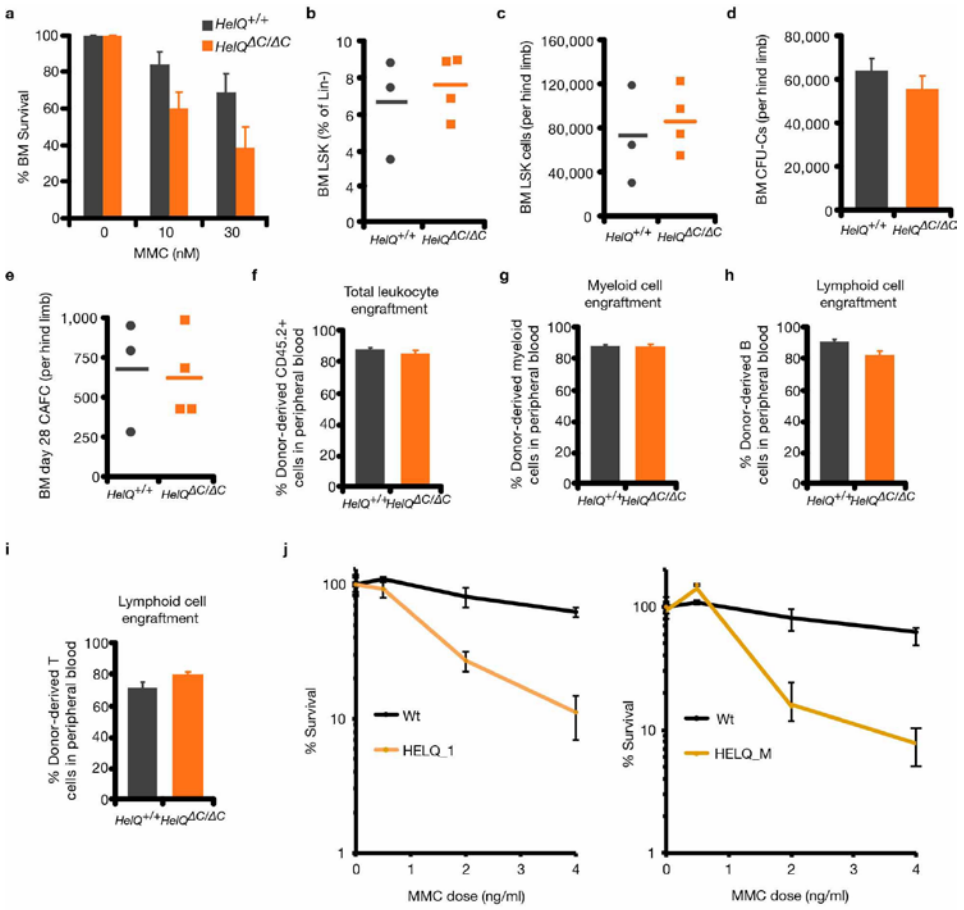

k

genotype	observed #	observed %	expected #	expected %
$HelQ^{+/+}$ $FancD2^{+/+}$	8	5.2	9.7	6.25
$HelQ^{+/+}$ $FancD2^{+/-}$	24	15.5	19.4	12.5
$HelQ^{+/+}$ $FancD2^{-/-}$	13	8.4	9.7	6.25
$HelQ^{+/\Delta C}$ $FancD2^{+/+}$	18	11.6	19.4	12.5
$HelQ^{+/\Delta C}$ $FancD2^{+/-}$	36	23.2	38.8	25
$HelQ^{+/\Delta C}$ $FancD2^{-/-}$	18	11.6	19.4	12.5
$HelQ^{\Delta C/\Delta C}$ $FancD2^{+/+}$	6	3.9	9.7	6.25
$HelQ^{\Delta C/\Delta C}$ $FancD2^{+/-}$	19	12.3	19.4	12.5
$HelQ^{\Delta C/\Delta C}$ $FancD2^{-/-}$	13	8.4	9.7	6.25
Total:	155			

P > 0.25

Extended Data Figure 4 | Characterization of *Helq*$^{\Delta C/\Delta C}$ bone marrow and generation of *Helq Fancd2* double-mutant offspring. **a**, *Helq*$^{\Delta C/\Delta C}$ and control bone marrow cells were isolated and exposed to MMC at the indicated doses and clonogenic survival of haematopoietic progenitors was plotted as percentage of surviving cells relative to untreated. Means ± s.e.m. for three mice per genotype are shown. **b**–**i**, Bone marrow (BM) from mutant and control mice was isolated and subjected to various haematopoietic stem and progenitor cell analyses: tabulation of bone marrow LSK (lineage$^-$ Sca-1$^+$ c-Kit$^+$) cell populations (**b**, **c**); bone marrow c.f.u.-c (colony-forming units in culture) assays (**d**); bone marrow day-28 cobblestone area-forming cells (CAFCs; **e**); and total donor-derived leukocyte (**f**), myeloid (**g**) and lymphoid (**h**, **i**) engraftment upon bone marrow transplantation. Raw data (symbols) and means (horizontal lines) from three mice are plotted (**b**, **c**, **e**); means ± s.e.m. for three mice per genotype (**d**); and means ± s.e.m. for 6–10 recipients for each genotype (**f**–**i**). **j**, siRNA-treated U2OS cells were plated for clonogenic survival and treated with the indicated reagents. **k**, Observed and expected Mendelian ratios calculated from *Helq*$^{+/\Delta C}$ *Fancd2*$^{+/-}$ double heterozygous matings. Chi-square analysis was used to test for deviation of observed from expected.

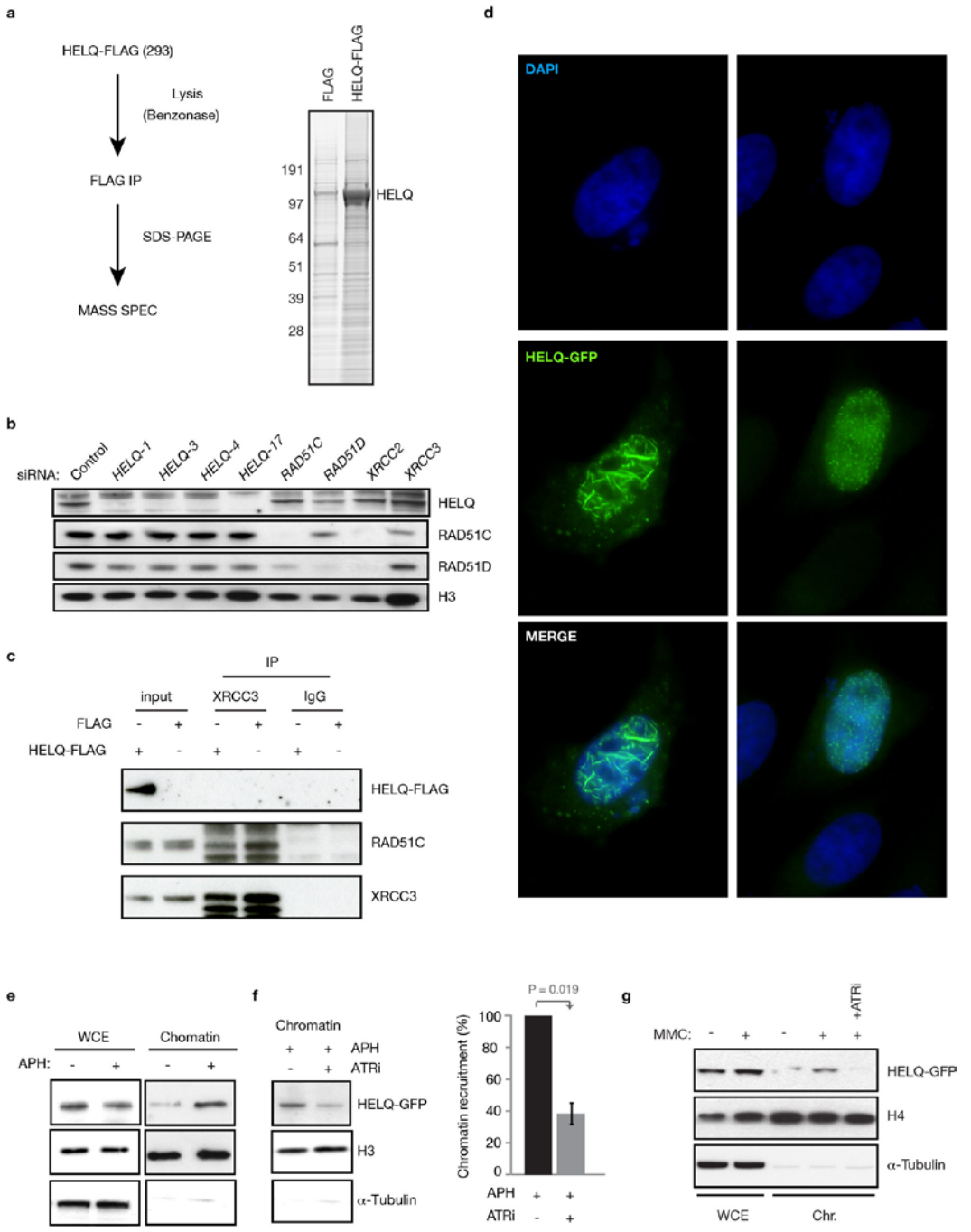

Extended Data Figure 5 | HELQ mass spectrometry, its relationship with the RAD51 paralogues, ATR, and overexpression. **a**, HELQ purification scheme and SDS–PAGE gel showing proteins co-purified with HELQ–Flag and control Flag immunoprecipitates. **b**, Cells treated with the indicated siRNAs were collected and probed for HELQ and the RAD51 paralogues. **c**, XRCC3 immunoprecipitated from HELQ–Flag and Flag control cell lysates and probed for Flag, XRCC3 and RAD51C (positive XRCC3 interacting protein control). IgG was used as a negative control. **d**, HeLa cells transiently expressing recombinant HELQ–GFP (green panels) fixed and stained with DAPI (blue panels) to identify nuclei. Two examples of spontaneous nuclear aggregation patterns are shown: small focal aggregates (right) and large filamentous aggregates (left). **e**, Chromatin fractions of HELQ–GFP cells treated with or without 2 μM APH for 24 h. **f**, Cells treated as in **e**, with or without 3 mM ATR inhibitor (ATRi). Quantification of HELQ in chromatin fractions normalized to H3 (right). **g**, Cells treated with or without 100 ng ml^{-1} MMC for 24 h and fractionated as in **e**.

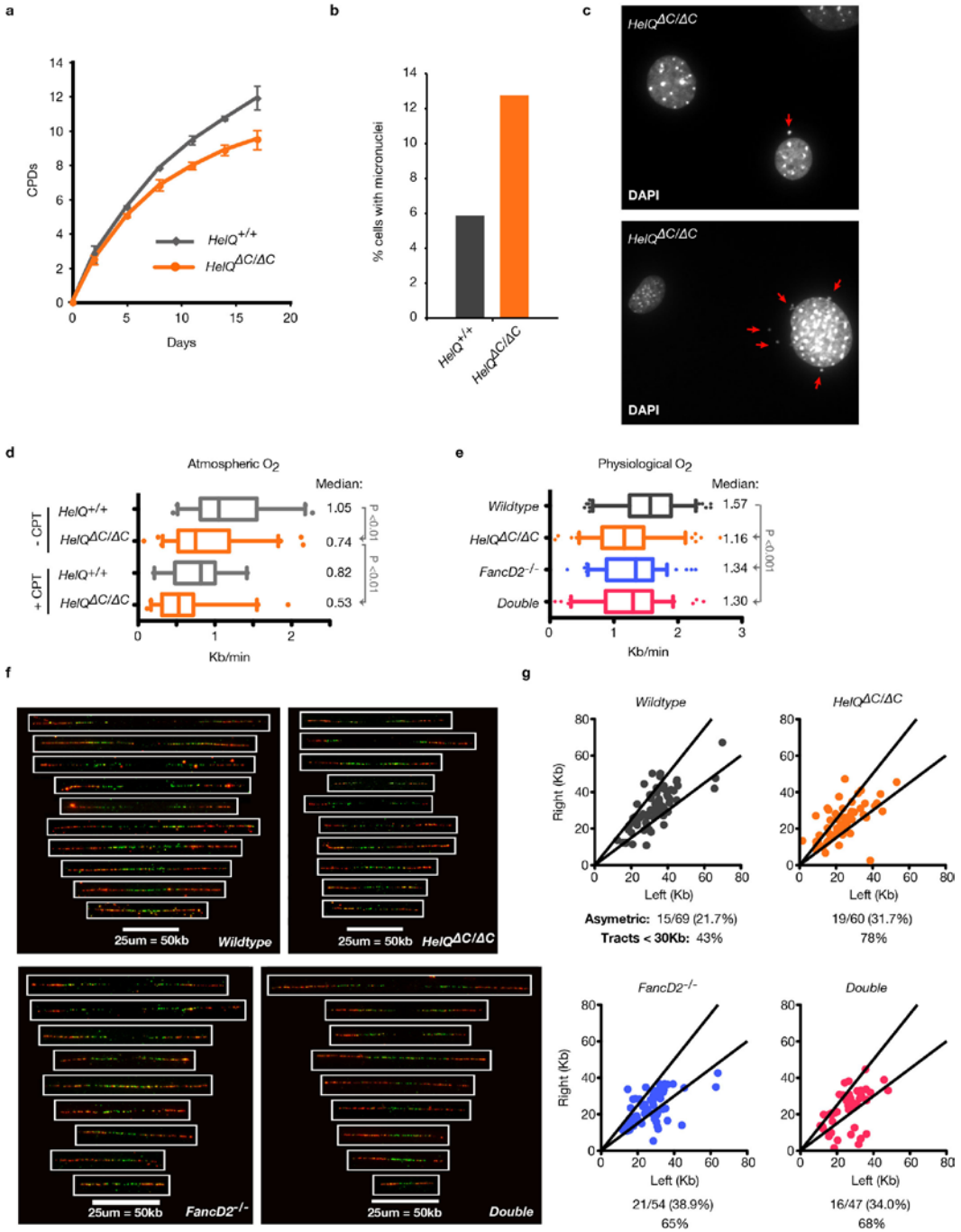

Extended Data Figure 6 | Spontaneous defects, checkpoint indices, damage foci and clonogenic survival of HELQ-deficient cells. **a**, Primary *Helq* mutant and control cell lines were grown in physiological O_2 for the indicated number of days and passaged regularly to generate a cumulative population doubling (CPD) curve. Means ± s.d. of triplicate replicas are shown. **b**, **c**, *Helq* mutant and control cells grown on coverslips were formaldehyde fixed and DAPI stained to determine levels of spontaneous micronuclei formation: percentage of 100 cells exhibiting 1 or more micronucleus (**b**); representative images (**c**), micronuclei (arrows). **d**, **e**, DNA combing used to calculate replication fork rates of primary cells grown under atmospheric (**d**) or physiological (**e**) O_2. Cells in **d** were treated with or without 2.5 μM CPT for 15 min during labelling. **f**, Examples of origin containing IdU (green)- and CldU (red)-labelled fibres. **g**, Right versus left replication tract lengths to determine fork asymmetry (defined as tracts falling outside the interquartile lines).

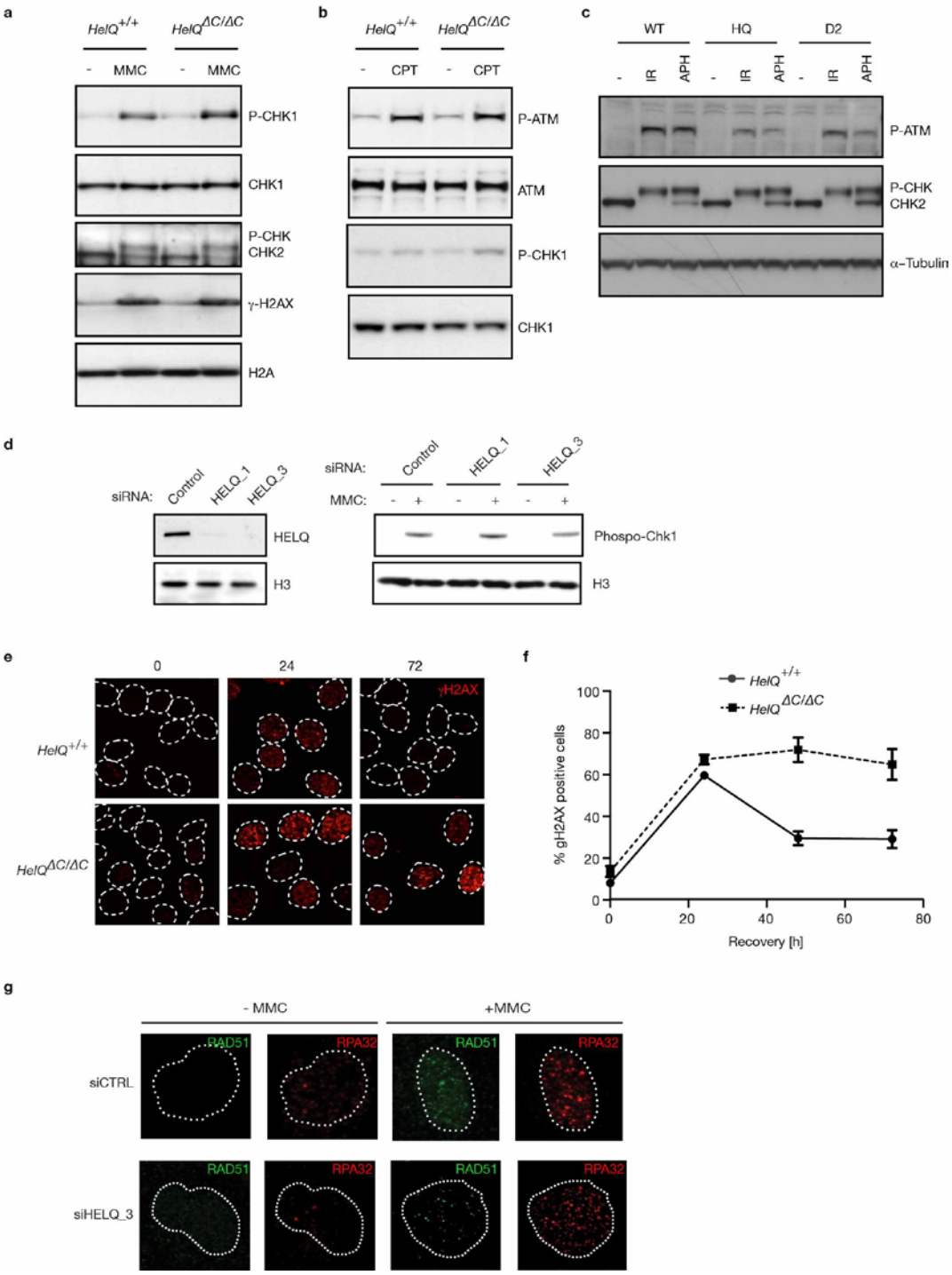

Extended Data Figure 7 | Checkpoint and double-strand break repair function. **a**, **b**, Immortalized $Helq^{\Delta C/\Delta C}$ and $Helq^{+/+}$ cells treated with or without 500 ng ml^{-1} MMC (**a**) or 50 nM CPT (**b**) for 20 h and probed for the indicated checkpoint indices. **c**, Primary wild-type (WT), HELQ-deficient (HQ) and FANCD2-deficient (D2) cells were left untreated (−), or exposed to 5 Gy irradiation and collected 30 min later, or 3 μM APH for 16 h and harvested 10 min later, and lysates were probed for the indicated checkpoint indices. **d**, Phospho-Ser 345 CHK1 levels in U2OS cells subjected to 1 μM MMC for 24 h. **e**, Immortalized mouse cells were treated with 1 μM MMC for 24 h, allowed to recover for the indicated times (in hours), and stained for γH2AX. **f**, Quantification of percentage of positive cells from **e**. **g**, RPA32 and RAD51 foci formation in U2OS cells ± 1 μM MMC for 24 h subjected to control and *HELQ* siRNA.

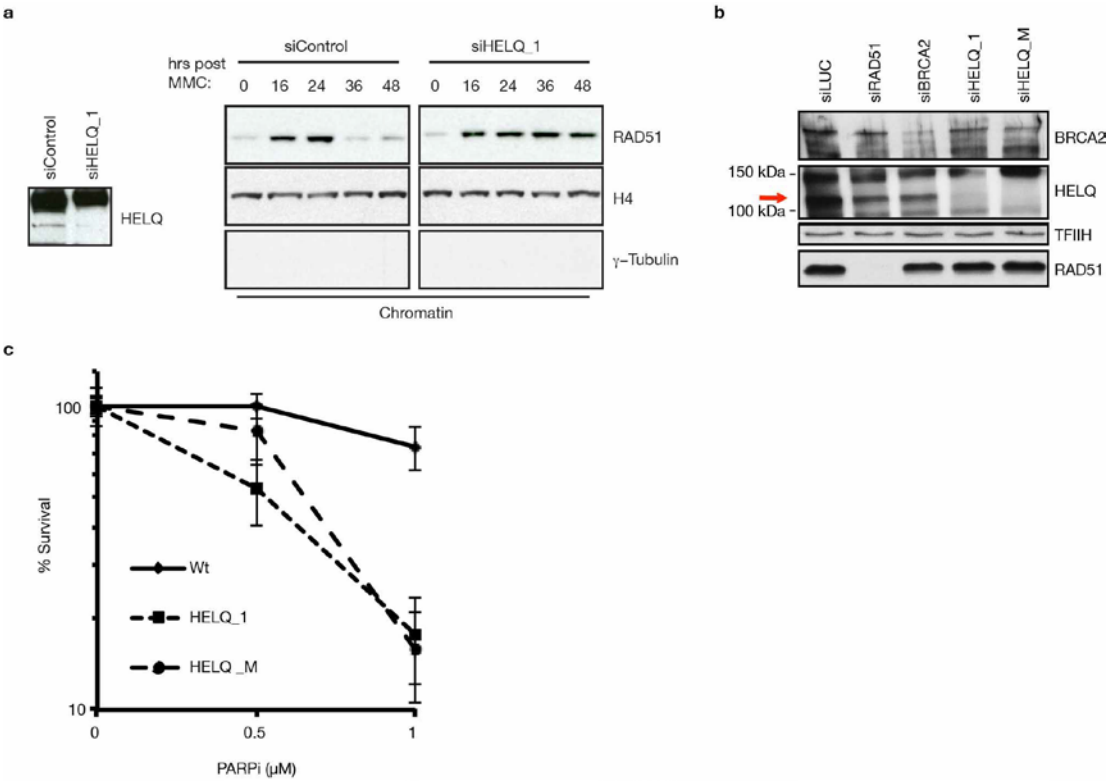

Extended Data Figure 8 | Homologous recombination dynamics and PARP inhibitor sensitivity. **a**, U2OS cells treated with or without 100 ng ml^{-1} MMC for 24 h, allowed to recover for the indicated times (in hours), fractionated and probed for RAD51. H4 and α-tubulin are shown as controls for chromatin fractionation. **b**, DR–GFP reporter cells treated with the indicated siRNAs were probed for BRCA2, HELQ and RAD51; transcription factor IIH (TFIIH) is shown as a loading control. **c**, siRNA-treated U2OS cells were plated for clonogenic survival and treated with the indicated reagents.